

**GEOLOGY, PETROCHEMISTRY AND TECTONICS  
OF THE LOWDER-MUDIAH AREA,  
ABYAN PROVINCE, YEMEN REPUBLIC**

**A thesis submitted to  
The University of Leicester  
for the degree of**

**Doctor of Philosophy**

**MAHFOOD ALI OBAID BA-BTTAT**

**February, 1991**

---

UMI Number: U039035

All rights reserved

INFORMATION TO ALL USERS

The quality of this reproduction is dependent upon the quality of the copy submitted.

In the unlikely event that the author did not send a complete manuscript and there are missing pages, these will be noted. Also, if material had to be removed, a note will indicate the deletion.



UMI U039035

Published by ProQuest LLC 2015. Copyright in the Dissertation held by the Author.  
Microform Edition © ProQuest LLC.

All rights reserved. This work is protected against  
unauthorized copying under Title 17, United States Code.



ProQuest LLC  
789 East Eisenhower Parkway  
P.O. Box 1346  
Ann Arbor, MI 48106-1346



7500646 047



#### DEDICATION

This work is dedicated to the spirit of my father, who died while I was in the first year in primary school. Almighty Allah, Bless him, and let him rest in peace in Paradise.

**GEOLOGY, PETROCHEMISTRY AND TECTONICS OF THE LOWDER-MUDIAH AREA, ABYAN PROVINCE, YEMEN REPUBLIC****MAHFOOD ALI OBAID BA-BTTAT****Abstract**

The Precambrian basement rocks of the Lowder-Mudiah area are divided into three main belts separated by two northeast-striking ductile shear (thrust) zones. The central belt consists of highly metamorphosed granitic gneisses intruded by granites. The eastern belt comprises greenschist-grade northeast-trending metavolcanics; these rocks are deformed in open antiforms and synforms. The western belt is composed of granite ( $740\pm 22$  Ma), diorite and gabbro traversed by two extensive dyke swarms, forming 75-90% of the total rock volume. The major swarm ( $709\pm 21$  Ma) trends NE-SW and the minor ( $587\pm 18$  Ma) E-W to NW-SE.

Three deformational episodes are recognized. Northeast trending recumbent isoclinal folds were followed by open folds with vertical axial planes and northwest trending crossfolds and kink bands. The thrust-lineation relationships suggest that there was an early phase of thrusting which produced down-dip lineations, and that these thrust surfaces were later reactivated to become dextral transcurrent ductile shear zones which gave rise to the present predominant shallow-plunging lineations. Tertiary block faulting occurred along reactivated Precambrian thrust planes.

Peraluminous, high silica, "A-type" granites formed from LILE- and LREE-enriched crustal melts in an extensional tectonic regime. These granitoids are similar to the felsic Mudiah metavolcanics, the felsic Mukeras dyke swarm and the "A-type" young granitoids (686 - 517 Ma) of Central Hijaz, Saudi Arabia.

The Mudiah metavolcanics and the NE-SW Mukeras dyke swarm are bimodal formed from LILE- and LREE-enriched source(s), and they exhibit Andean-type convergent margin characteristics. However, a large degree of compositional overlap may be expected between lavas in highly magmatic, rapidly distending rifts, and Andean-type convergent margins. Moreover, the Mudiah metavolcanics and the Mukeras dyke swarms are chemically similar to the dyke swarms in the Northeastern Desert of Egypt and the "sequence" A volcanics of Central Arabian Shield.

It is concluded that the late Precambrian accretion of arc systems resulted in a thickening of the crust, which led to deep crustal melting, which was probably triggered by upper mantle diapirism, caused by adiabatic decompression, updoming, stretching and crustal thinning and the injection of mantle-derived basaltic magma, that gave rise to the basaltic Mudiah metavolcanics and the basaltic Mukeras dyke swarms. In contrast, crustal melts are represented by the Lowder-Mudiah "A-type" granitoids, the felsic Mudiah metavolcanics, and the felsic Mukeras dyke swarms.

The host rocks of the dykes (granite ( $740\pm 22$  Ma), quartzdiorite, diorite and gabbro) have a calc-alkaline subduction zone signature, and they were probably emplaced in the roots of contemporary island arcs, similar to the old calc-alkaline granodiorite association (720 Ma) of Central Hijaz of Saudi Arabia.

Carbonatite bodies, mainly those which occur as dykes, which are either apatite-bearing or RE-mineral-bearing (group III and group IV) are confirmed as carbonatites. However, petrochemistry suggests that other carbonate sheets are sedimentary marbles enveloped by granitoid gneisses.

**Keywords:** Precambrian, Lowder-Mudiah granitoids, A-type, Mudiah metavolcanics, Mukeras dyke swarms, Bimodal, Carbonatites, Extension.

**ACKNOWLEDGEMENT**

I am especially grateful to my main supervisor at Leicester University, Prof. Brian F. Windley for his tireless supervision, kind advice and encouragement during field and laboratory work and for his great patience in reviewing this thesis.

I also wish to thank:

- a. my co-supervisors at Kuwait University, Prof. David C. Almond and Dr. Ali T. Al-Mishwat for their guidance and help during field and laboratory work and in reviewing this thesis, and Prof Ali A. Al-Shamian (Minister of Higher Education, Kuwait) and Dr. Sabeekah Abdul-Razag for their sincere help.
- b. the government of the Yemen Republic, represented by the Ministry of Oil and Minerals, Salih Bin Husinooon (Minister), and Omar A. Jabran (Immigrant Dept.) for the moral support and help during several field work seasons.
- c. the following people in Leicester University: Dr. Mike Le Bas, for his advice, checking and reviewing the work on the carbonatite problem. Mike Norry, Andy Saunders and John Tarney for their advice and criticism of the chemical interpretations, and to all members of staff for their friendly and helpful cooperation.
- d. Dr. David Rex, who kindly carried out the age determinations of the dyke swarms at Leeds University.
- e. Nick Marsh and Adelaide Holmes. Rob Wilson, Colin, Sue Button, Clive (Leiceester University), Takroni, Said, Ahmad Yahya, Azhar and Kambal (Kuwait University) for their help, and Ann Montgomery for her kindness, sisterly care and help.
- f. especially my family; my mother for raising me, praying for me and encouragement, my elder brother (Yeslam) for encouragement and moral support and finally my wife and my children for their patience, support and love, which gave me the motivation.
- g. the staff of the British Council, Mr. Tom White, Dr. James Taylor, Mr. David Brown, Dr. Frank Frankel (in Kuwait), Mrs Rosemary Gibson, and Marion Murphy (Nottingham), for their support and kindness.

---

**TABLE OF CONTENTS**

<b>Abstract</b> .....	III
<b>Acknowledgement</b> .....	IV
<b>Table of Contents</b> .....	V
<b>CHAPTER 1 INTRODUCTION</b> .....	1
1.1 Location.....	1
1.2 Transportation and Logistics.....	1
1.3 Population.....	1
1.4 Relief, Climate and Vegetation.....	1
1.5 Aim and Scope of the Work.....	3
1.6 Regional Geological Setting.....	3
1.6.1 The Arabian Shield.....	3
1.6.2 Northeast Africa.....	14
1.6.3 The Mozambique Belt.....	24
1.7 Local Geological Setting.....	25
1.8 Previous Work in the Lowder-Mudiah Area.....	27
1.9 Lay out of the Thesis.....	28
<b>CHAPTER 2 Field Relations and Petrography</b> .....	29
2.1 Introduction.....	29
2.2 The Central Belt (Granitoid gneisses, Amphibolites and Granitoids).....	31
2.3 The Eastern Belt (Mudiah Metavolcanics).....	45
2.4 The Western Belt	
(The Mukéras Escarpment Dyke Swarms and their Host rocks) .....	53
2.4.1 Thereh-Mukeras.....	56
2.4.2 Wadi Taran.....	56
2.4.3 Petrography of the Dykes and their Host rocks .....	61
2.4.3.1 The Dyke Swarms.....	61
2.4.3.1.1 Basaltic Andesite Dykes.....	61
2.4.3.1.2 Andesite Dykes.....	61

2.4.3.1.3 Rhyolite Dykes.....	61
2.4.3.2 The Host Rocks.....	64
2.4.3.2.1 Granite.....	64
2.4.3.2.2 Diorite-Granodiorite.....	64
2.4.3.2.3 Gabbro.....	67
2.4.4 Geochronology of the Dyke Swarms and thier Host rocks.....	67
2.5 Conclusion.....	69
<b>CHAPTER 3 Petrochemistry.....</b>	<b>71</b>
3.1 Introduction.....	71
3.2 Analytical Techniques.....	71
3.3 Nomenclature.....	77
3.4 Granitoids.....	77
3.5 Metavoicanics.....	82
3.6 The Mukeras Dyke Swarms and their Host rocks.....	89
3.6.1 Dyke Swarms.....	89
3.6.2 Host rocks.....	94
3.7 Discussion.....	94
3.7.1 Granitoids.....	94
3.7.2 Metavolcanics and Dyke Swarms.....	101
3.8 Mechanisms.....	110
3.9 Conclusion.....	111
<b>CHAPTER 4 Structural Geology.....</b>	<b>115</b>
4.1 Introduction.....	115
4.2 Folds .....	115
4.3 Foliation.....	118
4.4 Lineation.....	118
4.5 Thrusts.....	118
4.6 Present Topography and Block Faulting.....	125
4.7 Conclusion.....	129

<b>CHAPTER 5 The Carbonatites</b> .....	130
5.1 Introduction.....	130
5.1.1 Location.....	130
5.1.2 Geological Setting.....	130
5.1.3 Previous Work.....	131
5.1.4 Aim and Scope of the Work.....	131
5.2 Field Relations.....	131
5.2.1 Um Saiiamiah.....	131
5.2.2 Al-Arakbi.....	133
5.2.3 Durib.....	133
5.3 Petrography.....	133
5.4 Ore Microscopy.....	143
5.5 Microprobe analysis.....	143
5.6 Geochemistry.....	152
5.6.1 Analytical techniques.....	152
5.6.2 Trace and Rare Earth Elements.....	156
5.6.3 Group III and IV Carbonatites.....	162
5.7 Conclusion.....	169
<b>CHAPTER 6 Discussion and Conclusions</b> .....	171
6.1 Chapters 1-4.....	171
6.2 Chapter 5.....	176
<b>REFERENCES</b>	
<b>APPENDICES</b>	

## CHAPTER 1

### INTRODUCTION

#### 1.1 Location

The Yemen Republic is located in the southern part of the Arabian Peninsula, bordered on the north by Saudi Arabia, on the west the Red Sea, on the south by the Arabian Sea and Indian Ocean, and on the east by the Sultanate of Oman (Fig. 1.1). The Lowder-Mudiah area is situated within the Abyan Province of the Yemen Republic (Fig. 1.1) between longitudes 45° 40' E and 46° 10' E and latitudes 13° 40' N and 14° 00' N.

#### 1.2 Transportation and Logistics

The Lowder-Mudiah area is reasonably accessible because it is connected by the Aden-Mukalla Highway with Aden, about 200 Kms away, Sanaa to the WNW, and Mukaklla, the Hadramout Province capital about 800 Kms to the east. It is also connected with Sanaa by a highway via Al-bydha and Mukeras town to Thereh Escarpment, then by a gravel road through Thereh Pass to Lowder town then to Mudiah town. Within the wadis of the Lowder-Mudiah area 4-wheel drive Land Cruisers are the main transport means.

#### 1.3 Population

There are no recently accessible, statistical data, but the population in the Lowder-Mudiah area, may reach 40,000 people, mainly of originally nomadic tribes. They work either as farmers in rain fall-dependant farmlands or as shepherds of goats and camels. However, the majority are dependant on those who moved to the capital and work as civilian or military personnel.

#### 1.4 Relief, Climate and Vegetation

Elevation in the mapped area varies between 1100 and 1200 m above sea level, except at the Mukeras Escarpment, where elevations exceed 2500 meters. This escarpment separates the Lowder-Mudiah lowlands from the Mukeras Plateau.

The central and eastern parts (belts) of the area generally form lowlands, 1000 m above sea level, of 100 - 300 m high hills and mountains. In contrast the western part (belt), the Mukeras Plateau is an elevated area about 2500m above sea level extending from the

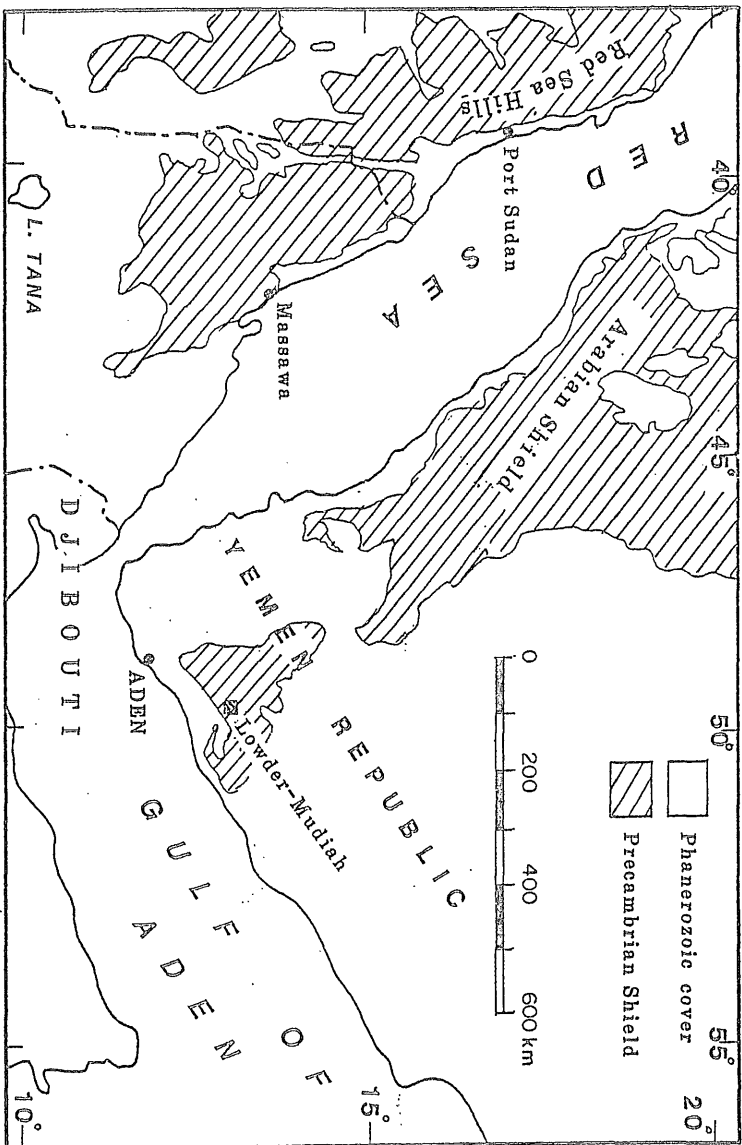


Fig. 1.1 Location map for the Lowder-Mudiah area, Yemen Republic

Mukeras Escarpment through Mukeras town and the villages of Um Salul and Awwein (beyond the mapped area) and northwestwards to the Yemen-Saudi border. The Mukeras Escarpment is a very prominent topographic, morphological and structural feature.

There is a wide range of temperatures between summer and winter, and between day and night. The hottest months are May to September; peak temperatures are in June and July, when they reach more than 40° C. During winter temperatures may reach 0° C.

Rain fall is irregular in summer, but more frequent in winter, when it may reach 20 inches in a month. Run off takes place as flash floods towards the sea and this partly recharges the shallow ground-water aquifer, that feeds shallow wells which are used for drinking and irrigation of very limited corn crops, vegetables and fruit farms.

The commonest trees in the Wadis are the Acacia and the Zizyphus spina-christi (Nebeg).

### **1.5 Aim and Scope of the Work**

The aim of this work is to study in detail the geology of the basement in this area, and to determine its tectonic setting within a Pan-African plate tectonic framework. It is hoped that this will provide a base for further studies of the geology and tectonics of Yemen. A total of 4 months was spent in the field at four different times. Six visits totalling 24 months were made to Leicester in the period of 5 years.

There was formerly no published geological map for the area and the only available report was technical and unpublished. Mapping was based on aerial photographs at a scale of 1 : 60,000. Geological and structural data and samples were collected along systematic traverses across strike during the fieldwork programme.

Petrographic study and the early stages of geochemical sample preparation were carried out at Kuwait University, but further preparation and geochemical analyses by XRF, AAS, ICP and electron-microprobe were carried out at the University of Leicester. Isotope analyses were undertaken by Dr. David Rex of Leeds University.

### **1.6 Regional Geological Setting**

#### **1.6.1 The Arabian Shield**

Geologically the Lowder-Mudiah area lies close to the southern boundary of the Arabian

Shield and the Mozambique Belt. An evolutionary model involving crustal growth, accretion-obduction processes of island arcs or microcontinents, and crustal thickening was first proposed by Brown (1972), Greenwood et al. (1976), Fleck et al. (1978) and Gass (1981) to explain the tectonic evolution of the Arabian Shield.

In general the Precambrian crystalline basement of the Arabian Shield is dominated by accreted island arcs, represented by metavolcanic rocks, gneisses, and granites with a subduction-related and calc-alkaline affinity (Camp, 1984; Stoesser and Camp, 1985; Roobol et al. 1983; Jackson et al., 1984; Jackson, 1986; Stacey and Hedge, 1984; Stacey et al. 1984). Greenwood et al. (1976, 1980) proposed that the southern Arabian Shield originated as an accreted island arc which evolved from early tholeiitic to later calc-alkaline volcanism.

Al-Shanti and Mitchell (1976) suggested that outer island arcs and collisional belts provide a possible model for evolution of part of the Arabian Shield. The thick volcanic, volcanoclastic and sedimentary succession of the Proterozoic Halaban Group in the east of the Shield, intruded by syn- to late tectonic plutons resembles Cenozoic subduction-related magmatic arcs. West of the Halaban Group, and separated from it by a major east-dipping thrust with associated ultrabasic rocks and carbonates, there are folded chlorite-sericite metasediments of the Abt Schist which is comparable to Cenozoic outer arc successions. West of and beneath the Abt Schist calcareous and arenaceous metasediments of the Ar-Ridaniyah Formation are analogous to the Mesozoic-Cenozoic continental margin shelf facies of a subducted plate. Eastward subduction with magmatism (Halaban Group) and tectonic emplacement of ocean-floor sediments (Abt Schist) was followed by continental collision and eastward under-thrusting by the Ar-Ridaniyah Group and cratonised central part of the Shield. Collision-related post-tectonic granites were emplaced during and following the collision. Al-Shanti and Mitchell (1976) concluded that in the Al Amar-Idsas region parallel magmatic and deformed sedimentary belts, separated by a tectonic line with associated ultrabasic bodies, are analogous to some Cenozoic island arc systems. Recognition of these belts provides evidence of subduction polarity and indicates the tectonic setting of post-tectonic granites. Similar belts should be preserved elsewhere in the Arabian Shield.

Camp (1984) described two northeast-trending Late Precambrian ensimatic island arc systems in western Saudi Arabia. Each displays lithotectonic provinces that are comparable to those in modern examples of plate convergence. The younger Hijaz island arc (800 - 700 Ma) contains a thick fore-arc sequence of Al Ays group turbidites which overlies an accretionary prism of metamorphosed and fragmented volcanosedimentary rocks and associated ophiolites. The older Asir island arc (900 - 700 Ma) is exposed at a much deeper erosional level, in which only remnant arc and fore-arc deposits are present. This arc is identified in part by a frontal-arc assemblage of abundant dioritic intrusions and high-grade metamorphic rocks that are interpreted as a high T-low P belt. A mafic back-arc volcanic assemblage appears to delineate an interarc basin situated between the At Taif frontal arc and a lithologically similar remnant arc west of Bishah. About 700 Ma ago the Hijaz island arc collided with the Asir arc along the Bir Umq-Port Sudan suture. Local uplift led to the creation of an intra-arc basin which was filled with volcanic molasse deposits of the Hadiyah and Fatimah groups. Continued convergence between 700 and 675 Ma resulted in development of the northeast-trending Samran fold belt. This collisional event marks the cessation of southeastward convergence, and this ended the initial phase in the progressive eastward evolution of the Arabian-Nubian Shield.

According to El-Ramly (1988) "It is now generally accepted that the Arabian-Nubian Shield, which forms large areas of the Middle East (mainly Saudi Arabia, Egypt, Sudan, Yemen, Somalia and Ethiopia) is of Late Proterozoic, Pan-African age". The term "Pan-African", first introduced by Kennedy (1964) defines an important and widespread tectonic and thermal event which affected the African continent during the Late Precambrian and early Paleozoic and led to its structural differentiation into cratons and orogenic areas some 500±100 Ma ago. Subsequent studies in several Pan-African regions in the continent and the Arabian Shield have shown that the Pan-African is not restricted to the ~ 500 Ma episode originally proposed by Kennedy, but covered a longer period of time (Clifford, 1967; Cahen and Snelling, 1966; Gass 1977; Al-Shanti, 1979; Kroner, 1979, 1984). Kroner (1984) assigned the time span 950-450 Ma to the Pan-African.

With regard to the Pan-African ages of granitic gneisses in the Saudi Arabian Shield, Kroner et al. (1979) stated that in the south-central Arabian Shield there are several areas of gneissic granitoid rocks which could represent Pan-African basement. They added that two suites selected as possible examples of fundamental basement can be shown not to be "ancient" in the conventional sense of having a prolonged PrePan-African crustal history. The Dahul gneiss/migmatite suite belongs to a major syntectonic granitoid batholith emplaced about 600 Ma ago during a period of major granite plutonism (the Pan-African event s.s.). The Dahul isotope data suggest that the rocks were derived from a basement up to 1150 Ma old, but there is no field evidence at present for the existence of such old rocks. The Jugjug gneisses represent plagioclase-rich, granitoid plutonic rocks emplaced between 780 and 870 Ma ago; they provide a pointer to the existence of Pre-Halaban basement, although the possibility of the pluton being coeval with the volcanics cannot be ruled out. The presence of significantly older crust is suggested by 2000 Ma-old zircons from a trondhjemite within a fault zone that forms the western margin of the Ar Rayn terrane (Calvez et al., 1982, 1983). Voluminous granitic crust with associated calc-alkaline volcanics of Pan-African age (960 - 520 Ma) is recorded from the Arabian-Nubian Shield. Minor enrichment in the  $^{87}\text{Sr}/^{86}\text{Sr}$  initial ratios of acidic magmas with time indicates that a continuum of mantle-derived partial melts from a subduction environment became progressively mixed with and partially assimilated with earlier stabilised crust. Further isotopic data are required to clarify details of the crustal thickening (to 35 km) or cratonisation process of the Shield before 500 Ma (Brown, 1979).

Geologic and isotopic evidence for early Proterozoic crust in the eastern Arabian Shield was presented by Stacey and Hedge (1984). Zircon U-Pb, feldspar-common Pb, whole-rock Sm-Nd and Rb-Sr data from a fine-grained granodiorite from the Jabal Khida region (lat.  $21^{\circ} 19' \text{ N}$ ; long.  $44^{\circ} 50' \text{ W}$ ) provide conclusive evidence for continental crust of early Proterozoic age (~1630 Ma).

Stacey et al., (1984) studied the geochronology and geologic evolution of the Halaban-Al Amar region of the Eastern Arabian Shield and found that U-Pb zircon model ages for eleven major units indicate three stages of evolution: (1) plate convergence, (2) plate

collision and (3) post-orogenic intracratonic activity. Convergence occurred between the western Afif and eastern Ar Rayn plates that were separated by oceanic crust. Remnants of oceanic crust now comprise the ophiolitic complexes of the Urd group. The oldest plutonic unit gave an age of  $694 \pm 8$  Ma. Detrital zircons from the sedimentary Abt formation of the Urd group, were derived from the source rocks that have a mean age of 710 Ma. Plate convergence was terminated by collision of the Afif and Ar Rayn plates during the Al Amar orogeny which began about 670 Ma. During collision, the Urd group rocks were deformed and in part obducted onto one or both plates. Synorogenic leucogranites were intruded from 670 to 640 Ma. From about 640 to 630 Ma widespread unfoliated dioritic plutons were emplaced in the Ar Rayn block. In their conclusions they recognized three orogenic events in the Halaban-Al Amar region: (1) Convergence of the Afif and Ar Rayn plates, with possible island arc formation, prior to 670 Ma. The Ard and Al Amar groups were emplaced during the period. (2) The Ad Dawadimi compressional orogeny, 670 - 630 Ma ago, is attributed to collision and suturing of the Afif and Ar Rayn plates. This collision terminated subduction, deformed the Ard group, and led to crustal remobilization and widespread emplacement of synorogenic plutonic rocks. (3) The Najd orogeny 620 - 570 Ma ago was a period of mild compressional deformation during which the Murdama molasse and associated volcanic rocks were deposited and folded, numerous granitic plutons were emplaced and the Najd left-lateral wrench fault system developed. Samples from four units, which had been proposed as belonging to a Middle Proterozoic or older sialic basement, have ages in the range 677 - 643 Ma. There appears to be no definitive evidence to indicate the presence of such a basement beneath this region. Stacey et al. (1984) produced Pb and Sr isotopic evidence which indicates that a small older continental component has been added to the crust of the region, but the nature and origin of this component is not understood.

Moreover, concerning the Pan-African microplate accretion of the Arabian Shield, Stoeser and Camp (1985) argued that the late Proterozoic Arabian Shield is composed of at least five geologically distinct terranes (microplates) separated by four ophiolite-bearing suture zones. Three ensimatic (intraoceanic) island-arc terranes (Asir, Hijaz, Midyan) occur in the western Shield and two terranes in the eastern Shield (the Afif of

continental affinity and the Ar Rayn with a possible continental affinity). The western two sutures are island arc-island arc junctions, whereas the eastern two sutures collectively form a major collisional orogenic belt. Accretion of the five terranes to form an Arabian neocraton occurred in the period 715 - 630 Ma. After accretion, intracratonic deformation and magmatism related to collision continued and resulted in the formation of molasse basins, intermediate to silicic volcanic rocks, peralkaline to peraluminous granites (640 - 570 Ma), and a major left-lateral wrench fault system (~630 - 550 Ma), which displaced the northern part of the Arabian neocraton ~250 km to the northwest. These tectonic events represent the accretion of the Arabian portion of Gondwanaland during the Pan-African event.

In his work on the distribution and tectonic setting of plutonic rocks of the Arabian Shield, Stoeser (1986) said that, although it is still not possible to model in detail the tectonic evolution of the Arabian Shield, its evolution can be interpreted in terms of the classic pattern of Phanerozoic plate tectonics (the "Wilson Cycle"). During the first stage of evolution (900 - 630 Ma) plutonism was dominated by intermediate plutonic rocks (diorite, quartz diorite, tonalite and trondhjemite) and involved a progressive evolution from primitive tholeiitic series arc rocks to mature calc-alkaline series rocks. These rocks formed in both ensimatic island arc and continental margin arc environments. The magmatic arc stage was terminated by two collisions (680 - 630 Ma); between an accreted ensimatic arc terrane and a continental microplate, and between the microplate and a continental (?) plate. These collisions resulted in a shift from arc magmatism dominated by intermediate plutonic rocks to collision-related granitic (granodiorite to monzogranite) magmatism 660 - 610 Ma. The final phase of plutonism within the Shield (610 - 510 Ma) was the formation of widespread post-orogenic intracratonic peraluminous to peralkaline alkali-feldspar granites. Such granites typically form during the terminal relaxation phase of continental collision tectonics. Although minor evolved peraluminous granites are present in the eastern part of the Shield, well-developed S-type granites (tourmaline- or cordierite-bearing) appear to be lacking, but may occur within the Afif basement domain. These alkali-feldspar peraluminous granites are similar to those of the Lowder-Mudiah area. Minor syenitic plutonic rocks were also emplaced

throughout the Shield from about 620 to 550 Ma. The peraluminous granites that do occur appear to be members of the A-type suite (Stukless et al., 1983, 1984; du Bray, 1983, 1986a,b; Ramsay et al., 1986a,b). If the definition of paired belts of I-and S-type granites is used, then, the Arabian Shield also contains a paired belt of early I-type granitoids along the Nabitah orogenic belt and somewhat younger evolved peraluminous S-type granites to the east. In the period 560 - 520 Ma alkali olivine basalt and alkaline andesite were deposited in pull-apart basins within the Najd fault system (Delfour, 1979). These basalts and basaltic-andesites are similar in age and trend to the late generation ( $587 \pm 18$  Ma) of the Mukeras dyke swarms which trend almost E-W to NW-SE (see Table. 3.6). Plutonic activity during this period included the emplacement of saturated and undersaturated syenites, the Jabal Radwa peralkaline granite, and possibly a few meta-aluminous granites. Small volumes of peralkaline granites were generated in the final phase of a Pan-African calc-alkaline igneous event which built the Arabian Peninsula. The peralkaline granites are closely associated with sutures related to ophiolites (Radain et al. 1981).

Stoeser and Stacey (1988) defined a major episode of collisional orogenesis and tectonism within the eastern half of the Arabian Shield between 680 and 600 Ma, based on U-Pb zircon age data. They stated that this orogenesis included two major orogenies, the Nabitah in the central Shield and Al-Amar in the east. The Nabitah orogeny resulted from the collision of an ensimatic accreted island arc terrane in the west with the Afif composite terrane in the east at about 690 - 683 Ma to form the Nabitah suture. Deformation and crustal remobilization along the Nabitah suture, during the period 680 - 640 Ma, resulted in the formation of the Nabitah orogenic belt. This belt is characterized by widespread early catazonal (680 - 650 Ma) synorogenic gneiss domes and complexes of leucocratic granodiorite, trondhjemite and monzogranite that are intruded by a bimodal mesozonal suite of late synorogenic (650 - 640 Ma) diorite, tonalite, and monzogranite. The early gneiss complexes are partly migmatitic and have metamorphic aureoles in the amphibolite facies. During the Al Amar orogeny (670 - 630 Ma) the Afif composite terrane collided with the Ar Rayn terrane to form the Al Amar suture zone. After orogenesis waned (640 - 600 Ma), the northwest-striking Najd left-lateral transcurrent fault system

and post-orogenic silicic magmatism developed throughout much of the Shield. The Al Amar orogeny and the Najd fault system are interpreted to be the result of collision and plate interaction between the Arabian Shield and a concealed continental plate to the east (Stoeser and Stacey, 1988). Berhe and Rothery (1986); Berhe (1988; 1990) suggested that the two sutures of Adola-Moyle and Baragol in NE Africa continue as the Nabitah and Idsas sutures of Arabia.

In their study of the geology, geochemistry, and petrogenesis of Late Precambrian granitoids in the Central Hijaz Region of the Arabian Shield, Jackson et al. (1984) suggested that Late Precambrian granitoid rocks occurring within a 44000 sq. km area of the western Arabian Shield are subdivided on the basis of geology and petrology into older (820 - 715 Ma) and younger (686 - 517 Ma) assemblages. The older assemblage contains major complexes which can be assigned to either one of a granodioritic or trondhjemitic petrologic association. The earliest granitoid rocks are trondhjemitic tonalites (trondhjemite association), depleted in Ba, Ce, F, La, Li, Nb, Rb, Y and Zr compared with granitoids of the slightly younger granodiorite association, which are related to a calcic calc-alkaline suite ranging in composition from gabbro to monzogranite. This association is similar to the granite-diorite-gabbro, host-rocks of the Mukeras dyke swarms, of which a granite gave an age of 740 Ma. The plutonic rocks of the older assemblage were probably emplaced in the cores of contemporary island arcs. The younger plutonic assemblage is dominated by three, geochemically distinct, coeval granitic associations: the alkali granite, alkali-feldspar granite and monzogranite. The alkali granite association is composed of perthite granites (alkali granites and genetically related alkali-feldspar granites). Rocks of this association are marginally peralkaline or metaluminous and are characterized by low contents of Ba, Co, Li, Rb, Sc, and Sr, and high contents of Be, Cu, F, REE, Nb, Sn, Y, Zn, and Zr. The alkali-feldspar granite association is mainly composed of alkali-feldspar granites and syenogranites; this association is similar to the Lowder-Mudiah granitoids. Rocks of this association are marginally peraluminous or metaluminous and contain low Ba, Sr, and high F, Rb, Sn, Th, U. The monzogranite association consists mainly of monzogranites and granodiorites. Rocks of this association are peraluminous or marginally metaluminous

and have the highest contents of Ba, Cu, Co, Li, Sc, Sr, Ta, and V, and the lowest contents of REE, Nb, Rb, Sn, Th, U, Y, Zn, and Zr of the three granitic associations. These voluminous granitic magmas, together with the felsic component of a coeval sequence of bimodal volcanic rocks, are partial melts of earlier island arc terrains produced during prolonged melting events. It should be noted that the Mudiah metavolcanics and the Mukeras dyke swarms are bimodal and similar to the "sequence" A volcanics of the Arabian Shield (Roobol, et al., 1983). Subsolvus, "high Ca" granites of the monzogranite association have I-type features and represent partial melts of previously unfused crust, while "low-Ca" perthite granites of the alkali granite and alkali-feldspar granite associations, have A-type features and represent partial melts of previously fused crust. Jackson et al. (1984) added that this type of petrogenetic model can account for much of the petrologic diversity of the Pan-African granitic terrain of the Arabian Shield.

Furthermore, as to the petrogenesis and evolution of Arabian felsic plutonic rocks, Jackson (1986) stated that two overlapping stages can be distinguished in the formation of the Arabian Shield : (1) an "island arc stage", between about 900 and 660 Ma, during which the formation and nature of plutonic magmas was controlled by subduction-related processes; and (2) a "post-accretion stage", between about 700 and 550 Ma, which was dominated by granitic magmas derived by massive crustal fusion. During the island arc stage, the earliest plutons were calcic gabbro-diorite or gabbro-diorite-tonalite-trondhjemite complexes. These were superceded by calc-alkaline gabbro-diorite-tonalite-granodiorite complexes, some of which contain small volumes of monzogranite (comparable to the granite-diorite-gabbro host-rocks of the Mukeras dyke swarms in Yemen), and by complexes composed predominantly of quartz diorite and tonalite. These plutonic complexes are analogous to intrusions emplaced in contemporary, immature to mature island arcs, and represent mantle (gabbro-diorite) and crustal (tonalite-trondhjemite-granodiorite) fusion products modified by fractionation processes. The post-accretion stage was characterized by a great diversity of rock types reflecting complex interaction of mantle and crustal fusion products. Crustal fusion produced voluminous granitic magmas whose composition was mainly determined by the nature of

the protolith and the degree of melting and differentiation. Fusion of primitive island arc protoliths produced low-K, tonalitic melts, whereas more evolved island-arc and continental crust protoliths yielded moderately potassic granites and granodiorites. Refusion of refractory crust from which a granitic melt had already been extracted produced low-Ca, alkali-feldspar granite and alkali granite. Reaction-melting, involving mantle-derived mafic magma and granulitic crust, produced intrusions of gabbro-anorthosite-syenite and monzodiorite-monzonite (Jackson, 1986). The granite-diorite-quartzdiorite-gabbro host rocks of the Mukeras dyke swarms ( $740 \pm 22$  Ma), are similar to the calc-alkaline, granodiorite association (720 Ma) of the Central Hijaz; whereas, the Lowder-Mudiah granitoids are similar to the younger A-type granitoids of the Central Hijaz of the Arabian-Shield.

As to the volcano-sedimentary belts in the Central Arabian Shield (CAS) the study of Roobol et al. (1983) revealed that the oldest volcano-sedimentary belts ("sequence" C; > 900 Ma), Bidah and Shayban, are chemically immature bimodal suites of low-K tholeiites and sodic dacite/rhyolite depleted in lithophile elements Rb, Nb, Zr, etc. These lavas have chemical characteristics similar to those of immature island arcs (IIA) such as the Tonga-Kermadec and Lesser Antilles arcs. Younger lavas of "sequence" B (900 - 700 Ma), Balas, Aqiq and Idsas, are slightly more mature in composition, being predominantly calc-alkaline and low-K arc tholeiite series with low lithophile element contents, but higher than "C" and high  $\text{Na}_2\text{O} : \text{K}_2\text{O}$  ratios. They are comparable with western Pacific Ocean modern island arc (IA) averages. The youngest voluminous lavas ("sequence" A; 700 - 570 Ma), Fatima, Arfan, Jugjug, Jahhad and Hummah, are generally calc-alkaline or high-K, calc-alkaline series lavas with moderately high lithophile element abundances, but much higher than "C and B" and lower  $\text{Na}_2\text{O} : \text{K}_2\text{O}$  ratios. They are comparable to transitional volcanic arcs (TVA) such as the Central American Cordillera or the Indonesian Sunda arc, which are transitional between island arcs and continental margin volcanic arcs. All suites of the CAS are strongly bimodal (basalt-basaltic andesite and dacite-rhyolite range) except Jugjug, Hummah and Idsas which appear to be unimodal (basaltic andesite-andesite range). Bimodality which may not be a normal feature of modern volcanic arc suites, but not unknown e.g Tonga islands, is a common feature of

the late Proterozoic stratovolcanoes of the CAS. Roobol et al. (1983) concluded that the cratonization process in the CAS thus involved the superimposition of three volcano-sedimentary sequences, rather than intraplate rifting or simple juxtaposition of oceanic island arcs, formed in progressively maturing volcanic arcs. Early formed immature island arcs were succeeded by chemically more mature island arc deposits and then by deposits formed in volcanic arc(s) transitional between island arcs and continental margins. The evolution ceased at this stage and probably did not advance to the equivalent of an Andean-type continental margin (Roobol et al., 1983). The Mukeras dyke swarms and Mudiah metavolcanics are similar to "sequence" A of the Central Arabian Shield. Moreover, Ba-bttat (1978, 1981, 1985); Ba-bttat and Husien, (1984) described the Late Precambrian Jabal Samran volcano-sedimentary rocks in Saudi Arabia and interpreted them as an island arc/active continental margin.

A Rb-Sr isotope study of the above volcano-sedimentary successions of the CAS by Darbyshire et al. (1983) showed that "sequence" A in the Central Arabian Shield indicates that very late Precambrian ca. 690 - 570 Ma volcanicity was an important event in the evolution of the Shield. The ages are considered to define or approximate to the age of lava extrusion: Fatima group  $688 \pm 30$  Ma; Jahhad unit  $616 \pm 13$  Ma; Jugjug formation  $612 \pm 22$  Ma; Arfan formation  $608 \pm 9$  Ma; Hummah unit  $572 \pm 23$  Ma. Initial  $^{87}\text{Sr}/^{86}\text{Sr}$  ratios range from 0.7027 to 0.7036, and Rb/Sr ratios are uniformly low ( $< 0.4$ ), except for a few metarhyolites. All the lavas appear to have been derived from a primitive, mantle-type source, although a slight increase of initial  $^{87}\text{Sr}/^{86}\text{Sr}$  ratio for the Jahhad and Hummah samples reflects the involvement of less-depleted mantle or possibly crustal contamination. These new data for "sequence" A together with those for other dated suites indicate that the eruption of low Rb/Sr magmas of probable mantle derivation continued from the earlier parts of the Hijaz Tectonic Cycle (i.e. "sequences" B and C, pre-dating 700 Ma) into the later parts (i.e. "sequence" A). There are, however, indications that some acidic lavas of "sequence" A were contaminated with crustal material or, possibly, were even crustally-derived (Darbyshire et al., 1983). The age of the Mukeras dyke swarms (709 - 587 Ma) is similar to that of the "sequence" A in the Central Arabian Shield. Hawkins et al. (1981) stated that a small segment of the SE Pan-

African Shield in Dhofar (Oman) is composed of quartz-feldspathic gneisses, granites, pegmatites, aplites and suggested that there is a basic dyke swarm in this region. The presence of this segment of the Pan-African Shield and the dyke swarms means that the Shield continues eastwards. Moreover, bimodal dyke swarms, granitoids and ultramafic rocks (ophiolites) of Precambrian age, in Oman about 2000 km to the east of Lowder-Mudiah area) were also reported by Gass et al., (1990), who concluded that this ophiolite suite implies a suture between colliding island arcs much further east than those recognized in Saudi Arabia.

### 1.6.2 Northeast Africa

Late Precambrian structures in NE Africa were attributed by Shackleton (1986) to successive gentle collision of island arcs; the sutures dip E or SE and relative plate motion was NE-SW. Widespread recumbent structures, complex and intense deformation and high-grade metamorphism imply crustal thickening and multistage collisional history. Relative NW-SE motion was probably followed by N-S post-collisional ductile shear zones. Shackleton (1988) added that of the many recognized types of ophiolites, which include obducted slabs, thrust slices, fault-bounded blocks, serpentinite thrust melanges, olistostromic and tectonic ophiolite melanges, ejected serpentinite lenses and serpentinite diapirs, most are found in the upper Proterozoic terranes of Arabia and NE and E Africa. Many of the occurrences are far from sutures: these must be identified on structural and other evidence. Ophiolite slabs obducted onto less dense continental crust tend to separate into units which subside, so that they are preserved in synforms. The Ingessena ophiolite in Sudan is an example. The general conclusion is that the region evolved by accretion and collision of a series of plates and microplates. Palaeomagnetic evidence (McWilliams, 1981) appears to indicate that the collision involved the eventual closure of a wide ocean, because there is a drastic difference between the apparent polar wander paths of East and West Gondwana, until the Ordovician when they coincide.

Moreover, there was a critical comment on the models of ophiolites, sutures, and microplates of the Arabian-Nubian Shield by Church (1988) who stated that the practice of identifying intra-arc oceanic crust and microplate boundaries in terms of the distribution

of ophiolite complexes in the Arabian-Nubian Shield may produce too simple a picture of the late Proterozoic paleogeography of northeast Africa. Some ultramafic-mafic complexes of the Arabian-Nubian Shield (cases similar to the mafic ultramafic complex at Mukeras town, in Yemen, for which no tectonic model has yet been proposed) considered to represent oceanic crust, are more likely to be intrusive complexes within arc sequences, whereas others, although correctly identified as having formed at a spreading centre, do not appear to have the characteristics of "normal" MOR material, and may rather have formed in a fore-arc environment during early stages of arc development. The tensional stress (spreading) regime required for ophiolite formation in a fore-arc environment can perhaps be generated by oblique subduction, which may also induce strike-slip transportation of slivers of the fore-arc ophiolite to locations far from the site of their formation. Such strike-slip displacements may have been more important in the assembly of the various arc terranes of the Arabian-Nubian Shield than has generally been considered, and the extreme width of the Shield owes more perhaps to microplate assembly involving lateral migration than to arc amalgamation by frontal collision.

El-Gaby and Greiling (1988) summarised the geology of Africa and the Pan-African event. The Precambrian of Africa consists of three major and several minor Archaean cratons surrounded and separated by upper Precambrian terranes (Clifford, 1970). Three categories can broadly be defined: (1) ensimatic terranes of volcanic arcs associated with ophiolitic melanges characterised by the Arabian-Nubian Shield. (2) Orogenically deformed upper Proterozoic sediments and igneous rocks deposited in geosynclines or aulacogen (e.g. Damara belt). (3) Belts of deformed and rejuvenated older basement rocks (e.g. Mozambique belt). In west Africa, a late Precambrian orogeny took place in Hoggar, Nigeria and Dahomey, followed in the Early Paleozoic by several post-tectonic granitic intrusions (Black, 1966). The Pan-African belt in East Africa comprises two contrasting units: the Arabian-Nubian Shield in the north and the Mozambique belt in the south. The Mozambique belt (Holmes, 1951) comprises a N-S trending structural belt extending from south of the Zambesi to the extreme north of Kenya and Uganda. There appears to be a general consensus that the Mozambique belt is a rejuvenated Pan-African cratonic basement. However, its relation to the Late

Proterozoic rocks of the Arabian-Nubian Shield is still unsettled. The Arabian-Nubian Shield is characterised by extensive thick volcanic and volcanoclastic successions enclosing several ophiolite complexes (Bakor et al., 1976; Shackleton et al., 1980). The Precambrian of Arabia, largely formed of greenschist assemblages, is intruded by calc-alkaline granitoids and believed to represent cratonized, late Proterozoic ensimatic island arcs without much contribution of older continental crust (Greenwood et al., 1976; Gass 1977). Kazmine et al., (1978, 1979) and Kroner (1979) assumed that the upper complex (=greenschist assemblage) of Ethiopia originated in rift zones which narrowed southwards within the ensialic Mozambique belt. Conversely, Hepworth (1979) interpreted the interdigitated boundary between the gneissose basement and the greenschist assemblage as defining an intensely folded surface with the basement plunging northeastwards on a regional scale beneath a greenschist cover. It seems most probable that the northern continuation of the Mozambique belt in Egypt, Sudan, and western Ethiopia represents an active continental margin towards the Late Proterozoic orogenic belt of the Arabian-Nubian Shield. Likewise, the Mozambique belt from Ethiopia to Mozambique might represent the active continental margin(s) of colliding East and West Gondwana cratons whereby the oceanic island arc material exposed in the Arabian-Nubian Shield was destroyed by subduction farther south rather than by erosion (Kroner, 1979; McWilliams, 1981; Vail, 1983; Warden and Daniels, 1984). El-Gaby et al. (1988) added that the basement of the Eastern Desert and Sinai, Egypt, constitutes the fold and thrust belt of a late Proterozoic (Pan-African) continental margin orogen. Late Proterozoic ophiolites and island arc volcanics and volcanoclastics occur as thrust sheets, and the suprastructure was thrust from an easterly direction over an early Proterozoic continental crust, the infrastructure. The rocks of the infrastructure are largely mylonitized at shallow depths along decollement surfaces, or remobilized at greater depths.

According to Kroner (1979) the Pan-African belts of the African mainland and the Arabian-Nubian Shield exhibit evolutionary features which are either compatible with inter-continental ensialic development or with plate margin and Wilson cycle tectonics during the time period 110 - 500 Ma. He suggested that both the ensialic and plate margin developments were caused by the same fundamental subcrustal forces that are

responsible for present-day lithospheric motion, and the Pan-African event is therefore representative of a transition from Precambrian ensialic plate tectonics to Phanerozoic Wilson cycle tectonics.

Much of the late Pan-African deformation in northeast Africa appears to have occurred by strike slip motion and there is a striking analogy with the Cenozoic deformation pattern behind the Himalayan belt in northeast Asia (Molnar and Tapponnier, 1975; Tapponnier et al. 1982; Tapponnier and Molnar, 1976; Molnar, 1984). The Pan-African structures and magmatism between the Hoggar and Egypt/Sudan may have been caused by continental collision and indentation of a hot crustal segment by a cold rigid plate (the West African craton).

Moreover, Kroner et al. (1988) pointed out that the inference of old continental crust underneath the Pan-African island arc assemblage in the Eastern Desert of Egypt is largely based on a few geochronological dates that indicate ages in excess of ~1000 Ma. They concluded that there is as yet no conclusive evidence for the existence of early Proterozoic or even Archaean crust east of the River Nile.

However, according to Schandelmeyer et al. (1988) a Precambrian basement west of the Nile (East Saharan Craton) in southern Egypt and northern Sudan comprises rock assemblages typical of cratonic areas. They are significantly different from the volcano-sedimentary-ophiolitic sequences which are exposed east of the Nile in the Late Proterozoic Arabian-Nubian Shield. Although these rocks are generally believed to be of Pre-Pan-African age, no radiometric age data are available to prove this view, except in the Gebel Uweinat basement inlier, where undoubtedly Archaean/Early Proterozoic and Mid-Proterozoic rocks are exposed. They added however, that new Sr and Nd isotopic data suggest a major crustal formation event in the Mid-Proterozoic.

Almond (1984) argued that in NE Africa there is good evidence of a major time break between stabilization of the Mozambique belt and the onset of late Proterozoic sedimentation and volcanicity. The length of this interval is open to debate, but a reasonable case can be made for an Eburnean age ( $2000 \pm 200$  Ma) for the major features of the Mozambique belt. The structural development of the Arabian-Nubian Shield falls mainly into the 1250 - 700 Ma range (i.e. largely Kibaran) and during this

period the rocks of the Mozambique belt acted as a foreland and, at least, local basement to the Late Proterozoic rocks. In this process the Mozambique metasediments were structurally modified, but only locally retrograded. The Pan-African episode followed closely and was essentially a thermal event in NE Africa, resetting many dates, but in some ways it can be likened to an aborted Hercyno-type orogeny which caused major intracontinental displacements along strike-slip faults and triggered intraplate alkaline magmatism.

According to Vail, (1988) two distinct lithologic-tectonic units underlie the Phanerozoic cover of northeast Africa between Egypt and Kenya and western Arabia between Sinai and Somalia. They are a granitic gneissose basement of granulite to amphibolite metamorphic facies overlain by interfolded supracrustal metasedimentary shallow shelf deposits. These rocks are in structural contact with dominantly greenschist facies volcano-sedimentary island arc-type assemblages with which are associated generally linear belts of fragmented ophiolite complexes intruded by syn- to late-tectonic calc-alkaline granitoid masses and post-tectonic granitic plutons. Many of the ophiolite belts mark suture zones which form tectonic boundaries to microplates. The oceanic terranes formed between about 950 and 650 Ma by crustal accretion, whereas the continental gneisses although isotopically overprinted and metamorphosed around 650 - 450 Ma (the Pan-African) are probably Early to Middle Proterozoic. The present structure is thought to have evolved through plate collision. Less disturbed Archaean cratonic areas lie further west in the Tanzania Shield and Uweinat inlier of the Nile Craton and possibly also to the east in southern Somalia.

With regard to the Precambrian metallogeny of NE-Africa, Pohl (1988) pointed out that the Precambrian of NE-Africa comprises essentially two major units; the Arabian-Nubian volcano-sedimentary greenschist-ophiolite assemblage, and the Mozambique belt *sensu lato*. Likewise, the metallogenic analysis of both units reveals comparable and differing features, the former including ophiolite and magmatic arc-related mineralisation, while the latter are characterized by the typically Mozambiquan metamorphogenic deposits, and the post-orogenic lithophile element mineralisation associated with A-type magmatism as well as gold-quartz veins which occur mainly within the greenschist

terrains. The ensimatic, central part of the Arabian Shield is characterized by Nb, Zr, Y, REE, U and Th occurrences, while Sn (exploited earlier) W and Be are more frequent in a marginal setting with continental influence. This appears to confirm the role of tin as an indicator of old sialic crust.

The central part of the Pan-African basement complex in the Eastern Desert of Egypt is dominated by low grade ophiolitic melanges and associated calc-alkaline rocks. Structurally, these rocks are part of a fold thrust belt, which formed during broadly E-W directed crustal shortening at the margin of a Pre-Pan-African craton in the west. Towards the south gneissic successions are exposed in tectonic windows beneath the low grade rocks. In contrast to earlier views these gneisses do not represent an autochthonous basement but form thrust units, which are an integral part of the fold and thrust belt. Such a situation is particularly well documented for the Migif-Hafafit gneisses. Cross-cutting relationships of stretching lineations show that NE-SW stretching, restricted to the Migif-Hafafit gneisses, predates SE-NW stretching related to regional nappe transport. A stretching lineation with a SE-NW orientation is the regionally most persistent feature and probably provides the strongest argument for a tectonic transport direction on a regional scale (Greiling et al., 1988). However, it should be indicated that the stretching, fragment, and mineral lineations in the Lowder-Mudiah gneisses are NE-SW accompanied by E-W directed crustal shortening (similar to that of the Migif-Hafafit gneisses in the Eastern Desert of Egypt).

Early stages in the geologic evolution of the central eastern desert of Egypt reflect an intense episode of ensimatic volcanic activity (e.g. the younger metavolcanics) similar to modern magmatism of the ocean floor and island arcs. The end of the Precambrian was a period of instability and melting in the mantle which lead to the formation of the entire crust of the central eastern desert of Egypt, the volcanic rocks of which record an episode of primitive crustal growth that is distinct from other terranes of similar age elsewhere in Africa which indicate that large-scale remobilization of older sial was common during the Late Precambrian (Stern, 1979, 1981).

igneous (and tectonic ?) activity in the Eastern Desert of Egypt began sometime prior to 765 Ma and ended by 540 Ma; the oldest rocks are found in the South Eastern Desert

and the youngest in the Northeastern Desert; the mean age of the basement decreases from south to north. A fundamental transition in tectonic and magmatic style, from compressional to extensional, occurred about 600 Ma and was especially important in the development of crust in the Northeastern Desert, and all igneous rocks in the Eastern Desert have low initial  $^{87}\text{Sr}/^{86}\text{Sr}$  (0.702 - 0.704), such that reworking of older continental crust is precluded. Instead, the basement of the Eastern Desert of Egypt must have evolved via melting of metasomatically enriched mantle and/or remelting of immature geosynclinal materials over 230 Ma at the end of the Precambrian (Stern and Hedge, 1985).

Large parts of northeast Africa and Saudi Arabia consist of a telescoped Proterozoic island arc ocean-basin complex less than 1 by old. In the central Eastern Desert of Egypt, the oldest units in the complex are a mafic and ultramafic sequence representing an ocean substrate. The oceanic-arc complex could have evolved and been intruded by progressively more voluminous and fractionated granitic rocks between about 550 and 850 Ma. In southwest Saudi Arabia these processes may have begun slightly earlier. Both the volcanic rocks within the complex and the granitic rocks intrusive into it have low initial ratios of  $^{87}\text{Sr}/^{86}\text{Sr}$  ( $< 0.704$ ), suggestive of a mantle origin (Engel et al., 1980). Moreover, Shimron (1984) suggested that the northern Arabian Shield evolved in part by subduction and island arc collision along an eastward-trending belt, which is marked by ultramafic complexes and extends from the southern Sinai Peninsula. He pointed out that the upper Proterozoic crystalline rocks in Sinai consist of three principal geologic units; (1) a high-metamorphic rank Basal Complex, (2) two generally lower grade calc-alkalic volcano-sedimentary successions (the Kid Group) and (3) late-kinematic to postkinematic (Pan-African) calc-alkalic and alkalic volcanic centers and plutonic masses. In his conclusion Shimron (1984) suggested that this region delineates the northernmost ophiolitic belt in the Arabian-Nubian Shield.

El-Ramly (1988) stated that the plate tectonic model and recognition of ophiolitic assemblages among basement rocks of the Eastern Desert of Egypt by Garson and Shalaby (1976) by considerable geochemical and isotopic evidence (Engel et al., 1980; Dixon, 1981; Stern, 1981; Stern and Hedge, 1985; Shackleton et al., 1980; Ries et al.,

1983).

Late Precambrian rifting and crustal evolution in the Northeastern Desert of Egypt was studied by Stern et al. (1984) who found that basement exposures along the northwestern flanks of the Gulf of Suez record the rapid formation of continental crust during the interval 670 - 550 Ma. A variety of field, petrologic and isotopic considerations indicate that this episode of crust formation took place in an extensional tectonic setting analogous to that of the late Paleozoic Oslo Rift of Norway. Crustal evolution in this region thus contrasts with other regions of the Afro-Arabian Shield where the crust appears to have formed by convergent margin accretionary processes and collisional tectonics. This imposes new constraints on our understanding of late Precambrian crustal evolution. Four principal rock associations make up nearly all the basement in the Northeastern Desert: (1) Hammamat Formation is a sequence of immature and poorly sorted breccia, sandstone, siltstone, and conglomerate. (2) Dokhan Volcanics are a thick sequence of slightly metamorphosed (lower greenschist facies) intermediate to felsic lavas. In some regions the Dokhan is a bimodal suite, in others rhyolitic ignimbrite is the eruptive equivalent of Younger Granite. (3) Dykes range in composition from basaltic 47% SiO<sub>2</sub> to rhyolitic 75% SiO<sub>2</sub> and from calc-alkalic to alkalic. They are bimodal with andesitic and rhyolitic dykes displaying contradictory intrusive relationships indicative of synchronous emplacement. These dykes trend east to northeast and therefore they are strong evidence for north-south to northwest-southeast -directed crustal extension. (4) Epizonal granite and granodiorite are variously known as the Younger Pan-African granites. They represent an anorogenic magmatic pulse unrelated to subduction-zone magmatism but rather associated with rifting and thus comparable with granites in the Oslo Rift. The mesozonal granodiorites are older than the granites and typically calc-alkaline. Stern et al. (1984) concluded that anatexis of metasomatically enriched mantle and/or first-cycle geosynclinal sediments and igneous rocks must be responsible for magma production.

Furthermore, study of the dyke swarms in the Northeastern Desert of Egypt by Stern et al. (1988) revealed that compositionally the bimodal dyke swarms are an important but poorly known aspect of the 575 - 600 Ma extensional event in northern Afro-Arabia. The

"mafic" suite consists of basalts and andesites with 49 - 66 %  $\text{SiO}_2$  and a mean of about 58 % silica. Porphyritic members contain phenocrysts of plagioclase and amphibole or clinopyroxene. The felsic suite consists of rhyolites that contain 70 - 78 %  $\text{SiO}_2$  with a mean of 75 %  $\text{SiO}_2$ , and are largely metaluminous. Porphyritic variants contain phenocrysts of K-feldspar and quartz, biotite, and/or amphibole. The field and chemical data indicate that the mafic dykes were hypabyssal feeders of the Dokhan Volcanics, while the felsic dykes fed epizonal sills and magma cushions emplaced at the base of the Dokhan. The large variations in felsic compositions indicate that the processes responsible for much of the chemical variability of the younger granites was established at depth and did not occur, for the most part, in the presently exposed epizonal plutons. Compositional variability may either reflect differences in the crustal sources or in deeper-seated magmatic fractionation processes. The composition of the mafic dykes provides a caveat for interpreting tectonic environments from the chemical composition of igneous rocks. These rift-related magmas show some chemical fingerprints of Andean-type calc-alkaline suites. This supports the suggestion that igneous rocks in rapidly extending, highly volcanic continental rifts show a large degree of compositional overlap with Andean margin magmatic suites (Stern et al., 1988). The bimodal dyke swarms in the Northeastern Desert of Egypt are very similar to the Mukeras dyke swarms and Mudiah metavolcanics of the Lowder-Mudiah area (see Tables 3.5, 3.6).

In their review of the mafic dyke swarms in the Arabian-Nubian Shield, Eyal and Eyal (1987) said that mafic dykes are mainly basaltic in composition, but andesitic and mafic lamprophyre dykes also occur. Dyke density is generally high and may form more than 50 % of an area. Six episodes of mafic dyke intrusion are distinguished in Saudi Arabia but only some of these are recognized in Sudan, the Eastern Desert, and Sinai. Most dykes were intruded after a period of calc-alkaline dioritic to granodioritic plutonism. The trend of the dykes in the shield is variable; N-S, NW and NE trends are common in Saudi Arabia, whereas E-W to ENE-WSW trends characterize the NE Sinai and Elat areas. In the Red Sea Hills also one episode of metamorphosed dyke intrusion is known.

The lithological units of NE Sudan have until recently been divided into three major groups separated by igneous phases and unconformities. Amphibolite facies para- and

ortho-gneisses, generally referred to as the Kashebib Series, were thought to underlie unconformably a metavolcanic and a metasedimentary sequence of greenschist facies basic and intermediate volcanics and associated clastic sediments, referred to variously as the Oyo Series, Nafirdeib Series, or Greenschist Assemblage. Both groups were extensively intruded by granitoids of batholithic dimensions, and by gabbroic and ultramafic masses. In turn they are overlain unconformably by younger more acidic volcanic sequences, the Awat, Homogar, and Asotriba Volcanics. The culminating event was considered to be the emplacement of younger granite complexes and associated dyke swarms. The recognition, within the volcano-sedimentary sequences, of two belts of ultramafic rocks, at Sol Hamed and Khor Nakasib, and their interpretation as probable ophiolite complexes, is a pattern closely comparable to that in Saudi Arabia (Embleton et al., 1984). Furthermore, the western quarter of a 500 km traverse line from the Nile at Abu Hamed to the Red Sea at Port Sudan crosses high-grade metasediments and gneisses similar to those occupying much of north-central Sudan, whereas the eastern section consists of low-grade metasedimentary and metavolcanic rocks correlatable with the Late Proterozoic of Arabia. A large batholith emplaced into low-grade rocks displays the full calc-alkaline range from gabbro to mildly alkalic granite, with granodiorites predominating. Then following stabilization, magmatic activity switched to the alkaline granite/syenite association characteristic of the Younger Granites of northern Africa. Most of these alkaline complexes were structurally controlled by the Wadi Oko-Wadi Odib-lineament, which follows one of the younger, N-S shear zones (Almond et al., 1984a,b).

In the Wadi Onib area of the northern Red Sea Hills there is a complete ophiolite succession, the individual units of which have been dismembered by intense tectonism, probably at the time of ophiolite emplacement (Hussein et al., 1984). A dismembered Proterozoic ophiolite in the Northeastern Nuba Mountains in Sudan was studied by Hirdes and Brinkmann (1985).

Numerous complexes, many in the form of ring structures, are located in Sudan, Egypt and Arabia. The regional pattern of ring complexes across the combined Arabian-Nubian Shield is an important element of the crustal evolution (Vail, 1984).

El-Ramly (1988) in his review of the geology of the Arabian-Nubian Shield stated that with regard to the Red Sea Hills of the Sudan, the similarity of the rock types and their tectonic setting with those in Saudi Arabia and the Eastern Desert of Egypt were recognized by Neary et al., (1976), who supported the evolutionary model developed in Arabia for these rocks.

Carbonatite dykes in Egypt occur at Gebel Tarbti (Serencsits et al., 1979). It could be that in the East African Rift, fracturing took place on an ancient and active lineament along which carbonatitic and alkaline igneous activity had long been focused (Woolley, 1989a).

### 1.6.3 The Mozambique Belt

The Mozambique Belt is dominated by granitic gneisses (Holmes, 1951; Shackleton, 1979, 1986; Almond, 1984; Warden and Daniels, 1984; Warden and Horkel, 1984). The coastal basement strip of northern Somalia provides a discontinuous section across the northeast branch of the Mozambique belt. The lithostratigraphic sequence is similar to that found further south in the Kenyan and Ethiopian segments of the belt. Sedimentation was initiated by rapid deposition of miogeoclinal arkosic and quartzitic clastics and greywackes on Pre-Mozambique gneisses. Deposition of the pelites and calcareous mudstones was succeeded by a carbonate-quartzite shelf sequence. The nature of the rocks flooring the layered succession is less certain than in S.Ethiopia and E.Kenya where relicts are characterised by Pre-Mozambique structures which occur in gneiss, domes and as tectonically upfaulted wedges. In N.Somalia they probably comprise granitoids and gneisses. Moreover, granitic gneiss collected from N. Somalia, between Berbera and Hergesa, during the Somali International Conference field trip, in which the author was a participant (1987) gave an isotopic age of 1800 Ma (Kroner, 1989, personal communication). Such source rocks are also reflected in the composition of the overlying clastics. The rocks were folded and metamorphosed under medium P/T mainly in the amphibolite facies but locally in the granulite facies in a culminating stage of the Mozambique orogeny. West of the northern Somalian basement variably metamorphosed crust of different origin (comprising basaltic and calc-alkaline volcanics with immature clastics and ophiolitic slices) was formed by closure of small island arc basins. The later

stages of evolution of the N.Somalian basement which occurred during the Pan-African event were characterised by andesitic to rhyolitic volcanism along the western flank possibly related to eastward subduction. Basaltic and dioritic magmatism along the E margin of the gneiss belt is probably related to collision and westward subduction of the eastern Gondwana plate. The volcanics in the margins of the belt are infolded with, but less strongly metamorphosed than, the gneisses. Deposition of predominantly argillaceous sediments with arenitic clastics and carbonates occurred along the eastern flank of the N.Somalian basement. Compression probably related to the eastern Gondwana collision folded these rocks about N-trending axes and reworked earlier basement structures of similar trend. The Pan-African event is also characterised by widespread granite intrusion and local dynamothermal reworking of the Mozambique gneisses which also deformed and metamorphosed mafic intrusions in the western part of the basement (Warden and Daniels, 1984). Precambrian carbonatite dykes in N.Somalia (NW of Berbera) at Darkainle intruded the granitic gneisses (Gellatly, 1962, 1963a,b, 1964; Heinrich, 1966; Gittens, 1966).

Warden and Horkel (1984) suggested that the north-east branch of the Mozambique belt extends into southern Arabia and constitutes a distinct geotectonic entity, characterized by a predominantly ensialic structure and lengthy polycyclic evolution.

### 1.7 Local Geological Setting

The Lowder-Mudiah area covers approximately 2200 sq. km and is underlain by a basement of Precambrian granitic gneisses and a sequence of metavolcanic rocks regarded by Greenwood and Bleackley (1967) as part of the Aden Metamorphic Group. These rocks are unconformably overlain by Jurassic limestone and Quaternary basalt of the Shugrah volcanic field (Cox et al., 1977).

Greenwood and Bleackley (1967) described the geology of the Western Aden Protectorate as: an assemblage of metamorphosed sedimentary and mafic igneous rocks (to which the term, Aden Metamorphic Group, is assigned) which rest upon older gneiss, is invaded by syntectonic granite and is associated with a zone of metasomatism and migmatization. Subsequent to the main period of regional metamorphism but prior to a later period of stress, plutonism of diorite, gabbro and granites were intruded. Older

volcanic rocks of the eastern Aden Protectorate are regarded as approximately contemporaneous with mafic intrusions of this phase. Slightly metamorphosed sedimentary rocks of Wadi Ghabar, Eastern Protectorate, represent uppermost basement rocks. Some Post-tectonic granites are early Paleozoic in age. Rare intrusions of alkaline granite have a Tertiary age. An early phase of regional (dynamothermal) metamorphism is distinguished from a later phase of essentially dynamic type. The highest grade of metamorphism recorded is that of the almandine-amphibolite facies. The Aden Trap Series are Late Cretaceous to Tertiary. The Aden Volcanic Series are Late Miocene, or Pliocene to Recent basaltic lava flows. The basement structural pattern resulted from the translation of a primary east-west stress by transcurrent movements.

Beydoun (1964, 1966) described the geology of the Eastern Aden Protectorate and part of Dhufar as follows : the basement rocks were in part subject to low-grade metamorphism, were folded, faulted, cleaved, and eroded. Intrusive activity may have extended into the upper Silurian as suggested by isotope dating. The oldest rocks overlying the basement peneplain are Middle and Upper Jurassic (?), and consist of basal sandstone, limestone, marbles, and local evaporites. Cretaceous transgression deposited clastics and limestone. Paleocene, Eocene, Oligocene and Miocene transgressions laid down limestone and local evaporites. The development of the Tertiary Hadramout uplifted compressional zone and a comparable parallel zone in Somalia are attributed to regional compression which buckled the crust. Important block and step faulting which followed buckling collapsed the flanks of the arches facing the Gulf of Aden.

A tectonized and dismembered ophiolite sequence is located about 100 km along strike to the southwest of the Lowder-Mudiah area (Al-Derweesh, 1988). Ultramafic rocks at Mukeras, Um Salul village, were reported by Dobrenky et al. (1977); Saeedan (1984) as mineral exploration targets, but they require detailed study to understand their geology in terms of plate tectonics.

Geukens (1966) stated that after the leveling of the Precambrian metamorphic basement toward the end of the Paleozoic, sandy formations of continental facies were deposited mainly in the northern part of Yemen. From the Liassic onward a zone of subsidence was

filled with fluvio-lacustrine sediments. From the Late Jurassic onwards, the marine transgression covered the entire territory. The zone of subsidence was more accentuated towards the Red Sea. Sandy conglomerates were deposited in the Mesozoic and there was a widespread marine transgression in the Paleocene age.

The landsat based geological map of the former Yemen Arab Republic by Grollier and Overstreet (1978) provides a general overview on the geology of the northern part of Yemen and the main different geological units including the basement, (in the south and southeastern parts), the sandstone and limestone cover rocks, the Tertiary and Quaternary volcanics (in the central parts) and the Tertiary (alkaline) granites mainly parallel to the Red Sea coast. The map shows that the basement to the north and north west of Lowder-Mudiah area is composed mainly of granitoid gneisses with NE-trending major shear zones, parallel to that of the Lowder-Mudiah area and there are dyke swarms intruded these basement rocks and extending to the north and northwest borders of Yemen.

### **1.8 Previous Work in the Lowder-Mudiah Area**

Greenwood and Bleackley (1967) made a reconnaissance study of the Lowder-Mudiah area when it was part of the former Western Aden Protectorate. Cox et al., (1977) studied the Quaternary Volcanics of Shugra, and the Russian Geological Mission (Kopechny, 1981) carried out geological prospecting for carbonatite at Lowder (Abouov et al., 1981).

Dobrenky et al. (1977) referred to the presence of mafic-ultramafic rocks, aplites of Palaeozoic age, diabase dykes of Mesozoic-Cenozoic, and strike-slip faults and thrusts at Mukeras town and the surrounding villages. Saeedan (1984, personal communication) pointed out that the mafic and ultramafic rocks at Mukeras town are associated with magnetite, chromite and sulphide mineralisation.

It should be noted that there is very little information about South Yemen in the international literature. With regard to the Shield in South Yemen, few geological details are known compared with those in Saudi Arabia and NE Africa. However, some geological activities were carried out by various geological missions, such as those of Czechoslovakia (Blumenthal, 1978) and East Germany, but no publications, data or

technical reports are available and accessible.

### 1.9 Lay out of the Thesis

Chapter 2. Is concerned with the field relations and petrography of the granitoid gneisses, amphibolites, Lowder-Mudiah granitoids, Mudiah bimodal metavolcanics, Mukeras bimodal dyke swarms and their granite-diorite-quartzdiorite-gabbro host rocks.

Chapter 3. The petrochemistry of the granitoids, Mudiah bimodal metavolcanics, Mukeras bimodal dyke swarms (the early generation,  $709\pm 21$  Ma) and their granite-diorite-quartzdiorite-gabbro host rocks. This includes XRF major and trace element analyses, triangular plots for some of the major oxides and normative minerals, and spider diagrams for the trace elements to compare with known areas as an attempt to determine the possible tectonic setting.

Chapter 4. This deals with the structural geology of the Lowder-Mudiah area, the folds, cross-folds, foliation and lineation. The faults in the area range from minor normal faults into major shears, thrusts and block faults.

Chapter 5. In this chapter a study of four groups of carbonatite dykes at Lowder, includes their mutual field relations and associations with their host rocks (the granitic gneisses), and petrography of the dykes: supported with electron microprobe analyses, XRF analyses for the major oxides and trace elements and ICP analyses for the REE.

Chapter 6. Discussion and conclusions for all the chapters which includes a schematic diagram for the possible paths of the magmatic evolution of the Lowder-Mudiah granitoids, Mudiah metavolcanics and Mukeras dyke swarms and their host rocks and their possible tectonic setting.

References cited in the thesis.

Appendixes. Tables of samples and locality Grid References, dyke swarm statistics, age date analyses, procedure of chemical analyses, tables of the chemical standards used with their mean and standard deviations.

## CHAPTER 2

### FIELD RELATIONS AND PETROGRAPHY

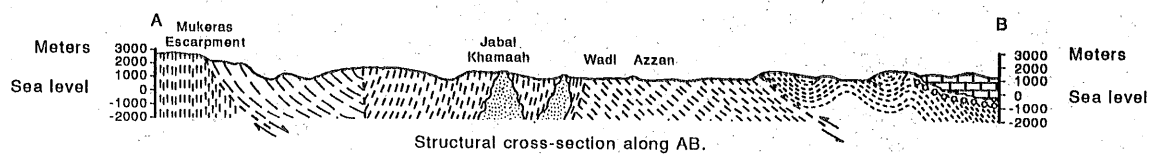
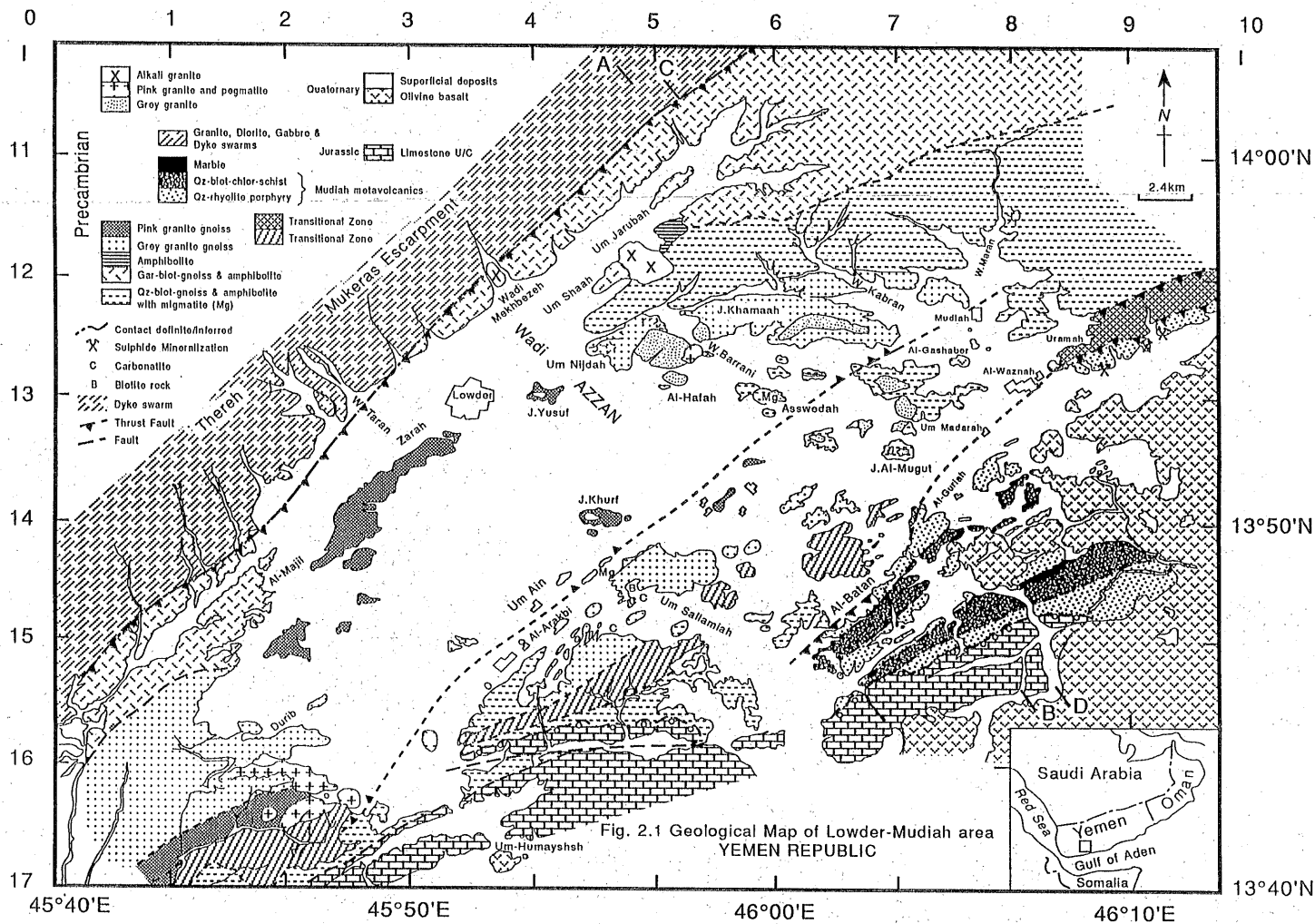
#### 2.1 Introduction

The Lowder-Mudiah area lies within the southwestern corner of Arabia (Fig. 1.1) and is made up dominantly of crystalline basement rocks, unconformably overlain by a cover of Jurassic limestone and Quaternary basalt. The basement rocks can be divided into three main belts, separated by two northeast-striking ductile shear (thrust) zones (Fig. 2.1).

The central belt is highly metamorphosed and underlies two thirds of the area in its central part. This belt trends northeast and is composed of grey and pink granitic gneisses, including lenses and patches of sheared quartz-biotite gneiss and amphibolites. These gneissose rocks are intruded by grey and pink pegmatitic granites that contain garnet and tourmaline. Migmatites occur locally within this belt at Asswedah, Al-Gashaber and Um Sallamiah. Carbonatite dykes intrude the grey granitic gneiss in the vicinity of Um Sallamiah, Al-Arakbi, and Durib (See Maps Figs. 2.1, 2.2 and 2.3, enclosed in accompanied pocket). However, it should be noted that, in Figs. 2.2 and 2.3, the locality numbers are not necessarily the same as the sample numbers for the same locality, but in some cases they are the same. The reason is that the locality was visited at different times for different purposes, e.g. following a sequence, recording information, or collecting samples, thus they might have the same or different numbers accordingly (for sample and locality Grid References list see Appendix Tables A2.7, A2.8).

The eastern belt comprises northeast-trending metavolcanic rocks, interlayered with subordinate marbles. These rocks display a low-grade greenschist facies mineralogy (Miyashiro and Aki, 1979) and are composed of quartz-biotite-chlorite schist, interlayered with amphibolite and schistose quartz-rhyolite porphyry. The sequence is deformed in open antiforms and synforms (see Fig. 4.1 enclosed in accompanied pocket) with vertical axial planes that trend northeast. Sulphide-bearing veins are common within the quartz-rhyolite porphyry and are shown on the field map as gossan.

The third belt occupies the western part of the area and is marked by a northeast-



trending, one kilometer high escarpment that reaches an elevation of 2500m. The main rock types are weakly altered and deformed medium grained granite, diorite and gabbro which are traversed by swarms of northeast-trending mafic and felsic dykes. These dykes have been metamorphosed to low-grade greenschist facies, weakly sheared and strongly epidotized.

Well-bedded Jurassic limestone forms discontinuous ridges that dip gently southeast and unconformably overlie the basement with a basal conglomeratic sandstone.

### **2.2 The Central Belt (Granitoid gneisses, Amphibolites and Granitoids)**

This belt is up to 20 km wide, composed of quartz-biotite gneiss, amphibolite, subordinate locally garnetiferous quartz-biotite schist, and quartzite (Table 2.1). The rocks have a porphyroblastic texture, and are foliated and friable. They contain lenticular rock fragments (Plate 2.2b), pinch and swell structures, and are traversed by numerous dykes and veins of granite and pegmatite (Plate 2.2d). These rocks contain isoclinal and open folds. Fragment and mineral lineations plunge shallowly to the northeast, and foliation mostly strikes northwest and dips steeply west (Plate 2.4 a-f, 2.5a & b).

The rocks are traversed by two generations of granitic and pegmatite veins. The older generation shows ptygmatic folds. The gneisses rocks also contain conformable foliated pegmatite sheets which show isoclinal closures and open folds. Individual pegmatitic-granitic veins consist of boudinaged en-echelon lenses which are themselves folded (Plate 4.5c & d).

There are transitional zones up to 2 km wide between the quartz-biotite gneiss, amphibolite and quartzite on the one hand and either the grey granitic gneiss (east of Al-Arakbi) or the metavolcanics (at Uramah) on the other. These transitions consist of alternating bands of the two adjacent rock types. These transition zones are high-grade ductile shear zones that result from thrust movements between rock groups in deep crustal conditions.

At Asswedah (Fig. 2.4), Um Sallamiah and Al-Gashaber, there are three very localized migmatite zones up to 600 m wide in quartz-biotite gneiss and amphibolite (Fig. 2.1) (Plate 2.1b). These are traversed by deformed dolerite dykes. Three phases of deformation can be recognized in these migmatites. These are:

**Abbreviations in Tables 2.1, 2.2, 2.3 and 2.4**

Qz = Quartz	C = Coarse
Pl = Plagioclase	F = Fine
Kf = K-feldspar	M = Medium
Bi = Biotite	Ph = Phaneritic
Ms = Muscovite	A = Aphanitic
Hb = Hornblende	Po = Porphyritic
Tr = Tremolite	Gr = Graphic
Ac = Actinolite	Mr = Myrmekitic
Cpx = Clinopyroxene	Pr = Perthitic
Opx = Orthopyroxene	Rp = Rapakivi
Ch = Chlorite	Sf = Shear fabric
Sc = Sericite	My = Mylonitic
Ep = Epidote	Fo = Microfolds
Ap = Apatite	Fl = Foliated
Zr = Zircon	Gn = Gneissose
Sp = Titanite (Sphene)	Sh = Schistose
Mg = Magnetite	Ef = Elongated fragment
Hm = Hematite	
Ga = Garnet	
Scp = Scapolite	
Ca = Calcite	
Tu = Tourmaline	

Table 2.1 Mineral assemblages and petrographic properties for representative samples of the Amphibolites, quartz-biotite-hornblende Gneisses of the Lower-Mudiah area, based on visually estimated percentages.

Minerals Sample No.	Qz	Pl	Kf	Bi	Ms	Hb	Cpx	Scp	Accessories	Alteration	Textures	Rock type
BY16K2	< 5	10 - 20		< 5		30 - 40		10 - 20	Sp	Sc,	Vc, Fl	Amphibolite
BY24A		20 - 30		< 5		30 - 40		10 - 20	Sp, Ap	Sc, Ca	Ph, M - C, Fl	Amphibolite
BY24B		30 - 40		< 5		30 - 40		10 - 20	Sp	Sc, Ca	Ph, M - C, Fl	Amphibolite
BY24C	5 - 10	30 - 40				30 - 40		10 - 20	Sp	Ca	Ph, C - F, Fl, My	Amphibolite
BY24D	5 - 10	20 - 30		5 - 10		20 - 30		20 - 30	Ap, Sp		Ph, M - C	Amphibolite
BY26I	10 - 20	10 - 20		5 - 10		30 - 40			Ap, Sp, Mg	Sc	M - C, Fl, Gn	Amphibolite
BY14B	5 - 10	20 - 30	< 5			30 - 40				Ep	C, Fl, Gn, Fo, Ef	Qz-hornb- Gneiss
BY17I	20 - 30	10 - 20	5 - 10	10 - 20		20 - 30			Zr, Ap		M, Fl, Gn	Qz-biot- hornb-Gneiss
BY36E	20 - 30	10 - 20		10 - 20		20 - 30					M, Fl, Gn, Fo, Sf	Qz-biot- hornb-Gneiss
BY38A2	20 - 30	10 - 20	10 - 20	10 - 20	5 - 10				Tu, Zr	Ch	M - C, Fl, Sh, Fo	Qz-biot- hornb-Gneiss
BY35B	> 40				5 - 10						Vc, Fl	Quartzite
BY26H	> 40			5 - 10						Ch	V - C, Fl, Ef	Quartzite

**Plate 2.1**

The following photographs illustrate the field characteristics and relationships of the granitoid gneisses, the amphibolites and the migmatites from the central belt and the metavolcanics and marble bands from the eastern belt.

(a) Alternating bands of quartz biotite gneiss (light) and amphibolite (dark) dip almost vertically. Al-Gashaber, Mudiah. Grid Reference 758 1295. Looking NE.

(b) The migmatite at Asswedah showing lenses and layers of amphibolite veined by quartz-feldspathic gneiss. Grid Reference 595 130. Looking SE.

(c) A discordant, intrusive contact between the grey granitoid gneiss (G) and the later pink granitoid gneiss (P). Jabal Al-Mugut. Grid Reference 710 134. Looking SW.

(d) Alternating dark and light bands of the metavolcanics with white bands of marble dip to the southeast. Mudiah. Grid Reference 755 1407. Looking NE.



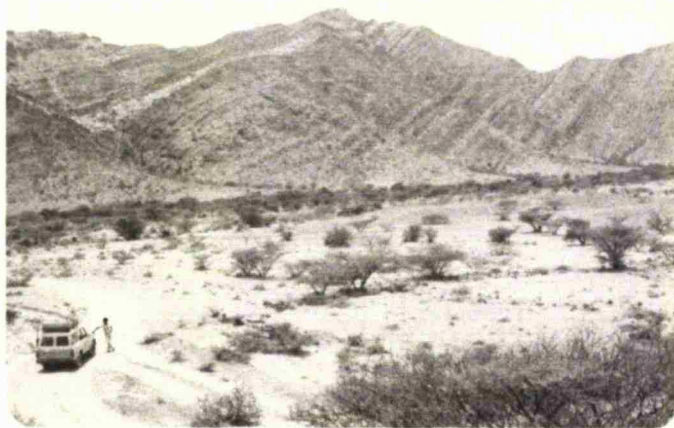
a



c



b



d

1. Deformation of the precursors of the gneiss and amphibolite.
2. Formation of shear zones.
3. Folding of the whole sequence. Finally, all rocks were intruded by unfoliated, undeformed grey granite.

A few small amphibolite bodies, up to 800 m across (Table 2.1) are concordant with the folded gneisses, and show mineral and crenulation lineations that plunge northeast. These amphibolites are transected by sheets of granite and pegmatite that have discordant contacts and chilled margins. The amphibolite also contain xenoliths up to few cm across of older granite and pegmatite.

The grey granitic gneiss is medium-grained, foliated, gneissose (Plate 2.5c & d) and is composed of quartz, K-feldspar, plagioclase, and biotite (Table 2.2). Its foliation trends NE-SW to NW-SE and dips SW and NE, respectively. Mineral and crenulation lineations plunge northeast. This gneiss is intercalated with minor quartz-biotite schist, amphibolite and quartzite. It is traversed by foliated, isoclinally folded, boudinaged sheets (Plate 2.2a) of granite and pegmatite.

The pink granitic gneiss (Plate 2.1c) is medium-grained (Table 2.2), foliated, trends NE and has a variable steep dip to the east and west. This is intercalated with quartz-biotite schist, amphibolite and quartzite. As indicated earlier it is transected by two generations of granite and pegmatite veins (Plate 2.2f), the older of which is folded and boudinaged. This indicates that there are at least two distinct phases of intrusive rocks. The first comprise granitic rocks (often in boudinaged and folded sheets) and pegmatite veins (Plate 2.2a), and the second comprises the post-tectonic granite and pegmatite sheets, which are finally followed by the alkali granite bodies (at Wadi Mekhbezeh and Jabal Um Hamra).

Petrographically the granitoid gneisses (see Table 2.2), are leucocratic, foliated (gneissose), with elongated fragments, mylonitic and myrmekitic, mylonitic textures. They are composed mainly of 20 - 30 % quartz, 20 - 40 % plagioclase, 20 - 40 % K-feldspar, 5 - 20 % biotite, 5 - 10 % muscovite and epidote < 5 % (in sample BY 30 A). FE - oxides (magnetite), zircon, sphene and apatite. The amphibolites (see Table 2.1) are melanocratic, medium to coarse grained, foliated (schistose to gneissose) with

Table 2.2 Mineral assemblages and petrographic properties for representative samples of the Granitoid Gneisses of the Lower-Mudiah area, based on visually estimated percentages.

Minerals	Qz	Pl	Kf	Bi	Ms	Ep			Accessories	Alteration	Texture	Rock type
Sample No.												
BY30B	20 - 30	20 - 30	20 - 30	10 - 20					Mg	Sc	Gr, Mr, Fl, Ef	Granitic gneiss
BY15E	20 - 30	30 - 40	30 - 40	10 - 20	< 5					Ch, Sc	M - C, Fl, Gn	Granitic gneiss
BY36B	20 - 30	20 - 30	20 - 30	5 - 10	< 5				Zr		C, Ef, Fl, Gn	Granitic gneiss
BY92	20 - 30	20 - 30	30 - 40	5 - 10					Sp, Ap, Zr, Mg		C, Ph, Mr	Granitic gneiss
BY21	20 - 30	20 - 30	20 - 30	10 - 20					Zr, Mg	Sc	C - M, Fl, Ef	Granitic gneiss
BY30A	20 - 30	20 - 30	30 - 40	10 - 20		< 5					M - C, Fl	Granitic gneiss
BY29G	20 - 30	30 - 40	20 - 30	5 - 10	5 - 10				Zr, Ap	Sc	C, Fl, Mr, Gn	Granitic gneiss
BY30D	20 - 30	30 - 40	20 - 30	5 - 10	5 - 10					Sc	M - C, Fl, Gn, Ef	Granitic gneiss
BY26M	20 - 30	30 - 40	30 - 40	5 - 10	5 - 10					Ch, Ca	M - C, Fl, Gn, My, Ef	Granitic gneiss
BY15A	20 - 30	20 - 30	20 - 30	5 - 10	5 - 10				Ap	Sc	M - C	Granitic gneiss

**Plate 2.2**

Photographs and a diagram to illustrate the field relationships of a boudinaged granitoid sheet, with intrusive contacts from the central belt; shear fabrics along the third central, shear zone; Shugrah volcanic field and the Jurassic limestone.

(a) Boudinaged white sheet of granitoid gneiss(S) within old grey granitoid gneiss. Mudiah. Grid Reference 758 1215. Looking SE.

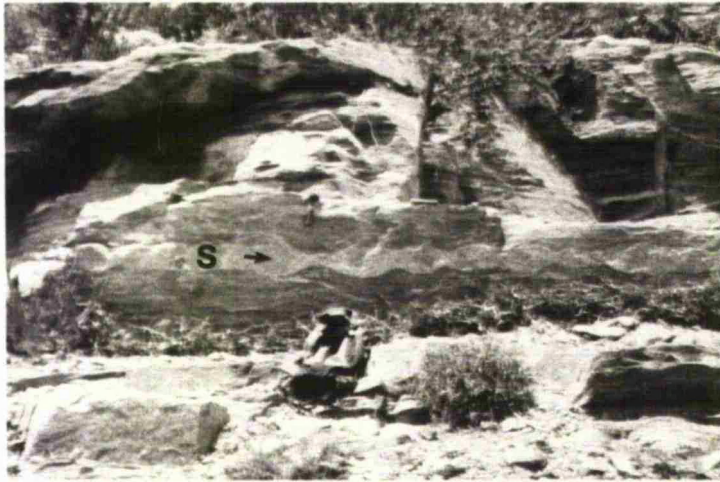
(b) Sheared, lensoidal granitic fragments within quartz-biotite gneiss and amphibolite, within the third central, shear zone west of Um Sallamiah, northeast of Um Ain. Grid Reference 45 145. Looking SE.

(c) A plug-like hill of grey granite with exfoliated surfaces. The granite has sharp contacts with the quartz-biotite gneiss and amphibolite. Al-Gashaber, Mudiah. Grid Reference 705 129. Looking SW.

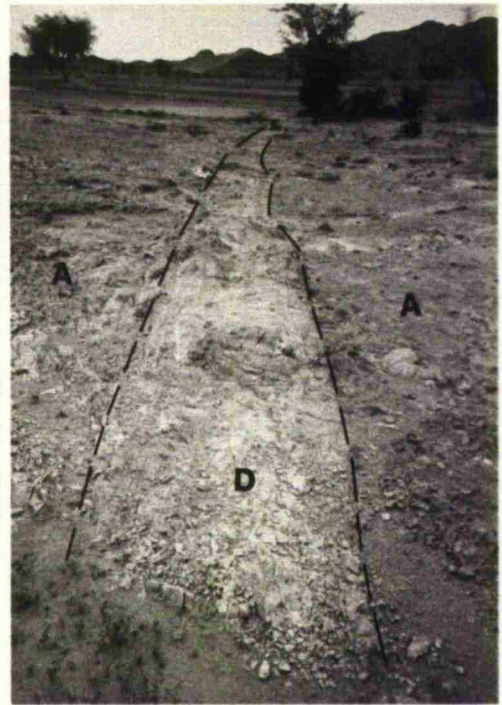
(d) Pink pegmatite dyke (D) traversing quartz-biotite gneiss and amphibolite (A) near Al-Arakbi. Grid Reference 41 15. Looking SW.

(e) The Shugrah volcanic field (dark low land), and the Jurassic limestone (light high ridges). Grid Reference 74 16. Looking NE.

(f) Diagram showing cross-cutting intrusive contacts between the grey granitic gneiss (GGn), the pink granitic gneiss (PGn) and the pegmatite dyke (P). Jabai Al-Yusuf. Grid Reference 41 13. Looking SE.



a



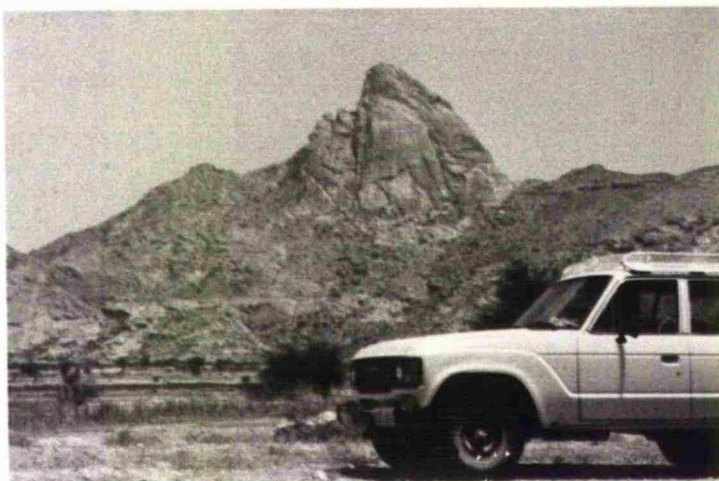
d



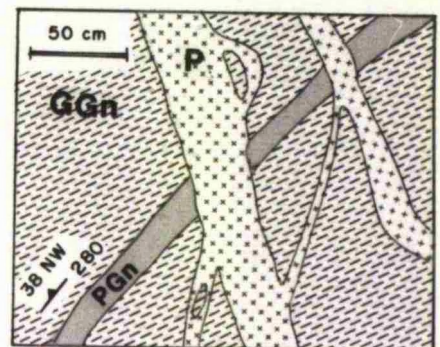
b



e



c



f

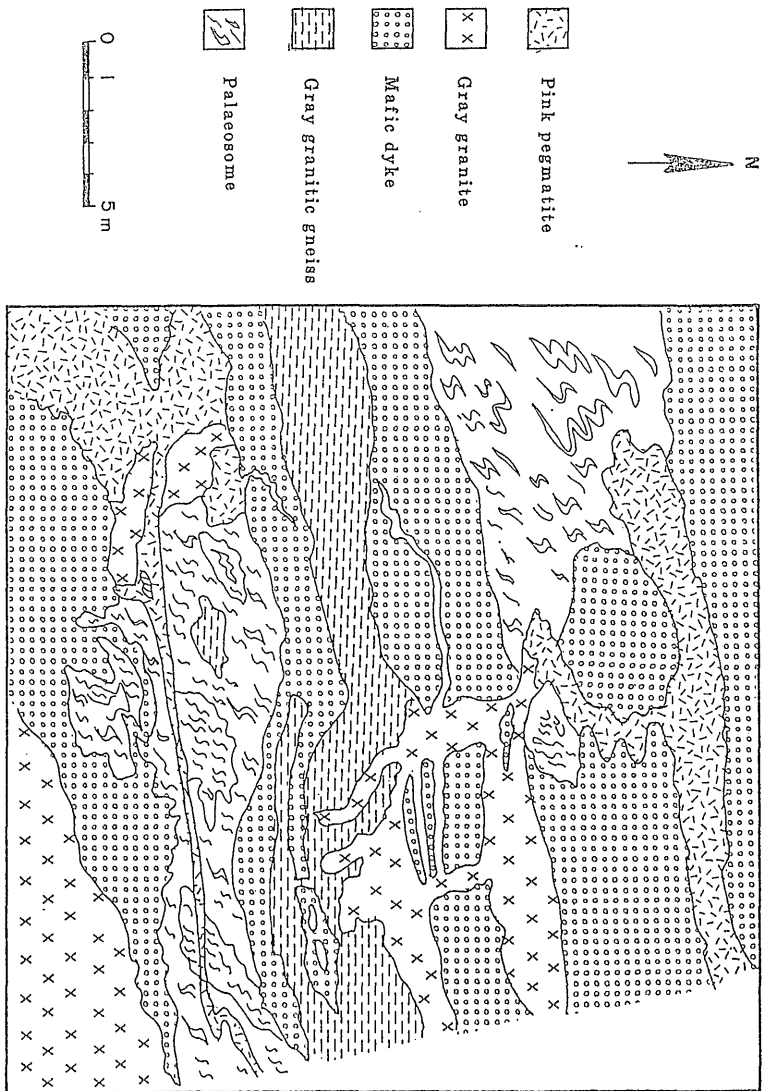


Fig. 2.4 Detailed sketch of part of the migmatite at Asswedah.

microfolds, elongated fragments, shear fabrics and myrmekitic texture. Composed of 20 - 40 % hornblende, 10 - 40 % plagioclase, 10 - 30 % scapolite (e.g. sample BY 24 C, see Plate 2.3 d), 5 - 10 % biotite and 5 - 20 % quartz. In addition to scapolite, other alteration minerals are sericite, chlorite and epidote. Fe-oxides (magnetite), sphene, zircon and apatite are accessories. The field association of some striped amphibolites (see Plate 2.1a) and quartzites is probably the result of isoclinal folding causing repetition of a simple original sequence. Moreover, the striped character of these rocks is probably the result of tectonic and metamorphic processes (Evans and Leake, 1960).

The grey granite forms up to 4 km wide, and is medium to coarse grained (Table 2.3), and it outcrops typically with exfoliation, blocky and rounded weathered surfaces (Plate 2.2c). This granite transects the granitic gneiss and amphibolite, with sharp contacts and chilled margins. It contains raft-like xenoliths of quartz-biotite schist gneiss and amphibolite, and is transected by the later pink granite and pegmatite veins.

The pink granite and pegmatite, up to 1 km in size (Table 2.3), intrude the granitic gneiss, amphibolite and the grey granite with sharp, discordant contacts and chilled margins. Some varieties contain garnet (Plate 2.3c), tourmaline and muscovite pockets, and show igneous flow bands made up of alternating biotite and quartz-feldspars. The granites contain raft-like xenoliths of gneiss and schist, some of which are partly assimilated.

The alkali granite, at Wadi Mekhbezeh and Jabal Um Hamra (Fig. 2.1), up to 1 km in diameter, is coarse grained, has a rounded exfoliation surface, and is composed of orthoclase, quartz, biotite and amphibole, and garnet in some varieties. The granite cuts the dyke swarms, their host rocks and the shear zone described above, and thus the granite intrusion represents the latest event in the region.

Petrographically the granitoid rocks (see Table 2.3) are leucocratic, petrographically showing graphic, myrmekitic and rapakivi textures. Composed of 10 - 30 % quartz, 20 - 30 % plagioclase, 20 - 40 % K - feldspar, 5 - 10 % biotite, 5 - 10 % muscovite and < 5 % hornblende (in some instances). Fe-oxide (magnetite), apatite, zircon, sphene, garnet and tourmaline (in some cases) are accessories. Most of these rocks show slight sericite and chlorite alterations. They have zoned plagioclase (e.g. sample BY16 N, see Plate 2.3e,f), rapakivi texture (e.g. sample BY19B, see Plate 2.3a), perthitic and graphic

Table 2.3 Mineral assemblages and petrographic properties for representative samples of the Granitoids of the Lowder-Mudtiah area, based on visually estimated percentages.

Minerals Sample No.	Qz	Pl	Kf	Bi	Ms	Hb	Accessories	Alteration	Texture	Rock type
BY30C	10 - 20	20 - 30	30 - 40	5 - 10	5 - 10		Ap, Mg	Sc, Ch	C, Ph	Granite
BY16N	10 - 20	30 - 40	20 - 30	5 - 10			Zr	Sc	C, Ph, Gr, Mt,	Granite
BY91	20 - 30	20 - 30	30 - 40	5 - 10	5 - 10		Mg	Sc	C - M, Ph, Gr	Granite
BY93	10 - 20	20 - 30	30 - 40	5 - 10	5 - 10		Sp, Zr, Ap, Mg		VC - C, Gr, Ph	Granite
BY36D	20 - 30	20 - 30	30 - 40	5 - 10	5 - 10		Ap, Mg	Sc, Ch	C, Mr	Granite
BY24E	20 - 30	20 - 30	30 - 40	< 5	< 5	< 5	Ga	Sc	VC, Ph	Granite
BY19C	20 - 30	20 - 30	30 - 40	< 5	< 5			Sc	VC, Pr, Gr	Granite
BY19B	20 - 30	20 - 30	30 - 40	< 5	< 5			Sc, Ch	VC, Rp	Granite
BY104	10 - 20	5 - 10	> 40			5 - 10	Zr, Sp, Mg	Ch	C, Gr, Pr, Mr	Alkali Granite

---

**Plate 2.3**

Photomicrographs to illustrate some textures and mineralogical constituents of the granitoids and the amphibolites.

(a) Rapakivi texture (R), shown by K-feldspar crystal with dark plagioclase rim in a rapakivi granite (Sample BY19B). Under C.P.L. Grid Reference 47 14.

(b) Perthitic and graphic textures in a graphic granite (Sample BY19C). Under C.P.L. Grid Reference 47 14.

(c) Garnet (G) in a granitic rock (Sample BY24E). Under P.P.L. Grid Reference 488 1435

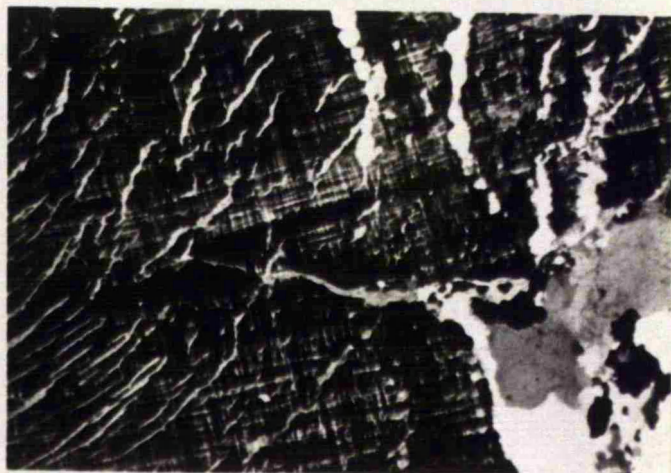
(d) Scapolite (S) and hornblende (H), in the amphibolites (Sample BY24C). Under P.P.L. Grid Reference 488 1442.

(e and f) Zoned plagioclase (P) and microcline (M) in a granitic rock (Sample BY16N). Under P.P.L. and C.P.L. respectively. Grid Reference 428 153.

0 3 mm



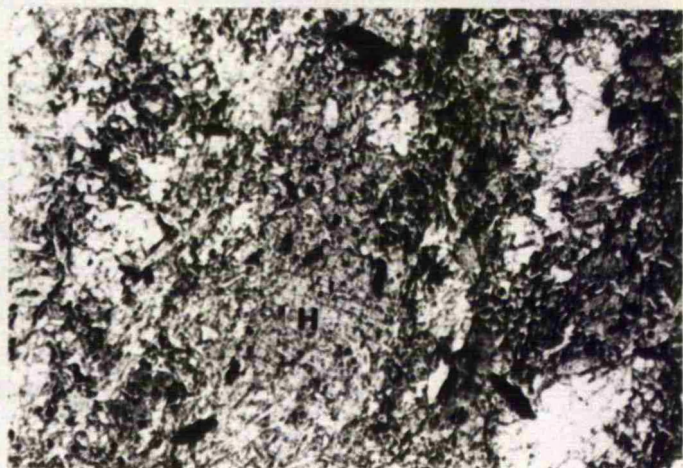
a



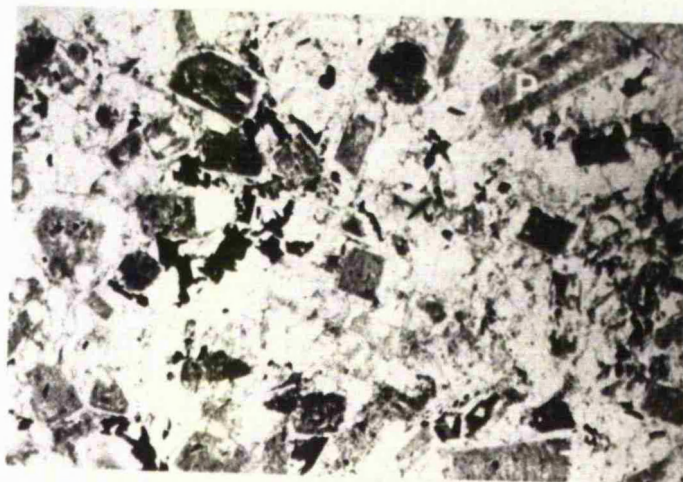
b



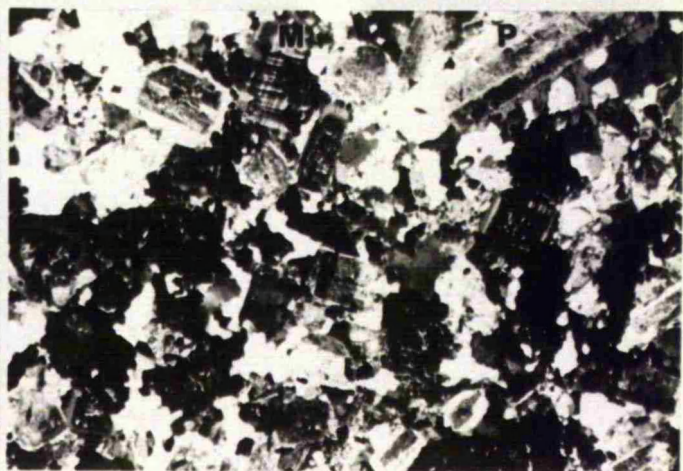
c



d



e



f

textures (e.g. sample BY19C, see Plate 2.3b).

### 2.3 The Eastern Belt (Mudiah Metavolcanics)

This is a northeast-trending belt, up to 4.5 km wide of alternating metavolcanic layers that are up to a few tens of meters wide (Plate 2.1d). They comprise epidote-chlorite-sericite and amphibole schists and quartz-rhyolite porphyry and basalt (Table 2.4). These rocks are strongly foliated, schistose, and lineated. Foliation trends NE-SW and dips shallowly SE and NW. The mineral lineation plunges gently NE. The whole sequence is folded into a first generation of synforms and antiforms that have vertical axial planes that strike NE and a second generation of open cross-folds. Quartz veins up to 10 cm wide, are associated with minor faults and shears. The quartz-rhyolite porphyry contains gossans, pyrite/galena-bearing quartz veins and stringers. The main sulphide mineralized quartz vein is about 1 meter thick and about 1 km long, and slightly discordant to the regional foliation. Its host porphyry shows evidence of strong shearing (Plate 2.5e & f), (Plate 2.6 a - f), leaching (bleaching) and haematization.

Petrographically the Mudiah Metavolcanics (see Table 2.4) are melanocratic, fine to medium grained, phaneritic, porphyritic, foliated (schistose), with shear fabrics and elongated fragments. The mafic varieties are composed of 30-40 % hornblende, 10-20 % plagioclase, 5 - 10 % biotite, < 5 % clinopyroxene, 5 - 10 % quartz, 5 - 10 % epidote and < 5 % chlorite and opaque Fe-oxides (magnetite). Epidote and chlorite are the main alteration minerals. The felsic metavolcanics are composed of 30-40 % quartz, 10 - 30 % plagioclase, 10 - 30 % K - feldspar, 10 - 30 % biotite, 10 - 20 % muscovite, 10 - 20 % epidote and < 5 % chlorite. The main alteration minerals are epidote and chlorite. Opaque Fe-oxides (magnetite) and apatite are accessories.

Between the conformable quartz-rhyolite porphyry and the quartz-biotite gneiss and amphibolite, there is a transitional zone up to 2 km wide, of banded gneisses within which there is a tectonic intercalation of these rocks from a few meters to a few tens of meters wide. This boundary zone is a ductile shear zone (Windley and Tarney, 1986). The tectonic interlayering makes the contact difficult to discern on aerial photos and on the ground. The metavolcanic rocks are unconformably overlain by the basal conglomeratic sandstone of the Jurassic limestone succession.

Table 2.4 Mineral assemblages and petrographic properties for representative samples of Muddiah Metavolcanics, based on visually estimated percentages.

Minerals SampleNo.	Qz	Pl	Kf	Bi	Ms	Hb	Ch	Ep	Qpx	Accessories & Alteration	Textures	Rock type
BY2C	< 5	10 - 20		5 - 10		30 - 40	< 5	5 - 10	< 5	Mg, Ch	F - M, Fl, Sh, Sf	Basalt
BY2E	10 - 20	20 - 30	10 - 20	10 - 20	5 - 10			10 - 20		Mg, Ch	F, Fl, Sh, Sf, Po	Andesite
BY5B	30 - 40	5 - 10	5 - 10	20 - 30	5 - 10		< 5	< 5		Ap, Mg, Ch	F - M, Po, Fl, Sf, Fo	Rhyolite
BY23A	20 - 30	5 - 10	20 - 30		10 - 20					Mg, Ch	F - M, Fl, Sh, Po, Sf, Ef	Rhyolite
BY86	30 - 40	5 - 10	10 - 20	5 - 10	10 - 20					Mg, Ch	F, Po, Fl, Sh, Sf	Rhyolite
BY87	< 5	10 - 20		5 - 10		30 - 40	< 5	5 - 10	< 5	Mg, Ch	F - M, Po, Fl	Basalt

**Plate 2.4**

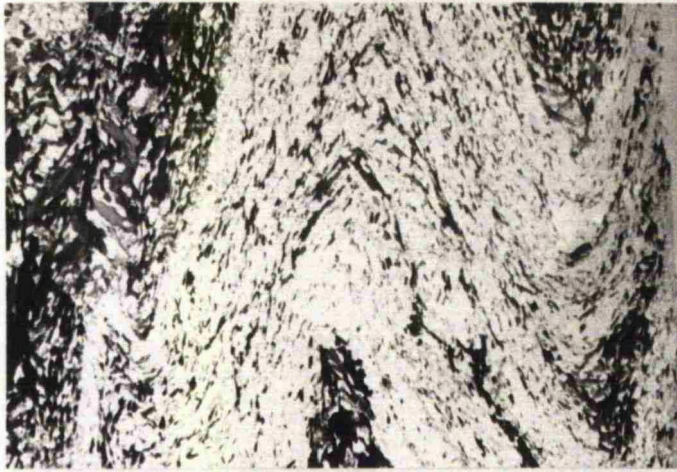
Photomicrographs, showing microfolds and fabrics in quartz-biotite gneiss from the central belt.

(a and b) Microfolds on the limb of a micro-isoclinal fold in the quartz-biotite gneiss (Sample BY26J). Under P.P.L. Grid Reference 482 1462.

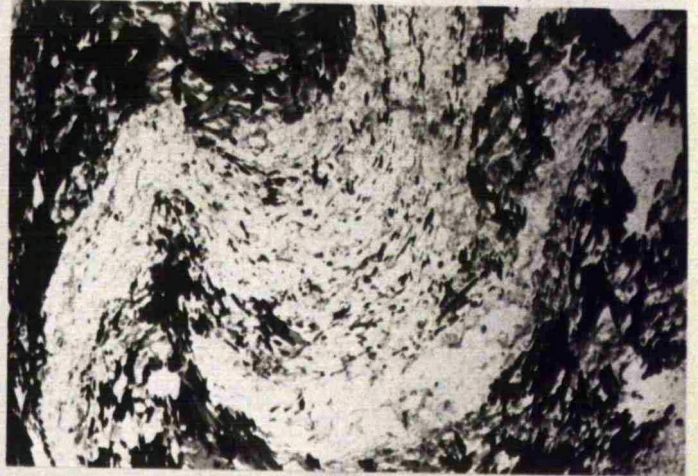
(c and b) Quartz-biotite gneiss (Sample BY38A2) showing the main foliation and microfolds, representing two phases of deformation. Under P.P.L. and C.P.L. respectively. Grid Reference 758 1295.

(e and f) Open micro-folds, and crenulation cleavage (possibly S2) in the quartz-biotite gneiss, (Sample BY13C) showing a post-tectonic crystallization of hornblende (H). Under P.P.L. and C.P.L. respectively. Grid Reference 810 1237

0 3 mm



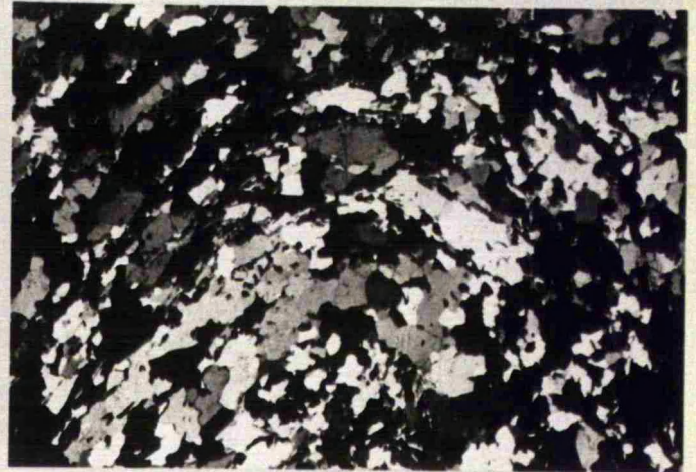
a



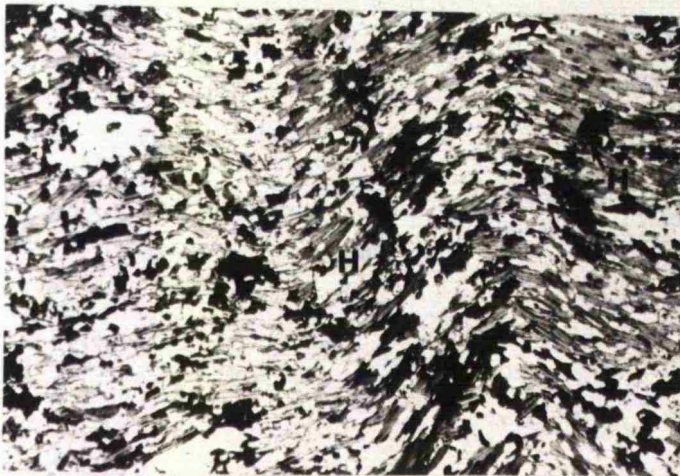
b



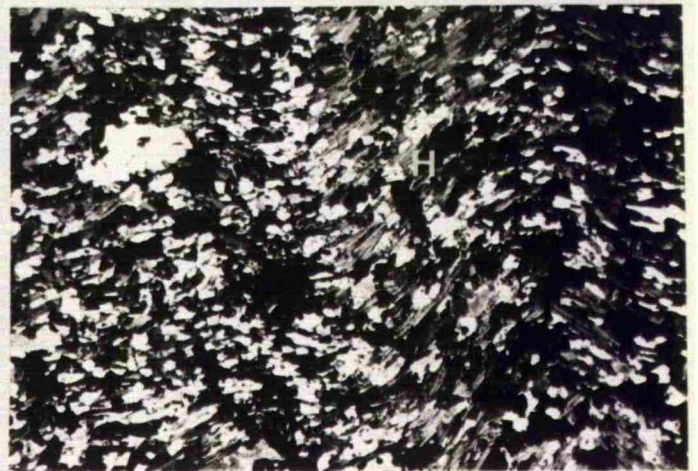
c



d



e



f

**Plate 2.5**

Photomicrographs showing microfolds and foliation in the granitoid gneisses from the central belt and shear fabrics in the metavolcanics from the eastern belt.

(a and b) An F1 fold hinge within a later isoclinal fold (F2), in the quartz-biotite hornblende gneiss (Sample BY36E from the central belt). Also it shows a post-tectonic crystallized hornblende (H). Under P.P.L. and C.P.L. respectively. Grid Reference 612 139

(c and d) Foliation in the granitic gneiss (Sample BY30D) from the central belt. Under P.P.L. and C.P.L. respectively. Grid Reference 7000 1348.

(e and f) The quartz-rhyolite porphyry (Sample BY23A) from the eastern belt, showing shear fabrics and flattening around quartz and K-feldspar fragments. Under P.P.L. and C.P.L. respectively. Grid Reference 775 1365.

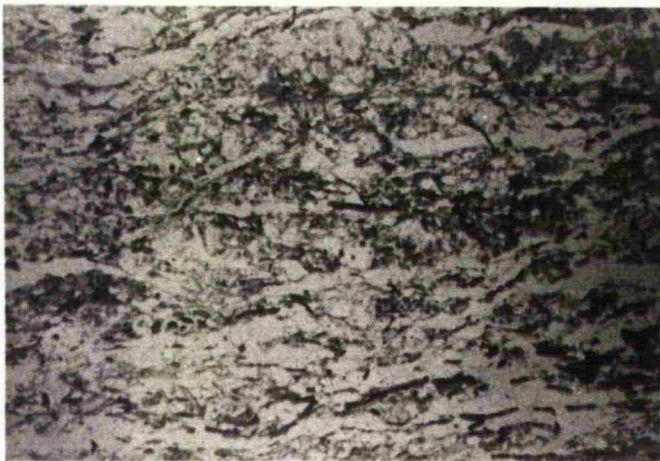
0 3 mm



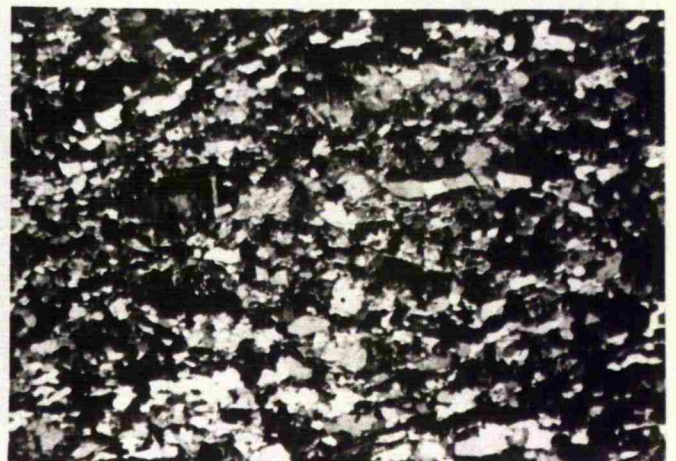
a



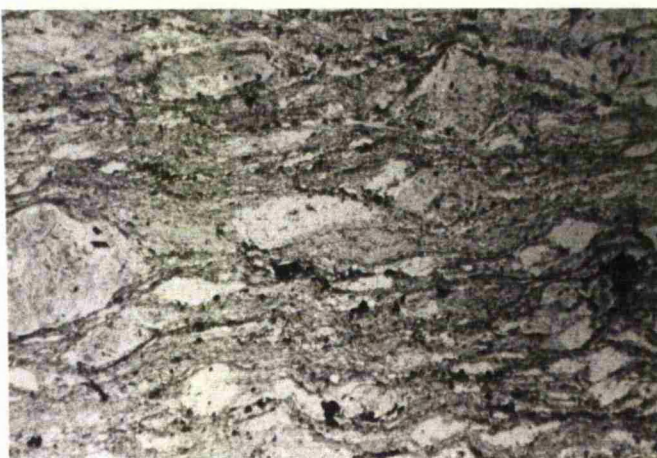
b



c



d



e



f

**Plate 2.6**

Photomicrographs to illustrate the shear fabrics in the metavolcanics from the eastern belt.

(a and b) Feldspar augen and shear fabrics in the metavolcanics, meta-andesite, (Sample BY2C) Under P.P.L. and C.P.L. respectively. Grid Reference 755 1407.

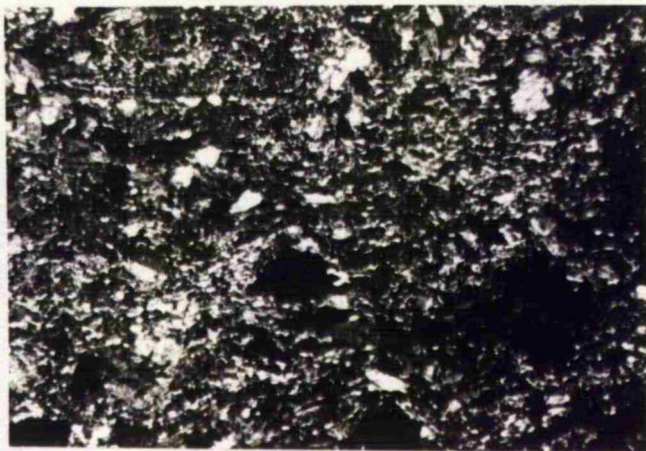
(c and d) Shear fabrics (shadow texture of quartz, feldspar and biotite) in the metavolcanics, meta-rhyolite to meta-rhyodacite, (Sample BY3). Under P.P.L. and C.P.L. respectively. Grid Reference 740 140.

(e and f) Shear fabrics, (shadow texture of feldspar, quartz and biotite) in the metavolcanics, meta-rhyodacites, (Sample BY5B). Under P.P.L. and C.P.L. respectively. Grid Reference 805 1448.

0 3 mm



a



b



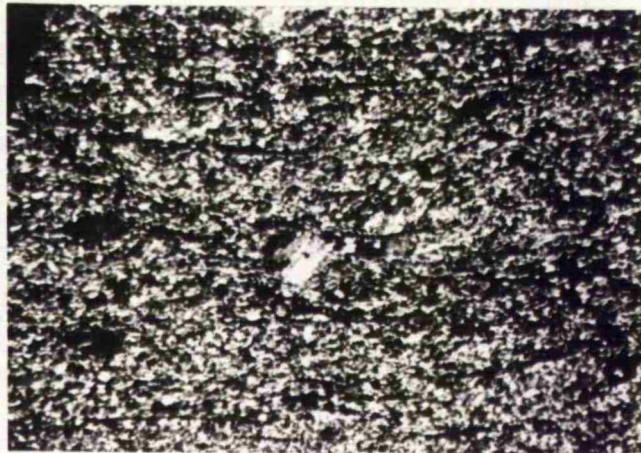
c



d



e



f

There are a few conformable lenses of banded marble up to 60 meters thick, within the metavolcanics, (Plate 2.1d). Contacts between the marble and the metavolcanics are faults with shears and epidote veins.

A bed of conglomeratic sandstone few tens of meters thick separates the Precambrian basement from the Jurassic limestone. It shows hematitic alteration and contains gossan-like pebbles. It is probably the lowest member of the Jurassic (Kohlan-formation) of the Amran group (Geukens, 1966; Greenwood Bleackley, 1967; Beydoun, 1966). The Jurassic limestone has coarse and fine-scale beds that strike NE-SW and dip gently SE. It ranges from fine-grained micritic fossiliferous to crystalline limestone.

A Quaternary basalt field (Plate 2.2e) extends from Shugrath Village to the borders of the Lowder-Mudiah area (Cox et al., 1977; Gass et al., 1965). There are basaltic cones and sheets of flow basalts with olivine phenocrysts and agglomeratic spiral bombs with onion-shaped weathered surfaces.

#### **2.4 The Western Belt (The Mukeras Escarpment Dyke Swarms and their Host Rocks)**

The Thereh-Mukeras Escarpment of the Lowder-Mudiah area is occupied by the major lithologic western belt (W.B) which is separated from the central belt (C.B) by a major southeasterly-dipping ductile thrust (Plate 2.7a). The belt is about 20 km in width and is essentially composed of (Fig. 2.6) intrusive batholiths composed of medium-grained granite in the northeast, and of granodiorite, diorite and gabbro in the southwest. These rocks are cut by an extensive swarm of northeast-trending, mafic to felsic dykes, which (Fig. 2.5; 2.6) represent an average about 75 % by volume of the host rocks and they reach about 90 % at Thereh passage (see Tables A2.1; A2.2 Appendix). Individual dykes reach up to 2 km in width at Wadi Taran (Plate 2.7 b, c). The dykes hosted by the granite are mainly intermediate and felsic, but those hosted by the diorite and gabbro are mainly mafic. A minor set of dykes trends almost east-west and cuts the NE-trending dykes.

At Thereh passage there are two types of diorite; an earlier foliated type is cut by a massive diorite with a clear discordant intrusive contact. Both diorites are cut by the mafic dykes, and all are cut by later grey granite and by the E-W dykes. The contacts between mafic and felsic NE-SW trending dykes are often sheared at their contacts with

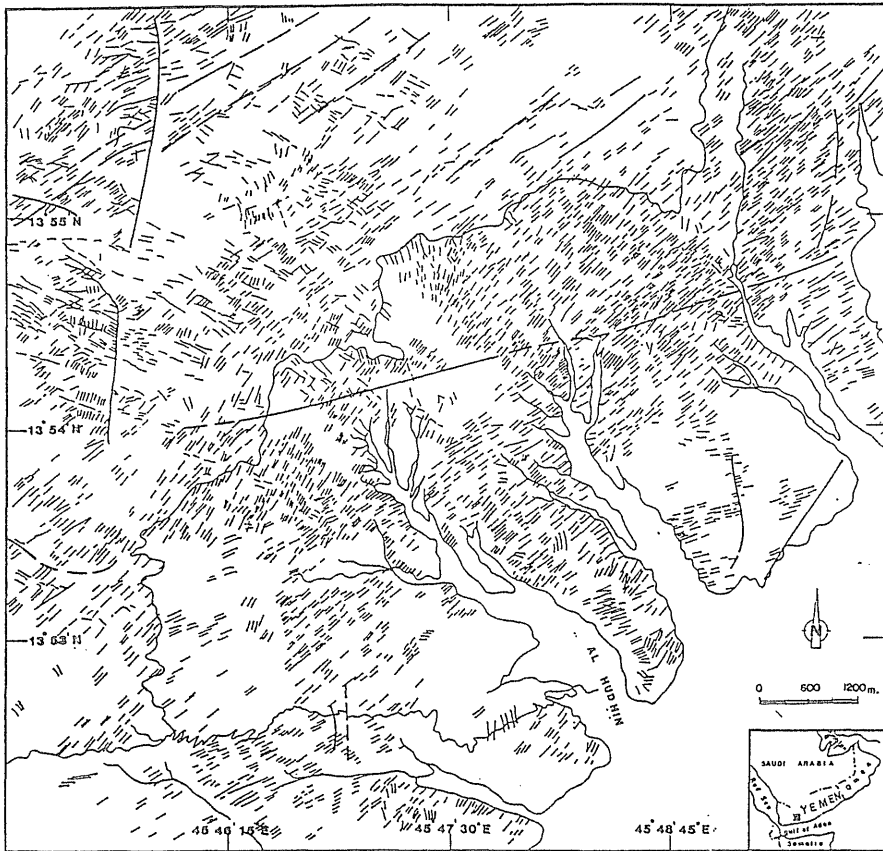


Fig. 2.5 Pattern of Late Precambrian dykes in the southeastern part of Mukeras Escarpment (light lines indicate the dykes, heavy lines the faults), obtained from study of aerial photos.



Fig-2.6 Distribution of the host rocks of the dykes shown in Fig. 2.5.

their host rocks.

Three traverses made across the escarpment at Wadi Taran, Wadi Mekhbezeh and Thereh-Mukeras (Fig. 2.7) revealed that the swarm is continuous and intense all along the escarpment for at least 60 km along strike, and that it is more than 20 km wide. The first and third of these traverses are described below:

#### **2.4.1 Thereh-Mukeras**

The two dyke swarms extend across the plateau to Mukeras about 25 km from Thereh. At Mukeras the predominant host rocks are diorite and gabbro, rather than the white granite so abundant at Wadi Taran. About 7 kms N10W of Mukeras town the diorite and the dykes are transected by a pink granite pluton, about 5 km in diameter that contains E-W trending inclusions of a reddish granite, identical to that at Wadi Mekhbezeh and Jabal Um Hamra.

It is important to note that the Thereh-Mukeras dykes extend at least another 20 kms across strike northwestwards towards the border of the Yemen Republic. This can be confirmed by consulting the Geologic Map of the Yemen Arab Republic (Grollier and Overstreet, 1978).

#### **2.4.2 Wadi Taran**

Here, the host rock is a white, medium-grained, weakly foliated and altered granite, intruded by two predominant sets of dykes that overall range from mafic and intermediate to felsic. The first set contains the majority of dykes and is oriented almost NE-SW. These dykes are cut by the second set oriented almost E-W (Plate 2.7b,c). The first dykes range in thickness from 2 m to 35 m (Fig. 2.8), are massive in their interiors, but are strongly sheared and foliated along their contacts and sometimes their centres especially within thinner dykes (about 1 m thick). Epidotization is prominent along joints and quartz veins, and pods of epidote are common in both the dykes and the granitic host rocks. These veins are oriented almost E-W. Some felsic dykes contain 5-15 cm long mafic xenoliths of unknown parentage.

The second set of dykes are unshaped, extend almost E-W and demonstrate at many intersections that they are later than the first dyke set.

An alkali granite at Wadi Mekhbezeh intrudes garnetiferous schist and gneisses of the

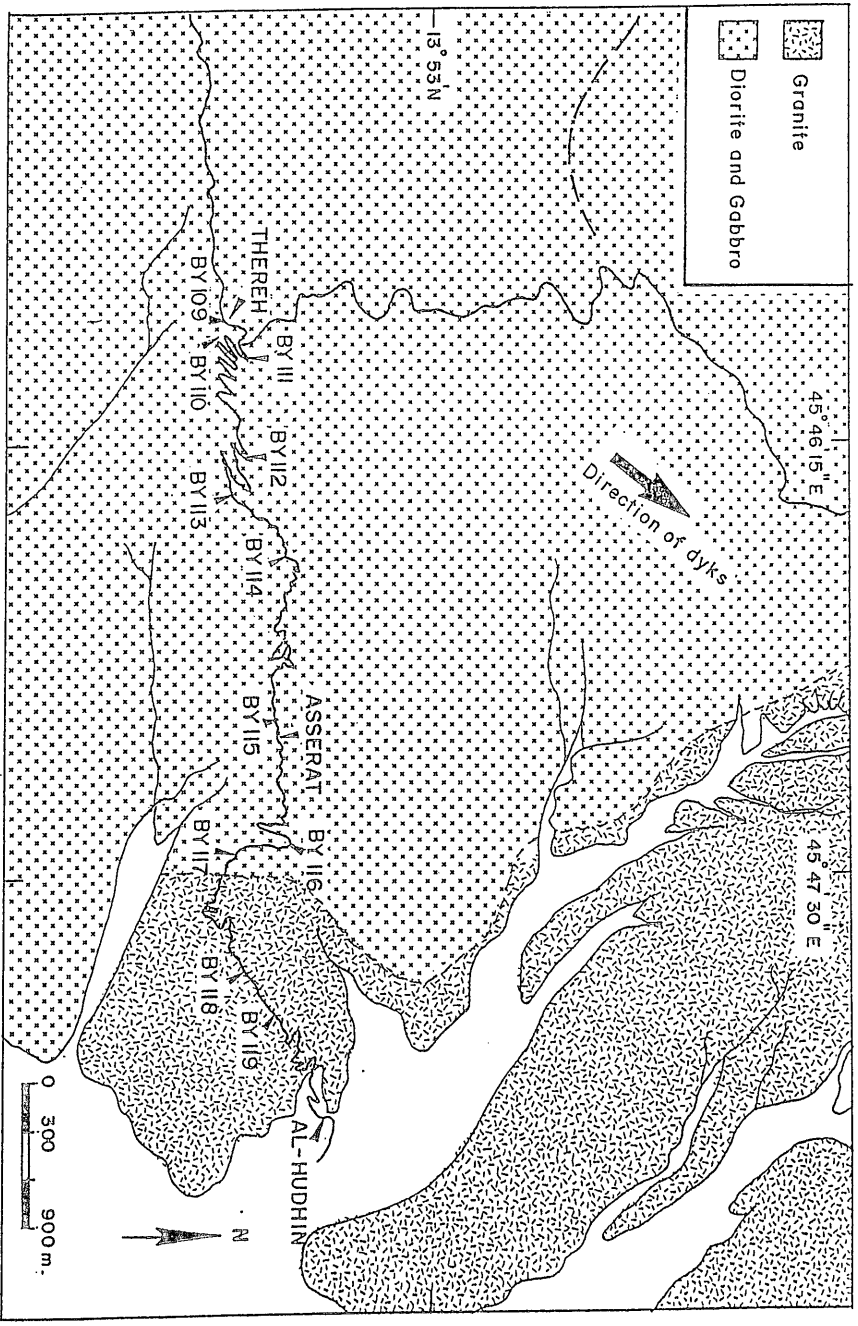


Fig. 2.7 Sample location map of dyke swarms and their host rocks along the Al Hudhin-Thereh escarpment road, the Mukeras Escarpment; Grid Reference between 170 132 & 200 135.

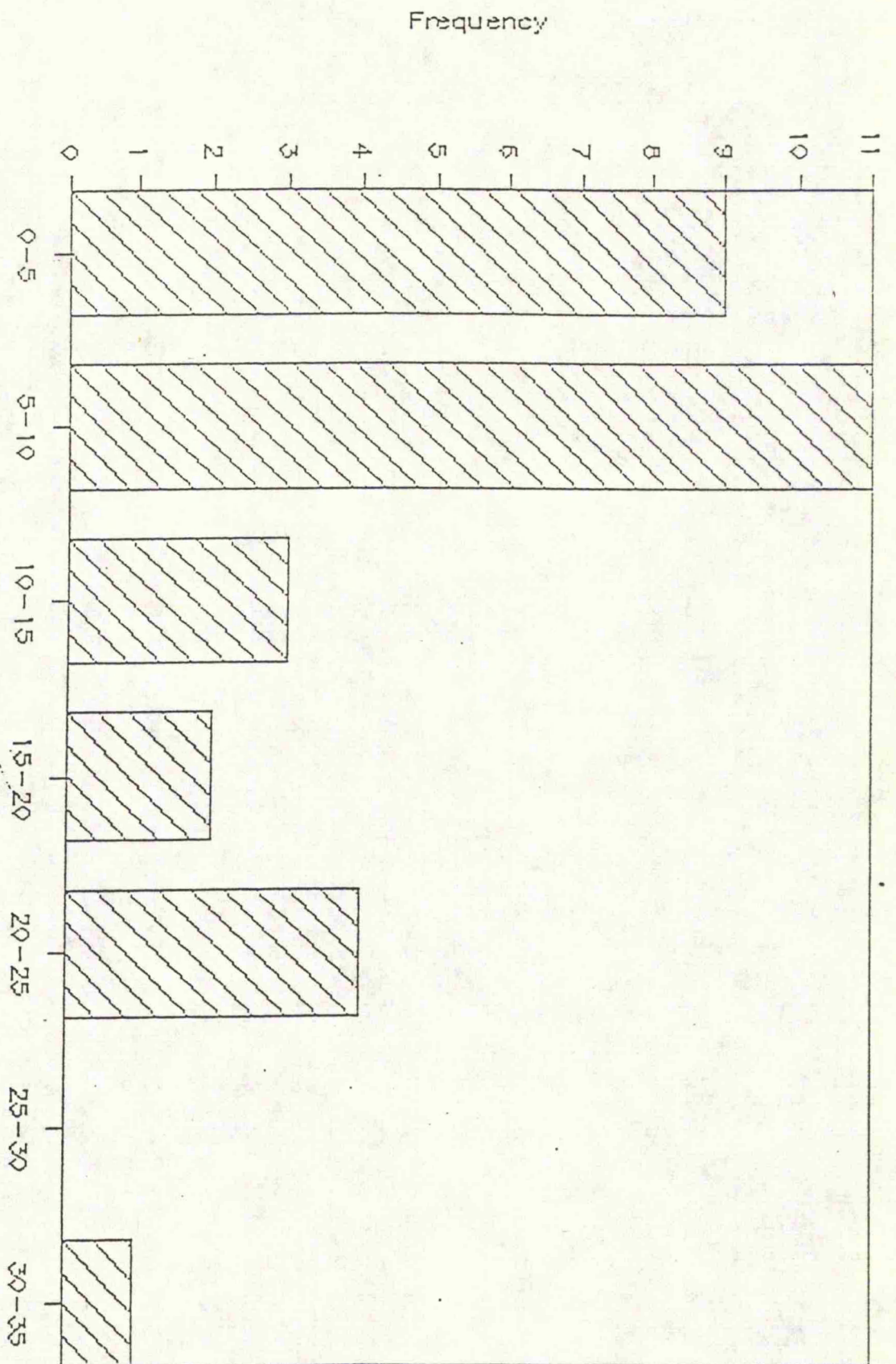


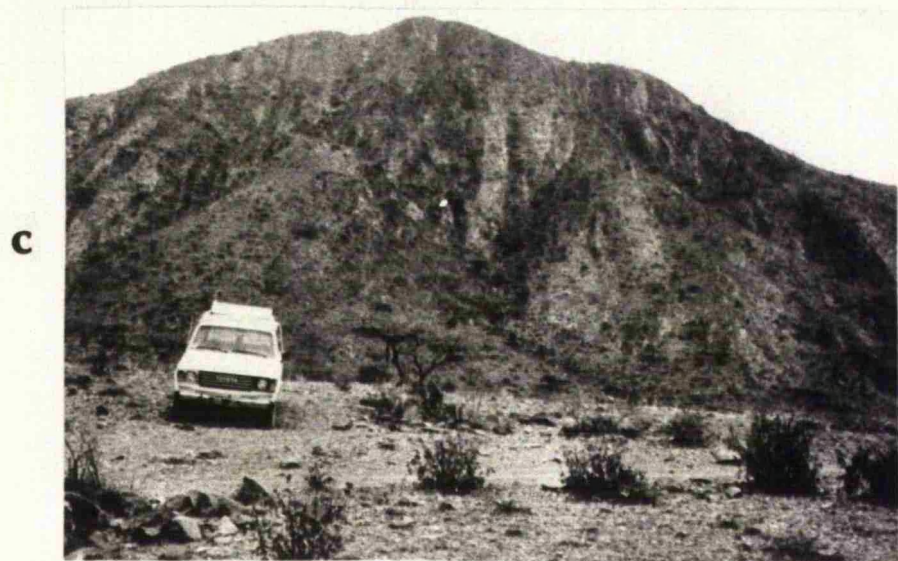
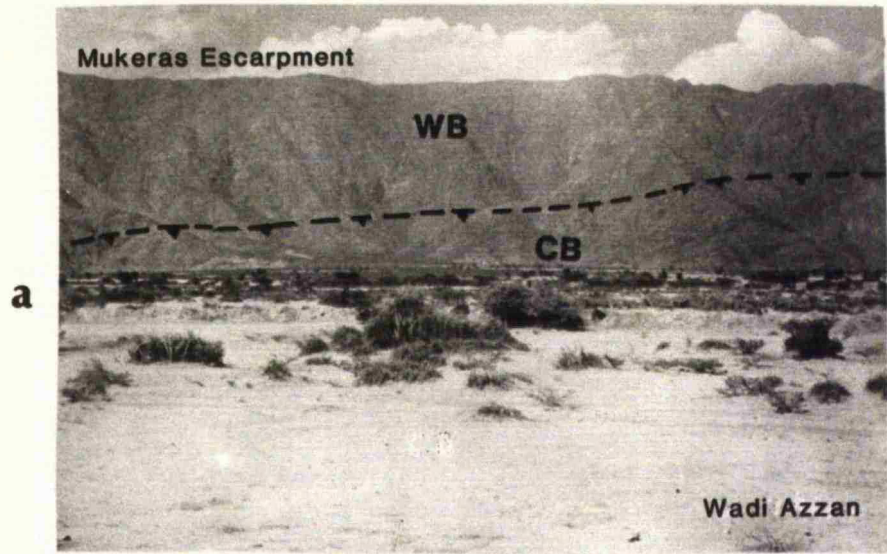
Fig. 2.8 Histograms showing the thickness of dykes with respect to their frequency.

**Plate 2.7**

Photographs to illustrate the field relations between the dyke swarms, their host rocks and the thrust zone between the western belt (W.B) and the central belt (C.B).

(a) General view of the Thereh-Mukeras Escarpment, host rock of the dyke swarms and the thrust zone between the western belt (W.B) and the central belt (C.B). Grid Reference 35 123. Looking SE.

(b & c) General view of the dyke swarms at Wadi Taran (Lowder), showing the intensity of the first NE-SW and the second E-W generations. Grid Reference 24 129. Looking NE.



central belt, as well as the dyke swarms, their host rocks and the thrust zone that separates the central (C.B) from the western belt (W.B) (see map Fig. 2.1 and plate 2.9 a,b). Therefore this alkali granite is the latest intrusion in the whole Lowder-Mudiah area.

### **2.4.3 Petrography of the Dykes and their Host Rocks**

#### **2.4.3.1 The Dyke Swarms**

Although these rocks are not strongly deformed, they do show recrystallization and greenschist facies mineralogy containing albite, epidote, actinolite and tremolite. Some have a mid-amphibolite facies mineralogy, and contain oligoclase, epidote, biotite, hornblende, and these dykes are enriched in opaque iron oxides and sphene, and are locally sheared.

##### **2.4.3.1.1 Basaltic Andesite Dykes**

These are melanocratic, porphyritic rocks that contain plagioclase phenocrysts in a matrix of ferromagnesian minerals, and minor quartz. They have ophitic and sub-ophitic textures. Main phases and modal contents are: slightly sericitized plagioclase (andesine, An 42) about 45%, clinopyroxene and weakly chloritized hornblende about 35%, slightly sericitized alkali feldspar (orthoclase) about 10%, and quartz 10%. Sericite, chlorite and calcite are alteration products of other minerals, and there is some opaque oxide (hematite).

##### **2.4.3.1.2 Andesite Dykes**

These rocks are melano- to mesocratic, some have a greenish colour and show porphyritic texture. In thin-section, the rocks show evidence of being altered, chloritized, sericitized and epidotized. Some rocks show locally preserved primary poikilitic textures but in others igneous textures have been destroyed during foliation development. Andesine (An 49) makes up about 55-60%, (actinolite-tremolite) and hornblende about 20-25%. Orthoclase amounts to about 20%, and shows poikilitic or poikiloblastic (sieve-like) texture and is slightly sericitized. Quartz (about 10%) shows myrmekitic texture. In addition there is minor biotite, chlorite and epidote, and opaque iron oxides (magnetite and hematite) and rare sphene.

##### **2.4.3.1.3 Rhyolite Dykes**

The rhyolites are leucocratic to mesocratic, porphyritic, with some glassy varieties.

**Plate 2.8**

Photomicrographs to illustrate the mineral constituents and textures of a gabbroic host rock and rhyolitic dykes.

(a and b) Augite (A) enclosed between plagioclases (P), ophitic texture, in gabbro host rock (sample BY111), under C.P.L. and P.P.L. respectively. See Fig. 2.7. Grid Reference 170 132 to 200 135.

(c and d) Phenocrysts of K-feldspar (K), and plagioclase (P) in a rhyolitic NE-SW dyke under C.P.L. and P.P.L. respectively. Sample BY64. Grid Reference 230 1285

(e and f) Sanidine phenocryst (S) and quartz-augen (Q) in rhyolite porphyry from a NE SW dyke (sample BY581), under C.P.L. and P.P.L. respectively. Grid Reference 231 1275

0 3 mm



a



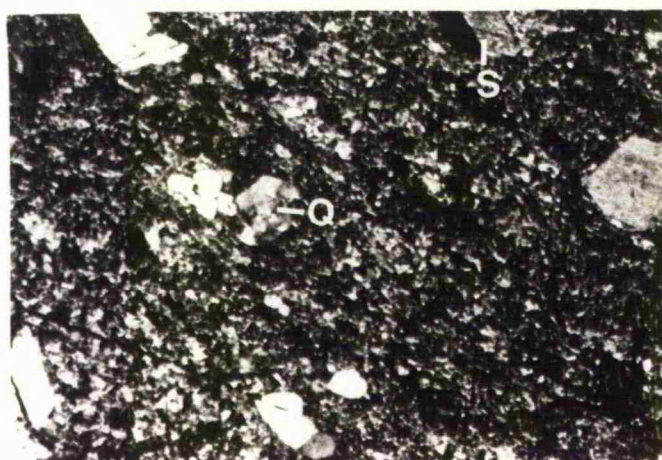
b



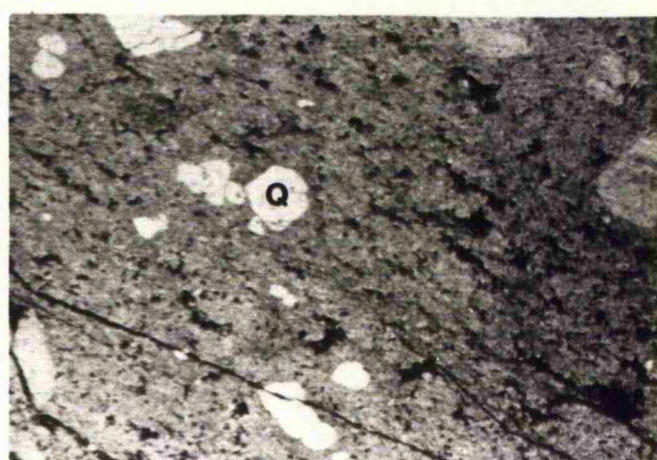
c



d



e



f

These rocks have a fine- to medium-grained groundmass with phenocrysts of quartz, and graphic, myrmekitic and perthitic textures. Some rocks contain glass and are slightly altered. Some show an early stage of cataclasis of quartz. Major constituents are: quartz about 20%. (some phenocrysts are augen-like (Plate 2.8 e&f), alkali feldspar (orthoclase, or sanidine Plate 2.8 e&f) and perthite is about 40%, plagioclase (albite, An 9) about 30%, is slightly sericitized and kaolinized, and mica (biotite and muscovite) about 10%. Alteration minerals include kaolinite, sericite, chlorite and epidote (sometimes along veins). There is a little accessory magnetite.

#### **2.4.3.2 The Host Rocks**

##### **2.4.3.2.1 Granite**

This is a coarse- and medium-grained, phaneritic, inequigranular, leucocratic, and slightly altered, epidotized granite. It shows early stages of cataclastic deformation (Plate 2.9 c, d) and is composed of the following major constituents: quartz 25%, showing wavy extinction, and myrmekitic texture; zoned K-feldspar (orthoclase, about 35%) shows perthitic texture (Plate 2.9 c,d), and is slightly sericitized and kaolinized; zoned plagioclase (albite, An10); about 30% and slightly sericitized and kaolinized; two generations of brown and green biotite form 10% and are chloritized. Other phases are hornblende, and epidote (in veins). Sericite, chlorite and kaolinite are alteration products. In addition, there are traces of opaque oxides, zircon, sphene and apatite. This granite has been weakly recrystallized, locally crushed and contains a considerable amount of epidote.

##### **2.4.3.2.2 Diorite-Granodiorite**

This is mesocratic, coarse- to medium-grained, and inequigranular and is composed of plagioclase, quartz and hornblende (Plate 2.9 e&f). Some rocks show a very weak foliation. Plagioclase (andesine, An32) amounts to about 30%, is sericitized and zoned (Plate 2.9 e&f). K-feldspar (orthoclase) is about 25% and slightly sericitized. Also there is Quartz (about 15%), hornblende (20%, slightly chloritized), and biotite (about 10%, slightly chloritized). Alteration minerals include chlorite, sericite and kaolinite; opaque oxide is magnetite. Accessories are zircon and sphene.

**Plate 2.9**

Photomicrographs to show textures and mineral constituents of the latest alkali granite of Wadi Mekhbezeh and the granite and granodiorite host rocks of the dyke swarm.

(a and b) Graphic and myrmekitic textures and green to brown amphiboles in the alkali granite of Wadi Mekhbezeh (Sample BY104), under C.P.L. and P.P.L. respectively. Grid Reference 370 119.

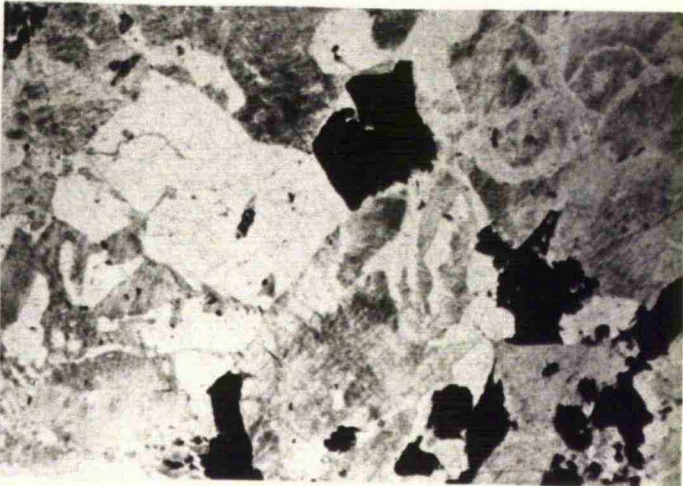
(c and d) Early stage cataclastic texture, perthite, sericitized zoned plagioclase, amphibole and epidote in the granite host rock of the dyke swarm (sample BY63), under C.P.L. and P.P.L. respectively. Grid Reference 2250 1282.

(e and f) Hornblende (H), quartz and zoned plagioclase (F), in granodiorite host rock of the dyke swarm (sample BY117), under C.P.L. and P.P.L. respectively. See Fig. 2.7. Grid Reference 170 132 to 200 135.

0 3mm



a



b



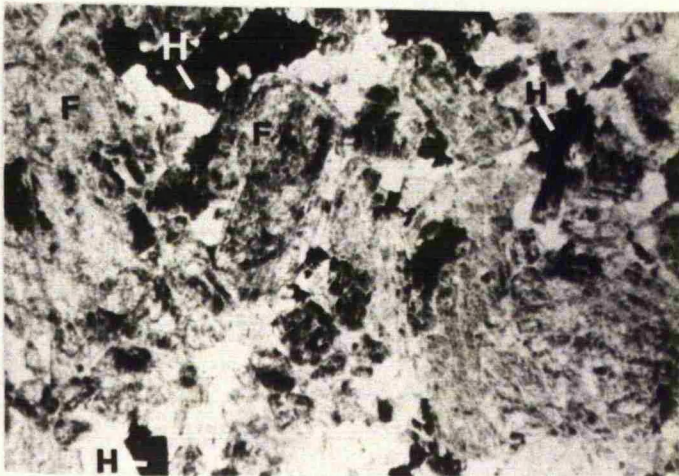
c



d



e



f

### 2.4.3.2.3 Gabbro

This is a melanocratic, coarse- to medium-grained, inequigranular rock, composed principally of plagioclase and pyroxenes, and it shows ophitic texture (Plate 2.8 a&b). Plagioclase (labradorite, An<sub>59</sub>) forms about 60%, and is very slightly sericitized. Clinopyroxene (augite) is about 35%. Minor constituents are, chlorite about 4%, sericite about 1% and magnetite 2%.

### 2.4.4 Geochronology of the Dyke Swarms and their Host Rocks

K/Ar and <sup>39</sup>Ar/<sup>40</sup>Ar dating was carried out at Leeds University by Dr. David Rex on four samples; two samples from the Thereh-Mukeras Escarpment representing the two different generations of dykes; one from the granitic host rock, and one from the alkali granite (for analytical details see Tables A 2.3, A2.4, A2.5, A2.6 Appendix).

Analyses for the hornblende concentrates from the early, NE-SW dykes yielded an age of 709±21 Ma, whereas the late set gave a K/Ar age of 587±18 Ma. Moreover, <sup>39</sup>Ar/<sup>40</sup>Ar analyses on hornblende concentrates from the two sets of dykes yielded ages of 694.1±23.1 Ma and 585.9±20.5 Ma, for the early and late sets respectively; the total average age is very near to the K/Ar age (see Fig. 2.9). These dates confirm the age relations established in the field, and also demonstrate that the dykes are Precambrian. A sample from the granitic host rock of the dykes yielded a K/Ar age of 740±22 Ma on biotite.

The alkali granitic intrusion at Wadi Mekhbezeh cuts the dyke swarms, host rocks, the gneisses of the central belt as well as the thrust zone, that separates the central belt (C.B) from the western belt (W.B), and is thus the latest intrusive body in the area. The age of this alkali granite given by K/Ar from a hornblende concentrate is 847±26 Ma, but this is older than the isotope age of the dykes. Thus the isotopic age relations are the reverse of the field relations. This sample was re-analyzed by the <sup>39</sup>Ar/<sup>40</sup>Ar method (see Fig. 2.9) which gave a value of 841.7±1.4 Ma. If this latest value of the alkali granite is correct, then the values given by the dyke swarm and their host rocks might represent reset ages rather than ages of intrusion; however, there are doubts concerning the alkali granite ages.

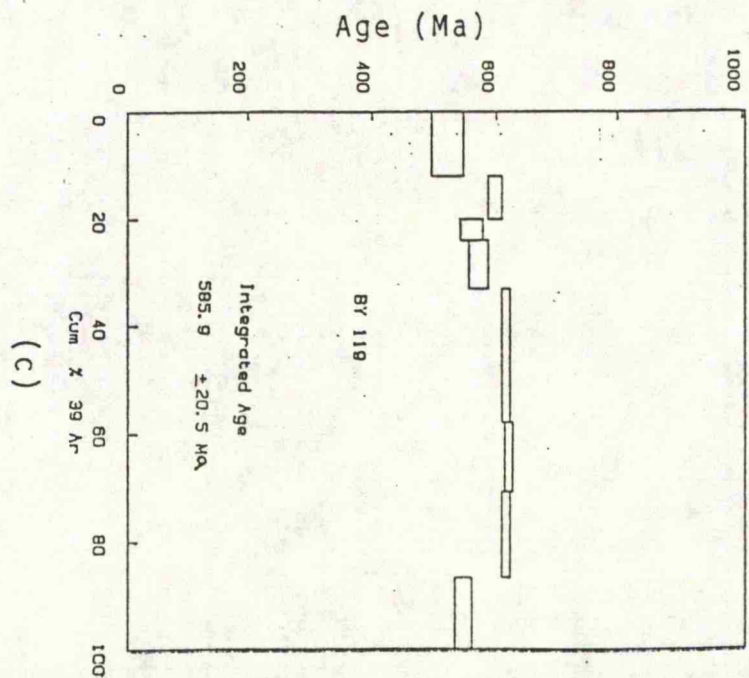
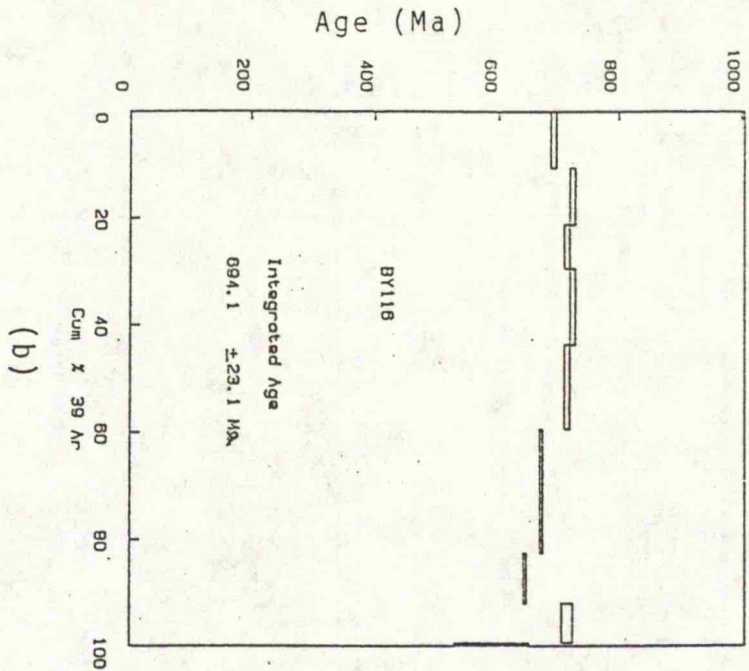
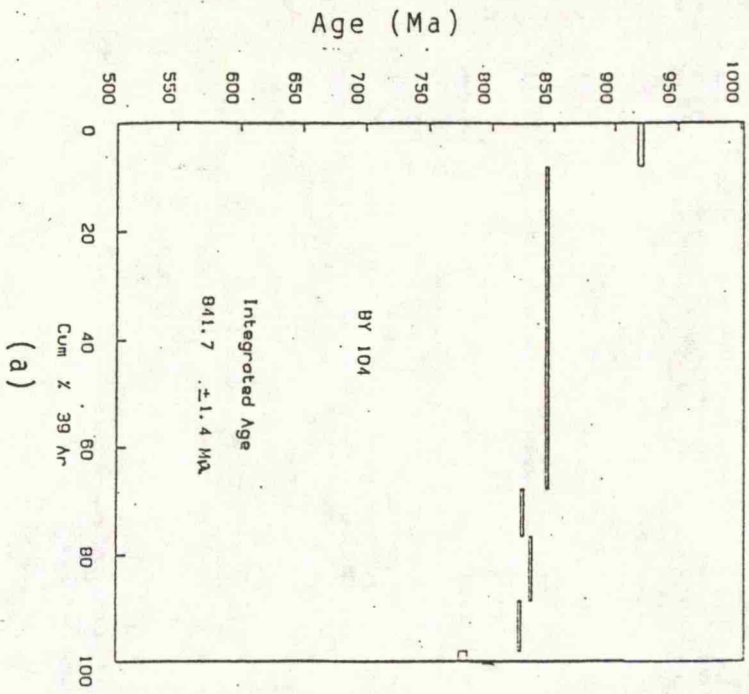


Fig. 2.9 Diagrams for  $^{39}\text{Ar}/^{40}\text{Ar}$  age determination on hornblende concentrates from the (a) latest alkali granite (sample BY104, Wdi Mekhbezh, Grid Reference 38 12), (b) early NE-SW dyke (sample BY116, see Fig. 2.7, Grid Reference between 170 132 & 200 135) and (c) late E-W to NW-SE dyke (sample BY119, see Fig. 2.7, Grid Reference between 170 132 & 200 135).

### 2.5 Conclusion

The basement rocks of the Lowder-Mudiah area are divided into three main belts, separated by two northeast-striking ductile shear (thrust) zones.

The highly metamorphosed central belt is composed of grey and pink granitic gneisses, including lenses and patches of sheared quartz-biotite gneiss and amphibolite intruded by grey and pink pegmatitic granites. Migmatites occur locally and carbonatite dykes intrude the granitic gneiss. Petrographically the granitoid gneisses are leucocratic, foliated (gneissose), with elongated fragments, mylonitic and myrmekitic, mylonitic textures. They are composed mainly of quartz, plagioclase, K-feldspar, biotite, muscovite and epidote. Zircon, sphene and apatite are accessories. The amphibolites are melanocratic, medium to coarse grained, foliated (schistose to gneissose) with microfolds, elongated fragments, shear fabrics and myrmekitic texture and are composed of hornblende, plagioclase, scapolite, biotite and quartz. In addition to scapolite, other alteration minerals are sericite, chlorite and epidote. Sphene, zircon and apatite are accessories.

The granitoid rocks are leucocratic, medium to coarse grained, showing graphic, perthitic, myrmekitic and rapakivi textures. Main constituents are quartz, plagioclase (zoned), K-feldspar, biotite, muscovite and hornblende (in some instances). Apatite, zircon, sphene, garnet and tourmaline (in some cases) are accessories. Most of these rocks show slight sericite and chlorite alterations.

The Mudiah metavolcanics with the subordinate marbles and sulphide-bearing veins, represent the eastern belt. These rocks were metamorphosed under low-grade greenschist facies conditions, and deformed in open antiforms and synforms. Petrographically the Mudiah metavolcanics are melanocratic, fine to medium grained, phaneritic, porphyritic, foliated (schistose), with shear fabrics and elongated fragments. The mafic varieties are composed of hornblende, plagioclase, biotite, clinopyroxene, quartz, epidote, and chlorite. Epidote and chlorite are the main alteration minerals. The felsic metavolcanics are composed of quartz, plagioclase, K-feldspar, biotite, muscovite, epidote and chlorite. The main alteration minerals are epidote and chlorite. Apatite is the accessory mineral.

The Mukeras Escarpment in the Lowder-Mudiah area is occupied by the third major lithologic western belt which is separated from the central belt by a major southeasterly-dipping ductile thrust. The belt contains mostly intrusive batholiths, composed of medium-grained granite in the northeast, and of granodiorite, diorite and gabbro in the southwest. These rocks are traversed by a major bimodal dyke swarms of an early generation ( $709 \pm 21$  Ma) striking northeast-southwest, and a minor late generation ( $587 \pm 18$  Ma) striking east-west to almost NW-SE cuts the early dykes. Although these rocks are not strongly deformed, they do show recrystallization and greenschist facies mineralogy with albite, epidote, actinolite and tremolite. Some have a mid- amphibolite facies mineralogy, and contain oligoclase, epidote, biotite, hornblende, and these dykes are enriched in opaque iron oxides and sphene, and are locally sheared. Other minerals are clinopyroxene (augite) and andesine in the basalts and basaltic-andesites; orthoclase and albite in the rhyolites. These rocks are, porphyritic and show graphic, perthitic and myrmekitic textures.

The basement rocks, in the eastern and southeastern Lowder-Mudiah area, are unconformably overlain by well-bedded southeasterly dipping Jurassic limestone, with a basal conglomeratic sandstone.

## CHAPTER 3

### PETROCHEMISTRY

#### 3.1 Introduction

One hundred and eighteen representative samples were collected (see Map Fig. 2.3; 2.7) of granitoids, (quartzo-feldspathic) granitoid gneisses, amphibolites, metavolcanics, dykes and their host rocks and carbonatites. Thirty five samples representing the Lowder-Muiah granitoids, Mudiah metavolcanics, the early generation ( $709 \pm 21$  Ma) Mukeras dykes and their host rocks (Tables 3.1, 3.2, 3.3, 3.4) were chemically analysed for their major and trace element contents. Forty one carbonatite samples were also chemically analysed and are discussed separately in Chapter 5. For the Grid References of the samples and localities, see the Appendix (A2.7; A2.8).

The normative minerals were calculated, using the  $\text{Fe}_2\text{O}_3/\text{FeO}$  ratio of 0.15 (see Tables 3.1, 3.2, 3.3, 3.4. Rock types for the Mudiah metavolcanics and Mukeras dykes in Tables 3.3, 3.4 and 3.5 were defined by  $\text{SiO}_2$  contents, thus: B = basalt (< 52%), BA = basaltic andesite (52 - 56%), A= andesite (56 - 63%), D= dacite (63-69%), R = rhyolite (> 69%).

The aim of this work was to place constraints on the petrogenetic processes and if possible the tectonic setting of the key rocks from the southern parts of the Arabian Shield in Yemen.

Spiderdiagrams were plotted using the Stern et al.(1988) data; in order to compare the Mudiah mtavolcanics and Mukeras dykes with the bimodal dykes in the Northeastern Desert of Egypt the data are given in the Appedix (A3).

#### 3.2 Analytical Techniques

The samples were cut into chips using a hammer and a hydraulic jaw splitter to remove weathered surfaces, and washed with tap water to remove dust, then dried. Chips were further crushed using a steel jaw crusher, coarse then fine. Quartering was carried out using a manual sample divider. About 150 grams were ground to a fine powder (< 240 mesh) in an agate Tema.

**Abbreviations in Tables 3.1, 3.2, 3.3 and 3.4**

L10040 = Leicester University Pellet Serial Number.

ALTTEX = Alteration and Textures

GR = Granite

R = Rhyolite

B = Basalt

BA = Basaltic Andesite

Ch = Chlorite

Sc = Sericite

Ep = Epidote

P = Pegmatite

Po = Porphyritic

Table 3.1 The granitoids of Lowder-Mudiah Yemen

PELLET SAMPLE ROCK TYP ALTTX	L10008 BY30C GR ScCh	L10015 BY18A GR ScCh	L10020 BY36C GR Sc	L10025 BY18C GR Sc	L10026 BY19A GR Sc	L10033 BY18B GR ScCh
SiO <sub>2</sub>	72.4	74.0	71.8	71.2	73.3	73.3
TiO <sub>2</sub>	0.26	0.22	0.39	0.38	0.26	0.21
Al <sub>2</sub> O <sub>3</sub>	13.6	13.9	13.9	13.7	13.5	14.1
Fe <sub>2</sub> O <sub>3</sub>	2.1	1.8	3.1	2.9	2.1	1.8
MnO	0.04	0.03	0.04	0.05	0.05	0.03
MgO	0.3	0.2	0.6	0.5	0.3	0.3
CaO	1.4	1.4	1.6	1.6	1.6	1.5
Na <sub>2</sub> O	3.1	3.2	3.2	3.1	3.4	3.4
K <sub>2</sub> O	4.83	4.93	4.74	4.85	4.45	4.89
P <sub>2</sub> O <sub>5</sub>	0.07	0.06	0.12	0.12	0.07	0.06
LOI	0.49	0.33	0.40	0.50	0.36	0.47
Total	98.55	100.09	99.93	98.94	99.36	100.02

## Trace elements in parts per million

CR	8.6	3.1	5.6	11.1	4.6	0.7
V	16.1	11.6	29.5	28.6	16.3	11.1
NB	13.4	13.4	9.6	10.7	15.9	11.8
ZN	38.0	38.7	45.5	53.1	45.4	35.2
NI	1.7	2.5	2.1	6.6	2.9	1.9
ZR	209.6	190.8	352.0	348.9	199.2	188.2
Y	21.8	15.8	21.9	20.9	21.4	15.7
BA	943.5	798.0	1306.2	966.1	659.6	804.8
SR	161.8	154.5	225.3	178.7	140.3	166.5
RB	214.4	216.8	159.1	235.5	203.7	214.6
TH	41.1	47.6	57.2	47.8	41.7	44.3
GA	16.0	19.5	18.4	18.1	21.5	19.7
LA	82.1	66.2	142.7	106.2	56.2	60.9
CE	149.4	111.3	248.6	189.6	102.4	100.9
ND	45.0	34.0	77.1	63.7	35.4	32.5

## Ratios

K / Na	1.7	1.7	1.7	1.7	1.5	1.6
Fe/Mg	7.2	8.6	5.5	6.6	7.8	7.9
K / RB	188.1	189.4	248.3	171.9	182.2	190.0
RB/SR	1.3	1.4	0.7	1.3	1.5	1.3
SR/BA	0.2	0.2	0.2	0.2	0.2	0.2
K / BA	42.7	51.4	30.2	41.9	56.3	50.7
K / ZR	192.4	215.2	112.2	116.0	186.3	216.6
ZR/NB	15.6	14.2	36.7	32.6	12.5	15.9

C.I.P.W. norms calculated using FeO:Fe<sub>2</sub>O<sub>3</sub>=0.85:0.15

Qtz	31.26	32.39	29.35	29.02	31.73	30.46
Cor	0.85	0.92	0.91	0.75	0.44	0.68
Or	28.57	29.13	28.01	28.67	26.33	28.89
Ab	26.53	26.99	27.05	26.61	28.75	28.55
An	6.32	6.60	7.15	6.98	7.30	7.11
Hy	3.33	2.70	5.24	4.67	3.26	2.85
Mt	0.36	0.31	0.53	0.50	0.36	0.31
Ilm	0.49	0.42	0.74	0.72	0.49	0.40
Ap	0.17	0.15	0.29	0.27	0.16	0.14

Table 3.1 The granitoids of Loucer-Mudiah Yemen

PELLET	L10040	L11663	L11665	L11678
SAMPLE	BY74	BY91	BY93	BY106
ROCK TYP	GR	GR	GR	GR
ALTTEX		Sc		
SiO <sub>2</sub>	72.4	74.1	73.6	72.3
TiO <sub>2</sub>	0.32	0.21	0.28	0.27
Al <sub>2</sub> O <sub>3</sub>	14.6	13.7	14.0	14.0
Fe <sub>2</sub> O <sub>3</sub>	2.4	1.6	1.9	2.2
MnO	0.05	0.05	0.05	0.04
MgO	0.5	0.2	0.3	0.4
CaO	1.6	1.2	1.2	1.4
Na <sub>2</sub> O	3.5	3.2	3.4	3.2
K <sub>2</sub> O	4.78	5.03	4.64	5.08
P <sub>2</sub> O <sub>5</sub>	0.10	0.04	0.06	0.07
LOI	0.42	0.61	0.59	0.35
Total	100.60	99.96	100.09	99.29

## Trace elements in parts per million

CR	4.9	4.1	8.4	11.6
V	22.2	12.3	15.1	15.2
NB	14.5	13.7	19.6	10.3
ZN	46.2	35.1	41.3	39.8
NI	3.3	0.8	0.2	1.2
ZR	266.7	148.3	188.6	225.0
Y	20.5	29.1	32.2	20.3
BA	1329.8	788.0	672.0	956.4
SR	232.0	154.8	171.8	166.3
RB	216.8	226.7	217.5	203.2
TH	52.4	40.7	34.5	47.3
GA	21.7	17.6	17.7	17.4
LA	98.1	64.0	63.0	84.6
CE	160.2	125.3	125.5	153.9
ND	47.8	43.8	40.9	48.7

## Ratios

K / Na	1.5	1.7	1.5	1.8
Fe / Mg	5.6	8.1	6.8	7.1
K / RB	183.8	185.1	178.1	208.4
RB / SR	0.9	1.5	1.3	1.2
SR / BA	0.2	0.2	0.3	0.2
K / BA	30.0	53.3	57.7	44.3
K / ZR	149.4	283.0	205.4	188.2
ZR / NB	18.4	10.8	9.6	21.8

C.I.P.W. norms calculated using FeO:Fe<sub>2</sub>O<sub>3</sub>=0.85:0.15

Qtz	28.84	32.40	32.17	29.64
Cor	1.07	0.88	1.35	0.79
Cr	28.25	29.70	27.42	30.05
Ab	29.41	27.42	28.69	27.07
An	7.10	5.58	5.65	6.66
Hy	4.05	2.48	3.07	3.50
Mt	0.41	0.27	0.33	0.38
Ilm	0.61	0.40	0.53	0.51
Ap	0.23	0.10	0.13	0.16

Table 3.2 Mudiah metovolcanics OF LOWDER-MUDIAH YEMEN

PELLET SAMPLE ROCK TYP ALTTEX	L10001 BY2A R Ch	L10003 BY3 R ScPo	L10004 BY7B R ScPo	L10029 BY2C B Ep	L10037 BY85 R ChSc	L10038 BY86 R ChSc	L10039 BY87 B Ep
SiO <sub>2</sub>	72.7	79.7	78.7	50.2	78.1	76.9	49.9
TiO <sub>2</sub>	0.29	0.16	0.18	1.45	0.26	0.28	1.35
Al <sub>2</sub> O <sub>3</sub>	15.3	10.2	11.5	14.4	11.4	11.3	15.1
Fe <sub>2</sub> O <sub>3</sub>	1.9	2.2	2.4	12.3	2.3	2.2	12.5
MnO	0.06	0.03	0.01	0.20	0.02	0.03	0.19
MgO	0.7	0.1	0.0	6.5	0.4	0.7	6.5
CaO	1.6	0.2	0.1	10.7	0.3	0.9	10.3
Na <sub>2</sub> O	4.6	0.3	3.9	1.8	1.8	1.8	2.1
K <sub>2</sub> O	3.20	7.42	3.79	0.44	4.94	4.33	0.44
P <sub>2</sub> O <sub>5</sub>	0.10	0.02	0.00	0.22	0.05	0.07	0.18
LOI	0.75	0.55	0.28	1.55	0.98	1.42	1.56
Total	101.30	100.87	101.03	99.77	100.62	99.75	100.18

Trace elements in parts per million

CR	0.0	3.6	1.5	226.9	6.6	5.3	249.4
V	17.1	13.3	2.1	276.3	19.1	33.3	273.4
NB	18.2	24.4	28.6	5.1	20.6	14.7	4.8
ZN	31.0	32.4	17.5	98.6	51.9	56.2	102.5
NI	1.9	1.3	2.0	48.9	3.0	5.9	53.6
ZR	385.1	656.9	844.3	115.4	437.5	314.8	93.0
Y	66.0	84.6	91.0	33.0	75.2	54.8	29.1
BA	293.9	103.1	52.8	128.4	303.0	284.8	135.9
SR	92.3	32.9	11.2	292.4	75.3	84.8	296.1
RB	104.9	283.5	98.0	11.5	143.6	136.8	9.2
TH	19.0	19.4	29.8	4.8	22.0	15.6	3.2
GA	14.6	19.9	23.0	22.8	24.3	18.0	24.4
LA	64.4	96.4	92.1	7.4	54.3	54.4	9.2
CE	124.7	168.4	167.8	23.9	115.3	111.0	15.6
ND	58.2	91.1	90.9	14.4	55.1	49.2	12.6

Ratios

K / Na	0.8	23.9	1.1	0.3	3.1	2.8	0.2
Fe/Mg	3.1	28.5	281.8	2.2	6.1	3.9	2.2
K / RB	255.1	218.6	321.6	322.7	288.5	266.3	398.8
RB/SR	1.1	8.6	8.8	0.0	1.9	1.6	0.0
SR/BA	0.3	0.3	0.2	2.3	0.2	0.3	2.2
K / BA	91.1	601.0	597.0	28.9	136.7	127.9	27.0
K / ZR	69.5	94.2	37.3	32.2	94.7	115.7	39.5
ZR/NB	21.2	26.9	29.5	22.6	21.2	21.4	19.4

C.I.P.W. norms calculated using FeO:Fe<sub>2</sub>O<sub>3</sub>=0.85:0.15

Qtz	28.32	48.52	39.59	4.18	46.31	46.33	2.25
Cor	1.66	1.24	0.63	--	2.64	2.34	--
Gr	18.91	43.87	22.38	2.60	29.20	25.57	2.57
Ab	39.31	2.95	33.42	14.91	15.25	14.85	17.49
An	7.05	0.83	0.72	30.15	1.15	3.83	30.73
Ei	--	--	--	17.90	--	--	16.01
Hy	4.03	3.00	3.04	22.02	3.88	4.18	23.35
Mt	0.33	0.38	0.42	2.13	0.40	0.38	2.16
Ilm	0.55	0.30	0.34	2.75	0.49	0.52	2.56
Ap	0.24	0.04	0.01	0.51	0.11	0.15	0.41

Table 3.3 The bimodal Mukeras dyke swarms (early NE-SW) LOWDER-MUDIAH YEMEN

PELLET SAMPLE ROCK TYP ALTTEX	L11673 BY101 B Ep	L11681 BY110 B Ch	L11683 BY112 B Ep	L11685 BY114 B Ep	L11687 BY116 BA Ch	L10045 BY64 R ScPo	L11671 BY99 R Sc	L11674 BY102 R Sc
SiO <sub>2</sub>	48.1	47.8	49.1	50.8	51.9	77.9	69.0	73.2
TiO <sub>2</sub>	2.08	1.45	1.60	2.17	1.60	0.17	0.33	0.36
Al <sub>2</sub> O <sub>3</sub>	13.4	15.3	14.2	13.4	13.5	10.8	14.7	12.9
Fe <sub>2</sub> O <sub>3</sub>	14.3	12.5	13.2	15.1	13.4	1.5	2.8	2.9
MnO	0.23	0.18	0.21	0.22	0.21	0.02	0.04	0.03
MgO	6.2	7.8	6.9	5.4	4.5	0.1	0.7	0.1
CaO	10.2	8.9	10.4	9.1	8.3	0.5	1.7	1.0
Na <sub>2</sub> O	2.6	2.6	2.4	2.7	2.9	2.5	4.8	4.8
K <sub>2</sub> O	0.47	1.09	0.60	0.87	1.11	5.19	2.92	3.01
P <sub>2</sub> O <sub>5</sub>	0.24	0.26	0.19	0.29	0.20	0.02	0.11	0.04
LOI	1.88	1.02	1.21	0.48	0.95	0.27	1.04	0.34
Total	99.74	98.83	100.02	100.52	98.50	98.95	98.18	98.67

## Trace elements in parts per million

CR	136.1	80.7	236.7	64.8	14.4	4.8	5.4	2.8
V	329.1	229.2	296.2	364.8	300.7	4.9	24.4	9.3
NB	5.8	5.1	4.1	5.6	8.2	29.2	7.8	18.7
ZN	116.5	84.8	111.8	128.5	103.1	14.3	23.5	11.0
NI	38.5	94.0	54.7	35.2	16.5	2.4	2.4	0.6
ZR	145.9	158.3	109.4	159.9	168.2	585.8	244.4	548.1
Y	34.4	34.1	30.0	40.4	37.9	96.3	21.9	60.6
BA	187.2	233.2	218.5	316.3	272.2	631.2	896.7	380.0
SR	259.6	348.4	279.6	297.1	258.6	69.5	205.1	86.7
RB	21.6	32.7	15.5	20.4	31.7	113.7	80.7	42.0
TH	5.2	0.0	2.5	2.8	0.0	30.1	11.9	19.4
GA	23.0	29.1	21.3	23.3	24.2	15.7	17.4	20.6
LA	11.0	15.6	8.3	11.2	17.5	47.6	30.5	50.7
CE	26.0	35.0	18.3	38.9	44.6	106.8	62.9	113.8
ND	16.3	20.5	10.1	19.9	22.0	54.8	22.1	50.1

## Ratios

K / Na	0.2	0.5	0.3	0.4	0.4	2.3	0.7	0.7
Fe / Mg	2.7	1.9	2.2	3.2	3.5	25.2	5.0	24.2
K / RB	182.9	279.3	327.8	354.0	293.0	380.1	303.1	596.9
RB / SR	0.1	0.1	0.1	0.1	0.1	1.6	0.4	0.5
SR / BA	1.4	1.5	1.3	0.9	1.0	0.1	0.2	0.2
K / BA	21.1	39.2	23.3	22.8	34.1	68.5	27.3	66.0
K / ZR	27.1	57.7	46.4	45.2	55.2	73.8	100.1	45.7
ZR / NB	25.2	31.0	26.7	28.6	20.5	20.1	31.3	29.3

C.I.P.W. norms calculated using FeO:Fe<sub>2</sub>O<sub>3</sub>=0.85:0.15

Qtz	--	--	--	1.84	4.01	41.39	23.97	29.97
Cor	--	--	--	--	--	0.19	0.75	0.05
Or	2.76	6.43	3.57	5.12	6.55	30.68	17.23	17.79
Ab	21.75	21.61	19.98	22.65	24.22	21.35	40.70	40.56
An	23.63	27.16	26.39	22.04	20.83	2.31	7.85	4.66
Di	21.16	12.63	19.85	17.55	15.92	--	--	--
Hy	17.18	10.89	19.72	22.14	19.02	1.99	5.05	3.77
Ol	3.14	12.51	2.38	--	--	--	--	--
Mt	2.47	2.15	2.28	2.61	2.30	0.26	0.49	0.50
Ilm	3.95	2.74	3.04	4.12	3.05	0.32	0.62	0.68
Ap	0.56	0.60	0.45	0.66	0.47	0.04	0.25	0.10

Table 3.3 The bimodal Mukeras dyke swarms (early NE-SW) LOWDER-MUDIAH YEMEN

PELLET SAMPLE ROCK TYP ALTTEX	L10017 BY34D1 B Ch	L10042 BY61 B Ch	L10046 BY65 B Ep	L10047 BY66 BA Ep	L11672 BY100 B Ch
SiO <sub>2</sub>	47.3	46.7	48.7	51.0	48.0
TiO <sub>2</sub>	1.39	1.31	2.07	1.32	1.61
Al <sub>2</sub> O <sub>3</sub>	12.9	12.5	13.6	15.3	11.8
Fe <sub>2</sub> O <sub>3</sub>	14.0	14.3	14.3	11.5	14.6
MnO	0.23	0.22	0.24	0.18	0.23
MgO	8.4	8.7	6.3	6.6	7.7
CaO	9.1	9.7	10.0	10.7	9.9
Na <sub>2</sub> O	2.3	2.3	2.6	2.1	2.1
K <sub>2</sub> O	0.70	0.47	0.88	0.56	0.58
P <sub>2</sub> O <sub>5</sub>	0.21	0.23	0.25	0.15	0.23
LOI	2.56	2.24	1.62	1.90	2.10
Total	99.11	98.64	100.64	101.22	98.86

## Trace elements in parts per millicn

CR	132.9	174.5	146.3	294.6	186.6
V	275.4	283.0	338.5	230.3	306.1
NB	4.5	5.2	7.6	4.5	5.9
ZN	77.5	102.1	92.8	94.3	113.2
NI	73.4	71.4	45.2	69.3	46.9
ZR	122.4	120.5	146.7	101.9	129.5
Y	30.8	30.0	38.9	25.3	30.4
BA	186.9	189.7	404.2	266.2	393.7
SR	294.4	291.9	245.0	267.6	273.9
RB	26.2	10.2	29.2	19.3	19.3
TH	0.0	0.7	2.7	0.2	5.2
GA	23.3	22.8	25.3	24.5	19.0
LA	7.2	6.3	9.8	8.0	12.3
CE	20.6	15.9	20.4	22.9	29.0
NC	11.2	13.8	13.4	12.1	17.5

## Ratios

K / Na	0.3	0.2	0.4	0.3	0.3
Fe / Mg	1.9	1.9	2.6	2.0	2.2
K / RB	228.1	390.7	254.6	243.9	253.8
RB / SR	0.1	0.0	0.1	0.1	0.1
SR / BA	1.6	0.6	1.5	1.0	0.7
K / BA	32.0	21.0	18.4	17.7	12.4
K / ZR	48.8	33.1	50.7	46.2	37.8
ZR / NB	27.2	23.2	19.3	22.6	21.9

C.I.P.W. norms calculated using FeO:Fe<sub>2</sub>O<sub>3</sub>=0.85:0.15

Qtz	--	--	--	2.88	--
Or	4.15	2.77	5.21	3.29	3.41
Ab	19.21	19.77	22.31	17.52	17.81
An	22.89	22.17	22.69	30.94	21.07
Di	16.94	20.02	21.10	17.38	21.87
H <sub>y</sub>	17.45	12.29	13.45	21.47	23.23
Ol	9.12	12.63	6.06	--	1.99
Mt	2.42	2.47	2.46	1.98	2.53
Ilm	2.65	2.49	3.92	2.52	3.05
Ap	0.50	0.54	0.58	0.35	0.53

Table 3.4 The host rocks for Mukerās dyke swarms LOWDER-MUDIAH YEMEN

PELLET SAMPLE ROCK TYP ALTTEX	L11682 BY111 GABBRO	L11684 BY113 DIORITE	L11686 BY115 QZDIOR	L11688 BY117 QZDIOR	L10044 BY63 GRANITE ScCh
SiO <sub>2</sub>	50.4	52.6	58.8	67.7	75.2
TiO <sub>2</sub>	1.37	1.01	0.88	0.50	0.26
Al <sub>2</sub> O <sub>3</sub>	15.9	14.2	19.3	15.7	13.3
Fe <sub>2</sub> O <sub>3</sub>	11.9	11.0	6.8	3.9	1.9
MnO	0.19	0.20	0.16	0.09	0.03
MgO	7.4	6.7	1.9	1.2	0.4
CaO	10.8	9.2	5.6	3.7	1.2
Na <sub>2</sub> O	2.4	2.1	4.5	4.0	3.9
K <sub>2</sub> O	0.45	1.22	1.85	2.33	4.04
P <sub>2</sub> O <sub>5</sub>	0.16	0.10	0.32	0.16	0.07
LOI	0.90	1.44	0.92	0.47	0.62
Total	101.76	99.58	100.98	99.64	100.96

Trace elements in parts per million

CR	167.1	228.7	6.5	8.1	1.5
V	214.3	246.0	65.2	52.3	15.0
NB	5.4	5.0	8.8	6.4	9.6
ZN	85.8	111.2	116.9	66.8	18.5
NI	96.9	81.9	1.1	1.2	2.1
ZR	91.9	63.9	445.0	187.3	160.8
Y	27.4	22.6	31.6	16.1	25.8
BA	141.0	291.0	1043.2	853.9	1054.2
SR	273.3	165.1	575.7	394.6	114.2
RB	9.3	37.6	52.5	70.0	112.4
TH	2.1	4.7	6.8	9.1	15.2
GA	13.3	17.6	25.7	18.4	18.1
LA	8.1	4.9	55.7	32.4	35.3
CE	31.8	9.6	108.5	62.2	66.1
ND	14.6	6.9	43.8	21.4	25.5

Ratios

K / Na	0.2	0.7	0.5	0.7	1.2
Fe/Mg	1.9	1.9	4.1	3.8	5.7
K / RB	406.2	272.9	294.7	278.0	300.4
RB/SR	0.0	0.2	0.1	0.2	1.0
SR/BA	1.9	0.6	0.6	0.5	0.1
K / BA	26.8	35.3	14.8	22.8	32.0
K / ZR	41.1	160.6	34.8	103.9	210.0
ZR/NB	17.0	12.8	50.6	29.3	16.8

C.I.P.W. norms calculated using FeO:Fe<sub>2</sub>O<sub>3</sub>=0.85:0.15

Qtz	--	4.45	7.97	24.32	33.18
Cor	--	--	0.46	0.33	0.58
Gr	2.66	7.20	10.91	13.79	23.89
Ab	20.29	17.51	37.98	33.52	32.97
An	31.37	25.76	25.75	17.30	5.30
Di	17.19	15.65	--	--	--
Hy	21.18	22.57	12.83	7.60	3.27
Ol	2.11	--	--	--	--
Mt	2.05	1.89	1.17	0.67	0.34
Ilm	2.60	1.91	1.67	0.95	0.49
Ap	0.38	0.24	0.73	0.36	0.17

Analyses were carried out on a Philips PW 1400 X-ray fluorescence spectrometer at the University of Leicester, using Rh and W tubes.

Major oxides were analysed by XRF, on fusion beads, using samples prepared by the technique of Marsh et al. (1980 and 1983) whereas trace elements were analysed by XRF from pressed pellets (see Appendix A3 for estimates of precision and accuracy). Pellets were made from the fine powder by adding 15-20 drops of an aqueous solution of polyvinyl alcohol (Moviol) at 15 tonnes per square inch pressure in a steel die.

The determination of the weight loss on ignition (LOI) was performed in Pt crucibles. The weight of the crucible (W1) and the weights of the crucible plus sample before (W2) and after ignition (W3) are recorded in order to determine the weight loss. The ignition was performed in a muffle furnace at 950° C for 1 to 1.5 hours. After ignition the samples were allowed to cool down to room temperature in a dessicator before reweighing.

The percentage weight loss (LOI) was then determined from the following formula :

$$\text{LOI} = 100 \times (W2 - W3) / (W2 - W1)$$

For further details of sample preparation and analytical techniques see Appendix A3.

### 3.3 Nomenclature

Element symbols and oxides rather than full names are used in the text. In addition various elements are assigned to groups according to their abundance or properties:

Major elements: Si, Al, Fe, Mg, Ca, Na, K, Ti, Mn, P, usually quoted as oxides in wt.%.

Trace elements: usually given in ppm (generally <1000 ppm) and include Cr, V, Nb, Zn, Ni, Zr, Y, Ba, Sr, Rb, Th, Ga, La, Ce, and Nd. Large ion lithophile elements (LILE): Rb, Ba, Sr, Th, U, and also K, have ionic radii larger than the common rock-forming elements. High field strength elements (HFSE): Zr, Nb, Hf, Ta. Refractory elements: Ni, Cr, V. Rare earth elements (REE) form their own group (the lanthanides) in the periodic table, and are also given in ppm. Light rare earth elements (LREE): La, Ce, Pr, Nd, Sm, Eu. Heavy rare earth elements (HREE): Gd, Dy, Ho, Er, Yb, Lu.

### 3.4 Granitoids

These rocks are mainly granites that typically contain muscovite and some biotite. In the granitoids muscovite pockets are common, and garnet and tourmaline are present in some types. The granitoid rocks (see Table 2.3) are leucocratic, coarse grained and

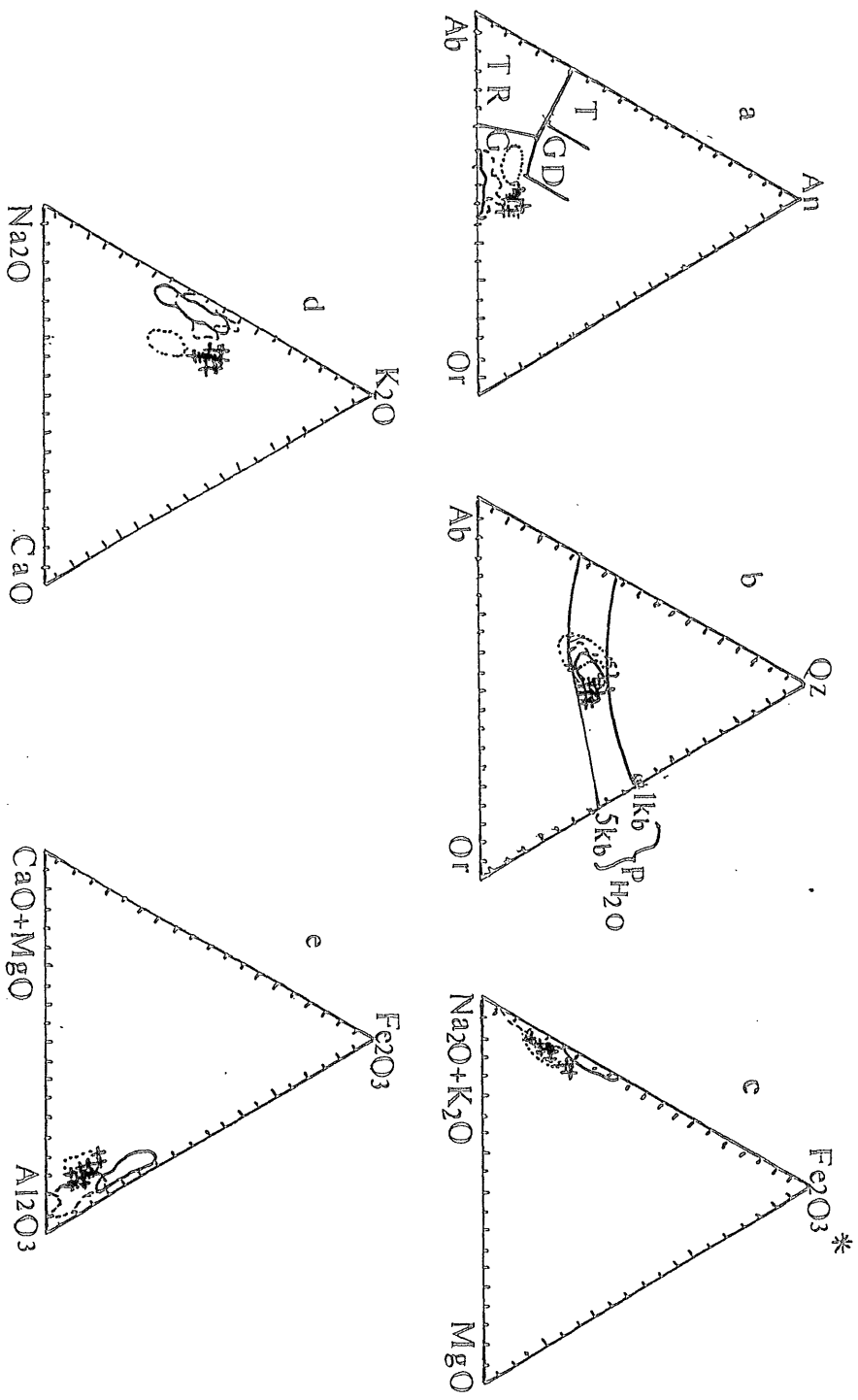


Fig. 3.1 a - e Triangular variation diagrams, for the Lower-Mudlah granitoids (crosses), the young assemblage of the Central Hijaz granitoids, alkali granite (solid line), alkali-feldspar granite (dashed line) and monzogranite (dotted line) (after Jackson et al., 1984). (fields, G=Granite, GD=Granodiorite, T=Tonalite, TR=Trondhjemite, after Barker, 1979).

show graphic, myrmekitic and rapakivi textures. They are composed of quartz (10 - 30%), plagioclase (20 - 30%), K - feldspar (20 - 40%), biotite (5 - 10%), muscovite (5 - 10%) and hornblende < 5% (in some types). Fe - oxide (magnetite), apatite, zircon, sphene, garnet and tourmaline (rarely) are accessories. Most rocks show slight sericite and chlorite alteration. They have zoned plagioclase (e.g. sample BY16N, see Plate 2.3e,f), rapakivi texture (e.g. sample BY19B, see Plate 2.3a), and perthitic and graphic textures (e.g. sample BY19C, see Plate 2.3 b).

Chemically the granitoids are very siliceous (70 - 74% SiO<sub>2</sub>) with high K<sub>2</sub>O/Na<sub>2</sub>O ratios (K<sub>2</sub>O about 5%, Na<sub>2</sub>O about 3%), with low Ba and Sr and high Rb. They are slightly peraluminous; this is reflected in the presence of small amounts of normative corundum and anorthite (see table 3.1).

In the normative Ab-An-Or diagram (Fig. 3.1a) these granitoids plot within the granite field of Barker (1979) in a zone between both the alkali-feldspar granite association and the monzogranite association of the Central Hijaz felsic rocks (see Fig. 3.1a) (Jackson et al., 1984; Jackson, 1986). In the Ab-Qtz-Or normative diagram (Fig. 3.1b) the majority of samples are situated near the ternary minimum for water pressures mainly between 1 to 5 Kbar in a zone overlapping the alkali-feldspar granite association of the Central Hijaz felsic plutonic rocks (see Fig. 3.1b) (Jackson, et al., 1984). In AFM space (Fig. 3.1c) they lie along the A-F side close to the Na<sub>2</sub>O+K<sub>2</sub>O apex, due to their very low MgO and low to moderate Fe contents, overlapping the fields of the Central Hijaz felsic plutonic rock associations (see Fig. 3.1c) (Jackson, et al., 1984; Jackson, 1986). Fig. 3.1d (Na<sub>2</sub>O-CaO-K<sub>2</sub>O) shows that the rocks plot almost midway along the Na<sub>2</sub>O-K<sub>2</sub>O side reflecting their small CaO content and almost 1 to 1.5 : 1 K<sub>2</sub>O/Na<sub>2</sub>O ratios. These rocks form a zone between the monzogranite and the alkali-feldspar granite associations of the Central Hijaz (see Fig. 3.1d) (Jackson et al., 1984; Jackson, 1986).

In a (CaO+MgO)-FeO\*-Al<sub>2</sub>O<sub>3</sub> diagram (Fig. 3.1e) these granitoids cluster near the Al<sub>2</sub>O<sub>3</sub> apex in a zone overlapping both the alkali-feldspar granite and the monzogranite associations of the Central Hijaz felsic plutonic rocks (see Fig. 3.1e) (Jackson, et al., 1984; Jackson, 1986).

The term 'spiderdiagram' is often used in this thesis in place of a multi-element diagram

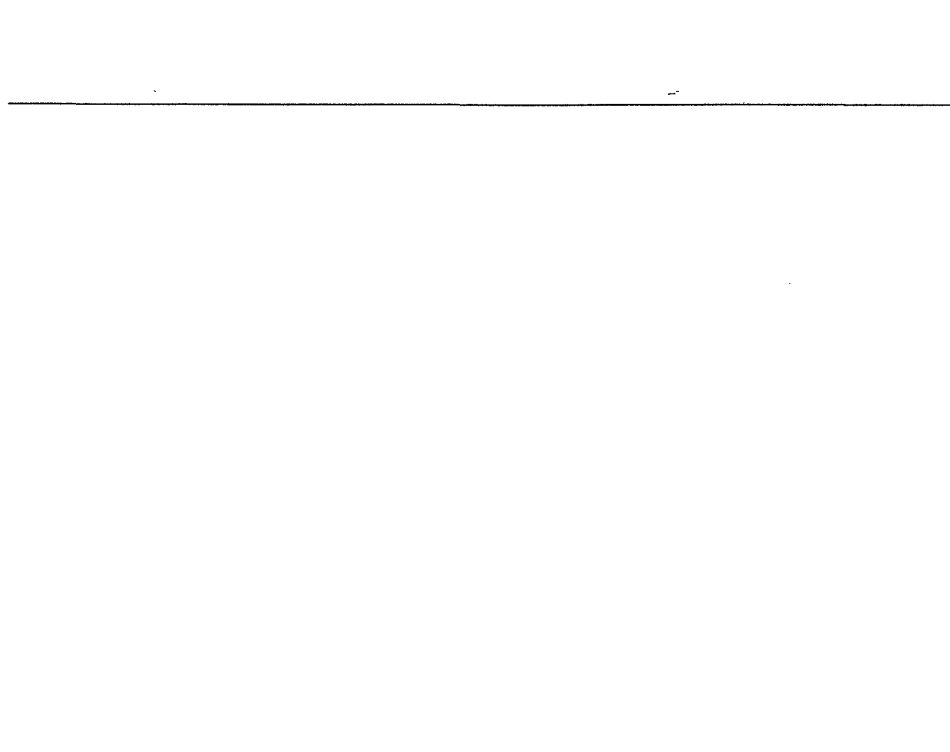
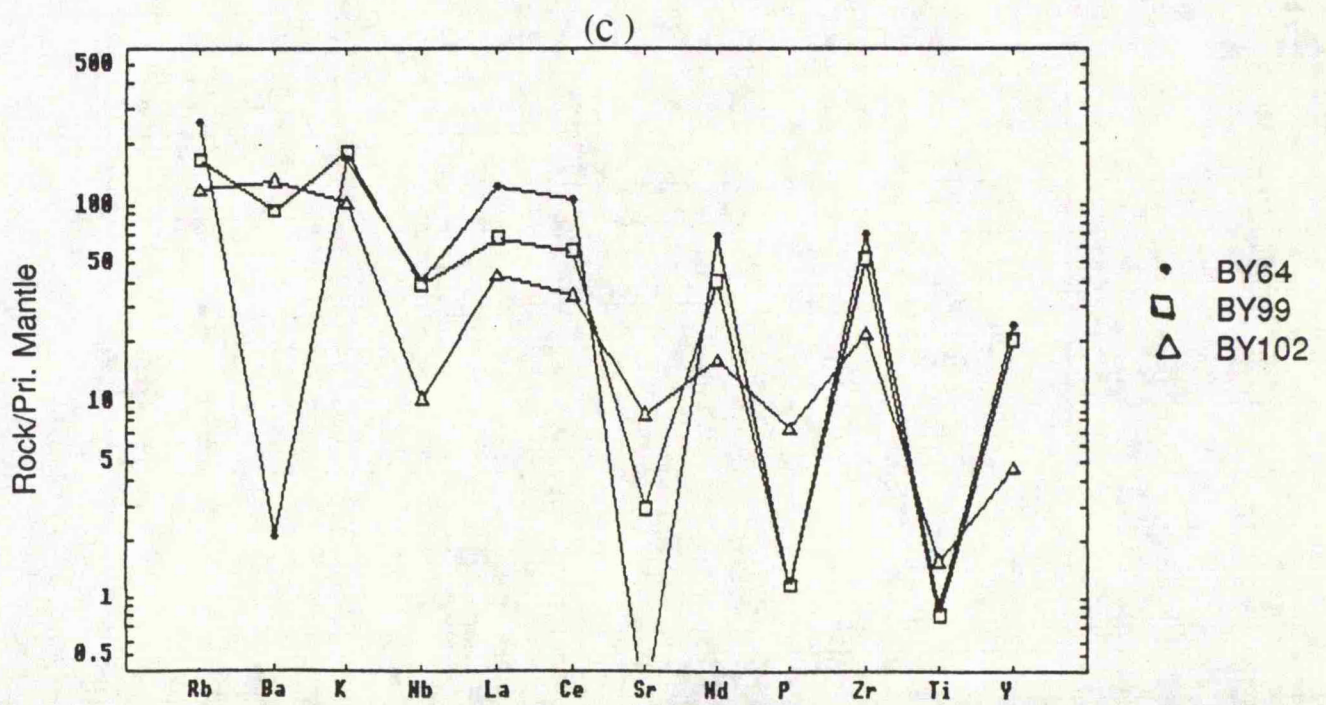
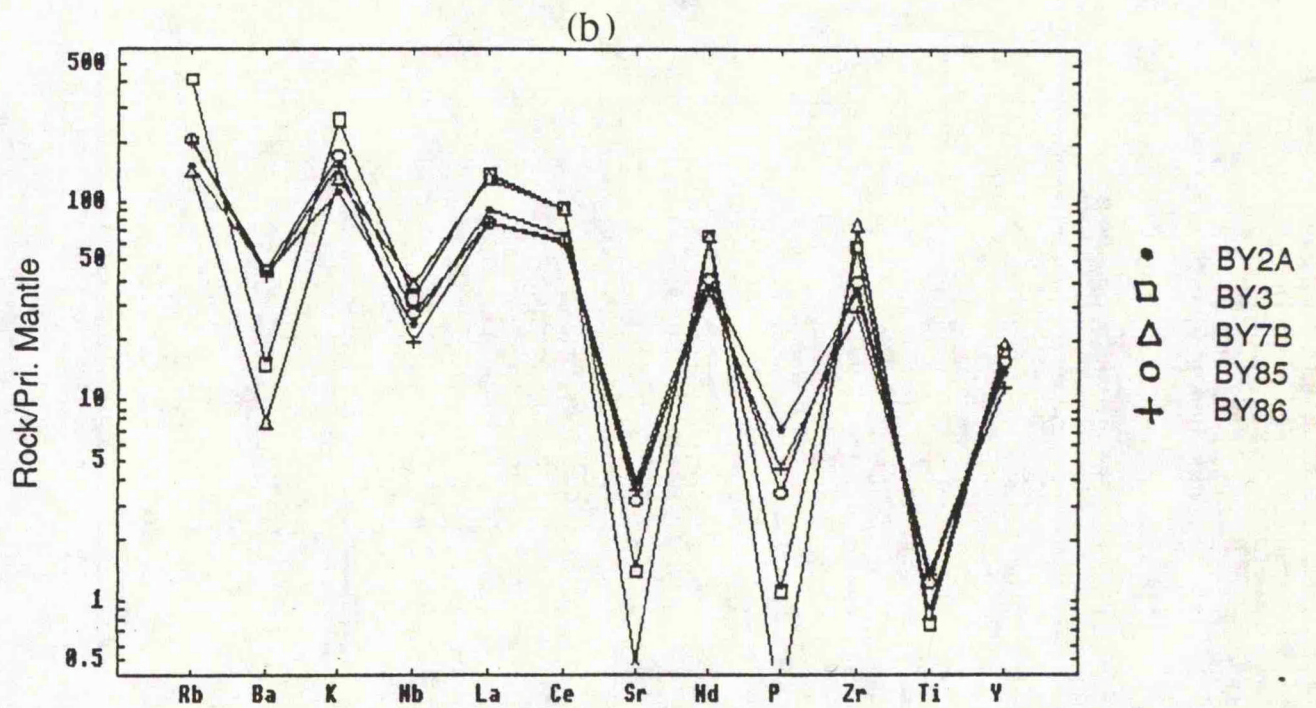
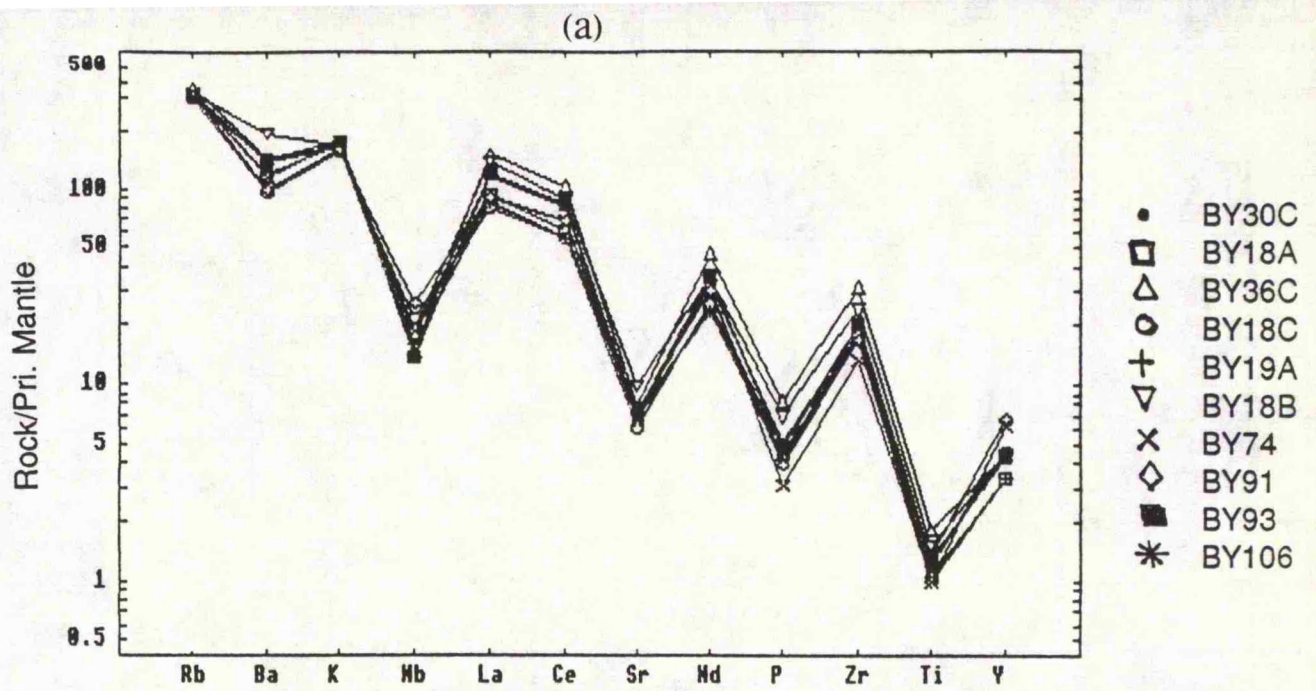


Fig. 3.2 Primordial Mantle-normalized spiderdiagrams for (a) the Lowder-Mudjah granitoids, (b) Mudjah felsic metavolcanics and (c) Mukeras felsic dykes. (normalizing values from Sun and McDonough, 1989)



in which individual traces are 'spidergrams' (Thompson et al., 1983; 1984). Such diagrams were normalised to primordial mantle, using the normalising values of Taylor and McLennan (1985), and Sun and McDonough (1989).

Fig. 3.2a shows a spiderdiagram for the incompatible trace elements of the granitoids. The patterns show a marked Nb trough, in addition to troughs at Ba, Sr, P and Ti, and positive spikes at the LREE. Since, Ba might substitute for K in K-feldspar and biotite, Sr for Ca in plagioclase; then troughs at Ba, Sr, P and Ti, are probably due to the fractionational crystallization of K-feldspar-biotite, plagioclase, apatite and sphene, respectively. These patterns are comparable with those of the felsic Mudiah metavolcanics (Fig. 3.2b), felsic Mukeras dyke swarms (Fig. 3.2c) and the felsic dykes of the Northeastern desert of Egypt (Stern et al., 1988) (see Fig. 3.4c). However, some deep troughs might be due to the use of strongly evolved rocks.

### 3.5 Metavolcanics

The Mudiah Metavolcanics (see Table 2.4) are melanocratic, fine to medium grained, phaneritic fragments. Mafic varieties are composed of hornblende plagioclase, biotite, clinopyroxene, quartz, epidote and chlorite and opaque Fe-oxides (magnetite). Epidote and chlorite are the main alteration minerals.

The felsic metavolcanics are composed of quartz, plagioclase, K-feldspar biotite, muscovite, epidote and chlorite. Epidote and chlorite are secondary. Opaque Fe-oxides (magnetite) and apatite are accessories.

Petrographically and chemically the Mudiah metavolcanics are bimodal, ranging from basalt, basaltic-andesite to rhyolite. Chemically the mafic metavolcanics (see Tables 3. 2, 3.5) range from 49.7 to 50.2% SiO<sub>2</sub>, Fe<sub>2</sub>O<sub>3</sub> \* (12.2 - 12.5%), Fe<sub>2</sub>O<sub>3</sub> \*/MgO (2.2) and TiO<sub>2</sub> (1.07 - 1.45%). Basalts contain up to 7% MgO, 249 ppm Cr, and 54 ppm Ni; which might be significant as indications of primary mantle melt. They are enriched in Fe and Ti (see Tables 3.2, 3.5). They are also enriched in K, Ba, Zr and LREE; K/Rb = 323 - 493, K/Ba = 6.3 - 29.

The felsic metavolcanics contain 73 to 79% SiO<sub>2</sub> and 3.2 to 7.42% K<sub>2</sub>O and have K<sub>2</sub>O/Na<sub>2</sub>O 0.8 to 3.1 (exception is sample BY3, K-feldspar porphyritic, up to 23.9) and are predominantly meta-aluminous. They contain high Fe<sub>2</sub>O<sub>3</sub>/MgO ratios (see Tables 3.2,

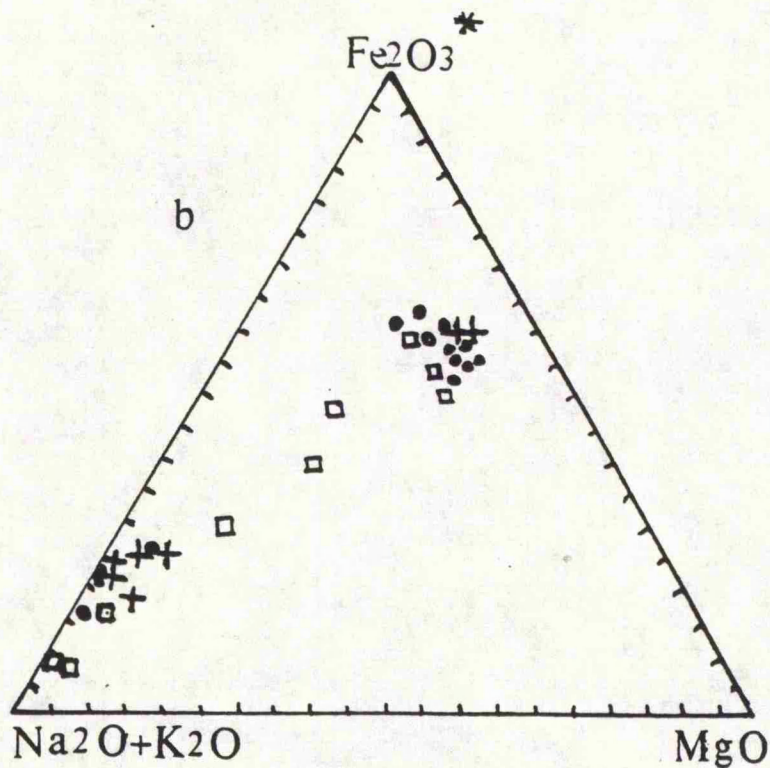
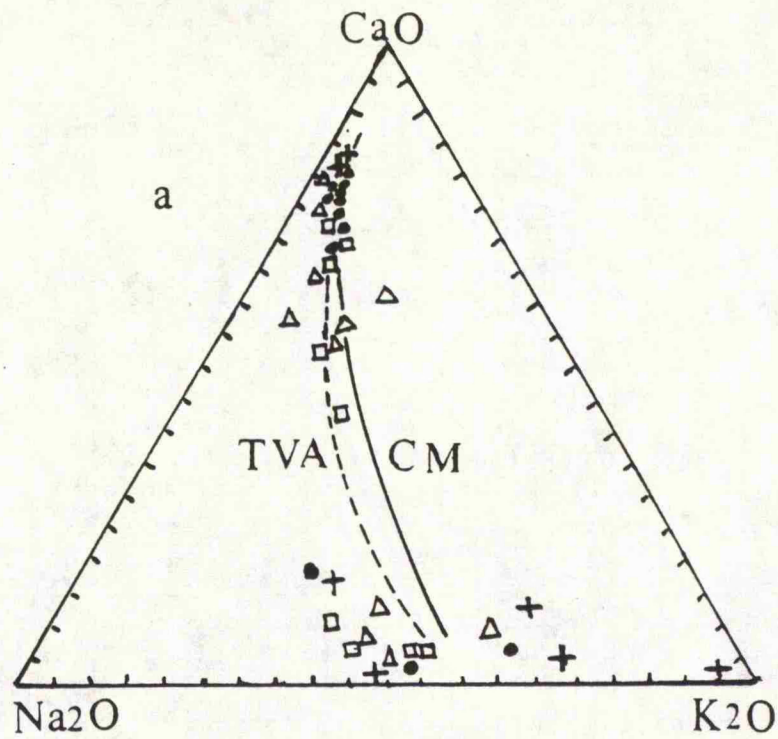


Fig. 3.3 a & b Triangular variation diagrams for the Mudiah metavolcanics (crosses), Mukeras dykes (closed circles), Northeastern Desert of Egypt dykes (open squares) (from Stern et al., 1988) and "sequence" A volcanics (Jahhad suite) of the Central Arabian Shield (open triangles) (from Roobol et al., 1983).

(trend reference from Roobol et al., 1983, TVA=transitional volcanic arc, CM=continental margin).

3.5), characteristic of post-tectonic suites (Anderson and Cullers, 1978).

Samples with a high silica content and high K relative to Na, have suffered alteration (e.g. samples BY3 and BY86, see Table 3.2). This alteration might affect the interpretation of their normative corundum. However, the presence of muscovite in their mineralogy, and of the normative corundum in all samples (e.g. BY2A and BY7B, see Table 3.2) which contain roughly equal amounts of K and Na (i.e. those with nil or negligible alteration), support the conclusion that the normative corundum, in the felsic metavolcanics, is a result of crustal contamination.

A Na<sub>2</sub>O-CaO-K<sub>2</sub>O diagram (Fig. 3.3a) shows that the metavolcanics lie along the boundary between the island arc and continental margin fields, similar to the Mukeras dyke swarms (Fig. 3.3a), the Egyptian dyke swarms (Stern et al., 1988) (see Fig. 3.3a), and the "sequence" A volcanics (Jahhad suite) of the Central Arabian Shield volcanics (Roobol et al., 1983) (see Fig. 3.3a).

Fig. 3.3b (AFM) shows that the metavolcanics occur within the tholeiitic field; however, the felsic varieties plot along the AF side towards the Na<sub>2</sub>O+K<sub>2</sub>O apex, on account of their very low Mg and low to moderate Fe contents.

In spiderdiagrams for the incompatible trace elements of the metavolcanics (Fig. 3.4a, 3.5a) two patterns are recognized:

a) The felsic varieties show a marked Nb trough, in addition to deep troughs at Ba, Sr, P and Ti, and positive spikes at the LREE. (Fig. 3.4a). Deep troughs might be attributed to the use of strongly evolved rocks. However, troughs at the Ba, Sr, P and Ti are probably due to the fractional crystallization of K-feldspar-biotite, plagioclase, apatite and sphene, respectively. These features of the felsic metavolcanic pattern are most likely subduction zone signatures (Tarney and Saunders, 1979). This pattern is comparable to that of the granitoids, the felsic Mukeras dyke swarms (see Fig. 3.2) and the Egyptian dykes (see Fig. 3.4a).

b) Mafic types have a relatively smooth distribution pattern, but with a moderate Nb trough and a trough at the P (Fig. 3.5a), which might indicate fractional crystallization of apatite. This pattern is comparable to that of the Mukeras mafic dyke swarms and the Egyptian dyke swarms (Stern et al., 1988) (see Fig. 3.5). However, the moderate Nb

Table 3.5 Comparison between the Mudiah metavolcanics, the Mukeras dyke swarms and the NE-Desert of Egypt dykes (data from Stern et al., 1988).

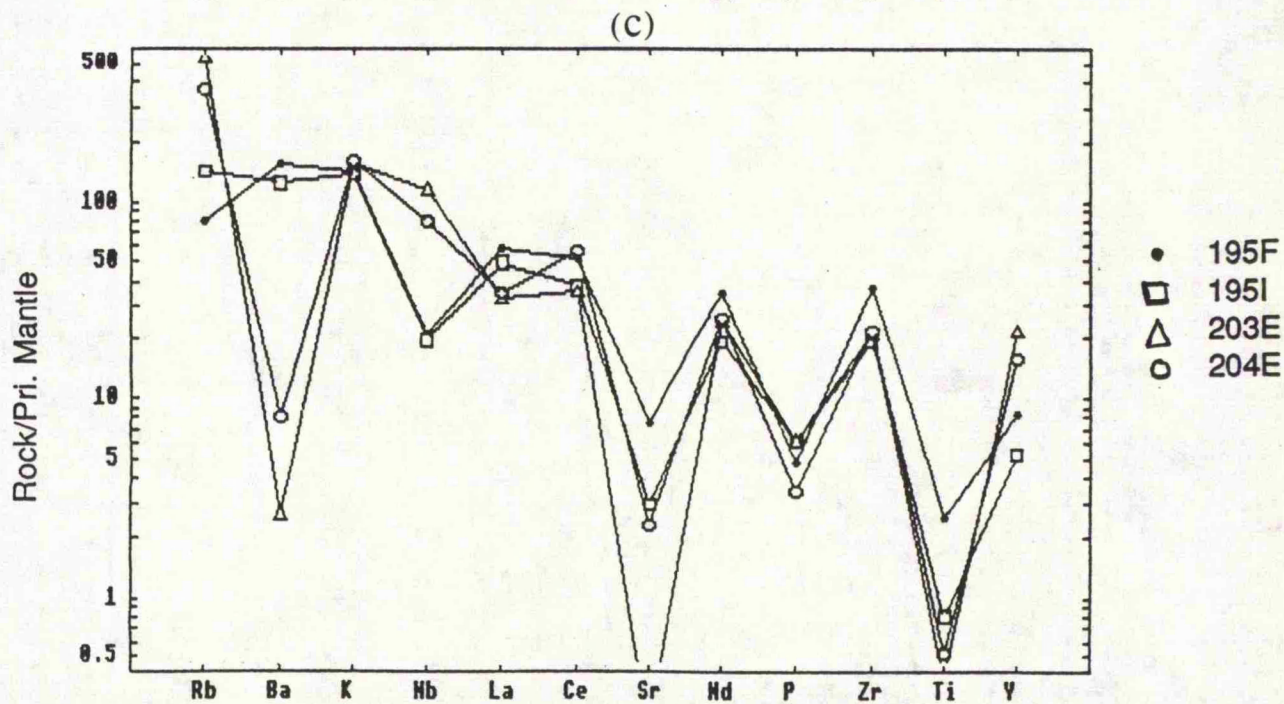
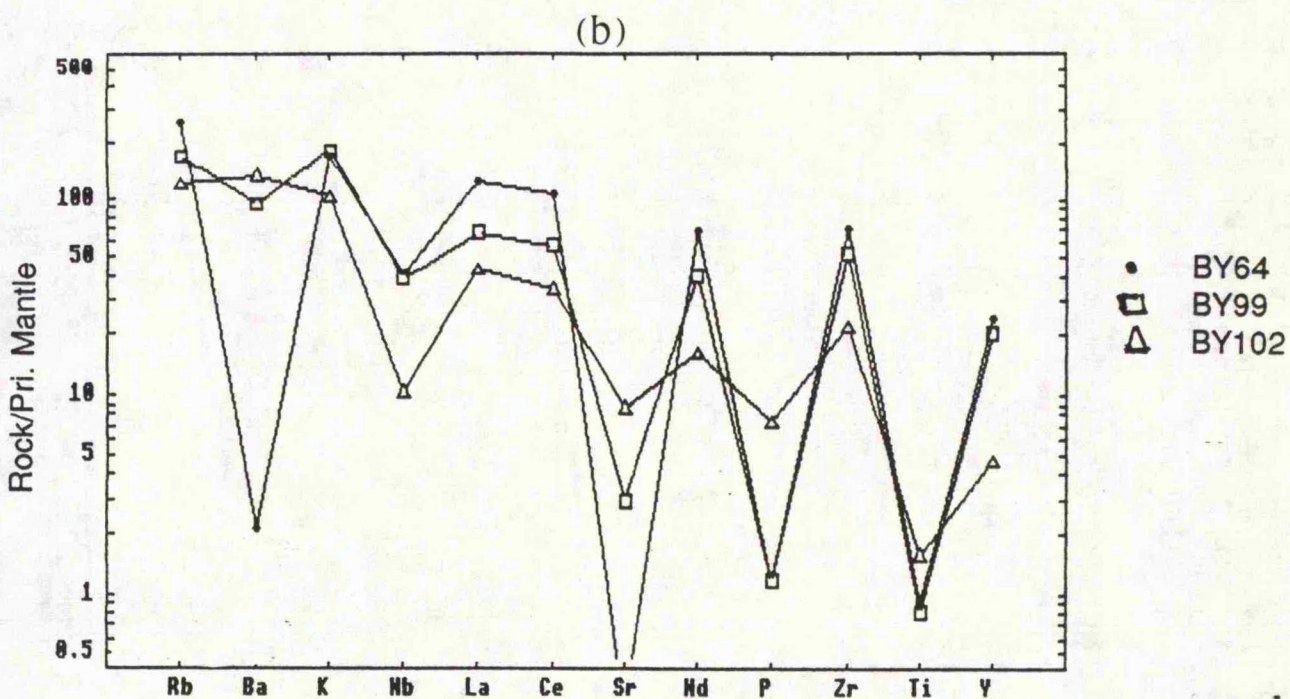
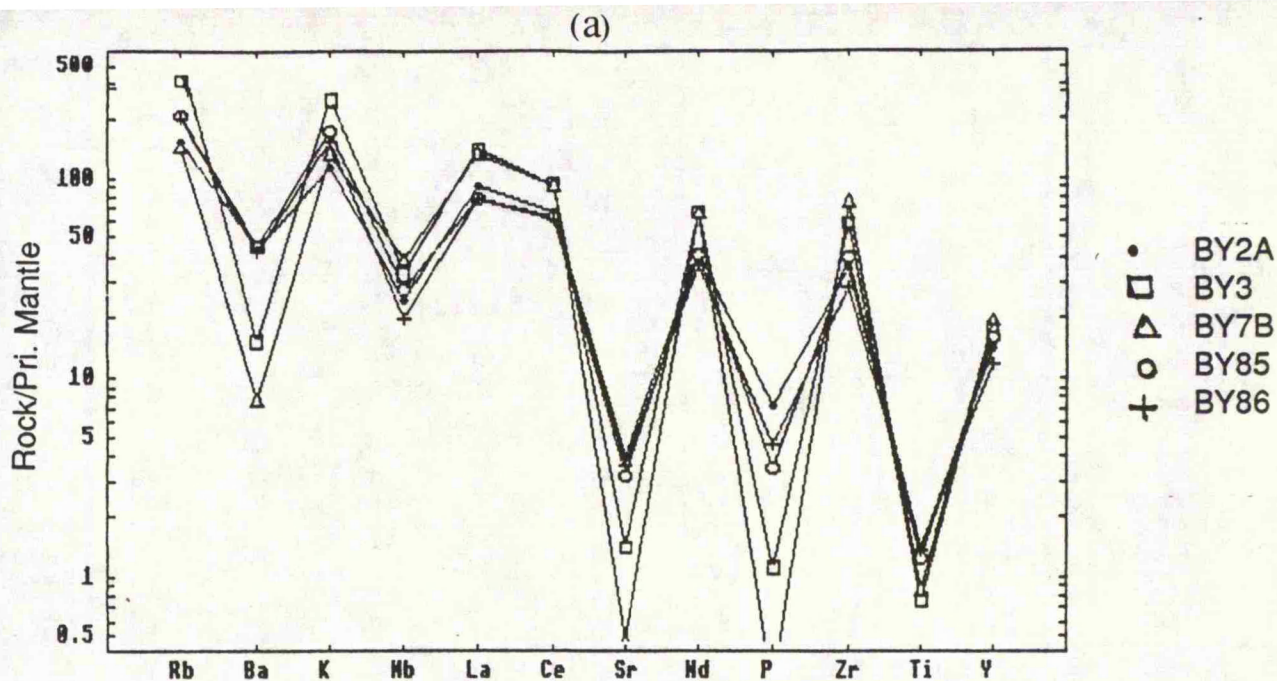
Locality Elements	Fesic Muiah Metavolcanics	Flsic Mukeras Dyke Swarms	Flsic Egypt Dyke Swarms
SiO <sub>2</sub>	73 - 80 %	69 - 78 %	70 - 78 %
K <sub>2</sub> O	3.2 - 7.4 %	2.9 - 5.2 %	3.2 - 5.9 %
K <sub>2</sub> O/Na <sub>2</sub> O	0.8 - 3.1	0.7 - 2.3	0.65 - 1.34
Fe <sub>2</sub> O <sub>3</sub> */MgO	3 - 29	5 - 25	3 - 25
TiO <sub>2</sub>	0.16 - 0.29 %	0.17 - 0.36 %	0.3 - 0.6 %
Fe <sub>2</sub> O <sub>3</sub> *	1.9 - 2.4 %	1.5 - 2.9 %	1.8 - 3.3 %
P <sub>2</sub> O <sub>5</sub>	0.02 - 0.10 %	0.02 - 0.11 %	0.07 - 0.18 %
MgO	0.1 - 0.7 %	0.1 - 0.7 %	0.4 - 1.0 %
CaO	0.1 - 1.6 % %	0.5 - 1.7%	0.9 - 2.2 %
Rb	98 - 284 ppm	42 - 114 ppm	55 - 210 ppm
Sr	11 - 92 ppm	70 - 205 ppm	90 - 400 ppm
Y	55 - 91 ppm	22 - 96 ppm	25 - 50 ppm
Ba	53 - 303 ppm	380 - 897 ppm	500 - 1300 ppm
Nb	15 - 29 ppm	8 - 29 ppm	10 - 25 ppm
Zr	315 - 657 ppm	245 - 586 %	240 - 780 %
Locality Elements	Mafic Mudiah Metavolcanics	Mafic Mukeras Dyke Swarms	Mafic Egypt Dyke Swarms
MgO	up to 7 %	up to 8.7 %	up to 8.9 %
Cr	249 ppm	295 ppm	556 ppm
Ni	54 ppm	94 ppm	176 ppm
Fe <sub>2</sub> O <sub>3</sub> *	12.3 - 12.5 %	11.5 - 15.1 %	9.8 - 13.1 %
Fe <sub>2</sub> O <sub>3</sub> */MgO	2.2	1.9 - 3.5	1.1 - 2.5
TiO <sub>2</sub>	1.35 - 1.45 %	1.32 - 2.17 %	1.5 - 2.4 %
K <sub>2</sub> O	0.44 %	0.47 - 1.11 %	0.8 - 1.8 %
Ba	128 - 136 ppm	187 - 404 ppm	290 - 650 ppm
Zr	93 - 115 ppm	102 - 168 ppm	210 - 270 ppm
K/Rb	323 - 399	183 - 391	425±94
K/Ba	27 - 29	12 - 39	24±6

Table 3.6 Age dates and comparison between, the Lowder-Mudiah (Yemen), the Arabian Shield, Saudi, (data from Roobol et al., 1983; Darbyshire et al., 1983; Jackson et al., 1984; Jackson 1986; Delfour, 1979) and the NE-Desert of Egypt (data from Stern et al., 1988; Stern and Hedge 1985),

Locality Description	Lowder-Mudiah Yemen	Arabian Shield Saudi Arabia	Northeastern Desert Egypt
Early Northeast-Southwest Mukeras dykes	K/Ar 709 $\pm$ 21 Ma 39Ar/40Ar 694 $\pm$ 23.1 Ma		
Late East-West to NW-SE Mukeras dykes	K/Ar 587 $\pm$ 18 Ma 39Ar/40Ar 585.9 $\pm$ 20.5 Ma		
Granite (host rock for dykes)	K/Ar 740 $\pm$ 22 Ma		
"sequence" A volcanics of Central Arabian Shield		700 - 570 Ma	
Young granitoid assemblage of Central Hijaz		686 - 517 Ma	
Old granitoid assemblage of Central Hijaz		820 - 715 Ma	
Granodiorite association of Central Hijaz		720 Ma	
Qattar-Dokhan dykes			589 $\pm$ 8 Ma
Dokhan volcanics			592 $\pm$ 13 Ma
Felsic plutonics			579 - 585 Ma
Alkali olivine basalt and alkaline andesites deposited in pull-apart basins within the Najd fault system Arabian Shield		560 - 520 Ma	

---

Fig. 3.4 Primordial Mantle-normalized spiderdiagrams for (a) Mudiah felsic metavolcanics, (b) Mukeras felsic dykes and (c) felsic dykes from NE. desert of Egypt (from Stern et al., 1988).  
(normalizing values from Sun and McDonough, 1989)



trough in the second pattern (Fig. 3.5a) of the metavolcanics is comparable with that of the first pattern (Fig. 3.4a), which might indicate that the Nb characteristics of the second have been inherited from a similar tectonic setting, i.e. the Nb trough might be an inherited subduction zone signature.

### 3.6 The Mukeras Escarpment Dyke Swarms and their Host Rocks

The Mukeras Escarpment is composed mainly of white granite, quartz-diorite, diorite and gabbro, intruded by a very extensive and intensive bimodal dyke swarms of two generations. The early (major) swarm strikes NE-SW ( $709 \pm 21$  Ma) and the late (minor) E-W to NW-SE ( $587 \pm 18$  Ma). Chemical analysis and modelling were carried out on the major (older) generation. However, age determinations were made on dykes from both swarms.

This is one of the most intense continental dyke swarms in the world (75 - 90% of the total rock volume in an area of  $\sim 20 \times 60$  km). Other comparably intense swarms, that are also Pan-African in age, are include the bimodal dykes in the Northeastern Desert of Egypt (Stern et al., 1988; Stern and Gottfried, 1986) and the dykes in the Hoggar of Algeria (Dostal et al., 1979).

#### 3.6.1 Dyke Swarms

Although these rocks are not strongly deformed, they do show recrystallization and greenschist facies mineralogy with albite, epidote, actinolite and tremolite. Some have a mid-amphibolite facies mineralogy, and contain oligoclase, epidote, biotite, hornblende, and these dykes are enriched in opaque iron oxides and sphene and are locally sheared. Other phases are clinopyroxene (augite) and andesine in the basalts and basaltic-andesites; orthoclase, sanidine (see Plate 2.8e,f) and albite in the rhyolites. These rocks are porphyritic (see Plate 2.8c,d), and show graphic, perthitic and myrmekitic textures.

The dyke swarms are petrographically and chemically bimodal in composition, ranging from basaltic andesite to rhyolite (see Tables 3.3, 3.5).

The mafic dykes up to 61% SiO<sub>2</sub>, Fe<sub>2</sub>O<sub>3</sub> \*(11.8 - 15.3%), Fe<sub>2</sub>O<sub>3</sub> \*/MgO ratio (1.9 - 4.7), TiO<sub>2</sub> (0.94 - 2.17 %). Basalts contain up to 8.7% MgO, 295 ppm Cr, and up to 94 ppm Ni, which might be significant as indications for primary mantle melt. The basalts are enriched in Fe and Ti (see Tables 3.3, 3.5). They are also enriched in K, Ba, Zr and

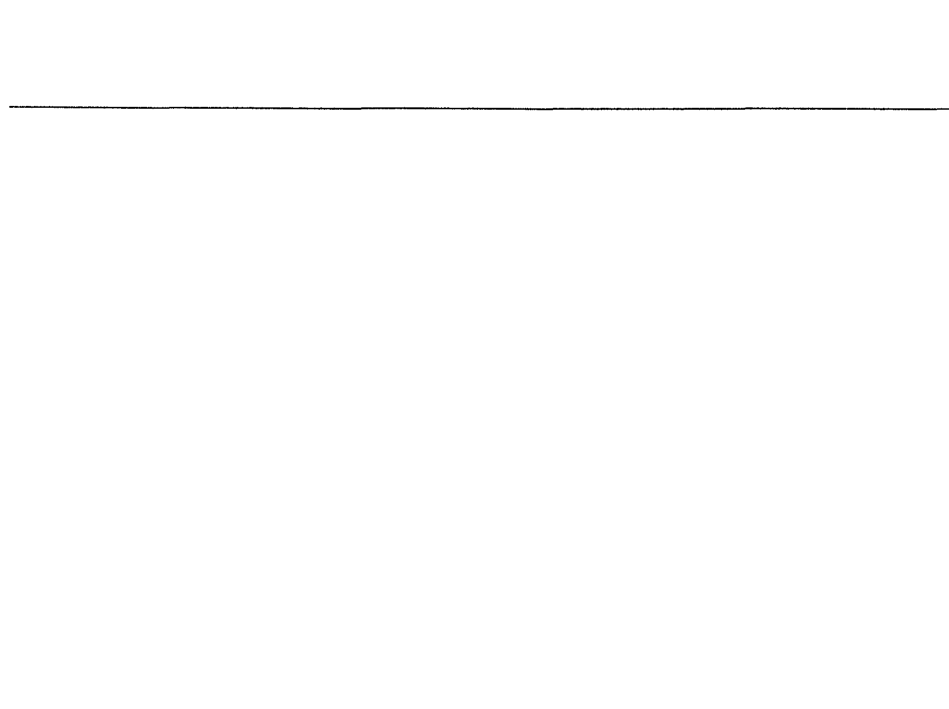
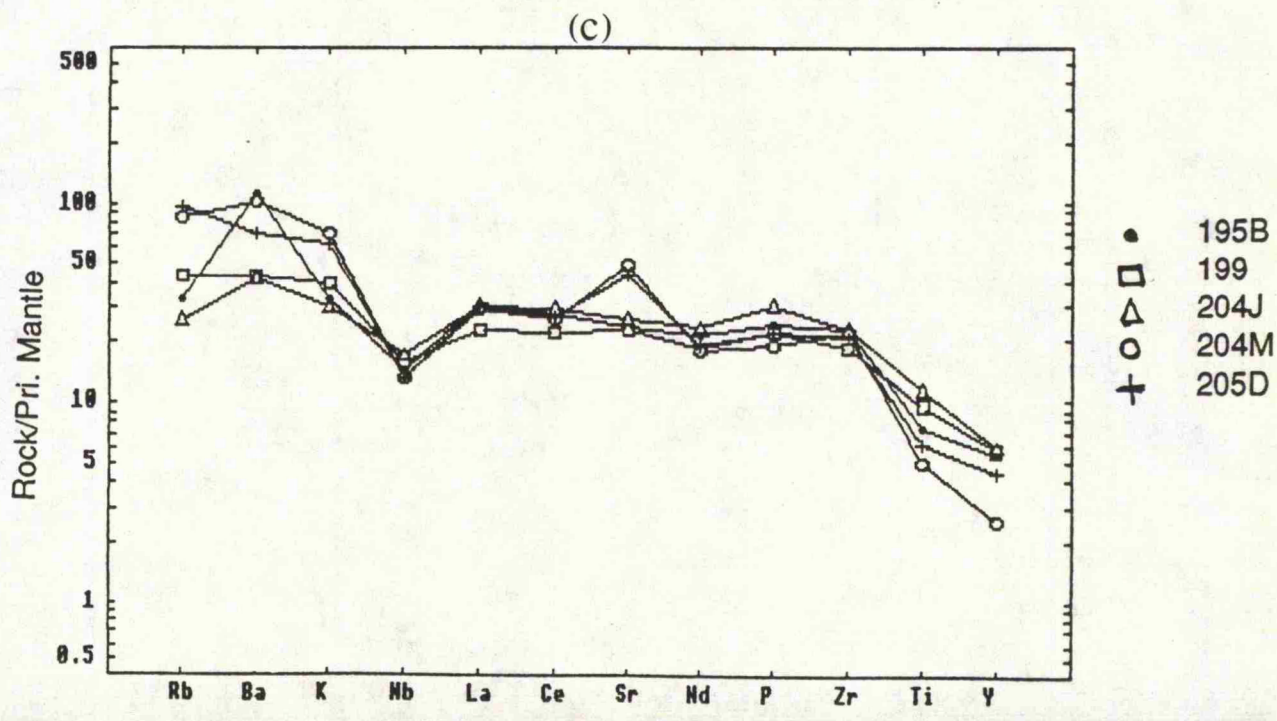
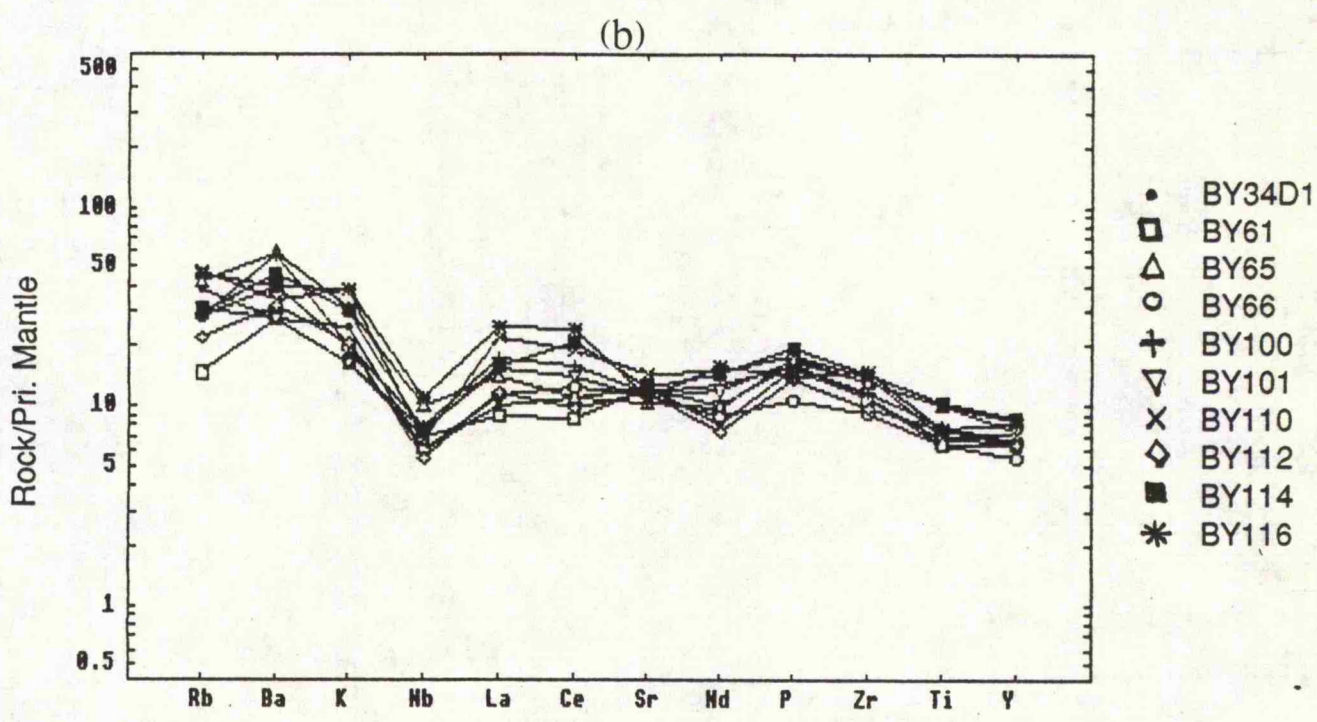
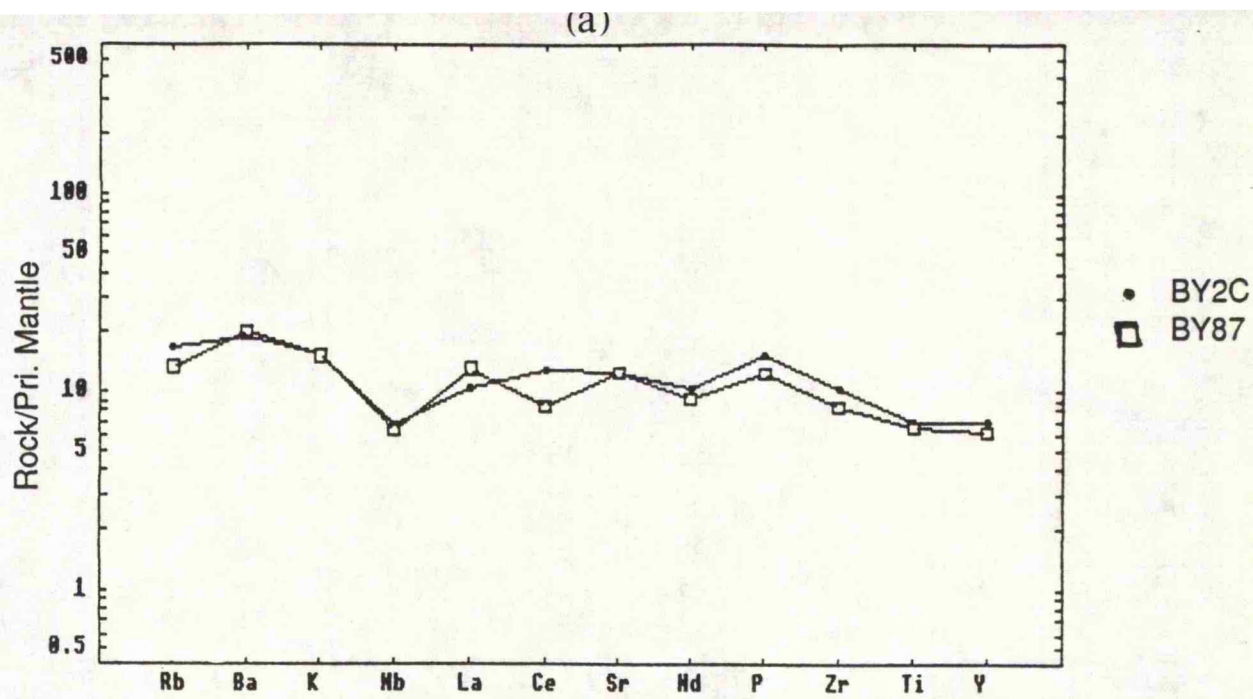


Fig. 3.5 Primordial Mantle-normalized spiderdiagrams for (a) Mudiah mafic metavolcanics, (b) Mukeras mafic dykes and (c) mafic dykes from NE desert of Egypt (from Stern et al., 1988).  
(normalizing values from Sun and McDonough, 1989)



---

LREE.

The felsic dykes contain 69 to 78% SiO<sub>2</sub> and 2.9 to 5.2% K<sub>2</sub>O, have K<sub>2</sub>O/Na<sub>2</sub>O (0.7 to 2.3) and are predominantly meta-aluminous. They contain high Fe<sub>2</sub>O<sub>3</sub>/MgO ratios, 5.0 up to 25, characteristic of post-tectonic suites (Anderson and Cullers, 1978) (see Tables 3.3, 3.5).

Moreover, in the Na<sub>2</sub>O-CaO-K<sub>2</sub>O ternary diagram (Fig. 3.3 a) these rocks fall along the boundary between the island arc and continental margin fields, similar to the Mudiah metavolcanics (Fig. 3.3a), the Egyptian bimodal dyke swarms (Fig. 3.3a) (Stern et al., 1988) and the "sequence" A volcanics (Jahhad suite) of the Central Arabian Shield (Fig. 3.3a) (Roobol et al., 1983).

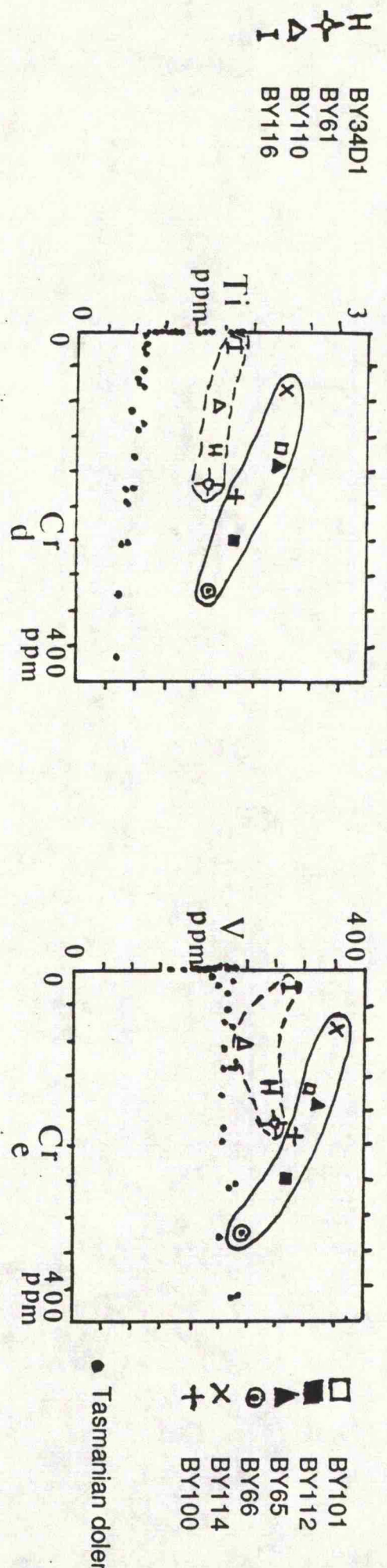
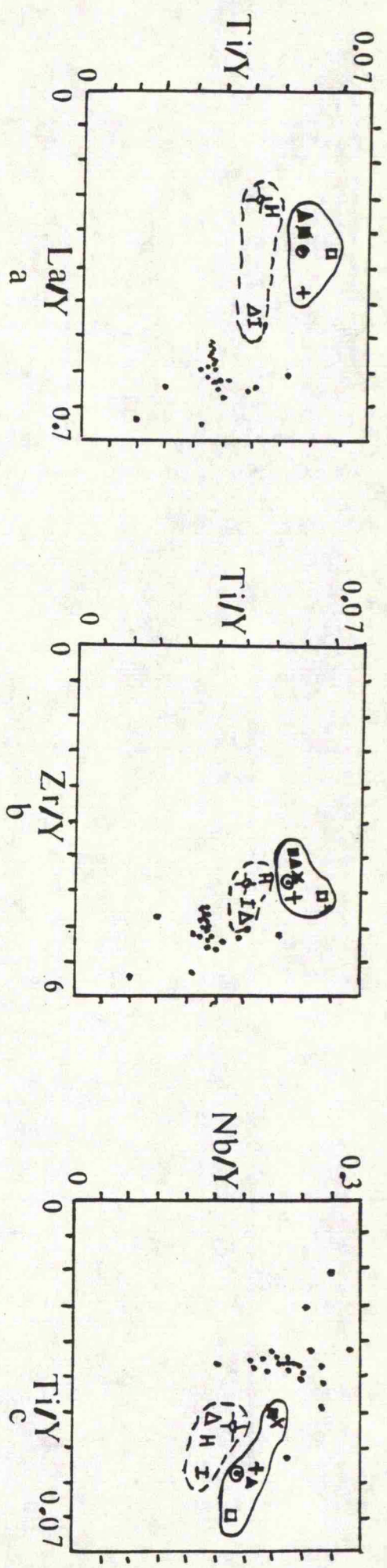
An AFM triangular plot for the dyke swarms (Fig. 3.3b) shows that they occur within the tholeiitic field. However, the felsic variety plots along the AF side towards the Na<sub>2</sub>O+K<sub>2</sub>O apex, on account of the very low MgO and low to moderate Fe contents.

The spiderdiagrams for the incompatible trace elements of the Mukeras dyke swarms reveal (Fig. 3.4b, 3.5b) two patterns :

a) The felsic dykes have a marked Nb trough, in addition to troughs at Ba, Sr, P and Ti, and positive spikes at the LREE (Fig. 3.4b). The deep troughs might reflect the presence of strongly evolved rocks. However, troughs at the Ba, Sr, P and Ti are probably due to the fractional crystallization of K-feldspar- biotite, plagioclase, apatite and sphene, respectively.

These features of the felsic dyke spiderdiagram are more likely subduction zone signatures (Tarney and Saunders, 1979). This pattern is comparable with that of the granitoids; the felsic Mudiah metavolcanics (Fig. 3.2) and the felsic Egyptian dykes (Fig. 3.4c) (Stern et al., 1988).

b) The mafic dykes have a relatively smooth patterns, but they have a moderate Nb trough in addition to a trough at P (Fig. 3.5b), which might indicate fractional crystallization of apatite. This pattern is comparable to that of the mafic Mudiah metavolcanics, the bimodal dyke swarms of the Northeastern Desert of Egypt (Fig. 3.5) (Stern et al., 1988). However, the moderate Nb trough of the Mukeras mafic dykes (Fig. 3.5b) is comparable to that of the felsic dykes (Fig.3.4b), which might indicate that the Nb



H BY34D1  
 + BY61  
 Δ BY110  
 I BY116

□ BY101  
 ■ BY112  
 ▲ BY65  
 ● BY66  
 ⊙ BY114  
 ⊙ BY100

● Tasmanian dolerite

Fig. 3.6 a - e Variation diagrams for the Mukeras mafic dykes and the Tasmanian dolerites (Hergt et al., 1989).

characteristics of the former were inherited from a similar tectonic setting, i.e. the Nb trough might be an inherited subduction characteristic (Tarney and Saunders 1979).

Moreover, variation diagrams for the Mukeras mafic dyke swarms (Fig. 3.6) of Ti/Y versus La/Y, Ti/Y versus Zr/Y, Nb/Y versus Ti/Y, Ti versus Cr, and V versus Cr were plotted with the Tasmanian dolerites (Hergt et al., 1989), show the Mukeras mafic dykes to split into two groups. This grouping indicates either, there are two different sources or two different amounts of partial melts (Pearce and Norry, 1979).

### 3.6.2 Host rocks

These rocks are leucocratic (granites) and meso to melanocratic (diorites to gabbros), medium to coarse-grained, slightly altered, sericitized, chloritized and epidotized and show perthitic (Plate 2.9c,d), myrmekitic and graphic textures, early cataclastic deformation in the granite (Plate 2.9c,d), and zoned feldspars (Plate 2.9e,f). The granites and granodiorites are composed mainly of quartz, albite to andesine, orthoclase and biotite; the gabbros of labradorite and augite, which show sub-ophitic textures Plate 2.8a,b).

In the Ab-Or-An normative ternary diagram (Fig. 3.7a) three samples of the host rocks plot within the granite, granodiorite, and tonalite fields Barker (1979); the other two fall closer to the anorthosite end-member being mafic diorites and gabbros. In AFM triangle diagram (Fig. 3.7b), Na<sub>2</sub>O-K<sub>2</sub>O-CaO (Fig. 3.7c) and CaO-MgO-Fe<sub>2</sub>O<sub>3</sub>\*-Al<sub>2</sub>O<sub>3</sub> (Fig. 3.7d) the host rocks lie on calc-alkaline trends. In Ab-Qz-Or normative diagram (Fig. 3.7e) the host rocks plot close to the cotectic surface, the P<sub>H<sub>2</sub>O</sub> 3 kb to 5 kb.

Moreover, these rocks, lie within or around the fields of the granodiorite association of the older assemblage of the Central Hijaz granitoids (Fig. 3.7). Therefore, since these host rocks have calc-alkaline affinity (Table 3.4, Fig. 3.7), the age of the granite (740 Ma), then this indicates that they are similar to the calc-alkaline granodiorite association (720 Ma) of the older assemblage of the Central Hijaz (Fig. 3.7), which were interpreted by Jackson et al., 1984; Jackson, 1986) as an island arc suite.

## 3.7 Discussion

### 3.7.1 Granitoids

The high siliceous content, the peraluminous nature, the high K<sub>2</sub>O/Na<sub>2</sub>O ratios, the

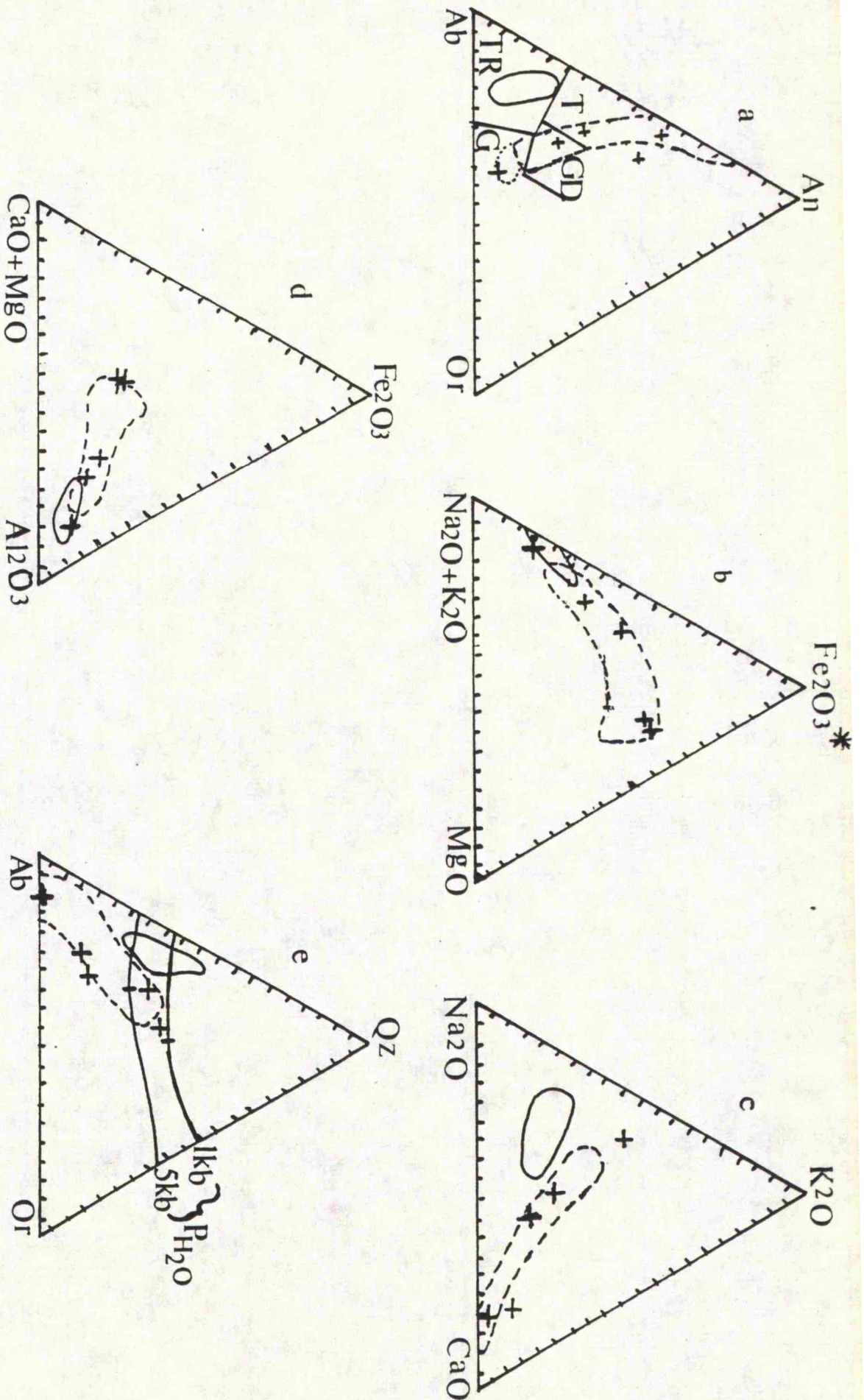


Fig. 3.7 a - e Triangular variation diagrams for the host rocks of the Mukeras dyke swarms (crosses) and the old assemblage of Central Hijaz granitoids, granodiorite association (dashed line) and trondhjemite association (solid line), granodiorite assemblage, the monzogranite association (from Jackson, et al., 1984). (fields, G=Granite, GD=Granodiorite, T=Tonalite, TR=Trondhjemite, after Barker, 1979).

presence of normative corundum and the presence of garnet and tourmaline in the mineralogy of the granitoids are all crustal melt (S-type) characteristics (Chappel and White, 1974; White and Chappel, 1977; 1988; Chappel and Stephens, 1988 and Crawford and Windley, 1990). However, the large ion lithophile element (LILE) enrichment, the high LREE / HREE ratios and the marked Nb troughs are all features related to stable phases in a subducted slab (Tarney and Saunders, 1979), i.e they are calc-alkaline subduction-related signatures.

According to White and Chappel (1988) S-type granites occur in many forms ranging from an association with migmatites and high grade regional metamorphic rocks, to large batholiths and their associated volcanic rocks, and most were derived from deeper parts of the crust. They argued that many greywackes (as source rocks that contain sufficient granite-forming elements, Si, Al, Na and K, and a high igneous component such as andesite), are peraluminous and would produce a magma of the same character by partial melting. Accordingly granitoids are probably derived from a highly evolved protolith (intermediate plutonics and metavolcanics of ? island arc origin) which must have had a pelitic component because they are peraluminous. The Lowder-Mudiah granitoids were possibly derived from similar source(s). Greater chemical variability might be attributed to a high degree of contamination from country rocks along with some effects of potassium metasomatism and the possible generation of an inhomogeneous magma during initial melting (White and Chappel, 1988). Mafic migmatites may also be the precursors of some calc-alkaline magmas in the lower crust and thus, of calc-alkaline granitoids (Tait and Harley, 1988).

According to Pitcher (1979) subduction energetics beneath an Andean-type continental margin provide sufficient heat and water to trigger remelting at various subcrustal and lower crustal levels. By such means material continuously accreting beneath a continental margin is episodically remobilized during periods of very rapid subduction by hot basic magmas that melt their way up into the crust along deep crustal fractures. The new I-type magmas are permissively accepted by the rigid crust at higher levels in cauldron structures, often accreting to form extensive batholiths. Within a Hercyno-type orogen produced by continent-continent collision tectonics shortening of the crust leads to

tectonic thickening and magmas are generated (particularly as a consequence of uplift) within the regionally-heated deep crust. It is in this environment that crustal-derived, S-type magmas most likely occur, less hot than those in a subduction regime, and they are emplaced by diapiric intrusion into ductile crust. Pitcher (1979) added that a multi-cyclic origin is necessary for granitoids that show I- and S-type characteristics, in order to model the complex geochemical patterns. Such complexity is exhibited in the Lowdert-Mudiah granitoids.

In his discussion of the formation of post-collisional monzogranites in the Karakoram, Crawford (1988) argued that the mantle wedge may be enriched during subduction by LILE-bearing fluids or by small-scale siliceous partial melts coming off the subducting slab. Amphibole, stable in a wet cool pre-collisional wedge, acts as a sink for the LILE, except for Rb which was released in the syn-subduction magmas. LILE-enriched amphibole dehydrate following collision and release LILE-enriched fluids, which flux the base of the crust, promote melting and contaminate the resultant crustal melts with LILE. The products of such a process resemble the post-collisional monzogranites.

Partial melting of the lower crust is considered in general to occur under fluid-absent conditions (Clemens and Vielzeuf, 1987; Vielzeuf and Holloway, 1988) through the breakdown of hydrous minerals such as mica and amphibole. Breakdown of muscovite occurs between 4 and 10 Kbar in a muscovite-quartz-feldspar assemblage at temperatures below 700° C. This produces small-scale melts which may resemble many of the garnet-muscovite leucogranites that intrude kyanite-sillimanite regional metamorphic belts (Clemens and Wall, 1981). To allow convective overturn and the generation of mobile plutons, the critical melt fraction must be exceeded in the source region (Clemens and Vielzeuf, 1987; Wickham, 1987). However, Wickham (1987) considered a critical melt fraction for granitic melts to be 30 - 50%, although any such parameter must be strongly dependant upon the specific nature of the melt and its environment. Recent experimental work has confirmed that voluminous peraluminous melts may be generated by biotite breakdown within a metapelitic source at temperatures in excess of 850° C (Vielzeuf and Holloway, 1988). Whether such high temperatures can be attained at the base of thickened continental crust during post-tectonic thermal

relaxation is debatable. Temperatures which only promote 5 - 20% lower crustal melting in such situations were predicted by England and Thompson (1986). Therefore, many workers have proposed additional heat sources from the mantle in order to promote sufficient crustal melting for the generation of migrating plutons (Clemens and Vielzeuf, 1987; Rutter and Wyllie, 1988). During and following collision, the thermal profile of the mantle and crust will change due to the removal of the cold slab input and crustal thickening. This will lead to conditions being simultaneously favourable for melting in both the subcontinental lithosphere and lower crust (Thompson, et al., 1984). Petrogenetic relationships that include direct fractionation, or assimilation of crust with subsequent fractionation of mantle-derived magma to yield granitic compositions were suggested by Leat et al. (1987), Nurmi and Haapala (1986), Rock and Hunter (1987) and Henney et al. (1989). However, recent modelling (Huppert and Sparks, 1988) has shown that intrusion of mantle magmas can melt the crust without any consequent mixing of the two components. The dominance of one of the above processes will obviously determine the nature of any granitic product.

According to Crawford and Windley, 1990) the post-tectonic granite magmatism of the Baitero Plutonic Unit of the Karakoram Batholith of NW Pakistan is temporally equivalent to the High Himalayan leucogranites. Both these rock groups have large ion lithophile element, LILE-enriched signatures, and are crustally derived melts, but they have distinct chemical and isotopic characters, suggesting different petrogeneses. This chemical signature results from a two-stage process; pre-collision subduction zone metasomatism of the mantle wedge by hydrous, silicious melts and / or fluids from the subducting slab, followed by destabilization of LILE-bearing mantle phase in response to post-tectonic thermal re-equilibration within the displaced modified mantle. Crustal thickening and the removal of the slab input leads to conditions being suitable for melting in both the mantle and crust at the same time. Lamprophyric melts from the mantle trigger or promote partial melting in the lower crust and contaminate the crustal melt by selective enrichment. This model provides an explanation for the collision-related granitoid/lamprophyre association and places constraints on mantle mechanisms with respect to tectonic evolution prior to and during continental collision.

A conceptual crustal profile by Jackson et al. (1984) in the Central Hijaz prior to the late Precambrian fusion event, includes a lower mafic layer composed of modified oceanic crust and mafic cumulates of the various calc-alkaline batholiths overlain by a 700 - 900 Ma crust which has an intermediate bulk composition and which is composed of calc-alkalic plutonic and volcanic rocks and derived sediments together with contemporary fragments of oceanic lithosphere. It is this crust which most likely formed the protolith from which the late Precambrian granitoids were derived. Therefore, the most likely source for the younger granitoids was the isotopically juvenile (700 to 900 Ma) calc-alkaline, plutonic, volcanic and volcanoclastic material. Moreover, Jackson et al. (1984) added that there are three phases of granitoid magmatism in the Central Hijaz. The earliest granitoids (820 Ma) are tonalites with trondhjemite affinities that have low - K contents (generally < 1.5% K<sub>2</sub>O), low K<sub>2</sub>O/Na<sub>2</sub>O ratio (0.3) and low abundances of granitophile elements such as F, Li, Nb, Rb, REE, Y and Zr; they probably formed the plutonic cores of immature oceanic island arcs. Granodiorites and tonalites of the second episode of magmatism have higher abundances of granitophile elements (2% to 3% K<sub>2</sub>O and K<sub>2</sub>O/Na<sub>2</sub>O ratios approximately 0.7). These granitoids together with gabbro, diorite and quartz diorite occur in batholithic intrusions which intrude coeval calc-alkaline volcanic successions. These batholiths probably represent the plutonic cores of more mature island arcs. Such calc-alkaline batholiths are considered to result from a combination of crustal melting with or without fractionation, and fractionation of mantle-derived basaltic and andesitic magma a model which can accommodate the geological and geochemical features observed in the Shufayyah Complex. The third episode of granitoid magmatism occurred between 686 Ma to 517 Ma when granites and perthite granites were emplaced. These granites have K<sub>2</sub>O contents of 3.5 to 4.5%, have K<sub>2</sub>O/Na<sub>2</sub>O ratios of approximately 1, and have enhanced granitophile element contents compared to earlier granitoids. No simple crustal melt model can account for the diversity and extremely variable major and minor element chemistry of the latest granitic magmas. However, most of the geological and chemical features observed in the Hijaz granites can be explained using a fusion-refusion model similar to that proposed by Collins et al., (1982), in which an initial fusion event produced "wet, high Ca" granites with I-type

characteristics (monzogranite association) and a later refusion of the same crust produced "dry, low Ca" granites with A-type characteristics (alkali granite and alkali-feldspar granite associations). The specific characteristics of each batch of I- or A-type granite magma would have been controlled by: 1) local compositional peculiarities of the melt zone, particularly with regard to minor phases; 2) local melt conditions and 3) fractionation processes during melting, or after separation of the melted fraction. Such a petrogenetic model may be applicable to large parts of the Arabian-Nubian Shield. However, a probable thickness for the Hijaz crust at 650 Ma would be 30 - 35 km. The likely low water and radio-element contents of this crust would tend to inhibit partial melting under normal geothermal gradients. According to Brown and Hennesy (1978) and Brown (1980) crustal fusion did occur on a grand scale, because an estimated 12,000 cubic kilometers of felsic magma is preserved in the upper 5 km of the crust. They added that according to Hildreth (1981) the energy needed to produce widespread crustal fusion is supplied by the introduction of large volumes of mafic magma into the lower and middle crust, usually within a tensional tectonic regime. The surface expression of such a phenomenon is likely to be represented by bimodal basalt/rhyolite volcanic activity, a situation which is apparent in the "sequence" A volcanics (Pellaton, 1979, 1981; Clark, 1981; Duyverman, et al., 1982). Moreover, Jackson et al. (1984) added, if it is assumed that the fundamental requirements of source material and melt mechanism are satisfied, then two types of granite melt could have been produced, namely: 1) I-types (Chappel and White, 1974) generated by melting the plutonic-volcanic-volcaniclastic island arc assemblage, one of the possibilities for the generation of the Mukeras granite-diorite-gabbro host rocks (see Fig. 6.1 path B); and 2) A-types (Loiselle and Wones, 1979; Collins et al., 1982) produced by remelting the already-melted residual island arc protolith, almost the case in the Lowder-Mudiah granitoids. S-type granite in the sense of Chappel and White (1974) would predictably be absent.

In discussing the melting processes for the Central Hijaz granitoid magmatism, Jackson et al. (1984) argued that the initial melt episode is likely to occur at lower temperatures and higher volatile pressures than the second episode of melting. Assuming that the main sources of water are from biotite and amphibole dehydration, initial melting could

occur in the 800 to 900° C temperature range at depths of 15 to 25 km. The I-type melts generated are likely to be more hydrous (i.e. crystallize more biotite and amphibole) than subsequent A-type melts. Remelting of the residual protoliths will only occur if (1) sufficient volatiles are available, e.g. release of F and Cl from residual amphiboles or new volatiles are added by degassing of mafic magma, and (2) there is additional heat input. Remelting could occur at temperatures of about 870 to 900° C (assuming water is derived from dehydration of residual micas and amphiboles). Such magmas are likely to be extremely dry and will thus be emplaced high in the crust or extruded on the surface. Such high temperature melting is also likely to involve the destruction of residual minor phases such as apatite, zircon, monazite and sphene and it is the involvement of these minerals that produces the characteristic enhancement of such elements as Nb, Zr, Y, REE and Sn (Collins, et al., 1982). The low Ca, Al, and Mg contents of the A-type granites are probably due to retention of these elements in highly refractory minerals, such as calcic plagioclase and pyroxene, whilst the high iron contents of the alkali granites might reflect the involvement of residual magnetite in the melt process.

The Lowder-Mudiah granitoids are similar to the A-type granitoids of the Central Hijaz, Arabian Shield (Fig. 3.1), and therefore a similar model to the A-type granitoids of the Central Hijaz can be applied. However, the host rocks (Fig. 3.7, Table 3.4) of the Mukeras dyke swarms are similar to the calc-alkaline monzogranite association of the Central Hijaz (Fig. 3.1), discussed above.

### 3.7.2 Metavolcanics and Dyke Swarms

The Mudiah metavolcanics and Mukeras dykes are petrographically and chemically bimodal. The mafic (basaltic) component shows indications of primary mantle melts that were enriched in LILE and LREE. Moreover, the mafic dyke swarms are of two different groups indicating that they are either of two different sources or of two different differential amounts of partial melts. In contrast the felsic (rhyolitic) component is predominantly meta-aluminous contain high Fe<sub>2</sub>O<sub>3</sub>/MgO ratio, characteristic of post-tectonic suite (Anderson and Cullers, 1978); however, they are also enriched in LILE and LREE with marked Nb trough.

There is a similarity between the Mudiah metavolcanics, Mukeras dyke swarms,

Northeastern desert of Egypt dyke swarms (see Tables 3.5, 3.6; Figs. 3.3, 3.4, 3.5) and "sequence" A volcanics (e.g. Jahhad Suite) of Central Arabian Shield (Fig. 3.3a; Table 3.6) as well as between their felsic component and the A-type granitoids of Central Hijaz (Jackson et al., 1984; Jackson, 1986). Therefore, the petrogenesis of these well studied and defined examples in Saudi Arabia and Egypt will be reviewed here, as a background for the conclusions reached on the petrogenesis of the Mudiah metavolcanics and Mukeras dyke swarms in particular and the magmatic evolution in the Lowder-Mudiah area in general.

The bimodal dyke swarms of the Northeastern Desert of Egypt were studied by Stern et al. (1988) who found that the mafic dykes are similar to the lavas of the Qattar-Dokhan Area in being dominated by andesites with medium to high contents of K<sub>2</sub>O. The andesitic dyke samples are virtually indistinguishable from the andesitic lavas of this region (Stern and Gottfried, 1986). This observation coupled with the field and geochronologic data further leads to the conclusion that these dykes were feeders for the Dokhan Volcanics. The dyke suite differs from the Dokhan Volcanics in containing more basalts (1/4 of the mafic suite contain less than 53% SiO<sub>2</sub>). These basalts are especially significant because one contains up to 8.9% MgO, 556 ppm Cr, and 176 ppm Ni, indicating that this sample must represent a primary mantle melt. The basalts are enriched in Fe and Ti, with Fe<sub>2</sub>O<sub>3</sub> \* = 9.8 to 13.1%, Fe<sub>2</sub>O<sub>3</sub> \*/MgO = 1.1 to 2.5 and TiO<sub>2</sub> = 1.5 to 2.4%. They are also enriched in K<sub>2</sub>O (0.8 - 1.8%), Ba (290 - 650 ppm), Zr (210 - 270 ppm) and LREE (La/Yb)<sub>n</sub> = 5.7 - 7.2. These are alkalic basalts that were derived from partial melting of enriched upper mantle. The relationships between the basalts and the andesites is problematic. A fractionation relationship is not indicated because incompatible elements, which would be expected to be enriched in the residual liquid are commonly as low or lower in the andesites as compared to the basalts. This is especially true for the high field strength cations (HFSE) such as Ti, P, Y, Nb, Zr, and the REE. There is an overall decrease in HFSE such as Y with increasing SiO<sub>2</sub>, that is largely inconsistent with a low-P fractionation relationship existing between the basalts and andesites. These lithologies nevertheless are petrogenetically related as shown by their similar isotopic compositions, REE patterns, K/Rb (basalt = 425±94; andesites =

$320 \pm 74$ ), K/Ba (basalts =  $24 \pm 6$ ; andesites =  $28 \pm 9$ ), and overall enrichment in LIL and HFSE incompatible elements. On the basis of REE modelling Stern and Gottfried (1986) suggested that the mafic members of the Northeastern Desert bimodal suites were formed either by 10% batch melting of LREE-enriched garnet lherzolite or by 10 - 20% batch melting of eclogite. The similarity of the mafic dyke bulk geochemistry and REE patterns to those of the mafic samples studied by Stern and Gottfried (1986) indicates that these conclusions hold for the mafic dykes as well. The fact that alkali basalts with high Cr, Ni, and Mg are more common in the dykes strongly indicates that these were formed by melting of LIL- and LREE-enriched garnet lherzolite in the upper mantle. The andesitic dyke rocks could either have been formed by lower degrees of hydrous melting of similar garnet lherzolite or by melting of eclogite. However, the felsic dykes are chemically indistinguishable from the Pink Granites of the Eastern Desert. They contain 70 - 78% SiO<sub>2</sub> and 3.2 - 5.9% K<sub>2</sub>O, have K<sub>2</sub>O/Na<sub>2</sub>O = 0.65 - 1.34 and are predominantly meta-aluminous. They contain high Fe<sub>2</sub>O<sub>3</sub>\*/MgO ratio, characteristic of post-tectonic suites. If found in a plutonic body, these compositions would correspond to "alkali granites" or "A-type" granites, terms that refer to the distinctive compositional characteristics observed for intrusive rocks of post-tectonic or extensional environments. Mukeras dyke swarms and Mudiah metavolcanics are both bimodal and are comparable to the dyke swarms of the Northeastern Desert of Egypt (see Figs. 3.3, 3.4, 3.5)

As to the petrogenetic relationship between the (bimodal) mafic and the felsic dyke swarms of the Northeastern Desert of Egypt Stern et al. (1988) pointed out that: two different hypotheses have been advocated for the generation of the late Precambrian "A-type" granites of Afro-Arabia, anatexis of the lower crust and fractional crystallization of mafic magma. Since the felsic dyke rocks are chemically indistinguishable from the "A-type" granite plutons, the same general types of models are applicable. One group of scientists argue that the late Precambrian accretion of arc systems to form the Afro-Arabian Shield resulted in a thickening of the juvenile crust which led to deep crustal anatexis (e.g. Greenberg, 1981). This was expanded on by Drysdai et al. (1984) who, following the model of Collins et al. (1982), argued that the "A-type" granites of Afro-Arabia were generated by partial melting, under high temperature vapour-absent

conditions, of a crust from which anatectic granodiorite melts had previously been extracted. This model faces the following objections: (1) How to produce such a large volume of K-rich melts from depleted lower crust ? (2) Flat HREE patterns indicate that the melts did not equilibrate with garnet - bearing rocks expected for the lower crust (Stern and Gottfried, 1986); (3) The felsic magmas are undersaturated in P<sub>2</sub>O<sub>5</sub> and all potential anatectic source rocks would produce saturated melts (Stern and Gottfried, 1986); and (4) Extensive melting of depleted lower crust cannot produce the observed enrichments of HFSE without also increasing Ca and Al (Harris et al., 1986a,b). Therefore, a modification of this model that overcomes objections 1 and 2 calls for anatexis of previously unmelted amphibolite-facies crust to generate the felsic magmas (Stern and Gottfried, 1986). In the case of the felsic dykes, this model would call on the intrusion of basic dykes into the juvenile crust to supply the heat necessary for melting. However, at the other extreme are models that call on the mafic and felsic members of the bimodal suite to have evolved, the latter from the former, by magmatic fractionation. One possibility is that the two members are immiscible liquids which separated during ascent through the crust. While this model is attractive in terms of the field relations (i.e. composite dykes with mafic margins and felsic centre; Voegeli, 1985) and in explaining the compositional gap between the mafic and felsic suites, this model is not favoured because the HFSE are not strongly partitioned into the mafic relative to the felsic rocks, as would be predicted from experimental studies (Watson, 1976; Ryerson and Hess, 1978). A second possibility is that the felsic magmas evolved from the mafic magmas by crystal-liquid fractionation. Stern and Gottfried (1986) developed a major-element fractionation model for the generation of Northeastern Desert felsic melts (75% SiO<sub>2</sub>; 4.8% K<sub>2</sub>O) by 67% fractional crystallization of Dokhan andesite (59% SiO<sub>2</sub>; 2.0 K<sub>2</sub>O). Testing of the model using the REE data did not support the model, because a match between the observed and predicted REE patterns could only be accomplished using partition coefficients appropriate for mafic magmas. A similar model can be proposed for the relationship between the mafic and felsic dykes and similar objections raised as well. Stern et al. (1988) added: we still have incomplete understanding of the petrogenesis of the felsic dyke rocks and, by inference, the petrogenesis of all the "A-type" granites in

northern Arabia. However, the Qattar-Dokhan dykes were intruded at  $589 \pm 8$  Ma; this is indistinguishable from the ages of the Dokhan Volcanics ( $592 \pm 13$  Ma) but is slightly older than the felsic plutons of the immediate area (579 to 583 Ma; Stern and Hedge, 1985). Were the felsic plutons emplaced (10 to 15 Ma) after the mafic volcanism ceased or do these differences reflect differences in cooling times? Age relationships among the felsic and the mafic dykes indicate these were emplaced during a similar time interval (Stern et al., 1988).

Stern et al. (1988) concluded that: the bimodal igneous activity in at least this part of northern Afro-Arabia occurred concurrently, and that the observed difference in radiometric ages largely manifests the slower cooling of the larger plutons relative to the dykes. The relationship between the mafic dykes and the Dokhan Volcanics is clear, the former represent magmatic conduits for the latter. The relationship between the felsic dykes and the Pink Granites, however, is more equivocal. Because both the felsic dykes and the plutons occupy similar crustal levels, it is not obvious whether the felsic dykes fed into or issued from the granite plutons; field observations, however, favour the first possibility. Moreover, the felsic dykes represent shallow feeders for the epizonal sill-like granite bodies of the Qattar-Dokhan area.

In their discussion of the significance for magmatic evolution Stern et al. (1988) pointed out that: one of the most important results from this study is the recognition that a wide range of chemical diversity was established prior to or during ascent through the crust. This observation is of limited importance for the Dokhan Volcanics/Mafic dykes, because there has never been any suggestion that these magmas fractionated within the upper 1 to 2 km of the crust that the exposed units represent. In the case of the felsic dykes, however, the observation that a wide range of especially LIL and HFSE trace elements existed in the felsic dykes is significant, and this is the case in Mukeras dykes. Recent studies have concluded that unusual enrichments of some trace elements (e.g. Ta, W, Mo, REE) may have occurred by vapor-transfer in the roof zones of shallow plutons in northern Arabia (Harris and Marriner, 1980; Drysdall et al. 1984). Similar, less extreme fractionation processes have been called on to explain a wide range of compositional variations observed in Northeastern Desert Pink Granites (Stern and Gottfried, 1986).

The fact that such large variations are observed in the felsic dykes indicates that the processes responsible occur relatively deep in the crust. The processes responsible for the generation of the felsic suite must also occur deeper than the present erosional level. As previously outlined, this may have occurred by anatexis within amphibolite facies rocks at mid-crustal levels or by fractional crystallization of alkali-rich andesitic melts. In the latter case, existence of long and extensive subparallel dyke swarms indicates that anatexis affected very large portions of the crust and that intense heating of the crust accompanied the strong crustal extension that affected northern Afro-Arabia at the end of the Precambrian. If the felsic melts formed by fractional crystallization, this also must have occurred relatively deep in the crust. In this case, the presence of extensive dyke swarms indicates that such magma reservoirs must have been abundant and occupied large portions of the mid-crust.

Therefore, the presence of the Mukeras extensive and intensive dyke swarms indicates that anatexis must have affected very large portions of the crust and the magma reservoirs probably occupied the mid-crust. The felsic Mukeras dykes are similar to the A-type granitoids of Lowder-Mudiah area and the felsic Mudiah volcanics (see Tables 3.1, 3.2, 3.3, 3.5; Fig. 3.2), thus the dykes might represent the feeders for the Mudiah metavolcanics (see Fig. 6.1)

As to the volcano-sedimentary belts in the Central Arabian Shield (CAS) the study of (Roobol et al. 1983) revealed that: the oldest volcano-sedimentary belts ("sequence" C; > 900 Ma), Bidah and Shayban are chemically immature bimodal suites of low-K tholeiites and sodic dacite/rhyolite depleted in lithophile elements Rb, Nb, Zr, etc. These lavas have chemical characteristics similar to immature island arcs (IIA) such as the Tonga-Kermadec and Lesser Antilles arcs. Younger lavas of "sequence" B (900 - 700 Ma) Balas, Aqiq and Idsas are slightly more mature in composition being predominantly calc-alkaline and low-K arc tholeiite series with low lithophile element contents, but higher than "C" and high Na<sub>2</sub>O : K<sub>2</sub>O ratios. They are comparable with western Pacific Ocean modern island arc (IA) averages. The youngest voluminous lavas ("sequence" A; 700 - 570 Ma) Fatima, Arfan, Jugjug, Jahhad and Hummah are generally calc-alkaline or high-K calc-alkaline series lavas with moderately high lithophile element abundances, but

much higher than "C and B" and lower Na<sub>2</sub>O : K<sub>2</sub>O ratios. They are comparable to transitional volcanic arcs (TVA) such as the Central American Cordillera or the Indonesian Sunda arc, which are transitional between island arcs and continental margin volcanic arcs. All suites of the CAS are strongly bimodal (basalt-basaltic andesite and dacite-rhyolite range) except Jugjug, Hummah and Idsas which appear to be unimodal (basaltic andesite-andesite range). Bimodality which may not be a normal feature of modern volcanic arc suites, but not unknown e.g. Tonga islands, is a common feature of the late Proterozoic stratovolcanoes of the CAS. Roobol et al. (1983) concluded that : the cratonization process in the CAS thus involved the superimposition of three volcano-sedimentary sequences, rather than intraplate rifting or simple juxtaposition of oceanic island arcs, formed in progressively maturing volcanic arcs. Early-formed immature island arcs were succeeded by chemically more mature island arcs, and then by volcanic arc(s) transitional between island arcs and continental margins. The evolution ceased at this stage and probably did not advance to the equivalent of an Andean-type continental margin.

Roobol et al. (1983) showed that none of the Central Arabian Shield lavas is a within-plate basalt and none of them, either felsic or mafic, is particularly alkalic; they are equally divided between calc-alkaline and high-K calc-alkaline, trace elements are not enriched relative to volcanic arc magmas, and TiO<sub>2</sub> has a low concentration (< 1.75%) typical for orogenic magmas. They concluded that the volcanic belts were formed in orogenic volcanic arc settings of the type associated with convergent plate margins. None has characteristics to be expected of the environments of rifting and crustal distension.

Stern et al. (1984) in their discussion of the tectonic geochemistry argued that : previous investigators have noted the enriched composition of the mafic to intermediate rocks associated with latest Precambrian magmatic activity throughout Afro-Arabia but a consensus has not been reached regarding the tectonic setting in which these lavas were erupted. The Dokhan Volcanics have previously been interpreted as products of Andean-type magmatism (Basta et al., 1980) as were analogous volcanics in the Kid Group, Sinai (Furnes et al., 1985) and "sequence" A volcanics in the Arabian Shield

(Roobol et al., 1983). These interpretations were first questioned by Resselar and Monrad (1983) who noted that the Dokhan lavas had elevated concentrations of incompatible trace elements with respect to igneous rocks typical of active continental margins. Stern and Gottfried (1986) interpreted the Dokhan Volcanics and Pink Granites as extrusive and intrusive components of a bimodal suite associated with crustal extension. Independantly, as a result of detailed field studies of "sequence" A in Arabia, Agar (1986) discounted the convergent-margin tectonic interpretation of Roobol et al. (1983). He argued instead that much of the "sequence" A volcanic activity occurred in pull-apart grabens of the Najed strike-slip orogen. Much of the disagreement stems from uncertainties in interpreting the geochemistry of especially the mafic igneous rocks. In general, all of the latest Precambrian igneous products in Afro-Arabia (Dokhan/mafic dykes in NE Egypt; Kid Group in Sinai; Jibalah, Shammar, Murdama, Furyh, and Hadlyah Groups in northern Saudi Arabia) share compositions that on a chemical basis alone could be interpreted as either related to intra-plate rifting or a mature convergent margin (e.g., Resselar and Monard, 1983). That is, these are largely calc-alkaline, show moderate enrichments of the incompatible elements, and are rarely silica-undersaturated. Until recently, proposed tectonic hypotheses for the evolution of Afro-Arabia were models of arc-accretion, and therefore it was appropriate to try to fit even late magmatic activity into that conceptual framework (e.g. Bakor et al., 1976; Fleck et al., 1980). More recent Interpretations of late crustal evolution in Afro-Arabia have emphasized the role of extensional tectonics and Najed strike-slip faulting (Stern et al., 1984; Stern, 1985; Burke and Sengor, 1986; Agar, 1986). Such recognition requires a re-interpretation of the tectonic signature of related igneous rocks. Tectono-magmatic interpretations are greatly simplified for the case of dyke swarms observed here. The field exposures give unequivocal evidence of a regional NW-SE extensional tectonic regime. The composition of the mafic suite volcanics is best explained in a within-plate magmatic setting. These rocks nevertheless present a problem in having high Zr/Nb (17 - 40) and Sr/Nd (19 - 39) considered otherwise diagnostic of convergent zone magmatism (Gill, 1981; De Paolo and Johnson, 1979). Barberi et al. (1982) pointed out that systematic compositional variations can be observed between continental rifts that

produce large and small volumes of melts. Low volcanicity rifts (e.g. Rhinegraben, Baikal, West Africa) erupt a wide range of mafic lavas but with relatively little felsic material. Instead, these rifts produce strongly alkalic and undersaturated lavas with strong LREE-enrichments ( $(La/Yb)_n$  about 10 to 50). High volcanicity rifts (e.g. Afar, East African Rifts) produce abundant felsic magmas and the mafic melts are less commonly undersaturated; much less LREE-enrichment is observed ( $(La/Yb)_n$  about 4 to 6). Barberi et al., (1982) suggested that the low- and high-volcanicity rifts are associated with rifts undergoing relatively little and great extension, respectively. The evolution of the Jemez Volcanic Field in the Rio Grande Rift is illuminating in this regard. Although this volcanic center began at about 16 Ma with the eruption of olivine tholeiites and high silica rhyolites, by 10 Ma magmatism it was dominated by andesites that are remarkably similar to the Dokhan andesites (Keres Group andesites; 60 - 63% SiO<sub>2</sub>; 0.8 - 1.1% TiO<sub>2</sub>; 2.5 - 3.2% K<sub>2</sub>O;  $(La/Yb)_n = 12 - 15$ ). Gardner et al. (1986) argued that these andesites comprise nearly half of the Jemez volcano. Rhyolitic domes and extrusives are common throughout the volcanic stratigraphy, becoming the dominant unit with the eruption of the 1.45 - 1.12 Ma Bandelier Tuff (Self et al., 1986). These rhyolites are very similar to the Egyptian felsics (68 - 78% SiO<sub>2</sub>; 0.04 - 0.44% TiO<sub>2</sub>; 3.2 - 5.4% K<sub>2</sub>O;  $(La/Yb)_n = 3 - 8$ ; Gardner et al., 1986; Self et al., 1986). Nearly all the Jemez volcanics with more than 53% SiO<sub>2</sub> are subalkaline (Gardner et al., 1986). If the tectonic setting of these rocks were not known a priori, their geochemical signature would very likely have been interpreted as indicating their formation in an Andean-type convergent margin. These results indicate that it may not be appropriate to expect all continental rifts to share common compositional characteristics but that the rate or degree of extension may be as important as the process itself in determining magma compositions. A large degree of compositional overlap thus may be expected between lavas erupted in highly magmatic, rapidly distending rifts and Andean-type convergent margins (Stern et al., 1988).

In Oman, about 2000 km to the east of Lowder-Mudiah area, dyke swarms of similar age to the late Mukeras dykes were reported by Gass et al. (1990). These dykes are bimodal, of Precambrian age (604 - 490 Ma) and are located in the NE and SE Oman, where

there are also granitoids and an ultramafic (ophiolitic) suite. Gass et al. (1990) pointed out that geochemical data show that most granitoids have the signature of volcanic arc granites and concluded that this reinforces the similarity with the Pan-African terranes of the western Half of the Arabian Plate, and that the ophiolitic suite implies a suture between colliding island arcs much further east than those recognized in Saudi Arabia (Gass et al., 1990).

### 3.8 Mechanisms

Based on the above discussion, the possible mechanism(s) for the magmatic evolution of magmatic activity of Lowder-Mudiah area is that, the calc-alkaline characteristics of some igneous rocks (as it is the case in Lowder-Mudiah) could be the result of melting a metapelite (Crawford and Windley, 1990), intermediate metavolcanics of ? island arc origin (White and Chappel, 1988), and/or mafic migmatites (Tait and Harley, 1988). However, the LILE- and LREE-enrichment in the Lowder-Mudiah area igneous rocks could have been related to a postulated metasomatic enrichment of the pre-collisional mantle wedge or sub-continental lithosphere through reaction with hydrous siliceous melts from a subducted slab. Crystallization of amphibole and other hydrous phases trapped LILE in a metasomatic mantle assemblage. Following collision, removal of the subducted slab input and vertical displacement of the mantle due to crustal thickening above led to elevated heat flow, destabilisation of the hydrous phase and consequent fluid-absent melting in the LILE-enriched mantle. These melts intruded the base of the thickened crust. The resultant heat influx triggered extensive dehydration melting of the hot lower crustal source. Once the critical melt fraction had been exceeded, convective overturn incorporated some of the fractionated magma into the granitic melt, thereby selectively contaminating it in LILE (Crawford and Windley, 1990). Extension and crustal thinning occurred, caused by and/or led to mantle upwelling or diapirism due to adiabatic decompression, and this enabled the felsic magma to rise through the crust leading to the formation of the Lowder-Mudiah "A-type" granitoids (intrusives), the Mukeras felsic dykes (hypabyssal) and the Mudiah metavolcanics (extrusives)(see Fig. 6.1). Remelting could occur at about 870 to 900° C. The A-type magmas are more likely to be extremely dry and thus be emplaced high in the crust or extruded (Jackson et al.1984). Injection of

mantle-derived basaltic magma, gave rise to the basaltic (mafic) Mukeras dyke swarms and the basaltic (mafic) Mudiah metavolcanics. The mafic Mukeras dyke swarms are of two groups representing either two different sources or two differential amounts of partial melts.

There is a possibility that the Mukeras dykes and Mudiah metavolcanic basalts were formed by partial melting of LILE- and LREE-enriched garnet lherzolite mantle (e.g. Kay and Gast, 1973). Whereas the andesite dykes could have been formed by lower degrees of hydrous melting of similar garnet lherzolite (e.g. Mysen and Boettcher, 1975), or by melting of eclogite (e.g. Apter, 1981) and may be with fractional crystallization of basaltic melts.

The felsic Mukeras dykes, the felsic Mudiah metavolcanics and the felsic dykes of the NE-Desert of Egypt (Stern et al. 1988) are chemically similar to the "A-type" granites of Afro-Arabia. Therefore, the fusion-refusion model for the Central Hijaz "A-type" granitoids (Jackson et al. 1984) and the ideas of mid-crustal anatexis (Stern et al. 1988) on the generation of the late Precambrian "A-type" granites of Afro-Arabia following the accretion of the arc systems in late Precambrian to form the Afro-Arabian Shield are applicable here. The variations observed in the felsic dykes and metavolcanics might indicate that the processes responsible occurred relatively deep in the crust and formed by anatexis with/or without fractional crystallization, and the extensive dyke swarms indicate that such magma reservoirs must have been abundant and occupied large portions of the mid-crust (Stern et al., 1988). Initial melting could occur at a depth of 15 - 25 km in a temperature range 800 - 900° C, and remelting at 870 - 900° C in (Hijaz) crust about 30 - 35 km thick at 650 Ma (Jackson et al., 1984).

### 3.9 Conclusion

The granitoids of the Lowder-Mudiah area are peraluminous, high silica, "A-type" granites that formed from LILE- and LREE-enriched crustal melts; such granites would be expected in an extensional tectonic regime. These granitoids are similar to the A-type younger (686 - 517 Ma) alkali-feldspar granite association (Fig. 3.1) of the Central Hijaz, Saudi Arabia (Jackson et al. 1984).

The Mudiah metavolcanics are bimodal, formed from LILE- and LREE-enriched

source(s), and exhibit Andean-type convergent margin characteristics. However, a large degree of compositional overlap may be expected between lavas in highly magmatic, rapidly distending rifts, and Andean-type convergent margins (Stern et al.1988).

The NE-SW Mukeras dyke swarms (early generation,  $709 \pm 21$  Ma -K/Ar,  $694.1 \pm 23.1$  Ma - $^{39}\text{Ar}/^{40}\text{Ar}$ ) provide evidence for NW-SE directed crustal extension accompanied by widespread bimodal igneous magmas which formed from LILE- and LREE-enriched source(s), and exhibit Andean-type convergent margin characteristics.

The mafic Mukeras dykes are of two groups reflecting two different sources or two different amounts of partial melts, and they may be hypabyssal conduits for the surficial eruption of the mafic component of the bimodal Mudiah metavolcanics. Basaltic melts were probably generated by melting in the upper mantle; the basaltic-andesite melts were probably produced either by a lower-degree of melting of a hydrous upper mantle, or of eclogite. In contrast, the felsic dykes probably represent the feeders of the felsic component of the bimodal Mudiah metavolcanics, and they might be related to the "A-type" granitoids of Lowder-Mudiah.

The felsic Mudiah metavolcanics and the felsic Mukeras dykes are chemically similar to the "A-type" granites of the Central Hijaz of the Arabian Shield, which were explained by a fusion-refusion model by Jackson et al.(1984), to the felsic dykes in the Northeastern Desert of Egypt (Stern et al. 1988), and to the crustal-melt monzogranites in the Karakoram of N. Pakistan (Crawford 1988; Crawford and Windley, 1990).

The petrochemical data combined with geological evidence lead to the following conclusions. The accretion of arc systems in the late Precambrian to form the Afro-Arabian Shield resulted in a thickening of the (juvenile) crust, which led to deep crustal melting (anatexis), which was probably triggered by a mantle disturbance and upper mantle upwelling or diapirism, probably caused by adiabatic decompression, that led to/ or was caused by updoming, stretching, crustal thinning (extensional regime), and the injection of mantle-derived basaltic magma, that gave rise to the basaltic (mafic) Mudiah metavolcanics and the basaltic (mafic) Mukeras dyke swarms. In contrast, the crustal melts are represented now by the felsic Mudiah metavolcanics, the Lowder-Mudiah "A-type" granitoids, and the felsic Mukeras dyke swarms.

The early generation of the Mukeras dyke swarms ( $709 \pm 21$  Ma), the Mudiah metavolcanics and the bimodal dyke swarms of the Northeastern Desert of Egypt (592 - 580 Ma) (Stern and Gottfried 1986; Stern et al. 1988; Stern and Hedge 1985) are very comparable (see Table 3.5; Figs. 3.3, 3.4, 3.5). All these are late Proterozoic bimodal basaltic-andesite to rhyolite suites that are LILE- and LREE-enriched and have marked Nb troughs, and thus they all probably contain an inherited subduction zone signature. Their felsic component is also comparable to the Lowder-Mudiah granitoids (Figs. 3.2, 3.4) and they both represent melts that developed from a remelted accreted arc in an extensional tectonic regime. Moreover, these rocks are similar to the bimodal "sequence" A; 700 - 570 Ma, volcanics (e.g. Jahhad suite) of the Central Arabian Shield (Roobol et al., 1983) (see Fig. 3.3, 3.4), which were considered by Agar (1986) to have extruded in pull-apart grabens of the Najed strike-slip orogen, rather than in a convergent plate margin as was previously interpreted by Roobol et al. (1983).

The host rocks ( $740 \pm 22$  Ma -K/Ar) of the Mukeras dyke swarms range in composition from granite, quartzdiorite, diorite to gabbro. These rocks collectively have a calc-alkaline subduction zone signature, and were probably emplaced in the roots of contemporary island arcs, similar to the older granodiorite association (720 Ma) of the Central Hijaz of Saudi Arabia (Fig. 3.7), which is calc-alkaline ranging in composition from gabbro through monzogranite (Jackson et al., 1984), therefore possibly formed along path A in the Lowder-Mudiah magmatic evolution (see Fig. 6.1). However, the only one granitic sample, show similarity with the Lowder-Mudiah granitoids and the monzogranite (Fig. 3.7a) of the younger assemblage (A-type granitoids) of the Central Hijaz (Jackson et al., 1984), giving rise to the possibility that the host rocks were post-tectonic and formed along path B rather than A in the proposed Lowder-Mudiah magmatic evolution (see Fig. 6.1).

The relationships between the mafic Mudiah metavolcanics and the mafic Mukeras dyke swarms on the one hand, and the Lowder-Mudiah granitoids, the felsic Mudiah metavolcanics and the Mukeras felsic dyke swarms on the other, are all based on their mutual spatial relations and their geochemical characteristics. More precise relationships require age determinations of the granitoids and metavolcanics.

---

The proposed mechanisms and relationships between the Lowder-Mudiah granitoids, Mudiah metavolcanics and the Mukeras dyke swarms should be considered as preliminary, due to the lack of isotopic constraints. However, this study is a first attempt to explore in modern detail the geology of South Yemen. It attempts to establish a possible mechanism(s) and evolutionary model especially by comparison with well-analysed comparable rocks in the Arabian and Afro-Arabian Shields. Further detailed study is recommended especially isotopic analysis in order to determine, confirm, develop, or reject the mechanism(s) and the evolutionary model proposed here.

## CHAPTER 4

### STRUCTURAL GEOLOGY

#### 4.1 Introduction

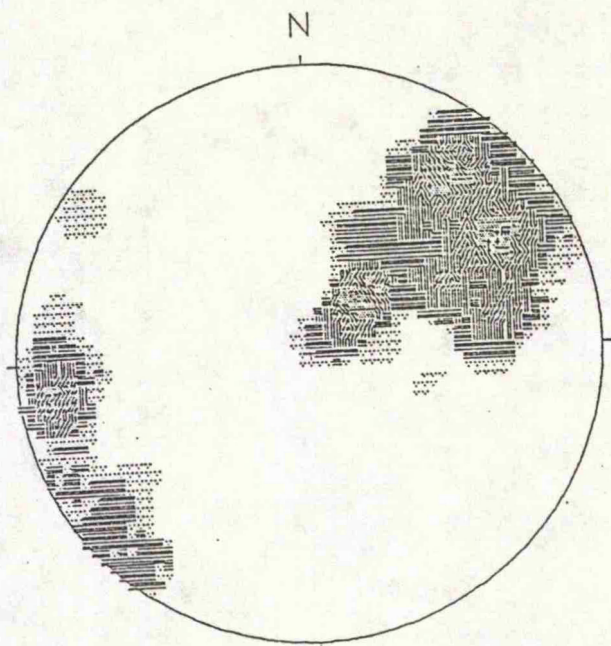
The basement rocks of the Lowder-Mudiah area are divisible into three major lithological (central, eastern and western) belts. These belts were subjected to several phases of folding and are separated by two major northeast-striking ductile shear (thrust) zones. Block faulting in the area is clearly evidenced by the uplifted western belt, the Mukeras escarpment, which represents a prominent topographic and structural feature, in addition to the east-southeastward block faulting in the Jurassic limestone. Structural features observed in the field and confirmed by structural analysis are shown in Fig. 4.1 (enclosed in the accompanied pocket).

#### 4.2 Folds

Multiple deformation has affected the area as indicated by three recognizable deformation episodes, each with its own distinctive style and orientation. Northeast trending isoclinal folds (Plate 4.3a,b) were followed by open folds with vertical axial planes and northwest-trending crossfolds and kink bands. Nomenclature of folds follows the terminology of Fleuty (1964).

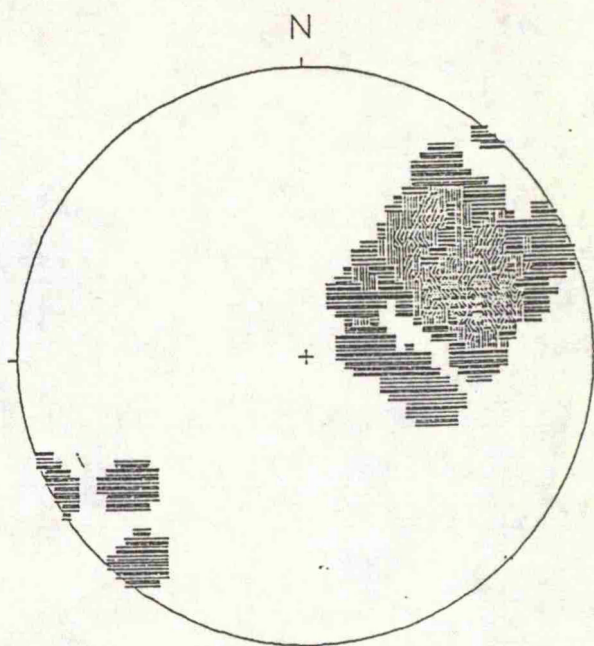
The earliest episode produced recumbent, tight isoclines with semi-horizontal axial planes (probably indicating the presence of nappe structures). There are others with vertical or northeastern and southwesterly plunging axes, but these are confined to the central belt. There appears to be some undulation in the trend and plunge of the fold axes, which in some places are almost horizontal. This is probably the effect of later crossfolding.

This early episode was followed by the development of large-scale open folds with vertical axial planes trending northeast, illustrated well by synforms and antiforms in the metavolcanics of the eastern belt, as well as in the quartz-biotite gneiss and amphibolite of the central belt, which is also folded into a northeast plunging antiform (see Fig. 4.1, enclosed in the accompanied pocket).



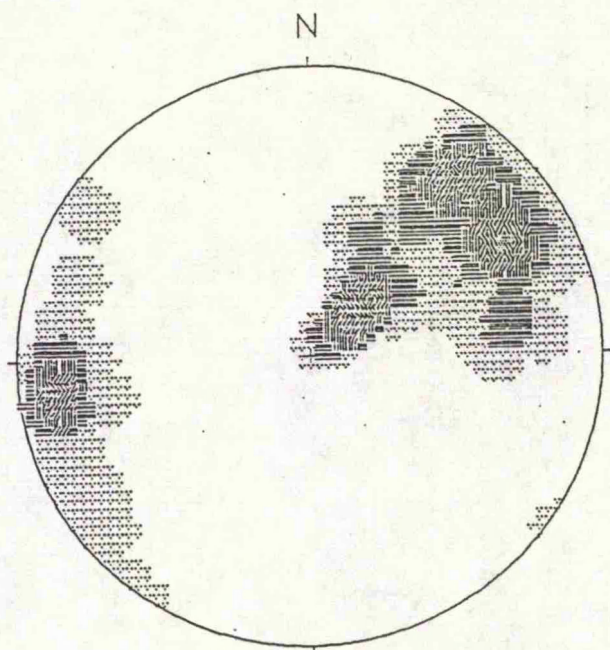
(a)

All lineation  
computed interval 2%



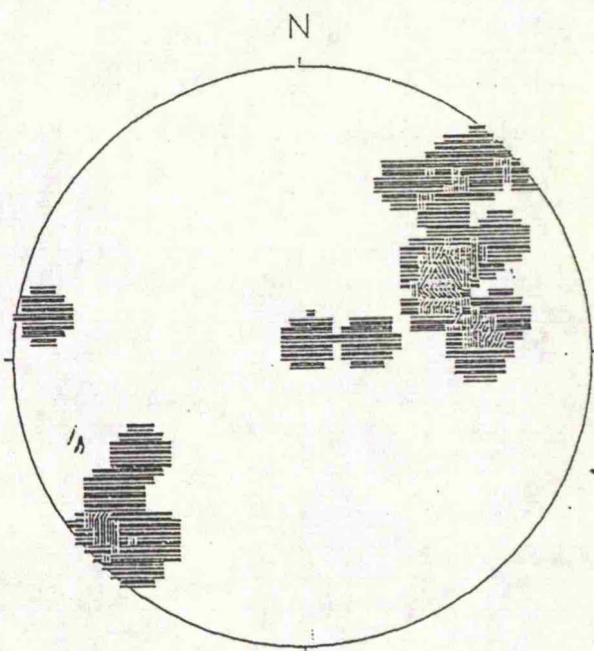
(b)

Mineral lineation  
computed interval .3%



(c)

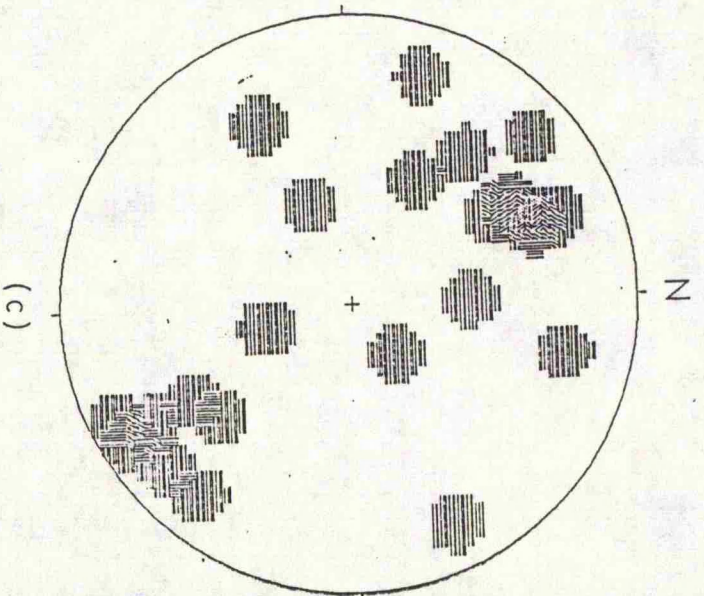
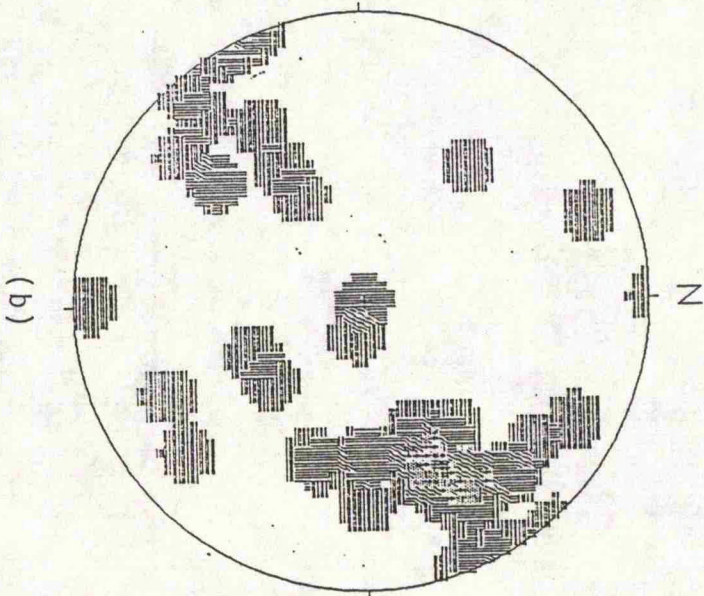
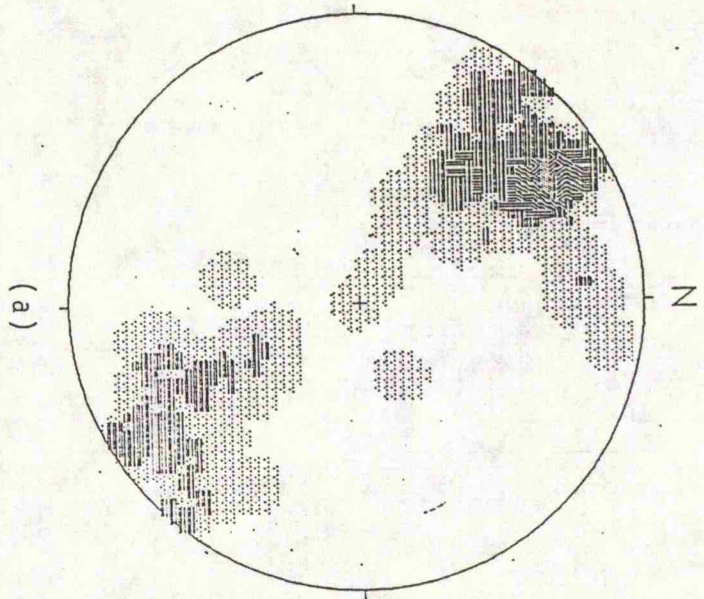
Fragment lineation  
computed interval 3%



(d)

Crenulation lineation  
computed interval 4%

Plate 4.1. Equal area lower hemisphere projections of (a) All the lineations, (b) Mineral lineation, (c) Fragment lineation, (d) Crenulation lineation. In the rocks of the central belt.



Foliation planes  
computed interval 4%

Fold axis  
computed interval 2%

Fold axial planes  
computed interval 4%

Plate 4.2. Equal area lower hemisphere projections of (a) Poles of foliation planes (b) Fold axes, (c) Poles of fold axial planes. In the rocks of the central belt.

Folding during the third episode is manifested by open cross folds and kink bands that plunge shallowly southwest and southeast, and have subvertical axial planes (Plate 4.4e). These folds deform both the earliest isoclines, the large-scale open folds and the shear zones between the major belts.

Equal area lower hemisphere projections of the fold axes (Plate 4.2b) and the fold axial planes (Plate 4.2c) show that there are two conspicuous, clearly defined point concentrations, one of which plunges northeast and the other mostly plunges southeast. In addition, there are two poorly defined concentrations, one north-south and the other around a vertical axis.

Measurements of folded granitic and pegmatic veins (the width of a whole vein divided by the length of that vein) reveal a shortening ratio of between 1/8 and 1/2.

### 4.3 Foliation

The metamorphic rocks of the central and the eastern belts are strongly foliated, and the foliation is expressed as either gneissosity in the granitoid gneisses of the central belt, or as schistosity in the amphibolites of the central belt and metavolcanics of the eastern belt. The foliation strikes generally to the northeast, and dips variably to the northwest and southeast. This is clearly demonstrated by the plots of foliations on an equal area lower hemisphere projection (Plate 4.2a).

### 4.4 Lineation

Linear structures in the area, particularly in the central belt, are expressed as mineral, crenulation and fragment lineations (Plate 4.1), the majority of which plunge northeast (Plate 4.1). Field observations suggest that an older southeast plunging lineation is locally preserved. Plotting the poles of all the lineations on an equal area lower hemisphere projection (Plate 4.1a) shows that the majority plunge northeast, and a minority southwest.

### 4.5 Thrusts

The three main ductile shear zones are deep-level major thrusts, which strike northeast (see Fig. 4.1).

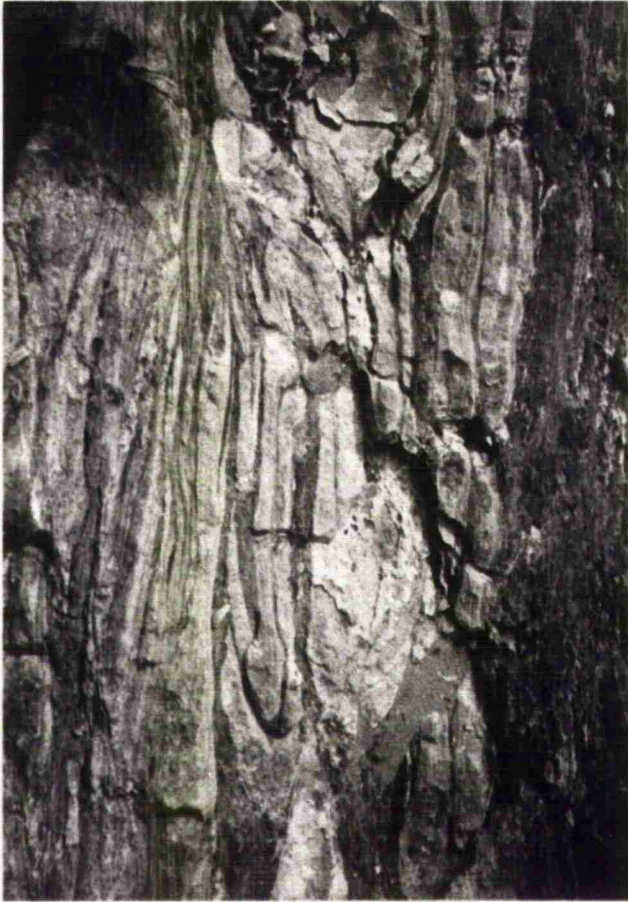
1. This major thrust is located in the eastern part of the area, strikes northeast-southwest, and dips moderately to the southeast. It separates the eastern belt of

**Plate 4.3**

Photographs to illustrate the isoclinal folds and the shear fabrics in the rocks of the central belt.

(a & b) Tight hinge of isoclinal fold (F1) in the quartz-biotite gneiss, and amphibolite. In the central belt, east of Al-Gashaber. Grid Reference 758 1295. Looking NE

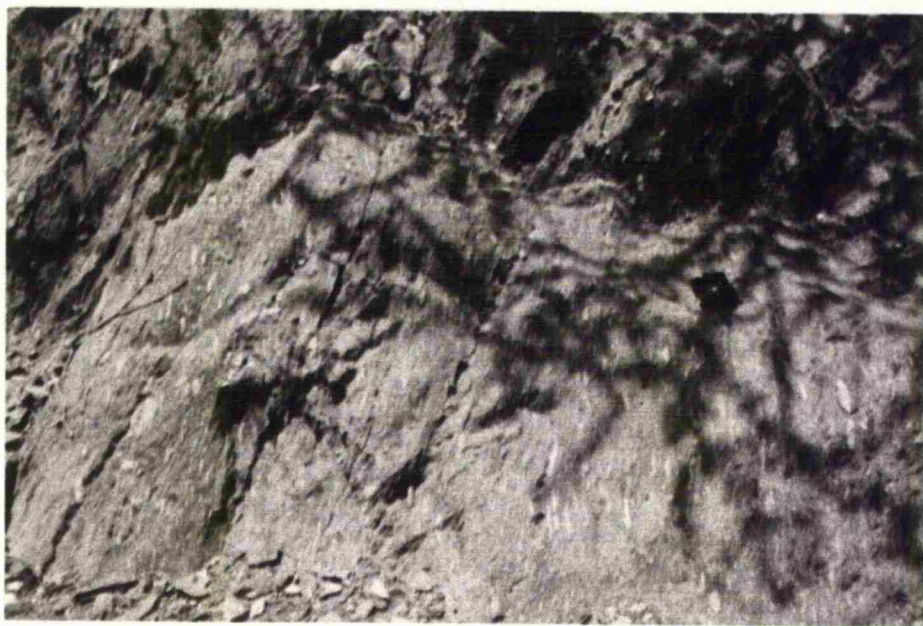
(c) Shear fabrics within garnetiferous quartz biotite schist and gneiss along the western shear zone (between the central and western belts) west of Um Jarubah (see Plate 4.6b). Looking NE. Grid Reference 51 11.



**a**



**b**

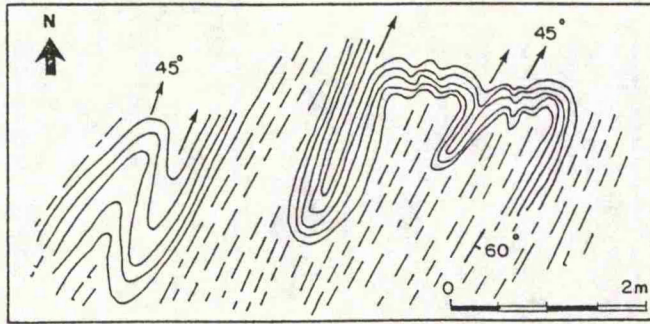


**c**

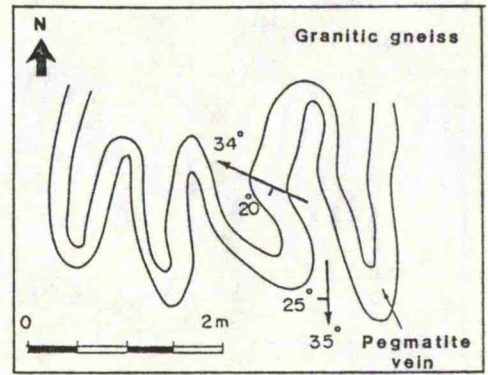
**Plate 4.4**

Sketches of different types of structures drawn in the field.

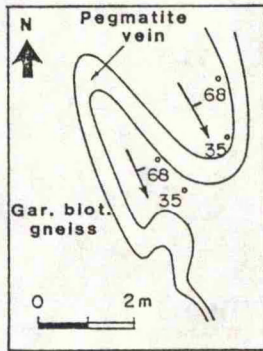
- (a) Isoclinal folds (F1) within the quartz-biotite gneiss and amphibolite. In the central belt east of Al-Gashaber (see plate 4.3a & b). Grid Reference 758 1295.
- (b) Early pegmatite isoclinally and cross folded, within the grey granitic gneiss of the central belt. Grid Reference 81 124.
- (c) Ptygmatically, isoclinally folded pegmatite within the quartz biotite gneiss and amphibolite of the central belt. Grid Reference 51 11.
- (d) Disharmonic folding shown by early pegmatite and a carbonatite dyke, at Um Sallamiah. Grid Reference 492 1453.
- (e) Fold interference pattern, shown by an isoclinal fold (F1) and a cross fold (F3) within the quartz-biotite gneiss and amphibolite of the central belt, at Al-Gashaber. Grid Reference 705 1282.
- (f) Sketch cross-section of part of the southwesterly-plunging antiform in the grey granitic gneiss, with folded pegmatite. Durib. Grid Reference 165 161.
- (g) Isoclinally folded early pegmatite within the quartz-biotite gneiss and amphibolite of the central belt. Grid Reference 230 119.
- (h) Tightly folded early pegmatite within the quartz-biotite gneiss and amphibolite, of the central belt, Mudiah. Grid Reference 820 119.
- (i) Sketch of fold interference pattern showing the augen structure, that might indicate two generations of folds  $F_n$  and  $F_{n+1}$  (F1, F2) in the quartz-biotite gneiss and amphibolite of the central belt, Mudiah. Grid Reference 705 1282



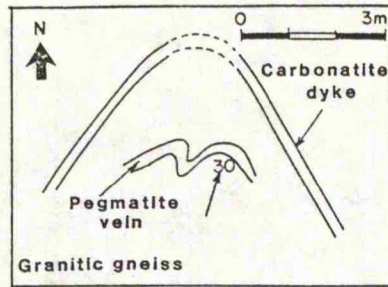
a



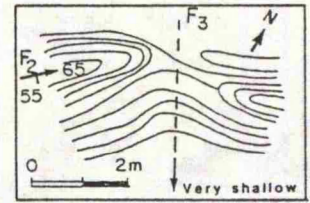
b



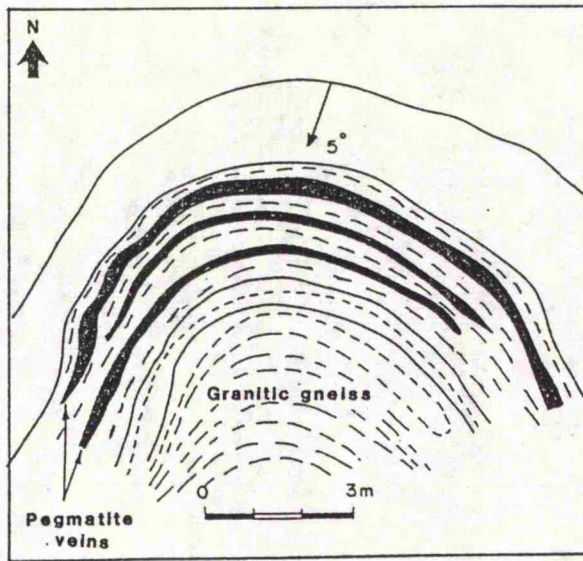
c



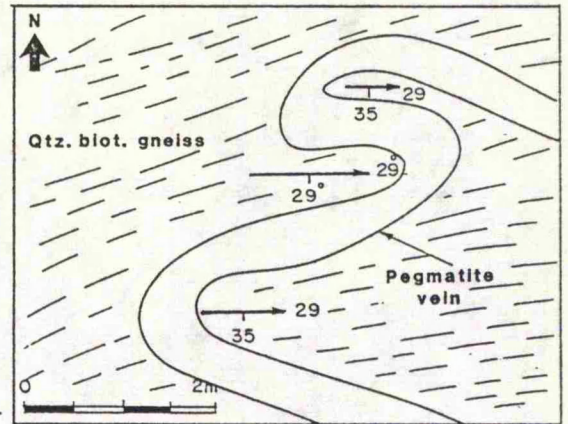
d



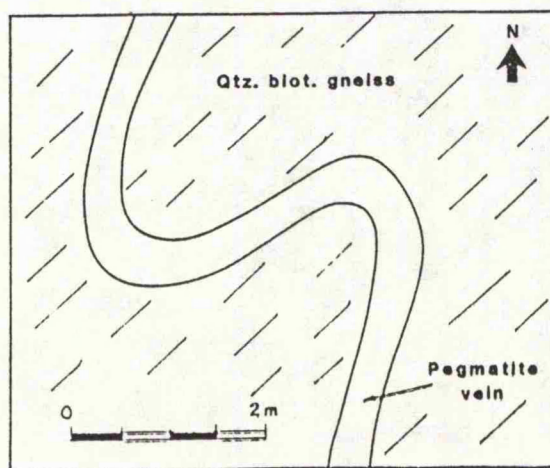
e



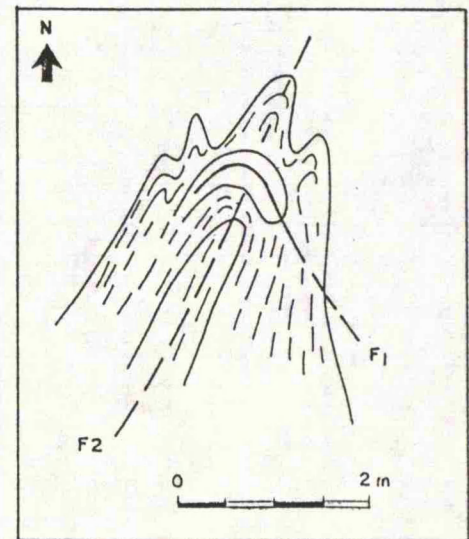
f



g



h



i

**Plate 4.5**

Sketches of different types of structures drawn in the field.

(a) Folded and boudinaged pegmatite within the garnetiferous quartz-biotite gneiss and schist of the western shear zone, between the central and western belts, west of Um Jarubah. Grid Reference 51 11.

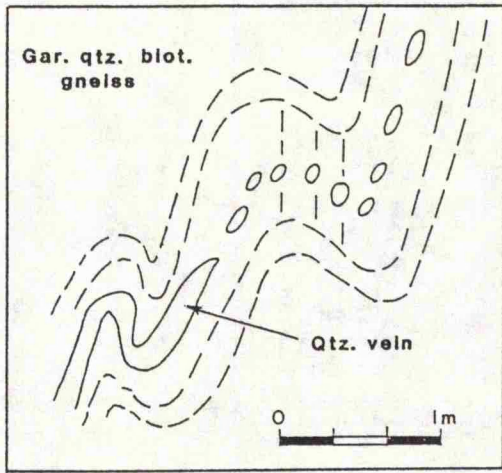
(b) Sigmoidal tension gashes of pegmatite within the garnetiferous quartz-biotite gneiss and schist of the western shear zone, west of Um Jarubah. Grid Reference 51 11.

(c) Boudinage of extended pegmatite vein, within the quartz-biotite gneiss and amphibolite, of the central belt at Al-Gashaber. Grid Reference 705 1282.

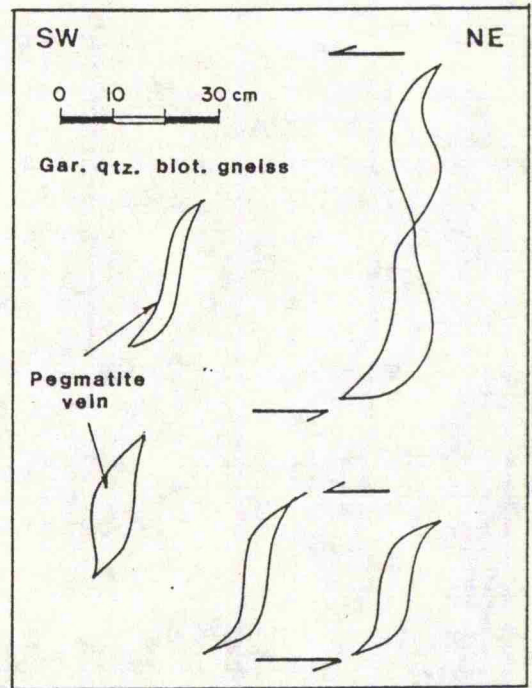
(d) A folded pegmatite, faulted in an echelon shape, offset sinistrally, in the garnetiferous quartz-biotite gneiss and schist of the western shear zone, west of Um Jarubah. Grid Reference 51 11.

(e) Folds of early pegmatite within the grey granitic gneiss, of the central belt at Jabal Al-Yusuf. Grid Reference 41 13.

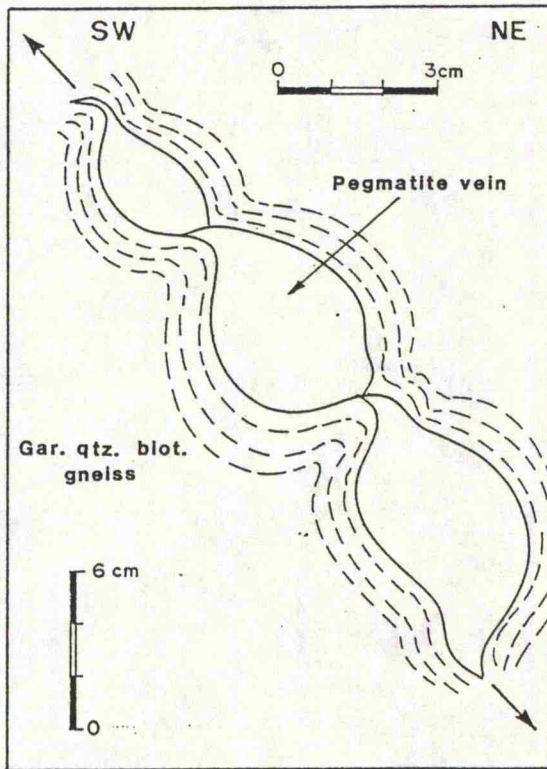
Plate 4.5



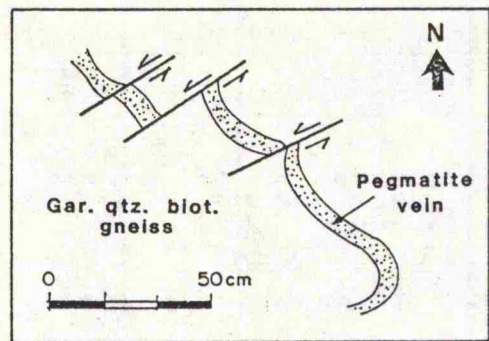
a



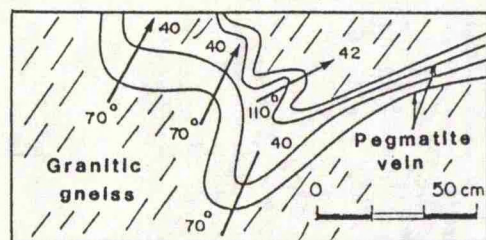
b



c



d



e

metavolcanics from the central belt of granitoid gneisses and amphibolites. This thrust shows a zone of interlayered, structurally concordant lithological slices of the metavolcanics (quartz-rhyolite porphyry) and of the quartz-biotite gneiss and amphibolite (of the central belt), clearly illustrated at Uramah (Mudiah) (Fig. 2.1). In this zone there are boudinaged and sheared pegmatites (Fig. 4.1).

2. This thrust is located in the western part of the area, trends northeast-southwest and dips moderately to the southeast. It separates the central lithological belt from the western belt of the dyke swarms and their granite, diorite and gabbro host rocks. This thrust is marked by strong shear zone that strikes northeast-southwest and dips moderately to the southeast. At Wadi Mekhbezeh the foliations of the garnetiferous quartz-biotite gneiss and schist of the central belt are dragged into the thrust over a distance of 300 m (Plate 4.6).

Shears along both these thrusts are indicated by mylonitization, lensoidal fragmentation and sigmoidal textures that are characteristic of shear fabrics (Sylvester, 1988; Fleuty, 1964) (Plate 4.3c; Plate 4.5a,b,c). Although the dip of the two major thrust planes is generally southeast, the majority of lineations plunge shallowly northeast. In a few localities there is evidence of a weak lineation that plunges steeply to the southeast; this appears to be an older relict lineation.

A dextral sense of movement is indicated by sigmoidal structures (Sylvester, 1988; Simpson et al., 1983) (Plate 4.5b). Some later, folded, pegmatite veins show a sinistral displacement (Plate 4.5d).

3. A third major thrust is located within the central lithological belt. This strikes northeast-southwest and dips to the northwest. On the thrust surfaces are lenticular rock fragments that define a lineation that plunges gently to the northeast. The thrust is marked by strongly sheared quartz-biotite gneiss and amphibolite. Shear surfaces are indicated by the lens-shaped fragments, the sigmoidal fabrics and by the interlayering of slices of different lithological units (Fig. 2.1).

#### 4.6 Present Topography and Block faulting

Topographically the Lowder-Mudiah area is divided into three main parts. The eastern is relatively higher than the central part, which represents the lowlands, and the western

**Plate 4.6**

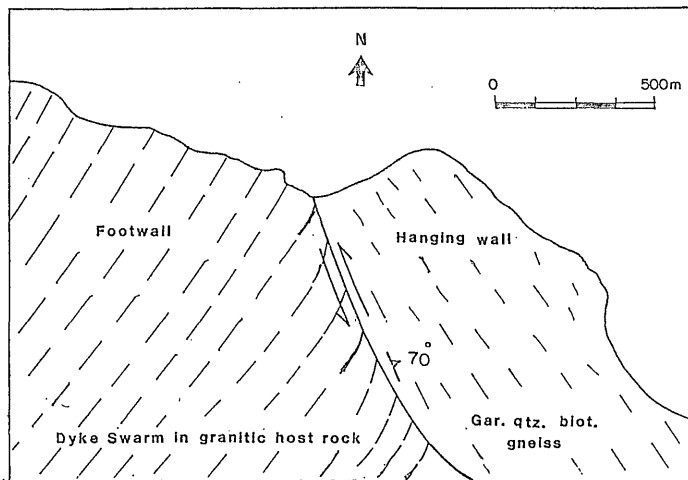
Sketches drawn in the field to illustrate the relationships between the dyke swarms, their host rock (western belt), the thrust and shear zone and the rocks of the central belt at Wadi Mekhbezeh. Grid Reference 38 119.

(a) Schematic diagram showing the relationships between the western thrust, the shear zone within the garnetiferous-quartz-biotite gneiss and schist of the central belt, and the dyke swarms of the western belt. Grid Reference 38 119.

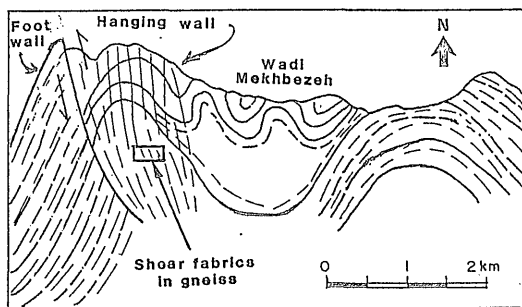
(b) A schematic diagram across the western thrust and shear zone, viewed between Wadi Mekhbezeh and Um Najdah. Grid Reference between 37 118 and 45 126.

(c) A diagrammatic view across the western thrust and shear zone, at Wadi Mekhbezeh. Grid Reference 38 119.

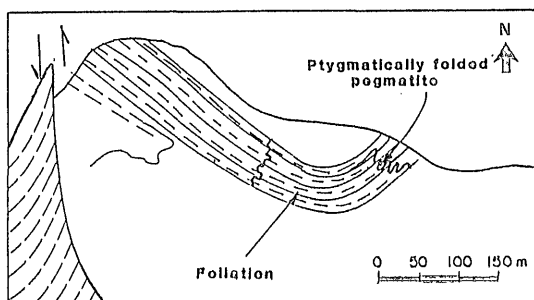
Plate 4.6



a



b



c

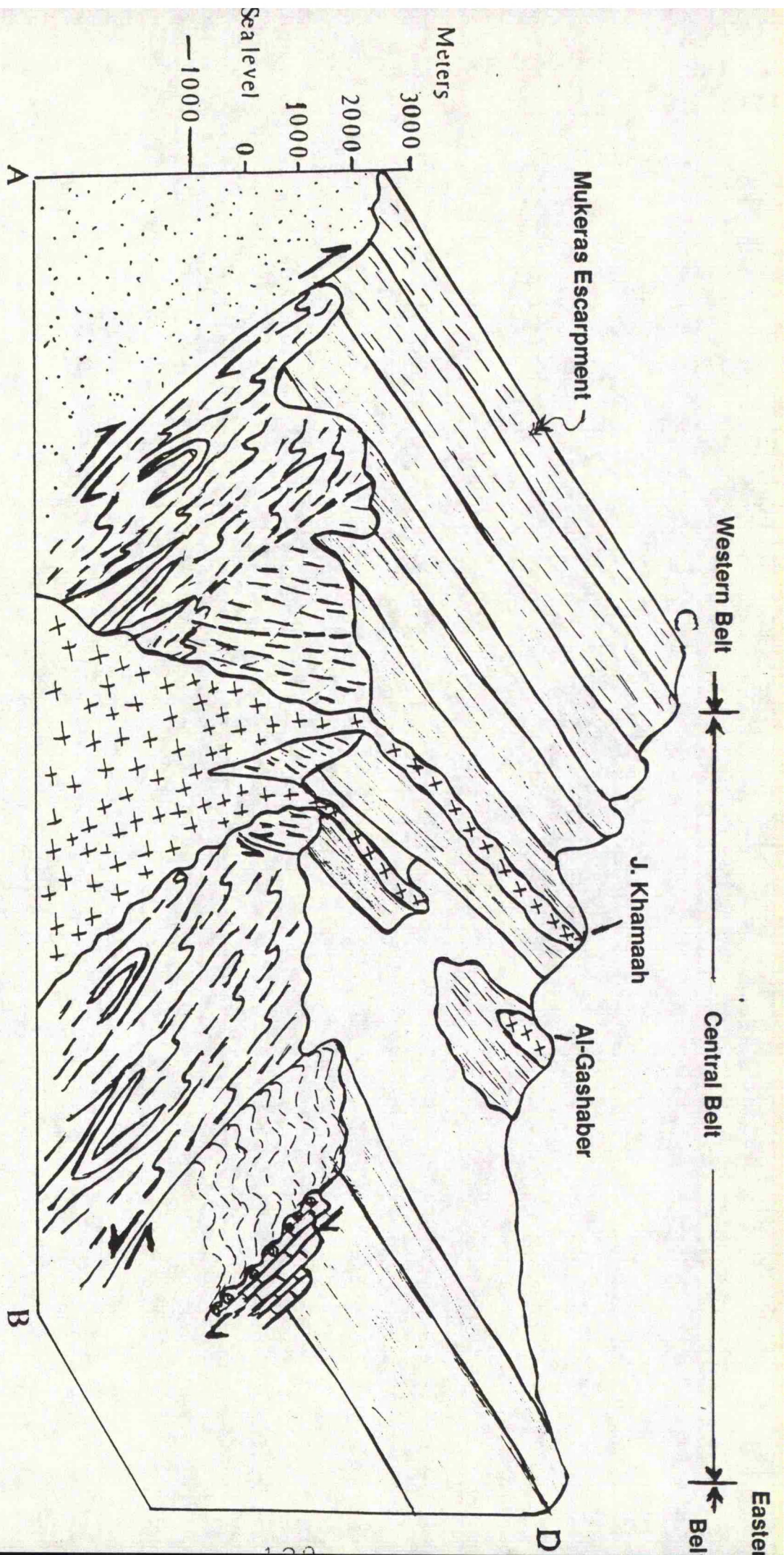


Fig. 4.2 Block-diagram (ABCD; see map Fig. 2.1) showing structure of the area. The Mukeras Escarpment (Western Belt) and the Mudiiah metavolcanics (Eastern Belt) were uplifted relative to the Central Belt, and the Jurassic limestone down-faulted in the east.

part is the highest of the area (Mukeras Escarpment). The Mukeras Escarpment is a prominent topographic and structural feature. The three parts now represent a slightly uplifted eastern block, a subsided central block and a strongly uplifted western block. This indicates block faulting in the area, associated with east-southeast-ward step faulting in the Jurassic limestone. Beydoun (1964, 1966) pointed out that important block and step faulting, which followed buckling, collapsed the flanks of the arches facing the Gulf of Aden. Therefore, the Mukeras Escarpment is a result of late Tertiary uplift and block faulting, which has faulted the Jurassic limestone. However, the late Tertiary normal (block) faulting was controlled by the earlier Pan-African thrust structures (Fig. 4.2).

#### 4.7 Conclusion

The basement rocks in the Lowder-Mudiah area were multiply deformed and dissected by two major northeast-striking ductile shear (thrust) zones, which were reactivated during the late Tertiary in the form of block faulting which led to the uplift of the western part (Mukeras Escarpment) and the eastern part (Mudiah metavolcanics) relative to the central part. However, there was an early phase of thrusting which produced down-dip lineations, and these thrust surfaces were later reactivated to become transcurrent ductile shear zones which gave rise to the present predominant shallow-plunging lineations. Most kinematic evidence indicates that the transcurrent shear zones have a dextral sense of movement. Three deformation episodes were recognized: northeast-trending isoclinal folds, followed by open folds with vertical axial planes and northwest-trending crossfolds and kink bands.

## CHAPTER 5

### The CARBONATITES

#### 5.1 Introduction

##### 5.1.1 Location

The carbonatite dykes are located in the low lands at Um Sallamlah, Al-Arakbi and Durib, in the Lowder-Mudiah area, which is part of Abyan province of the Yemen Republic (see the map Fig. 2.1).

##### 5.1.2 Geological Setting

The geology of the Lowder-Mudiah area consists of Precambrian basement rocks ranging from granitoids, granitoid gneisses, amphibolites and metavolcanics (Ba-bttat, et al., 1988, 1989). These rocks are unconformably overlain by Jurassic limestone (Greenwood and Bleackley, 1967) and partly covered by Quaternary (Shugrah) volcanic basalts (Cox, et al. 1977).

Subparallel discontinuous lenses of carbonatite dykes of variable thickness and colour, brownish, yellowish and pinkish, intruded the basement rocks. The host rocks into which the carbonatite dykes are intruded consists mostly of grey granitic gneiss, amphibolite and quartzite (Ba-bttat, et al. 1988, 1989).

However, it should be pointed out that to the SW of Lowder-Mudiah area, across the Gulf of Aden, Precambrian carbonatites were reported to occur in N.Somalia, NW of Berbera, at Darkainle in the form of discordant dykes intruded the basement rocks (syenites and gneisses) in association with marble bands and exhibit fenitization. These carbonatites are sovites to dolomitic carbonatites enriched in Ba, La, Sr and Y and contain pyrochlore and barite (Gellatly, 1962, 1963a,b, 1964; Heinrich, 1966; Gittlins, 1966).

In Egypt, carbonatites (351 Ma) occur at Gebel Tarbt (Serencsits et al., 1979). Although they concentrated along the Red Sea coast, their age seem to be much older for it to be related to the initial fracturing and opening of the Red Sea. On the other hand, it could be that, as in the East African Rift, fracturing took place on an ancient and active lineament along which carbonatitic and alkaline igneous activity had long been focused (Woolley,

1989).

### 5.1.3 Previous Work

Although the Quaternary volcanics have been subjected to relatively detailed examination, the Precambrian basement of the Lowder-Mudiah area has been only very broadly studied as part of the former Western Aden Protectorate (Greenwood and Bleackley, 1967).

As to the carbonatites, the only available information is in an unpublished technical report by Abouov et al., (1981). This was the result of a Russian Project on the carbonatites involving diamond drill coring at Um Sal-lamiah and Al-Arakbi.

### 5.1.4 Aim and Scope of the Work

The geological study of Lowder-Mudiah area has laid emphasis on field relations, mineralogical constituents, through petrographical examination, electron microprobe analysis, whole-rock petrochemistry and rare earth element analyses. A particular problem was to decide whether these are dykes of carbonatite *senso stricto*, or mineralized lenses of marble variably enriched in REE.

## 5.2 Field Relations

### 5.2.1 Um Sallamiah

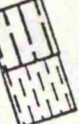
The carbonatite dykes vary in colour from pink to yellowish brown. Some are ferruginous (Plate 5.1b), discontinuous lens-like bodies, 2 - 20 m thick, subparallel to each other and trending almost NE-SW. They intrude grey granitic gneiss and subordinate amphibolite, quartz-biotite gneiss and small quartzite patches. There are clear cross-cutting intrusive contact relationships between the carbonatite dykes and their host rocks, (see Figure 5.1).

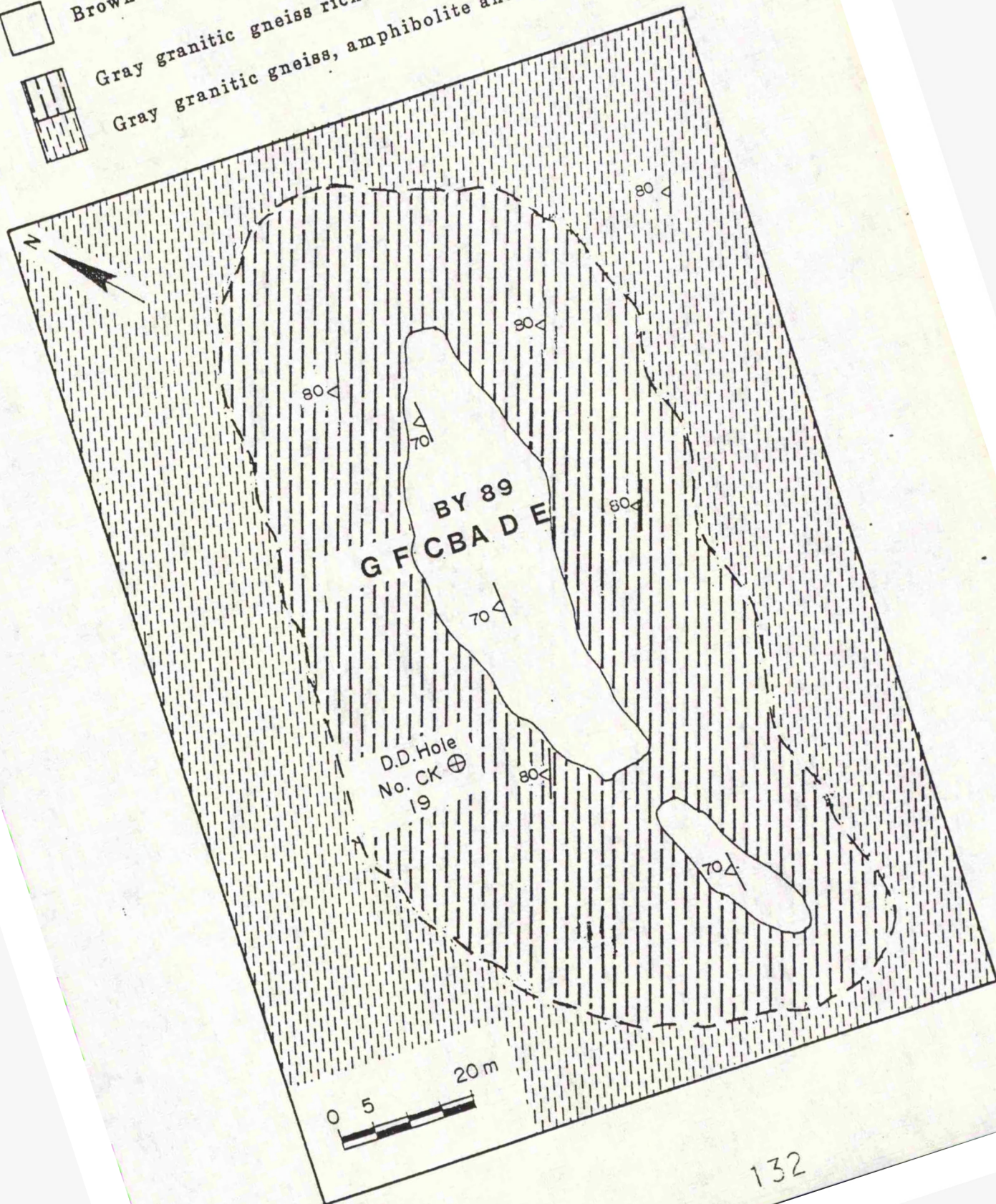
In the vicinity of the carbonatite dykes, the granitic gneiss becomes richer in pink K-feldspar (both in size and amount) (Fig. 5.1). Moreover, at Um Sallamiah (Fig. 2.1), about 300 m to the west of the carbonatite dyke BY89, there is an unfoliated body of biotite about 15 m wide and about 100 m long, with flakes of mica 0.5 to 2.0 cm in size, and hornblende. This body shows cross-cutting intrusive contact relationship with the granitic gneiss, but has no direct contact relationship with the carbonatite dykes.

The enrichment of alkalis shown by the growth of K-feldspars in the granitic gneiss; the

Fig. 5.1 Sketch map of carbonatite at Um Sallamiah .

Grid Reference 482 1455

-  Brown carbonatite
-  Gray granitic gneiss rich in pink K-feldspar
-  Gray granitic gneiss, amphibolite and quartzite



presence of the biotite body as well the mobilized hornblende and aegirine along the joints of the fractured granitic gneiss host rock; might be considered as evidence for the fenitization commonly associated with carbonatite intrusions (Mian and Le Bas, 1986; Andersen, 1989).

Some carbonatite dykes show large open antiform folds with disrupted crests (Plate 5.1a) while others contain xenoliths of the granitic gneiss, which indicate that the carbonatites, although younger than their granitic gneiss, host rocks, also suffered deformation.

### 5.2.2 Al-Arakbi

About three kilometers south of Um Sallamiah, and east of Al-Arakbi, sets of carbonatite dykes sharply cross-cut the grey granitic gneiss and amphibolite host rock. Moreover, there is a concordant body of amphibolite, within the gneiss, which has no clear contact relationship with the carbonatite dykes.

### 5.2.3 Durib

The carbonatitic rocks near Durib are located about 15 km southwest of Um Sallamiah. The host rocks here again consist of grey granitic gneiss, with foliation trending northeast and steeply dipping to the west, associated with quartz-biotite gneisses, amphibolite and quartzite. The carbonatitic sheets, range from 0.5 to 15.0 m wide, and are folded, with a moderate plunge to the southwest. These carbonatitic sheets have fine grained margins, becoming coarser inwards towards the centre, and contain raft-like xenoliths from the host rocks. There is also a concordant body of amphibolite in the vicinity of the carbonatitic sheets, similar to that at Al-Arakbi but with no clear contact relationship with these carbonatitic sheets.

## 5.3 Petrography

The carbonatites are generally coarse-grained, but sometimes medium- to fine-grained, and inequigranular (Plate 5.2a & b). They are yellowish brownish, greyish, pink or white in colour, jointed, altered, banded (in some instances) contain lenticular bands of coarse grained crystalline calcite. They are weakly foliated, react vigorously with HCl and are composed of calcite, dolomite or iron-rich calcite and/or dolomite with patches of pink-coloured barite. Mica is represented mainly by phlogopite, and there is also a little green amphibole, opaque octahedral spots of iron oxides, hematite and limonite. Some

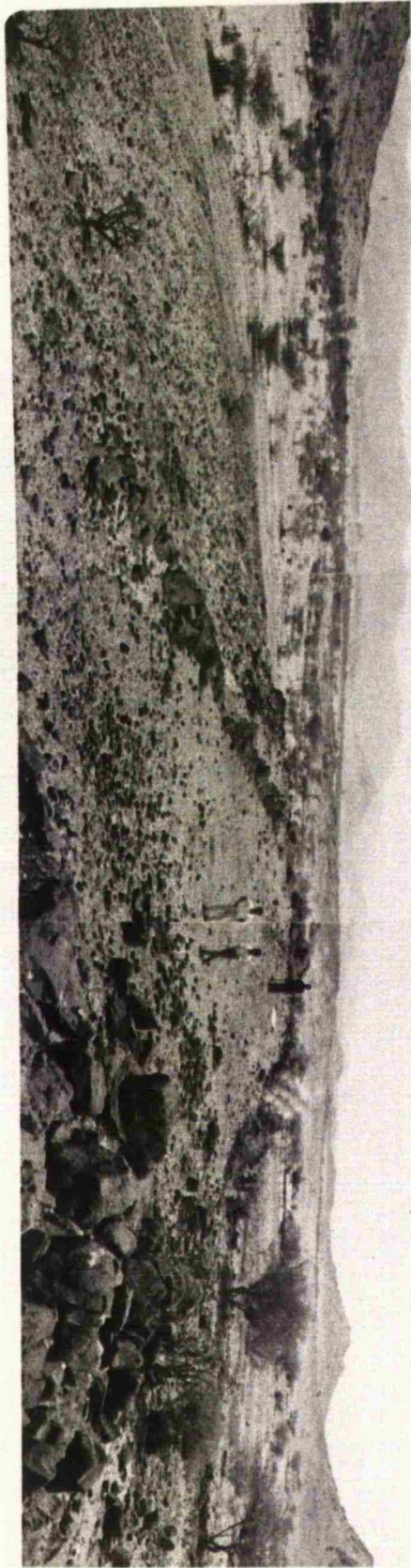
**Plate 5.1**

The following figures, illustrate the field relationship of the carbonatite dykes at Um Sallamlah.

(a) A panoramic view of a ferro-carbonatite dyke or sill (MKY4), in the form of an open plunging antiform fold, with grey granitic gneiss in the core of the fold. Grid Reference 492 1453. Looking SW.

(b) Carbonatite dyke (BY90) with streaks or very thin bands of magnetite (M). Grid Reference 482 1455. Looking west.

p



q

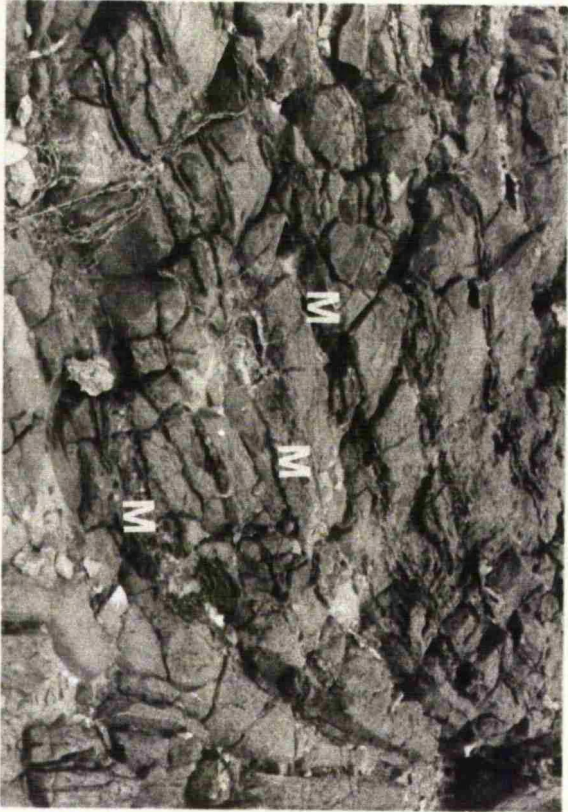


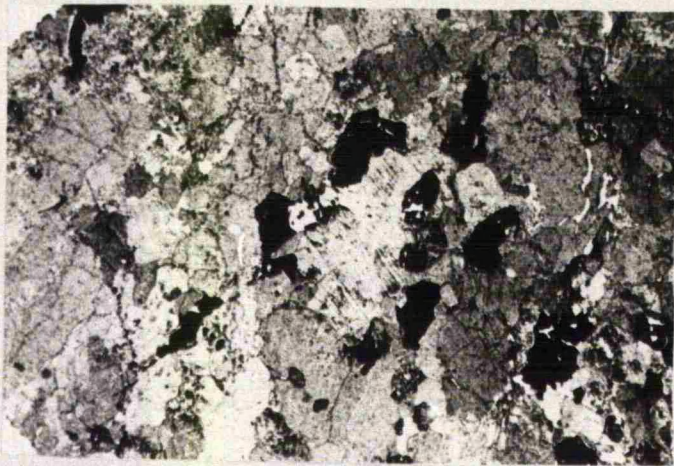
**Plate 5.2**

Photomicrographs showing the main textures and mineral constituents of the carbonatite dyke MKY4. Grid Reference 482 1455.

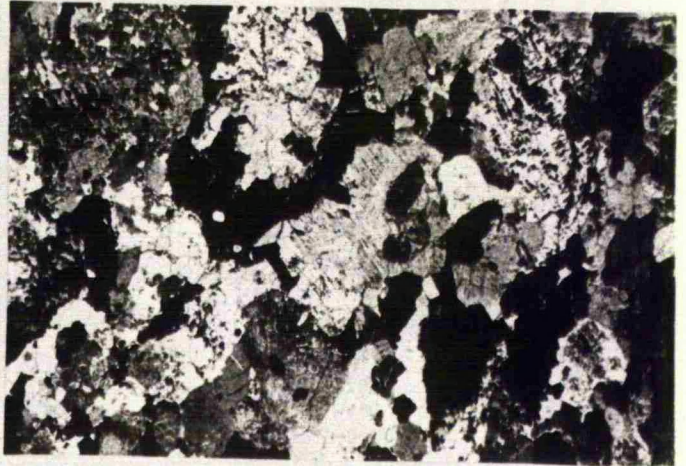
(a and b) Phaneritic, inequigranular texture in ferrocarnatite (MKY4), from Um Sallamiah, with monazite(z) and magnetite(M), as seen under P.P.L. and C.P.L. respectively.

(c and d) Dark barite (B), dusty looking ankeritic dolomite (D), clear calcite (C), Monazite(z) and dark magnetite(M), in carbonatite dyke (MKY4) from Um Sallamiah, as seen under P.P.L. and C.P.L. respectively.

(e and f) Barite (B) and ankeritic dolomite (D) in perthite-like intergrowth texture, in carbonatite dyke (MKY4), from Um Sallamiah, as seen under P.P.L. and C.P.L. respectively.

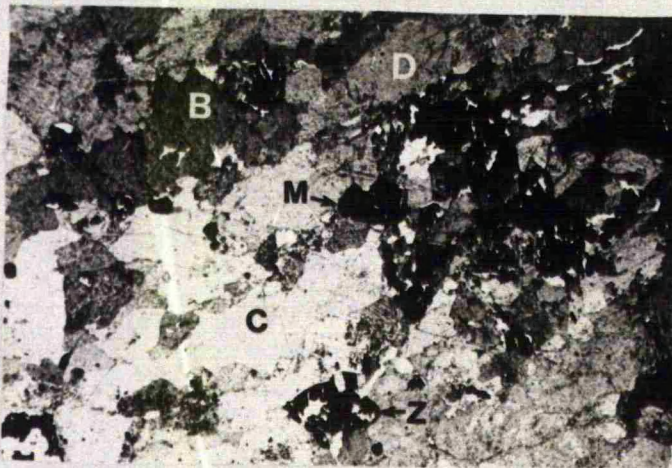


a

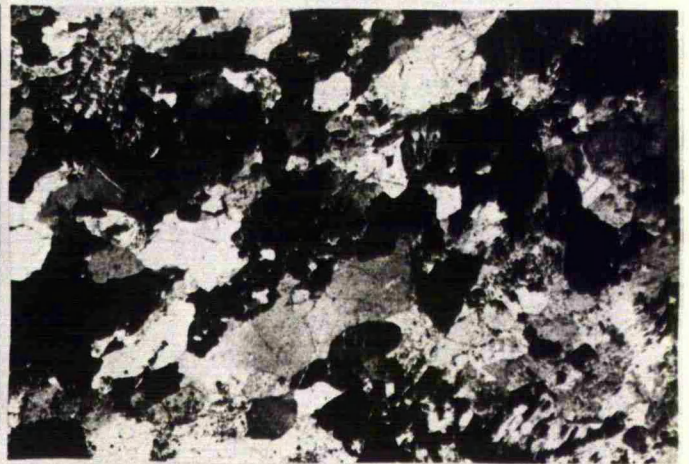


b

0 3mm

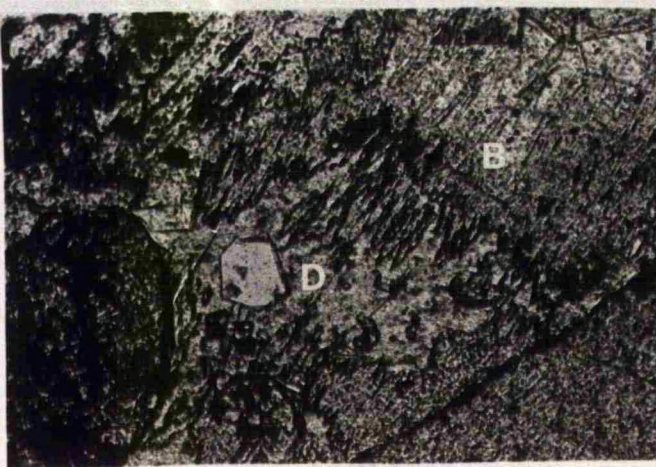


c

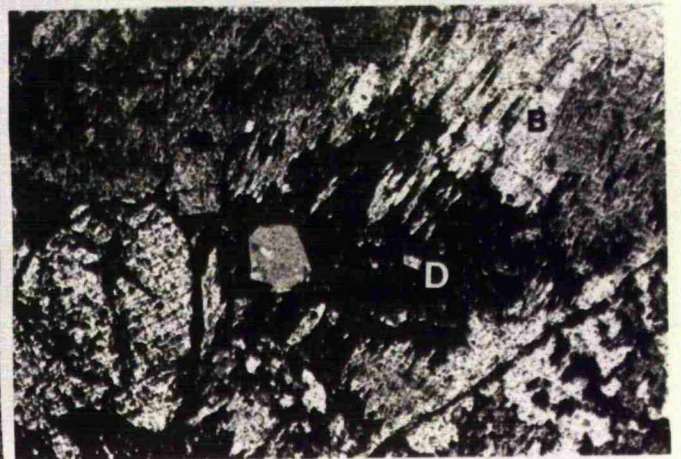


d

0 3mm



e



f

0 0.5mm

carbonatites are very rich in magnetite (Plate 5.1b; 5.2c,d and 5.3c). Surface voids are present in some varieties due to the weathering away of the octahedral grains of magnetite. Alteration along some grain boundaries may indicate leaching. Deformation is expressed by kink bands of mica, while the weak foliation and lineation is expressed by the arrangement of mica and apatite (Plate 5.4a, b, c & d). Perthite-like intergrowth texture occurs between barite and dolomite, and/or calcite, in samples from Um Sailamiah and Al-Arakbi. These intergrowths are in the form of interfingering growths of comb-like texture, between these minerals (Plate 5.2e & f). At least three generations of carbonate (calcite and/or dolomite), are present. The oldest generation is seen in the groundmass and is usually dusty-looking. It is surrounded by the second generation, in the form of clear granular, polygonal, crystallized calcite. The two older generations are cut by the third generation (mainly calcite) in the form of veins and veinlets, (Plate 5.3e & f). Zoned calcite is also present in some varieties. Some of the calcite crystals show elongation (lens-shaped), in samples from the margin of dykes (e.g. sample BY89 C & E, from Um Sailamiah, see fig. 5.1). The calcite, dusty-looking dolomite to ankeritic dolomite (Plate 5.2c, d, e & f) are forming about 40-50% (All percentages are based on visual estimates).

Barite forms about 20-40% of all carbonatites and is pink in colour, showing very weak pleochroism, sometimes to deep pink (Plate 5.2c, d, e & f). Mica, mainly phlogopite, but in places biotite, make up about 10% of the rock. Phlogopite has a characteristic golden yellow colour (Plate 5.4e). Banding and bending of mica (phlogopite) might indicate deformation, and some mica is altered into chlorite, usually along fractures. Apatite, comprising some 10-20%, it exhibits foliation and lineation (Plate 5.3e & f; Plate 5.4a, b, c & d). Certain varieties of the carbonatites (e.g. MKY6) are very rich in apatite, which has a typical stubby morphology of carbonatitic apatite (Plate 5.4c & d). Large crystals of monazite (plate 5.4e) make up about 5-10% of the rock. Amphibole (winchite) pale green to brownish green, form about 5-10%. Pyrochlore is about 3%. Quartz present in some instances as veins and veinlets, showing wavy extinction.

Iron oxides are present either in the form of cubic, octahedral crystals of magnetite (Plate 5.1b, plate 5.3c & d), or in the form of hematite and limonite which has been remobilized

**Plate 5.3**

Photomicrographs, to illustrate textures and mineral constituents of the carbonatite dykes at Um Sallamiah.

(a and b) Euhedral crystal of calcite (C), in a carbonatite dyke (BY26DI), Um Sallamiah, as seen under P.P.L. and C.P.L. respectively. Grid Reference 482 1462.

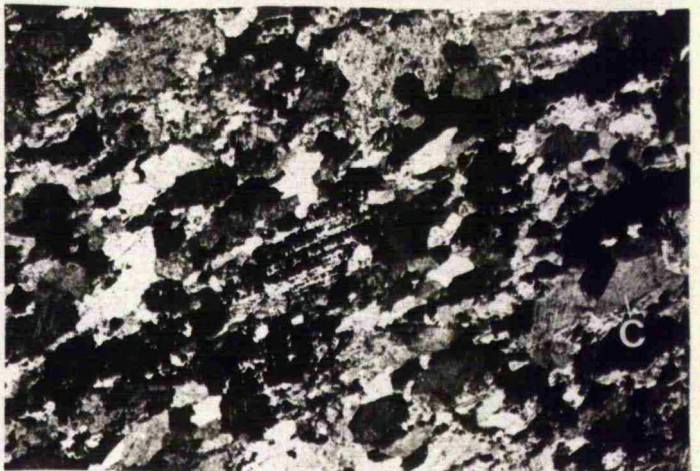
(c and d) Anhedral calcite, dolomite and barite, with monazite (Z) and magnetite (M), in the carbonatite from Um Sallamiah (BY26DI), as seen under P.P.L. and C.P.L. respectively. Grid Reference 482 1462.

(e and f) Carbonatite from Um Sallamiah (BY89D), with apatite (A) mineral and vein of calcite. Apatite crystals show foliation, as seen under P.P.L. and C.P.L. respectively. Grid Reference 482 1455.

0 3 mm



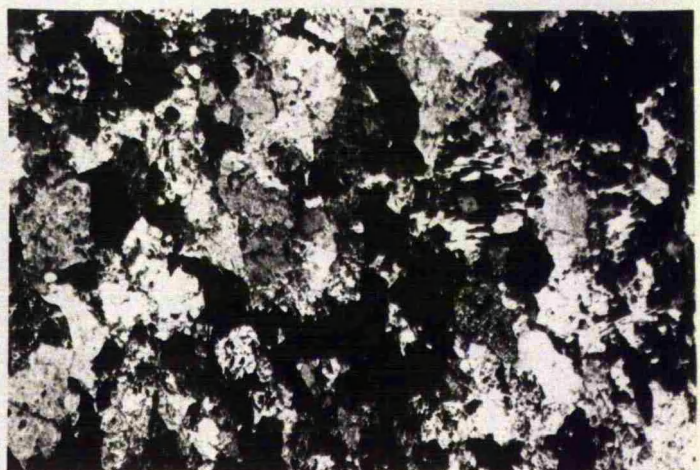
a



b



c



d



e



f

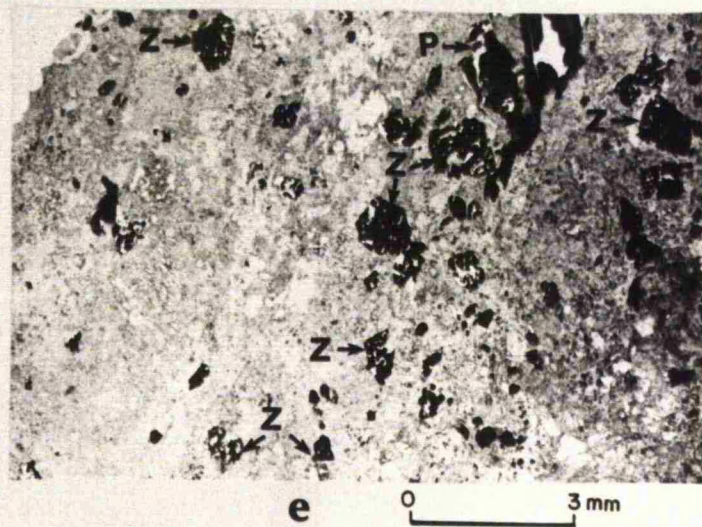
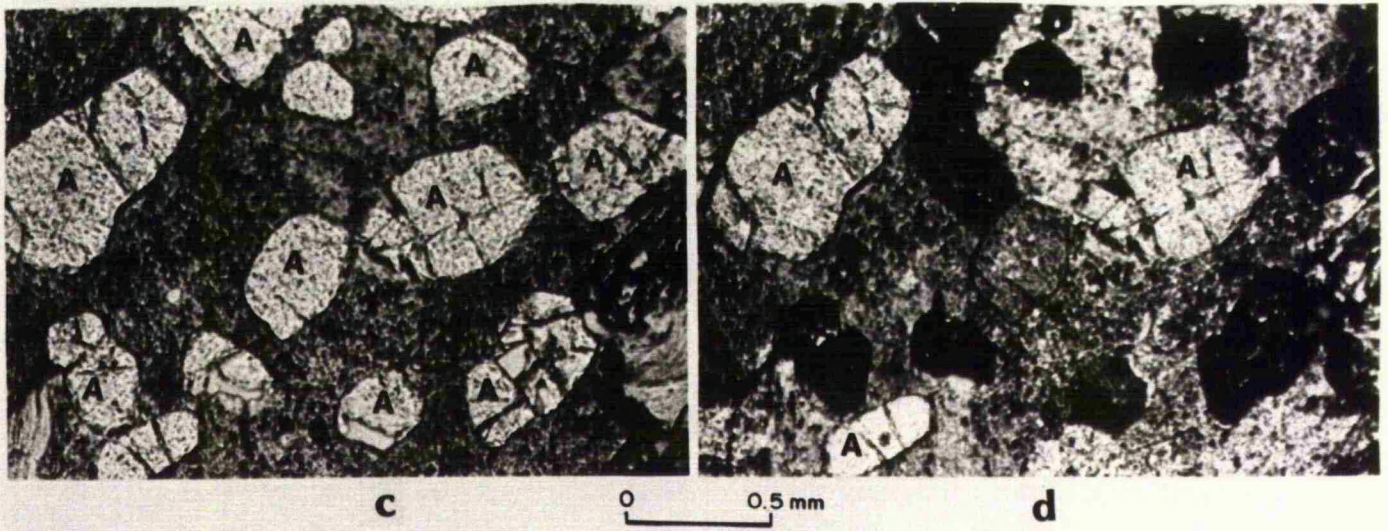
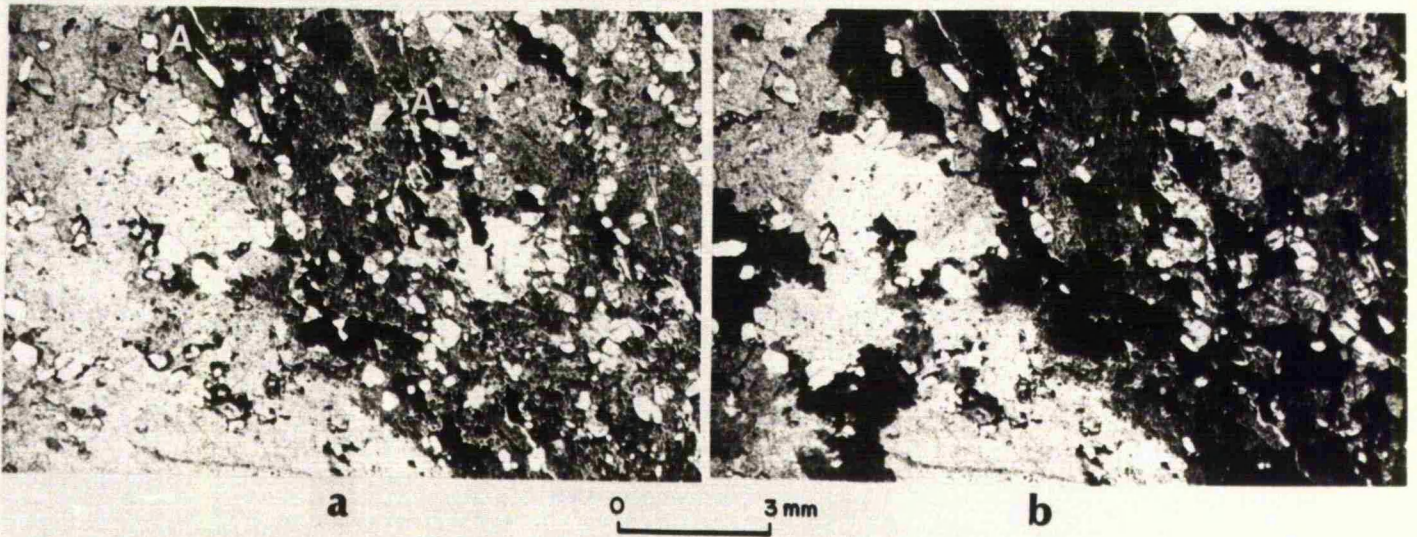
**Plate 5.4**

Photomicrographs for the carbonatite, showing foliated texture and stubby habit of apatite, from Um Sallamiah.

(a and b) Carbonatite sovite, rich in apatite (A) foliated (MKY6) Um Sallamiah, as seen under P.P.L. and C.P.L. respectively. Grid Reference 480 1448.

(c and d) Stubby habit and foliation of apatite (A) in carbonatite sovite (MKY6), Um Sallamiah, as seen under P.P.L. and C.P.L. respectively. Grid Reference 480 1448.

(e) Monazite (Z) and phlogopite (P) in ankeritic ferrocarnatite, BY90c, Um Sallamiah, as seen under P.P.L. Grid Reference 492 1453.



and moved along, the grain boundaries, or the fractures.

Petrographic study reveal that, apatite, monazite, pyrochlore and barite minerals are of the main constituents of group III and group IV carbonatites, whereas group I and group II are composed mainly of calcite and/or dolomite with granular and mozaic textures (The grouping is based on trace and rare earth elements spiderdiagrams, which will be discussed later).

Group III carbonatites are very rich in apatite, while group IV has less apatite, but very rich in monazite and barite. The presence of the characteristic carbonatite minerals (apatite, monazite, and pyrochlore) in group III and IV, and the absence of these minerals in group I and II, might indicate, mineralogically, that group III and group IV are definitely carbonatite rocks.

Mineralogically group III and group IV carbonatite can be classified (Woolley, 1982; Woolley and Kempe, 1989) as apatite sovites, ankeritic to dolomitic magnesio-carbonatites and Ba-rich ferrocarnatites.

#### **5.4 Ore Microscopy**

Ore microscopic identification of the opaque minerals reveal that they are mainly perfect euhedral crystals of magnetite, strongly martitized and fractured, and healed with the non-opaque minerals, minor geothite and hematite. Geothite is mantled by martitized magnetite (this geothite is probably after sulphides). More details are in the appendix A5.

#### **5.5 Microprobe Analysis**

Microprobe analysis were carried out at the University of Leicester, using a Mark V Cambridge Electron Microprobe and Geol-JXA-8600 Electron Microprobe on carbon-coated polished sections. The analysis reveal that, the carbonate minerals range from pure calcite to ankeritic dolomite, ankerite, to dolomite (Table 5.1). Amphiboles, winchite (Table 5.2a), sub-calcic actinolite (Table 5.2b), actinolite (Table 5.2c) and tremolite (Table 5.2d).

Winchite have been identified from carbonatites (Hogarth, 1989). Actinolite and tremolite were reported to be optically determined from carbonatite, but without chemical analysis (Hogarth, 1989, p. 132).

Monazite analysis (Table 5.3), shows noticeably low totals, and a high Th peak seen

TABLE 5.1: REPRESENTATIVE MICROPROBE ANALYSIS OF CARBONATES  
FROM THE CARBONATITES FROM LOWDER-MUDIAH AREA,  
YEMEN REPUBLIC

Group	III	IV	IV	IV	IV
Sample	BY25E	BY11	MKY4	MKY4	MKY4
Locality	UMS	UMS	UMS	UMS	UMS
SiO <sub>2</sub>	.15	.00	.21	.16	.17
Fe <sub>2</sub> O <sub>3</sub>	4.26	.00	1.40	.01	.67
MnO	.56	2.21	.81	.65	.44
MgO	17.06	.57	19.21	.25	11.84
CaO	29.02	56.51	30.46	58.94	39.03
SrO	.49	NA	NA	NA	NA
TOTAL	51.54	59.29	52.09	60.01	52.15

NA = Not analysed

UMS = Um Sallamiah

TABLE 5.2a: REPRESENTATIVE MICROPROBE ANALYSIS OF AMPHIBOLE (WINCHITE)  
 SAMPLE HKY4, FROM THE CARBONATITES FROM, UM SALLAMIAH,  
 LOWDER-HUDIAH AREA, YEMEN REPUBLIC

OXIDE %		NOS. OF IONS		SITE OCCUPANCIES		
SI 02	55.45	SI	7.983	TET	SI	7.983
TI 02	0.18	TI	0.019		AL	0.017
AL2O3	0.62	AL	0.105		SUM	8.000
FE2O3	2.92	FE3	0.317	C(M1,M2,M3)	AL	0.088
FE 0	6.53	FE2	0.786		TI	0.019
MN 0	0.27	MN	0.033		FE3	0.317
HG 0	17.64	HG	3.786		HG	3.786
CA 0	6.96	CA	1.074		FE2	0.786
NA2O	4.54	NA	1.267		MN	0.005
K 2O	0.56	K	0.103		SUM	5.000
		SUM	15.472	B(M4)	MN	0.028
	95.67	O	23.000		CA	1.074
					NA	0.898
					SUM	2.000
				A	NA	0.369
					K	0.103
					SUM	0.472

TABLE 5.2b: REPRESENTATIVE MICROPROBE ANALYSIS OF AMPHIBOLE  
 (SUBCALCIC ACTINOLITE) SAMPLE BY26C FROM THE CARBONATITES  
 FROM, UM SALLAHIAH, LOWDER-HUDIAH AREA, YEMEN REPUBLIC

OXIDE %		NOS. OF IONS		SITE OCCUPANCIES		
SI 02	56.39	SI	8.000	TET	SI	8.000
TI 02	0.07	TI	0.007		SUM	8.000
AL2O3	0.44	AL	0.074	C(M1,H2,H3)	AL	0.074
FE2O3	0.02	FE3	0.002		TI	0.007
FE 0	4.74	FE2	0.562		FE3	0.002
MN 0	0.20	MN	0.024		HG	4.331
MG 0	20.48	MG	4.331		FE2	0.562
CA 0	9.72	CA	1.478		MN	0.024
NA2O	3.16	NA	0.869		SUM	5.000
K 2O	0.47	K	0.085	B(M4)	CA	1.478
		SUM	15.432		NA	0.522
	95.68	O	23.000		SUM	2.000
				A	NA	0.347
					K	0.085
					SUM	0.432

TABLE 5.2c: REPRESENTATIVE MICROPROBE ANALYSIS OF AMPHIBOLE  
(ACTINOLITE) SAMPLE MKY6 FROM THE CARBONATITES  
FROM, UM SALLAMIAH, LOUDER-MUDIAH AREA,  
YEMEN REPUBLIC

OXIDE %		NOS. OF IONS		SITE OCCUPANCIES		
SI 02	55.93	SI	7.930	TET	SI	7.938
TI 02	0.02	TI	0.002		AL	0.062
AL203	0.84	AL	0.141		SUM	8.000
FE 0	4.56	FE2	0.541	C(M1,M2,M3)	AL	0.079
HN 0	0.01	HN	0.001		TI	0.002
MG 0	20.27	MG	4.207		MG	4.289
CA 0	12.79	CA	1.945		FE2	0.541
NA2O	0.82	NA	0.226		HN	0.001
K 20	0.21	K	0.030		SUM	4.912
		SUM	15.121	D(H4)	CA	1.945
	95.45	O	23.000		NA	0.055
					SUM	2.000
				A	NA	0.171
					K	0.038
					SUM	0.209

TABLE 5.2d: REPRESENTATIVE MICROPROBE ANALYSIS OF AMPHIBOLE (TREMOLITE)  
 SAMPLE HKY6 FROM THE CARBONATITE FROM, UH SALLAMIAH, LOWDER-  
 MUDIAH AREA, YEMEN REPUBLIC

OXIDE %	NOS. OF IONS	SITE OCCUPANCIES		
SI 02	55.86	SI	7.835	TET SI 7.835
TI 02	0.04	TI	0.004	AL 0.165
AL2O3	1.13	AL	0.187	SUM 8.000
FE 0	3.07	FE2	0.360	C(M1,M2,M3) AL 0.022
MN 0	0.17	MN	0.020	TI 0.004
HG 0	21.79	HG	4.556	HG 4.556
CA 0	12.96	CA	1.948	FE2 0.360
NA2O	1.01	NA	0.275	MN 0.020
K 2O	0.21	K	0.038	SUM 4.963
		SUM	15.223	B(M4) CA 1.948
96.24	0	23.000		NA 0.052
				SUM 2.000
				A NA 0.223
				K 0.038
				SUM 0.260

TABLE 5.3: REPRESENTATIVE MICROPROBE ANALYSIS OF MONAZITE  
FROM THE CARBONATITES FROM LOWDER-MUDIAH  
AREA, YEMEN REPUBLIC

Group	IV	III	IV
Sample	BY26D2	BY25E	BY42D1
Locality	UMS	UMS	ARA
SiO <sub>2</sub>	.08	.66	.29
TiO <sub>2</sub>	.18	.00	.58
Al <sub>2</sub> O <sub>3</sub>	.04	.00	.26
CaO	.25	.44	.00
SrO	.91	.07	.00
La <sub>2</sub> O <sub>3</sub>	21.52	22.20	21.73
Ce <sub>2</sub> O <sub>3</sub>	32.30	32.76	32.48
SO <sub>3</sub>	.12	.80	.00
P <sub>2</sub> O <sub>5</sub>	27.95	28.62	27.76
TOTAL	83.35	85.55	82.84

N.B. Low totals might be attributed to not analysing for thorium, which show high peak through screen, during analysis. According to Deer et al. 1965, ThO<sub>2</sub> in monazite might form 4% to 12% and up to 30% of the total oxides.

UMS = Um Sallamiah

ARA = Al-Arakbi

TABLE 5.4: REPRESENTATIVE MICROPROBE ANALYSIS OF APATITE FROM THE CARBONATITES FROM LOWER-MUDIAH AREA, YEMEN REPUBLIC

Group	III	III	III	III
Sample	BY26C	MKY6	MKY6	MKY6
Locality	UMS	UMS	UMS	UMS
MgO	.29	.00	.30	.17
CaO	52.13	54.60	52.24	52.97
Na2O	.56	.10	.20	.20
K2O	.13	.01	.07	.04
P2O5	39.36	38.27	38.48	38.22
SrO	.79	NA	NA	NA
La2O3	.18	NA	NA	NA
Ce2O3	.64	NA	NA	NA
TOTAL	94.08	91.98	91.29	91.6

NA = Not analysed

TABLE 5.5: REPRESENTATIVE MICROPROBE ANALYSIS OF BARITE  
FROM THE CARBONATITES FROM LOWDER-MUDIAH AREA,  
YEMEN REPUBLIC

Group	IV	IV	IV	IV	IV
Sample	BY26D2	BY42D1	BY11	MKY4	MKY4
Locality	UMS	ARA	UMS	UMS	UMS
SiO <sub>2</sub>	.31	.41	.95	.82	.98
Na <sub>2</sub> O	.99	1.12	.34	1.05	.76
K <sub>2</sub> O	.08	.02	.03	.07	.89
BaO	61.35	63.27	62.63	64.83	61.95
SrO	2.58	1.79	2.56	NA	NA
La <sub>2</sub> O <sub>3</sub>	.00	1.57	0.1	NA	NA
SO <sub>3</sub>	34.30	34.65	34.16	34.26	33.07
TOTAL	99.61	102.83	100.77	101.03	97.65

NA = Not analysed

during analysis. According to Deer et al., (1965), Th in monazite might form 30% of the total oxides composition of this mineral, so the low totals of monazite might be attributed to the absence of Th in the microprobe analytical results. Other minerals probed were apatite (Table 5.4) and barite (Table 5.5).

## 5.6 Geochemistry

### 5.6.1 Analytical Techniques

Thirty carbonatitic rocks, three limestones and two marble samples were cut into chips using hammer and hydraulic jaw splitter to remove weathered surfaces. Selected homogeneous chips were crushed using a steel jaw crusher and about 150 grams of the coarse material was ground to a fine powder in an agate, Tema swing ball mill.

Pressed pellets were made from the fine powders by adding 15-20 drops of an aqueous solution of polyvinyl alcohol (Moviol) at 15 tonnes per square inch pressure in a steel die. These pellets were analysed for major and trace elements on Phillips PW1400, X-ray spectrometer, at the University of Leicester, using Rh and W tubes.

Rare earth elements (REE) were separated from the ignited powder at the University of Leicester, using the method of Walsh et al. (1981) and analysed by Inductively Coupled Plasma Optical Emission Spectrometer (ICP). With each batch of six samples, one standard (BOB-I) and one blank were run during the separation of the REE for calibration purposes and determining errors which might have arisen, particularly in the concentration of solutions used. Details for the analytical techniques and accuracy are in the appendices, A3 and A5.

Whole rock (major oxides), trace elements and rare earth element analysis are listed in Tables 5.6, 5.7 and 5.8. In some of the analysis, low totals of the major oxides (less than 60%), are attributed to the presence of very high concentration of BaSO<sub>4</sub> (Barite). Moreover, there is a noticeable difference between the values of some REE (La, Ce, Nd) obtained by XRF and that obtained by ICP. This attributed, according to Marsh (1990 personal communication), to that, for many of the samples the abundances of the REE, Ba and Sr are possibly one or two orders of magnitude outside the routine calibration ranges. For XRF the routine calibration ranges for the LREE as follows: La = 0 - 200 ppm, Ce = 0 - 400 ppm, Nd = 0 - 200 ppm. Routine calibration ranges on the XRF for Ba

Table 5.6: CARBONATITIC ROCKS OF LOWDER-MUDIAH AREA ABYAN,  
PROVINCE, YEMEN REPUBLIC

GROUP	III	III	IV	IV	II	III	III
LOCALITY	UMS						
PELLET	L10055	L10056	L10057	L10058	L10064	L10065	L10066
SAMPLE	BY26A	BY26C	BY26D1	BY26D2	BY25B	BY25C	BY25D
SiO <sub>2</sub>	2.2	5.4	0.3	2.4	0.5	3.9	1.5
TiO <sub>2</sub>	0.05	0.18	0.20	0.23	0.02	0.23	0.04
Al <sub>2</sub> O <sub>3</sub>	0.3	0.1	0.1	0.1	0.1	0.5	0.0
Fe <sub>2</sub> O <sub>3</sub>	0.2	0.3	0.4	0.3	0.1	0.2	0.4
MnO	0.40	0.49	0.48	0.46	0.18	0.16	0.53
MgO	5.9	16.3	9.5	10.2	20.1	1.9	14.8
CaO	45.7	36.1	23.8	25.3	37.5	47.5	36.7
Na <sub>2</sub> O	0.1	0.0	0.1	0.1	0.0	0.1	0.1
K <sub>2</sub> O	0.0	0.0	0.0	0.0	0.0	0.0	0.0
P <sub>2</sub> O <sub>5</sub>	0.08	3.21	1.29	0.63	0.03	4.73	3.60
Total	54.93	62.14	36.19	39.75	58.64	59.29	57.66

Trace elements in ppm

Cr	1	3	0	0	2	0	0
V	21	49	23	47	0	93	10
Nb	12	42	694	457	1	14	734
Zn	17	10	13	11	14	21	50
Ni	7	6	10	16	2	4	5
Zr	0	47	0	0	0	0	0
Y	53	82	118	129	4	68	35
Ba	1944	224	136996	123835	95	2497	1423
Sr	12784	788	9284	4497	852	1809	13317
Rb	0	0	12	10	0	0	0
Th	2	26	249	408	4	18	13
Ga	8	5	24	16	3	9	9
La	357	577	3764	4938	39	363	311
Ce	753	1171	4581	6458	58	789	722
Nd	300	464	1189	1714	20	372	321

Rare earth elements ICP analysis in ppm

La	374.3	791.21	5833.7	8673.69	32.8	556.6	431.6
Ce	756.0	1445.20	8957.8	13237.66	50.7	1106.7	961.6
Pr	86.4	154.22	831.3	1215.26	4.3	129.7	114.9
Nd	287.4	484.97	2206.9	3153.92	13.63	451.8	413.2
Sm	42.1	63.27	198.3	279.15	1.57	66.7	55.1
Eu	12.4	17.03	45.1	61.88	0.51	18.0	15.1
Gd	27.6	38.43	95.2	130.41	0.91	43.9	33.8
Dy	14.8	19.83	42.7	54.86	0.68	19.8	14.5
Er	7.2	9.56	29.2	42.77	0.18	9.3	6.1
Yb	4.8	5.76	10.5	13.18	0.23	4.4	2.7
Lu	0.7	0.75	1.3	1.72	0.27	0.6	0.3
LREE/HREE	112	169	415	435	143	148	199

Localities

UMS = Um Sallamiah  
DUR = Durib  
ARA = Al-Arakbi

GROUP	III	III	IV	IV
LOCALITY	UMS	UMS	UMS	UMS
PELLET	L10067	L10068	L10074	L10075
SAMPLE	BY25E	BY25A	BY26E	BY11
SiO2	0.2	0.3	5.8	2.7
TiO2	0.07	0.04	0.18	0.24
Al2O3	0.1	0.1	0.3	0.1
Fe2O3	0.4	0.4	0.4	0.4
HnO	0.55	0.54	0.35	0.47
MgO	18.5	18.6	5.9	8.5
CaO	36.0	36.3	24.0	26.5
Na2O	0.0	0.0	0.1	0.1
K2O	0.00	0.00	0.00	0.00
P2O5	1.87	0.95	1.32	0.86
Total	57.65	57.16	38.27	41.80

Trace elements in ppm

Cr	0	0	0	0
V	27	16	37	17
Nb	36	43	652	318
Zn	24	28	13	18
Ni	3	1	14	13
Zr	0	0	0	0
Y	62	66	139	84
Ba	52	49	134072	104694
Sr	1741	1769	8961	5958
Rb	0	0	10	9
Th	13	20	366	229
Ga	6	3	23	18
La	530	544	5126	4609
Ce	1069	1098	6353	6369
Nd	418	417	1680	1760

Rare earth elements ICP analysis in ppm

La	740.12	785.42	7092.51	8261.29
Ce	1368.23	1435.48	10759.14	12916.64
Pr	136.95	150.68	995.44	1200.90
Nd	420.86	462.34	2604.40	3175.10
Sm	53.20	53.05	237.37	278.41
Eu	13.76	14.02	57.10	57.74
Gd	32.73	31.97	115.36	120.33
Dy	15.06	15.64	52.63	44.25
Er	7.74	8.06	36.65	37.56
Yb	4.14	4.38	12.01	10.09
Lu	0.57	0.56	1.47	1.37
LREE/HREE	203	206	408	497

GROUP	I	I	IV	I	I
LOCALITY	ARA	ARA	ARA	ARA	ARA
PELLET	L10069	L10070	L10071	L10072	L10073
SAMPLE	BY16J1	BY16J2	BY42D1	BY42D4	BY42G1
SiO2	3.9	4.3	1.1	1.9	3.7
TiO2	0.03	0.03	0.03	0.04	0.03
Al2O3	0.3	0.3	0.1	0.5	0.3
Fe2O3	0.5	0.3	0.2	0.1	0.1
MnO	0.35	0.21	0.29	0.06	0.16
MgO	16.5	16.4	0.2	14.0	18.2
CaO	37.3	38.7	37.6	42.6	38.5
Na2O	0.0	0.0	0.1	0.0	0.0
K2O	0.01	0.00	0.00	0.05	0.02
P2O5	0.10	0.10	0.55	0.05	0.02
Total	58.93	60.32	40.45	59.28	61.08

Trace elements in ppm

Cr	2	5	0	6	1
V	7	13	2	17	9
Nb	1	1	1341	1	0
Zn	32	38	0	20	19
Ni	11	9	17	6	2
Zr	0	0	0	0	1
Y	8	9	70	5	7
Ba	38	53	124492	208	36
Sr	160	252	5984	279	114
Rb	0	0	14	1	2
Th	0	2	305	4	5
Ga	3	5	23	6	5
La	7	5	7224	9	5
Ce	5	3	9420	6	9
Nd	6	4	2384	7	6

Rare earth elements ICP analysis in ppm

La	4.45	0.23	13272.5	7.16	5.00
Ce	7.00	0.0	20044.8	10.36	7.70
Pr	0.0	0.0	1858.9	1.07	0.77
Nd	2.49	0.0	4798.7	3.59	3.07
Sm	0.45	0.0	360.2	0.80	0.73
Eu	0.23	0.0	70.0	0.06	0.14
Gd	0.63	0.0	146.1	0.44	0.75
Dy	1.00	0.0	54.0	0.36	0.61
Er	0.34	0.0	48.7	0.01	0.48
Yb	0.43	0.0	10.5	0.20	0.33
Lu	0.05	0.0	1.2	0.04	0.05
LREE/HREE	17	0.0	631	84	18

GROUP	II	II	I	III	I	II
LOCALITY	DUR	DUR	DUR	DUR	DUR	DUR
PELLET	L10076	L10077	L10078	L10079	L10080	L10081
SAMPLE	BY44	BY45	BY46	BY47A	BY48	BY49
	*P	*C	*P			
SiO <sub>2</sub>	3.2	13.8	2.9	0.4	1.9	4.3
TiO <sub>2</sub>	0.04	0.05	0.04	0.02	0.03	0.06
Al <sub>2</sub> O <sub>3</sub>	0.7	0.8	0.5	0.1	0.2	1.1
Fe <sub>2</sub> O <sub>3</sub>	0.1	0.2	0.1	0.1	0.0	0.1
MnO	0.68	0.90	0.22	0.66	0.06	0.49
MgO	16.7	14.7	22.9	6.5	4.8	10.4
CaO	39.2	36.2	35.1	46.9	48.0	44.0
Na <sub>2</sub> O	0.0	0.0	0.0	0.0	0.0	0.0
K <sub>2</sub> O	0.11	0.35	0.26	0.00	0.10	0.98
P <sub>2</sub> O <sub>5</sub>	0.03	0.03	0.04	0.02	0.04	0.03
Total	60.76	66.96	61.98	54.76	55.12	61.48

Trace elements in ppm

Cr	0	0	2	2	2	2
V	4	2	6	0	1	17
Nb	2	2	1	3	0	0
Zn	16	5	321	5	4	13
Ni	1	3	0	6	0	3
Zr	5	6	0	0	0	5
Y	36	103	9	129	4	33
Ba	98	87	79	9	16	471
Sr	83	61	465	115	208	273
Rb	5	21	6	0	1	26
Th	3	3	0	0	0	2
Ga	8	7	4	4	5	7
La	38	27	6	500	4	33
Ce	64	57	16	1001	0	56
Nd	30	33	7	405	3	29

Rare earth elements ICP analysis in ppm

La	26.69	19.94	4.14	409.54	1.50	23.5
Ce	50.67	49.64	8.79	811.08	2.43	44.3
Pr	5.20	6.23	0.29	90.47	0.0	4.9
Nd	19.71	23.08	3.18	303.25	0.78	18.6
Sm	4.49	8.43	0.58	52.41	0.03	4.4
Eu	0.81	1.41	0.15	7.24	0.03	0.68
Gd	5.23	11.85	0.82	41.83	0.0	4.92
Dy	5.18	15.06	1.07	25.15	0.22	4.43
Er	2.63	8.38	0.63	11.98	0.0	1.72
Yb	1.92	6.13	0.53	8.04	0.16	1.92
Lu	0.27	0.86	0.06	1.13	0.02	0.28

LREE/HREE 20 6 13 72 26 22

\*P = Periphery of the dyke

\*C = Centre of the same dyke

-V-

GROUP	IV	III	III	III	III	IV	IV	IV
LOCALITY	UMS							
PELLET	L10082	L10083	L11657	L11658	L11659	L11660	L11661	L11662
SAMPLE	MKY4	MKY6	BY89A	BY89D	BY89E	BY90A	BY90B	BY90C
			*C	*M	*P	*P	*C	*P
SiO2	2.5	4.4	0.60	1.62	0.79	2.39	1.54	3.05
TiO2	0.19	0.2	0.06	0.08	0.06	0.06	0.05	0.04
Al2O3	0.2	0.6	0.17	0.27	0.15	0.11	0.14	0.16
Fe2O3	0.4	0.3	7.01	6.24	6.91	7.61	5.47	4.37
MnO	0.41	0.1	0.50	0.22	0.55	0.39	0.31	0.30
MgO	10.5	3.1	17.65	3.02	15.47	7.64	3.35	0.53
CaO	24.3	46.2	35.56	46.53	38.42	23.56	17.39	30.86
Na2O	0.1	0.1	0.03	0.10	0.0	0.09	0.14	0.0
K2O	0.02	0.0	0.005	0.026	0.003	0.00	0.00	0.00
P2O5	0.54	4.6	3.569	3.460	3.256	1.12	0.461	0.782
Total	39.14	59.7	65.14	61.56	65.61	42.95	28.84	39.87

Trace elements in ppm

Cr	0	0	1	2	27	BDL	BDL	BDL
V	25	68	50	78	95	18	15	13
Nb	428	11	88	58	81	544	201	397
Zn	19	39	28	43	28	BDL	58	BDL
Ni	10	5	2	6	2	15	32	4
Zr	0	144	10	14	31	BDL	BDL	BDL
Y	77	73	67	63	59	135	BDL	98
Ba	122241	1715	99	2128	306	120945	82721	133897
Sr	5495	6755	2022	5779	1451	11263	185642	7956
Rb	13	0	0	BDL	1	10	BDL	20
Th	657	13	34	24	29	432	601	519
Ga	18	8	5	7	4	BDL	3	BDL
La	6185	434	628	557	630	5054	3644	6928
Ce	7748	912	1314	1154	1290	6156	5661	8703
Nd	1915	394	506	455	475	1690	1148	2323

Rare earth elements ICP analysis in ppm

La	11573.0	554.8
Ce	17078.0	1122.0
Pr	1515.0	129.7
Nd	3766.0	441.1
Sm	281.0	62.9
Eu	58.0	17.5
Gd	123.0	41.8
Dy	49.0	19.1
Er	55.0	9.3
Yb	10.0	4.2
Lu	1.21	0.53

LREE/HREE 490 151

- \*C = Centre of the dyke
- \*M = Midway between centre and periphery of the same dyke
- \*P = Periphery of the same dyke

TABLE 5.7: JURASSIC LIMESTONE ROCKS OF LOWDER-MUDIAH AREA,  
 ABYAN PROVINCE, YEMEN REPUBLIC

PELLET SAMPLE	L10051 BY35A1	L10052 BY35A2	L10053 BY35A4
SiO <sub>2</sub>	4.3	1.6	11.9
TiO <sub>2</sub>	0.04	0.04	0.13
Al <sub>2</sub> O <sub>3</sub>	0.3	0.3	1.9
Fe <sub>2</sub> O <sub>3</sub>	0.0	0.0	0.1
MnO	0.03	0.03	0.07
MgO	1.9	1.2	13.6
CaO	49.0	49.4	36.5
Na <sub>2</sub> O	0.1	0.1	0.1
K <sub>2</sub> O	0.11	0.05	0.80
P <sub>2</sub> O <sub>5</sub>	0.02	0.05	0.04
Total	55.78	52.70	67.09

Trace elements in ppm

Cr	4	6	9
V	4	24	13
Nb	0	0	1
Zn	20	9	6
Ni	4	7	3
Zr	0	0	13
Y	1	5	5
Ba	19	15	53
Sr	308	753	110
Rb	5	3	24
Th	1	3	3
Ga	9	6	6
La	4	3	6
Ce	0	5	9
Nd	5	9	10

Rare earth elements ICP analysis in ppm

La	0.0	0.0	0.0
Ce	0.82	1.75	7.10
Pr	0.0	0.0	0.0
Nd	0.02	1.47	3.47
Sm	0.0	0.07	0.57
Eu	0.0	0.0	0.0
Gd	0.0	0.0	0.0
Dy	0.0	0.0	0.0
Er	0.0	0.0	0.0
Yb	0.0	0.09	0.03
Lu	0.0	0.01	0.03
LREE/HREE	0.0	3.2	176

TABLE 5.8: MARBLE ROCKS OF LOWDER-MUDIAH AREA, ABYAN PROVINCE, YEMEN REPUBLIC

PELLET SAMPLE	L10049 BY1	L10050 BY6
SiO <sub>2</sub>	0.1	0.8
TiO <sub>2</sub>	0.02	0.04
Al <sub>2</sub> O <sub>3</sub>	0.1	0.3
Fe <sub>2</sub> O <sub>3</sub>	0.0	0.0
MnO	0.06	0.02
MgO	22.6	0.6
CaO	37.2	49.6
Na <sub>2</sub> O	0.0	0.1
K <sub>2</sub> O	0.00	0.17
P <sub>2</sub> O <sub>5</sub>	0.05	0.03
Total	60.18	51.59

Trace elements in ppm

Cr	3	0
V	6	12
Nb	0	0
Zn	98	3
Ni	0	1
Zr	0	0
Y	3	1
Ba	12	69
Sr	78	1482
Rb	1	3
Th	2	4
Ga	3	6
La	3	3
Ce	0	1
Nd	3	0

Rare earth elements ICP analysis in ppm

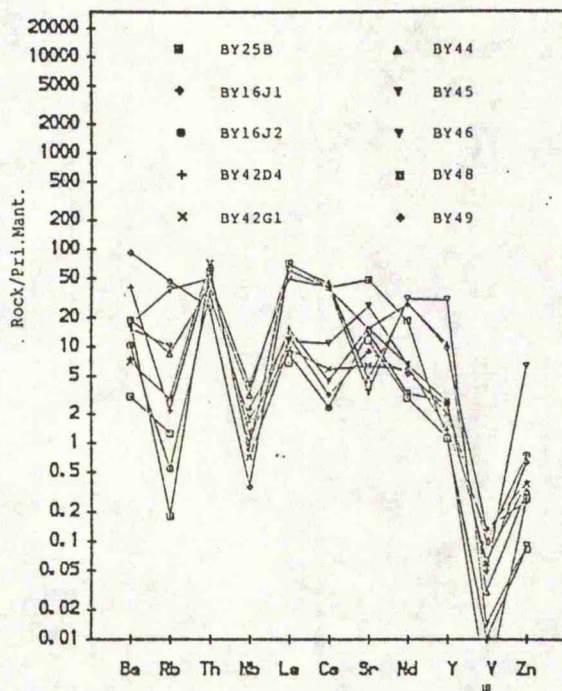
La	0.36	1.2
Ce	0.12	2.3
Pr	0.0	0.05
Nd	0.0	0.09
Sm	0.0	0.2
Eu	0.0	0.03
Gd	0.0	0.03
Dy	0.0	0.02
Er	0.39	0.005
Yb	0.02	0.6
Lu	0.0	0.03

LREE/HREE	1	6
-----------	---	---

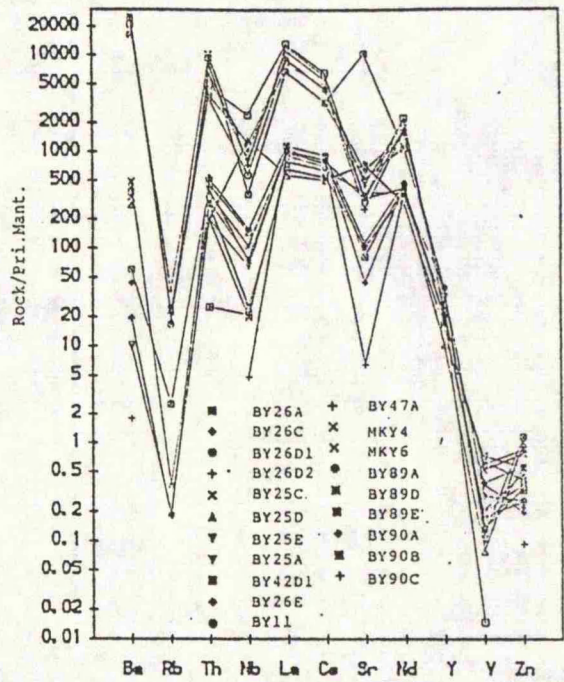
and Sr are: Ba = 0 - 2000 ppm, Sr = 0 - 5000 ppm. Whilst not having a range of suitable standards with reliable values higher than those quoted above, determinations for La, Ce and Nd on SY-3 plus comparison with the behaviour of other similar trace elements suggest that the calibrations, for the LREE's, are probably reasonable up to around 1000 ppm but this is without the additional complication of elevated Ba and Sr contents. High levels of Ba particularly could create problems of background interference during the determination of the LREE's by XRF, leading to over correction of the measured peak intensities. Another problem that may arise is that if the REE's are concentrated in minor phases with a very high mean atomic weight compared to those of the major phases the estimate mass absorption coefficient will not truly reflect the mass absorption history of the REE analyte lines i.e. they will be under corrected and give lowered intensities and hence lowered abundances. Concomitantly, high Ba and Sr levels in the rocks will lead to higher Ba and Sr levels in the separated and concentrated solutions for ICP analysis. Whilst these enhancing interferences are corrected for within the routine range of operation the interferences are non-linear and will increase with concentration hence ICP determination on these compositions may well be elevated. This is really sufficient work for several PhD.'s solely devoted to developing analytical techniques which would give the same degree of confidence of analytical quality for rocks of these compositions as for routine silicates e.g. basalts, granites, metamorphic silicates and mudstones/shales. Until some efforts put into this area I'm afraid the picture will not improve dramatically (Marsh, 1990, personal communication).

#### 5.6.2 Trace and Rare Earth Elements

Spider-diagrams for the trace and REE's of the carbonatites as well as limestone and marble samples from Lowder-Mudiah area, were plotted to illustrate the chemical characteristics and behaviour of these carbonatites. Trace element plotted against Primordial Mantle values (Taylor and McLennan, 1985), show that the carbonatitic rocks fall into four groups of patterns (Fig. 5.2a & b and Fig. 5.4a-d). To verify this four patterns phenomenon, these rocks and samples of the Jurassic limestone and the marble were analysed by ICP for REE. The same four groups emerged when the REE were plotted against chondrite values (Taylor and McLennan, 1981), as seen in Fig. 5.3a & b and Fig.

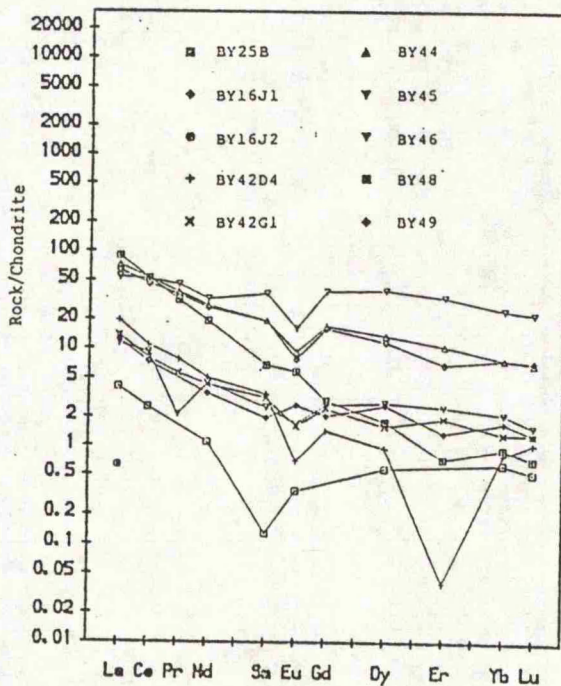


(a)

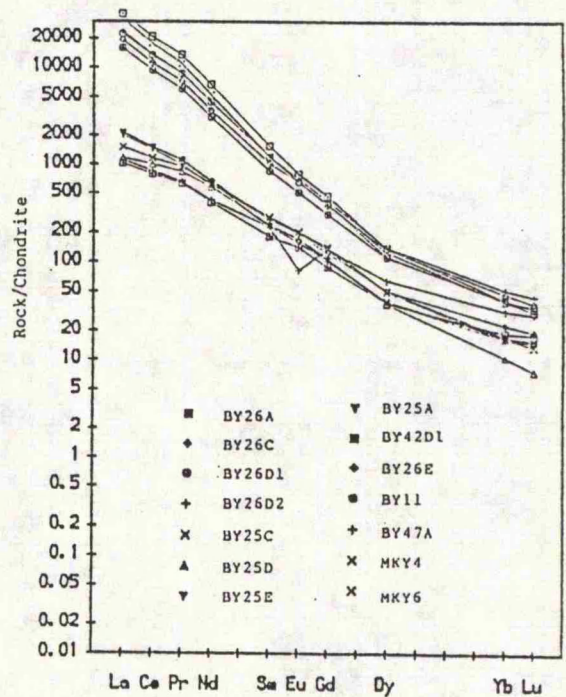


(b)

Fig. 5.2. Primordial Mantle-normalized trace element spiderdiagrams for (a) group I and II (b) group III and IV carbonatites.

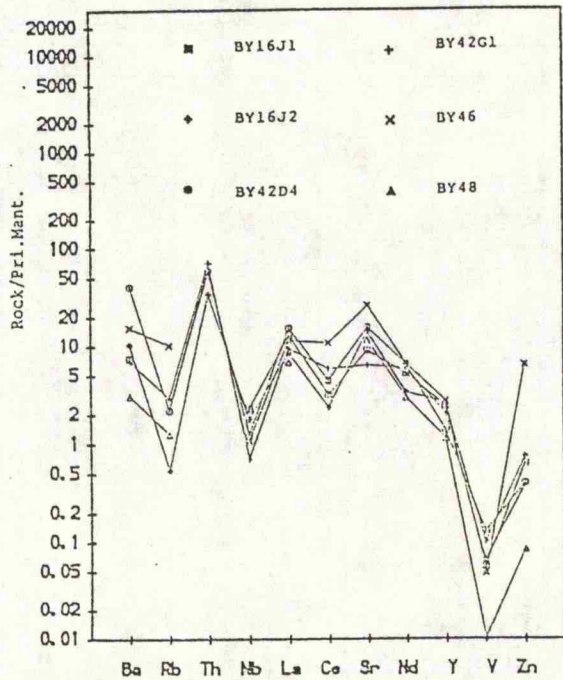


(a)

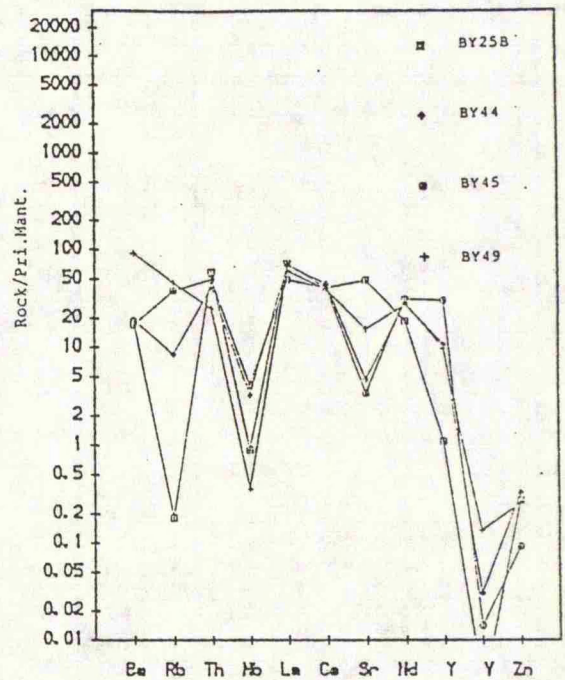


(b)

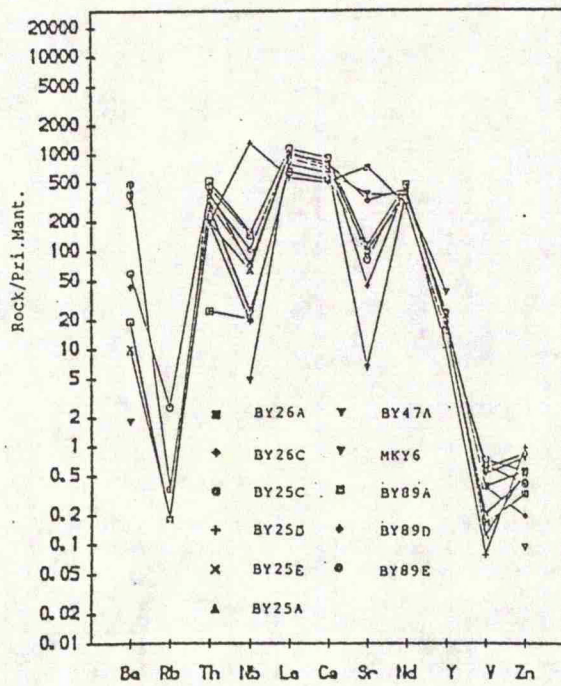
Fig. 5.3. Chondrite-normalized rare earth element spiderdiagrams for (a) group I and II (b) group III and IV carbonatites.



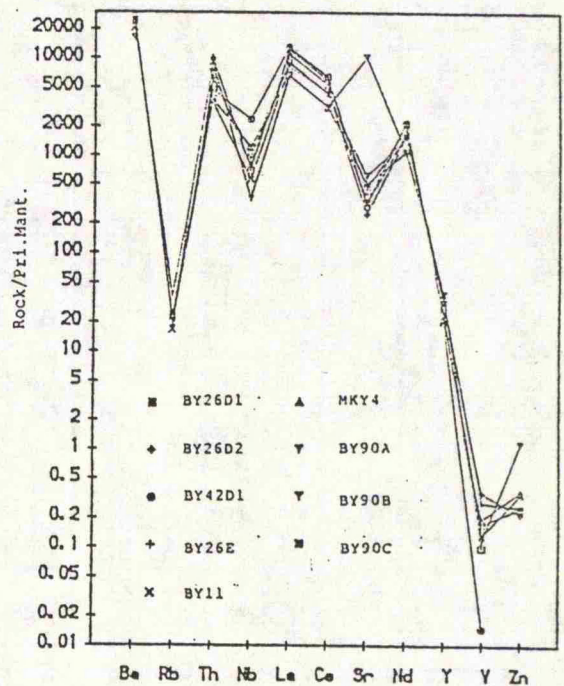
(a)



(b)

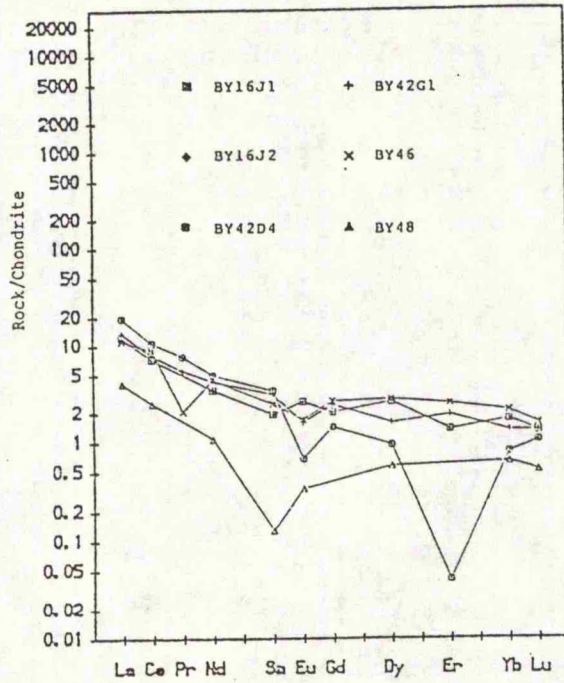


(c)

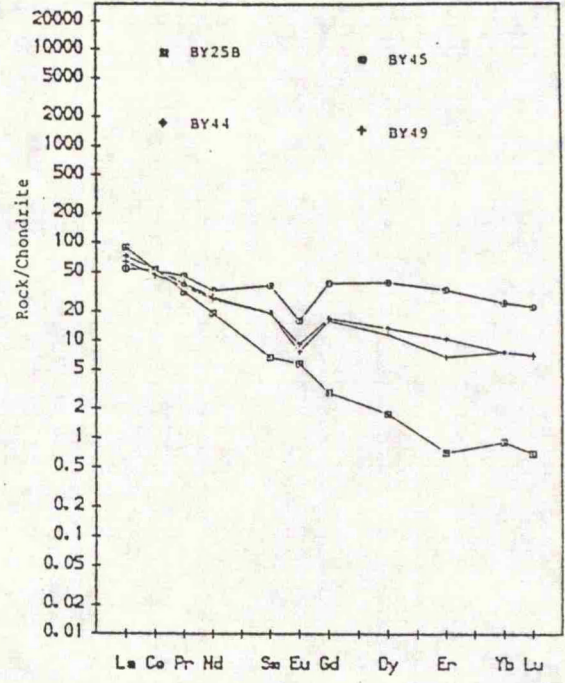


(d)

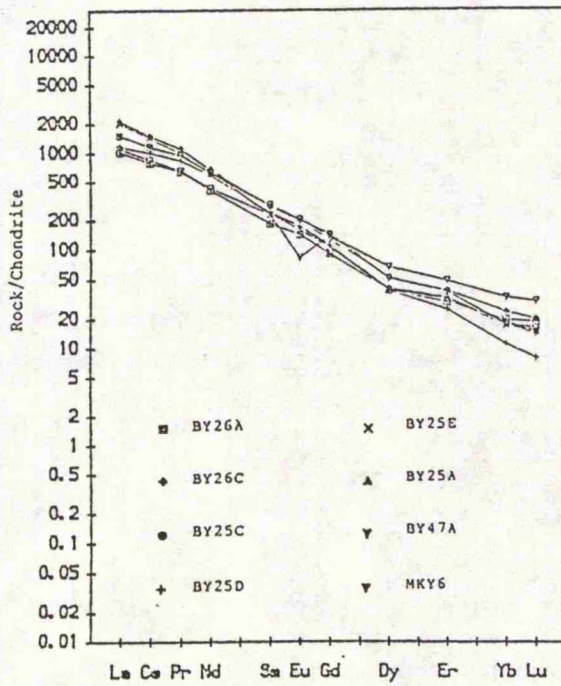
Fig. 5.4. Primordial Mantle-normalized trace element spiderdiagrams for (a) group I, (b) group II, (c) group III and (d) group IV carbonatites.



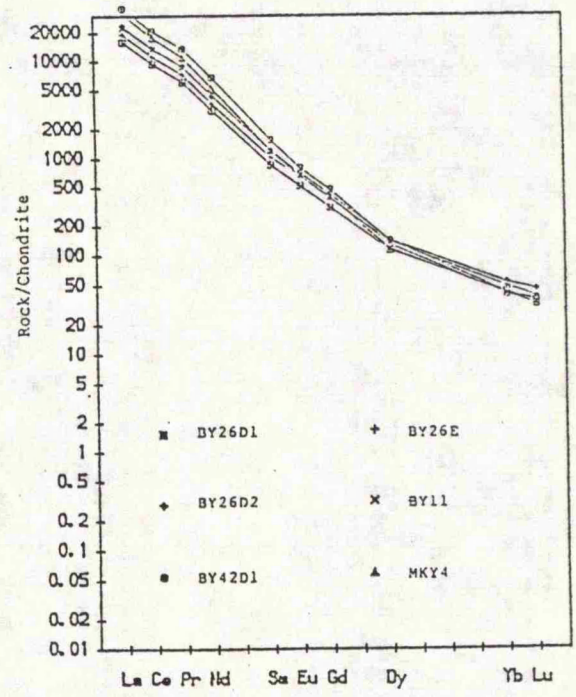
(a)



(b)

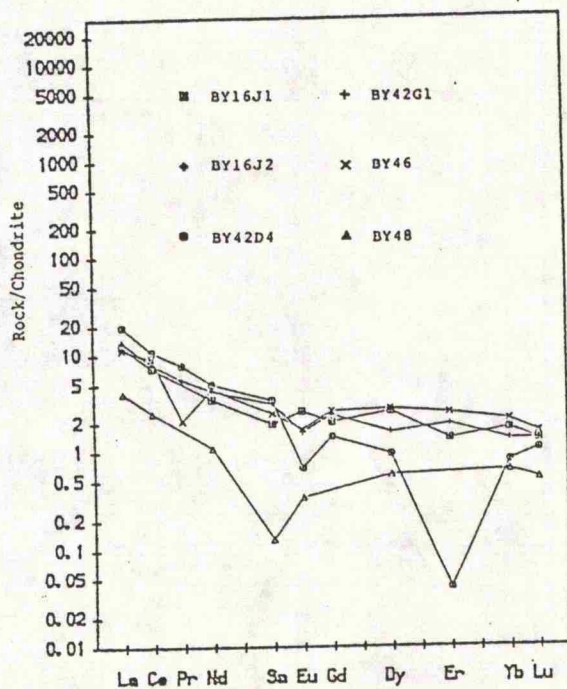


(c)

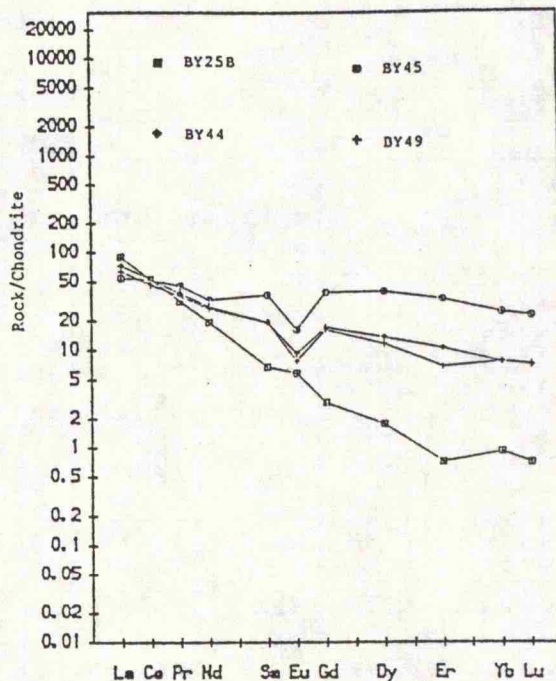


(d)

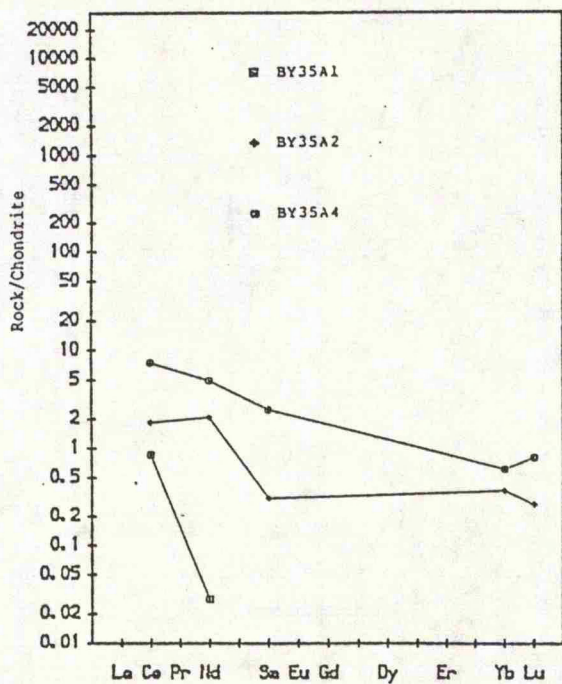
Fig. 5.5. Chondrite-normalized rare earth elements spiderdiagrams for (a) group I, (b) group II, (c) group III and (d) group IV carbonatite.



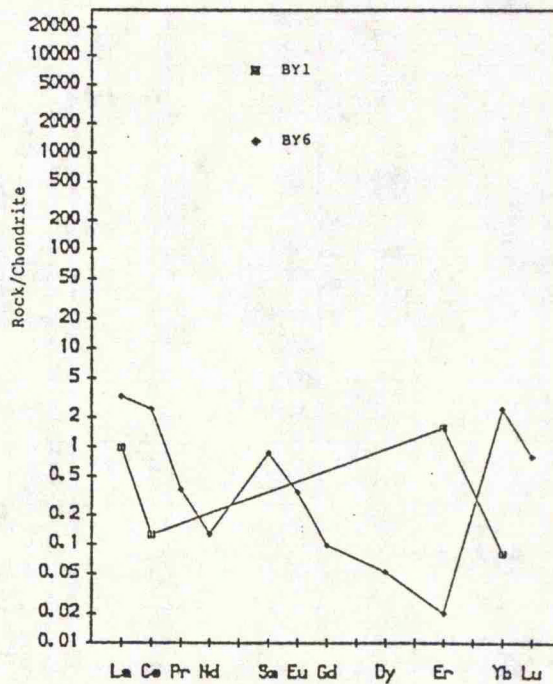
(a)



(b)



(c)



(d)

Fig. 5.6. Chondrite-normalized rare earth element spiderdiagrams for (a) group I carbonatite, (b) group II carbonatite, (c) limestone and (d) marble.

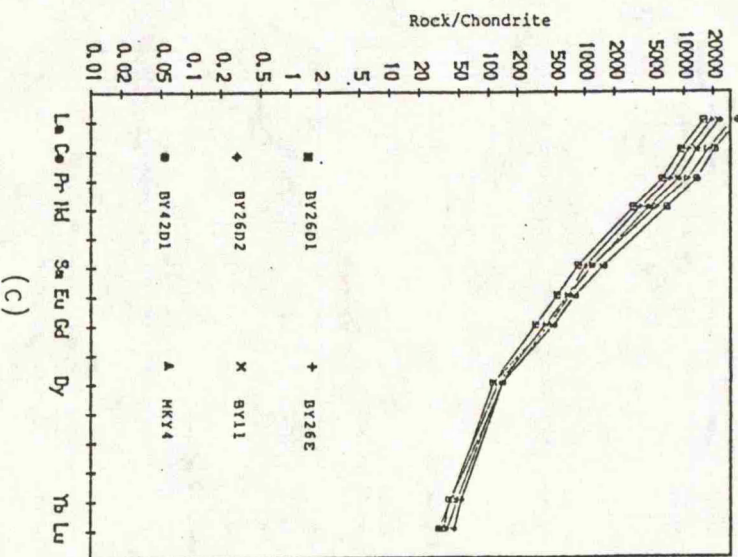
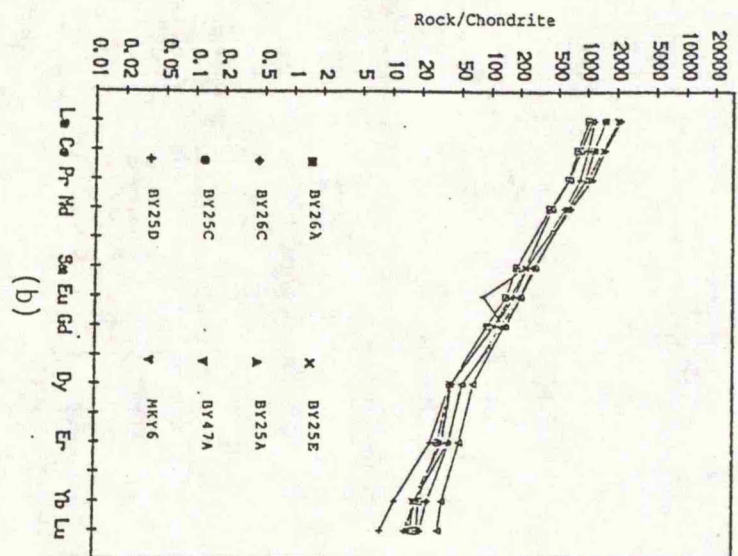
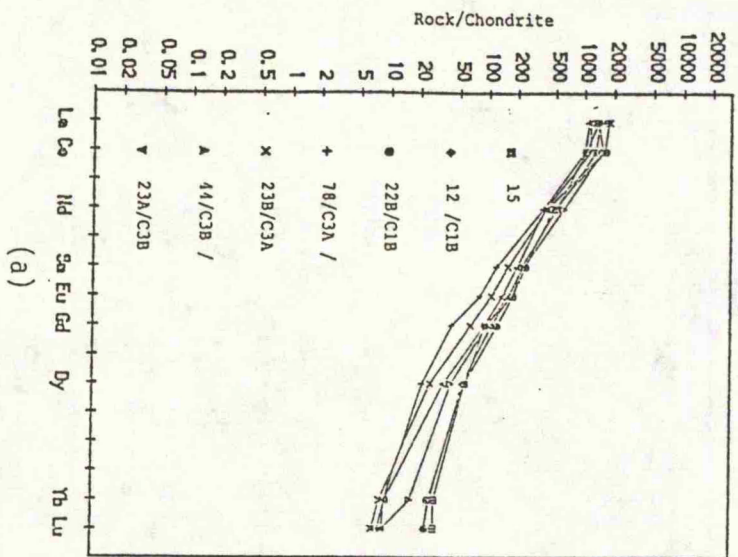


Fig. 5.7. Chondrite-normalized rare earth elements, comparative spiderdiagrams for (a) Loe Shilman, Pakistan, carbonatites (Mian, 1987), (b) group III and (c) group IV carbonatites, Lower-Mudiah.

5.5a-d.

Groups III and IV (Fig. 5.3b and Fig. 5.5c & d) show steep REE distribution patterns typical for carbonatites (Moller et al., 1980) which have high LREE/HREE ratios, compared with that of groups I and II (see table 5.6). Moreover, group III is closely comparable with the Loe Shilman of Pakistan (Mian, 1987) (Fig. 5.7a-c).

Group I and II patterns (Fig. 5.3a and Fig. 5.5a and b) exhibit very low LREE/HREE ratio (see table 5.6), compared with that of groups III and IV, and show negative Eu anomalies, characteristic of limestones. Although group II generally has low concentration of REE, it is still higher than that of group I (see table 5.6). However, there is similarity between the group I patterns and that of the marble and the Jurassic limestone (Fig. 5.6 a-d) which themselves show very low LREE/HREE ratios (see tables 5.6, 5.7 and 5.8). Therefore, groups III and IV are definitely carbonatites, while groups I and II appear not to be.

It should be emphasized that all the carbonatite dykes look alike apart from colour, and are all parallel. The groups are not geographically (spatially) controlled (see Table 5.6).

### 5.6.3 Group III and IV Carbonatites

To classify the group III and IV carbonatites and to understand in more details their chemical behaviour and characteristics, eighteen samples from Um Sallamiah were selected and plotted. These samples were numbered serially from 1 to 18 for plotting simplicity (see Fig. 5.8).

A ternary diagram for whole rock, CaO, MgO, and FeOT + MnO (Fig. 5.8), for carbonatite classification, show that these rocks fall within the calciocarbonatite (Sovite), magnesiocarbonatite and ferrocarnatite fields (Woolley and Kempe, 1989). Fractionation trends where Ca decreases with the increase of Mg and Fe (Le Bas, 1989), (bold arrows in Fig. 5.8) were recognized in groups III and IV carbonatites, and these are: Normal trend of fractionation (Le Bas, 1989) for group III carbonatites, as seen from three samples of a single dyke, 1, 2, 3 (Fig. 5.8). Similar trend is seen in dykes 12, 13, 16 and 17, but are less Fe-rich, and this may be the result of fractionation, also, from a Ca-rich carbonatite magma but which is more oxidizing, on the principles that the more oxidizing a carbonatite magma is, the less Fe-rich will be the carbonatite crystallizing. Samples 14

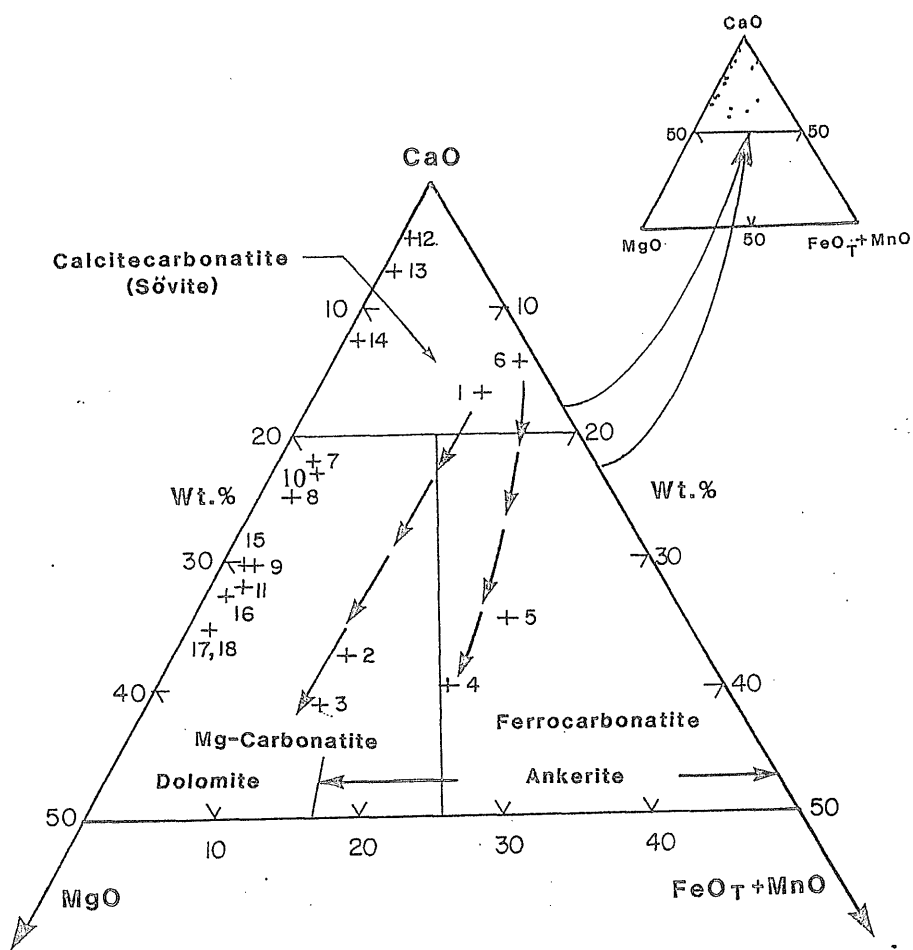


Fig. 5.8. Plot on the carbonatite classification (see Woolley and Kempe (1989), and two evolutionary paths for group III and IV carbonatites, from Um Sallamiah, where 1 = BY89D, 2 = BY89E, 3 = BY89A, 4 = BY90B, 5 = BY90A, 6 = BY90C, 7 = BY11, 8 = MKY4, 9 = BY26D2, 10 = BY26E, 11 = BY26D1, 12 = BY25C, 13 = MKY6, 14 = BY26A, 15 = BY25D, 16 = BY26C, 17 = BY25E, and 18 = BY25A. 1,2 and 3 are from a single dyke of group III, and 4,5 and 6 are from a single dyke of group IV.

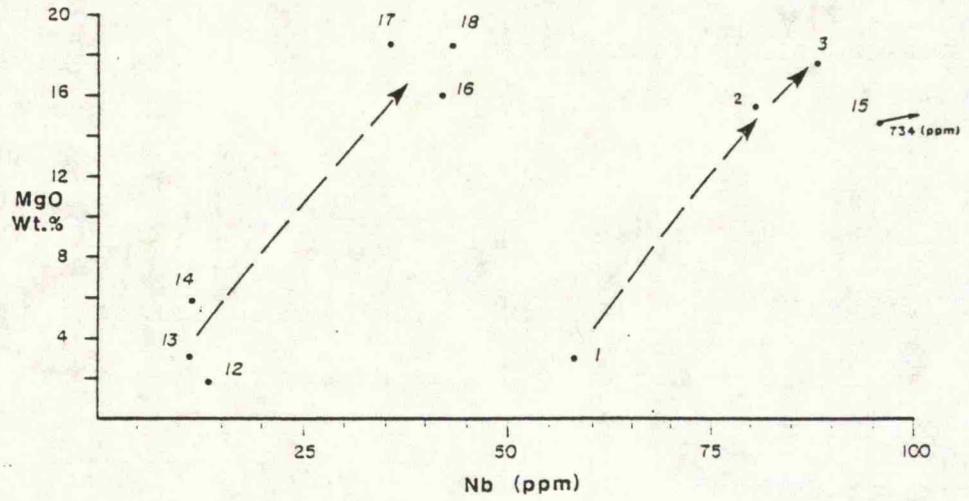


Fig. 5.9 Nb versus MgO plots for group III carbonatite. Um Sallamiah.  
(for sample numbers refer to Fig. 5.8).

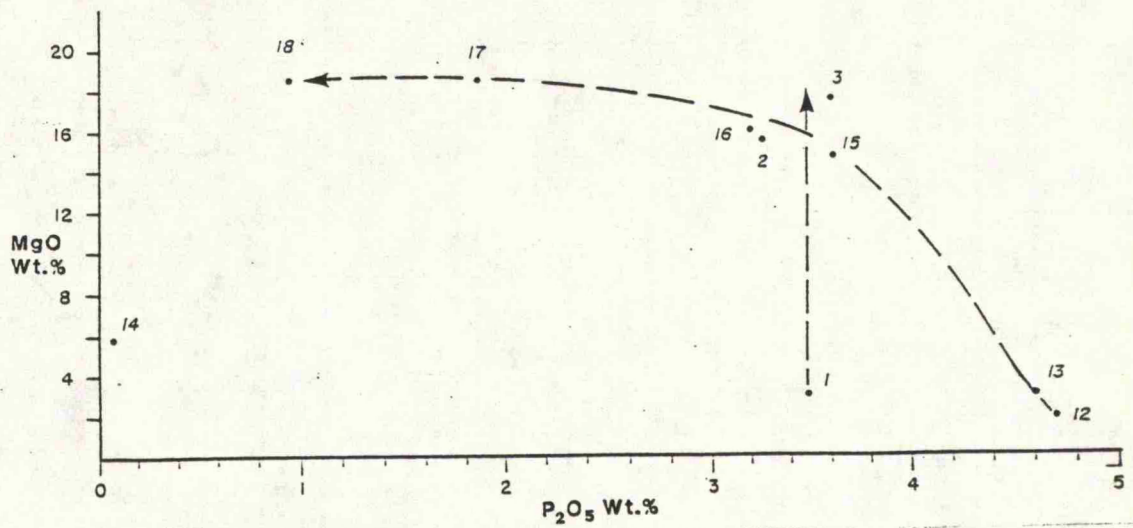


Fig. 5.10 P<sub>2</sub>O<sub>5</sub> versus MgO plots for group III carbonatite. Um Sallamiah.  
(for sample numbers refer to Fig. 5.8).

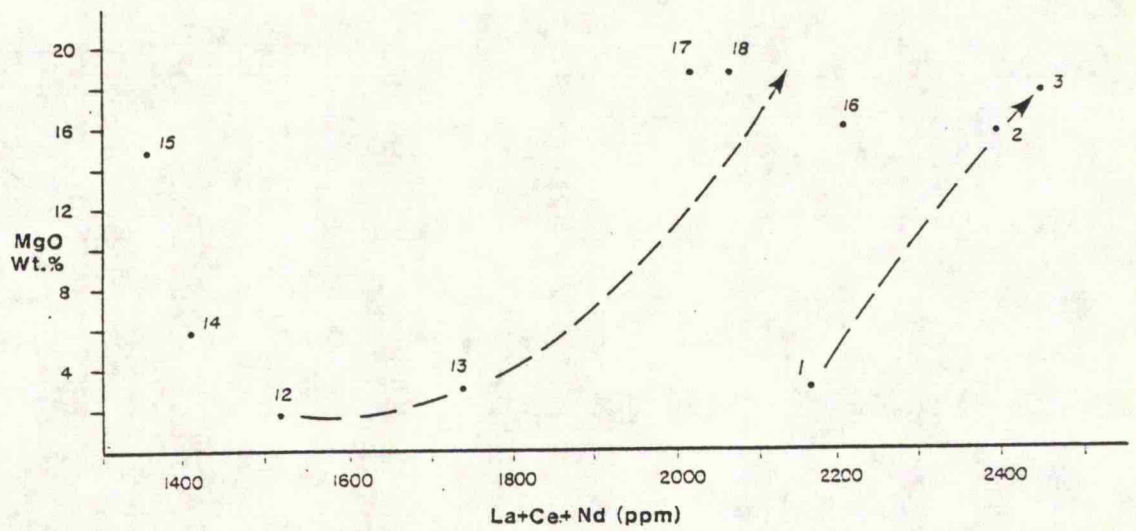


Fig. 5.11 REE (La+Ce+Nd) versus MgO plots for group III carbonatite (1, 2, 3 from one dyke BY89). Um Sallamiah.

(for sample numbers refer to Fig. 5.8).

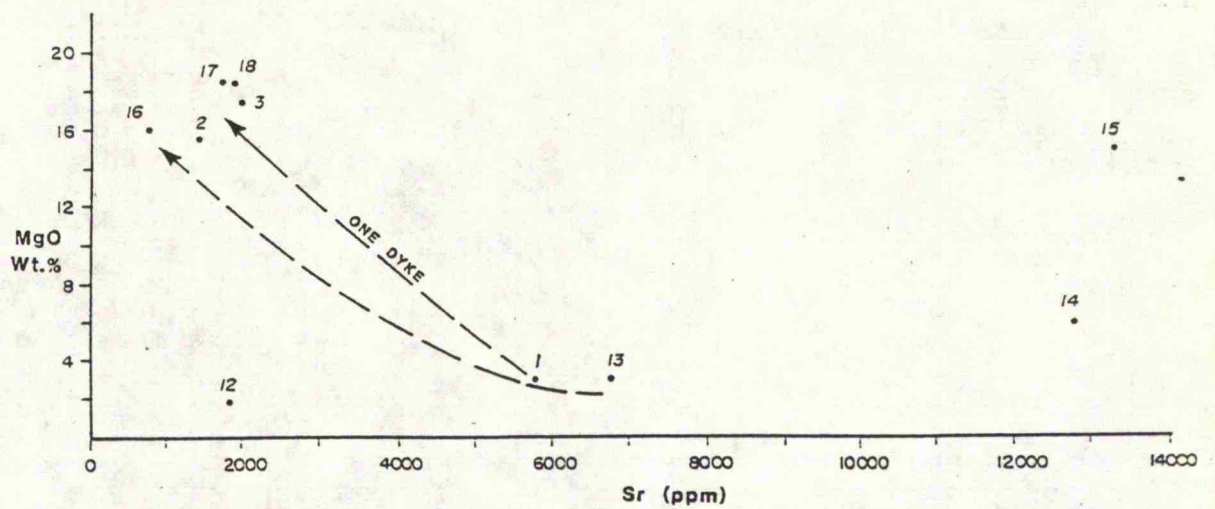


Fig. 5.12 Sr versus MgO plots for group III carbonatite. Um Sallamiah.

(for sample numbers refer to Fig. 5.8).

and 15, however, are anomalous and for which no explanation can at present be offered. Nb against MgO plot (Fig. 5.9) show that sample 15 is Nb-rich and its anomalous geochemistry may result from the sample being pyrochlore-rich and the product of an accumulation processes.

Since sample 14 is P205-poor, (as seen from P205 against MgO), plot (Fig. 5.10), compared with the others of the same group, it is interpreted to be a carbonatite from which apatite has been removed by accumulation processes.

There is a linear positive correlation trend between REE and MgO, in three different samples from one single dyke (dyke BY89) from group III (Fig. 5.11, samples 1, 2, 3) and possibly other dykes also from the same group i.e. BY25, MKY6, BY26, BY25E and BY25A (Fig. 5.11, samples 12, 13, 16, 17, and 18) and a negative correlation trend between Sr and MgO (see Fig. 5.12)

As to group IV carbonatites, if normal fractionation of carbonatite (Le Bas, 1989) is accepted i.e. Ca decreases and Mg increases, then normal trends of fractionation for group IV were recognized as seen from three different samples of a single dyke, 4, 5 and 6 (Fig. 5.8) and different dykes 7, 8, 9, 10, 11. Moreover, sample 6 would seem to be an earlier carbonatite relative to all the others of group IV. Although the REE (Fig. 5.13) and the other plots (Figs. 5.14, 5.15, 5.16 and 5.17) show much scatter, therefore no trend lines can be drawn between most of the group IV points, however, tie lines were drawn between points 4, 5 and 6 as an indication that they are related since they represent three different samples from one single dyke (dyke BY90). There is indication assuming that sample 6 is earlier, that REE decreases with fractionation. This is likely to be the case because, since total REE exceed 1%, they can be considered as compatible elements and therefore are precipitated early. This is confirmed by the presence of abundant euhedral monazite in thin-section of BY90C (Plate 5.4e). Furthermore, since all the group IV carbonatites are REE-rich, although less REE-rich than sample BY90C, the fractionation of these carbonatites is dominated by the crystallization and variable accumulation (or extraction) of monazite.

Since the REE and P205; (the MgO and P205, too) contents do not vary sympathetically (Fig. 5.14; fig. 5.15), it is evident that other RE minerals must be present, such as ?

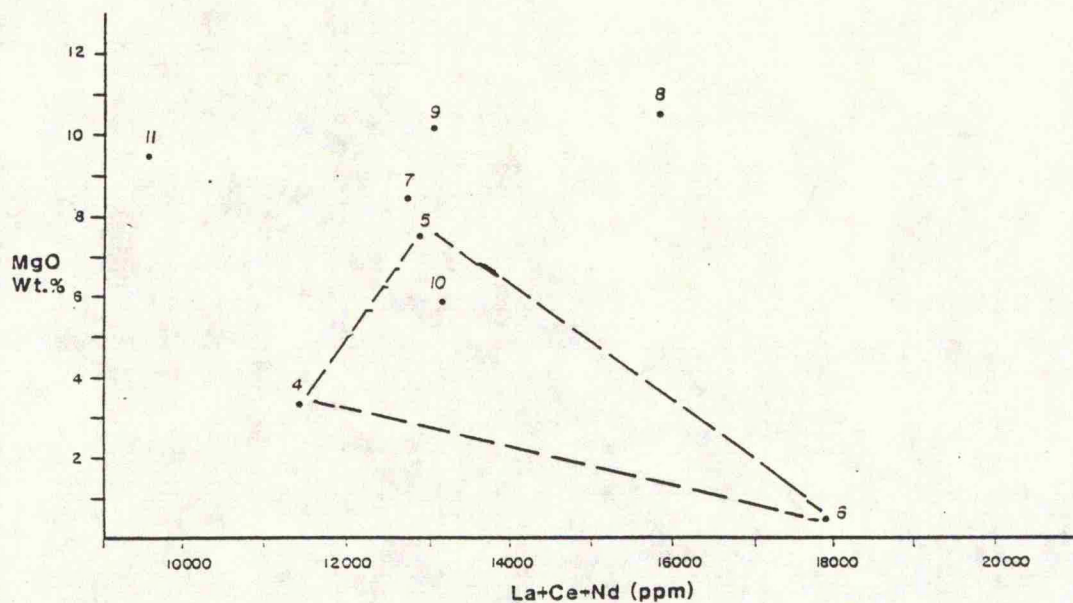


Fig. 5.13 REE (La+Ce+Nd) versus MgO plots for group IV carbonatite (4, 5, 6 from one dyke BY90). Um Sallamiah.

Tie lines were drawn (in this figure and Figs. 5.14, 5.15, 5.16, 5.17 & 5.18) between points; 4, 5 and 6 as they represent different samples from a single dyke BY90).

(for sample numbers refer to Fig. 5.8).

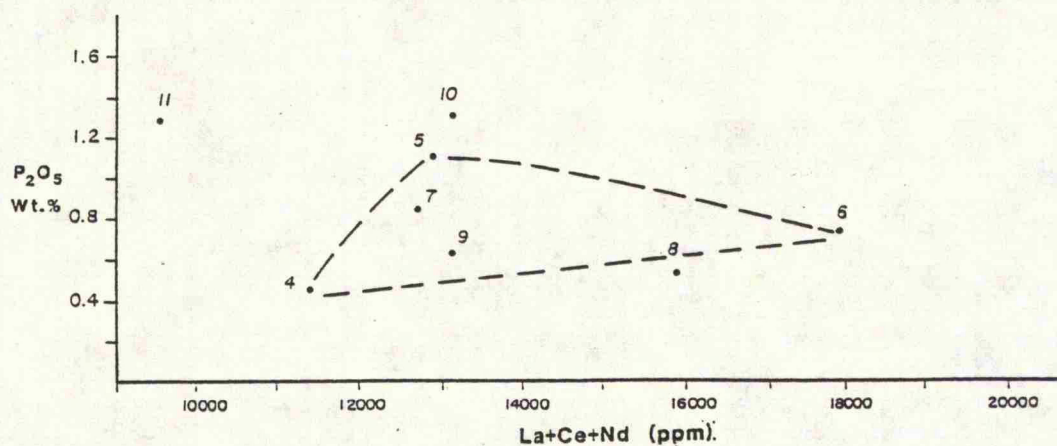


Fig. 5.14 REE (La+Ce+Nd) versus P<sub>2</sub>O<sub>5</sub> plots for group IV carbonatite. Um Sallamiah.

(for sample numbers refer to Fig. 5.8).

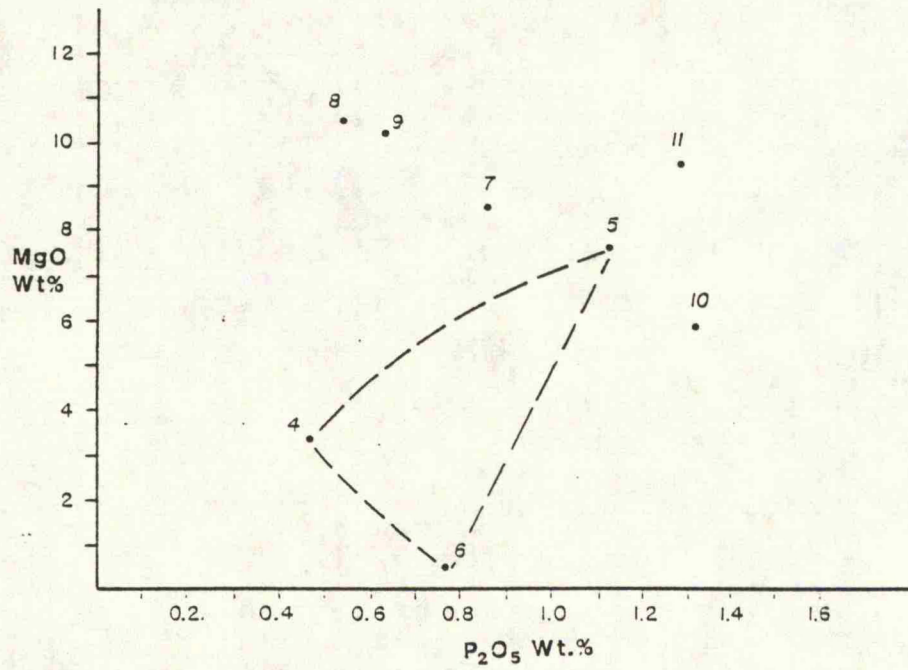


Fig. 5.15 P<sub>2</sub>O<sub>5</sub> versus MgO plots for group IV carbonatite. Um Sallamiah.  
(for sample numbers refer to Fig. 5.8).

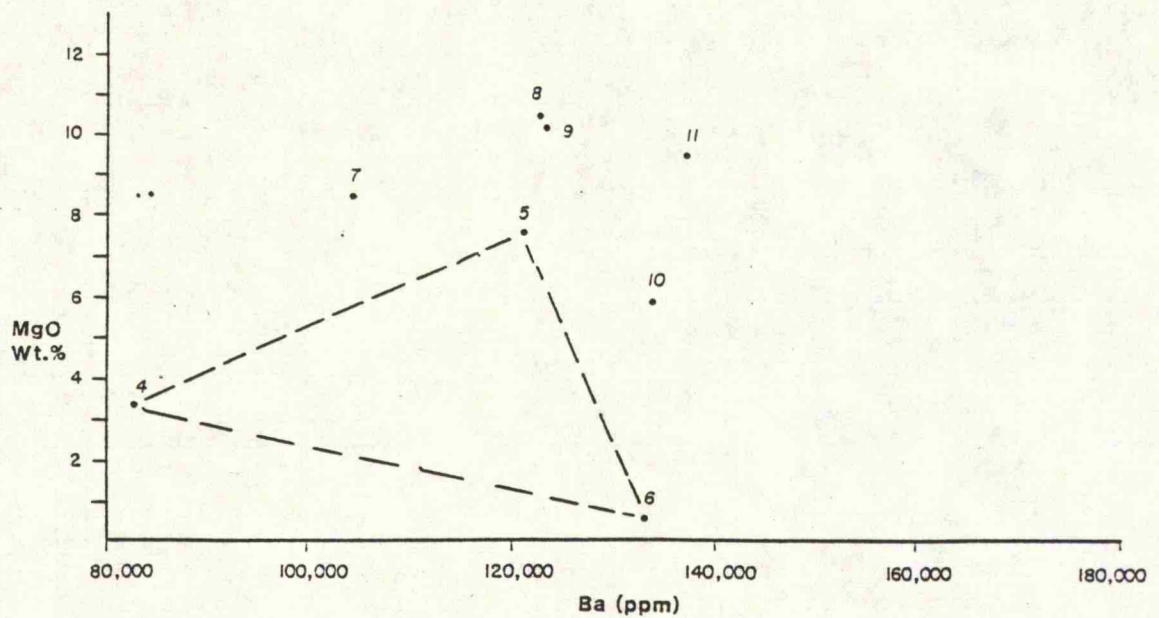


Fig. 5.16 Ba versus MgO plots for group IV carbonatite. Um Sallamiah.  
(for sample numbers refer to Fig. 5.8).

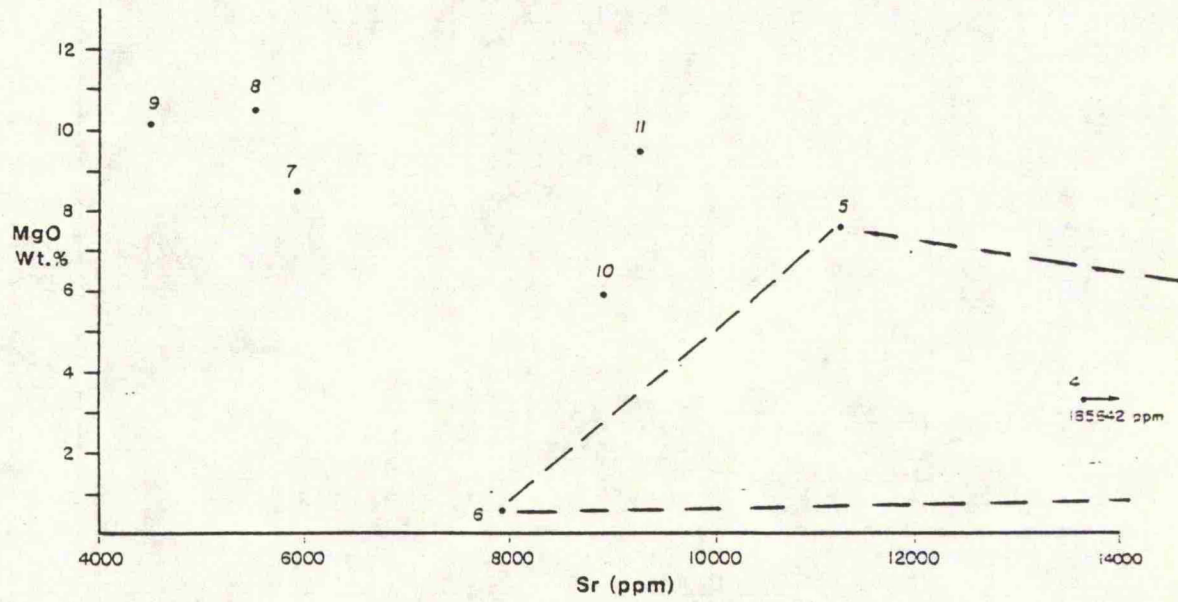


Fig. 5.17 Sr versus MgO plots for group IV carbonatite. Um Sallamiah.  
(for sample numbers refer to Fig. 5.8).

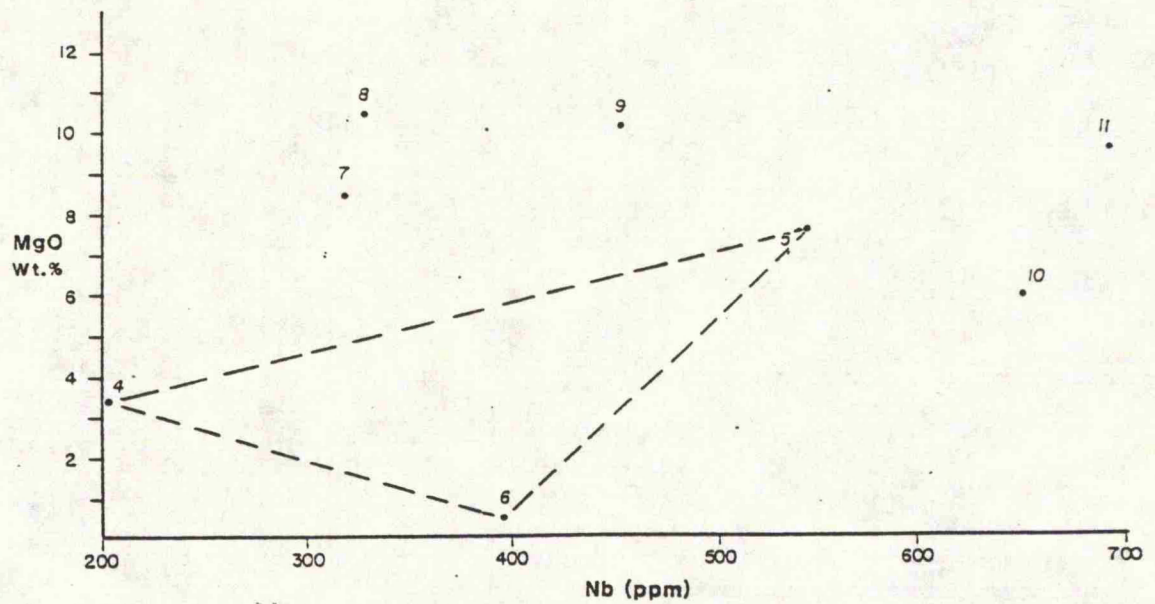


Fig. 5.18 Nb versus MgO plots for group IV carbonatite. Um Sallamiah.  
(for sample numbers refer to Fig. 5.8).

bastnaesite.

Not only can REE be considered as compatible but also Ba (Fig. 5.16). Ba varies from 8 to 14% (equivalent to 14- 24 wt % barite) and it would seem that this high content of Ba causes it also to behave compatibly. Thus both REE and Ba dominate the fractionation processes, other than the Ca, Mg and Fe which behave normally. In Sr versus MgO plot (Fig. 5.17), Sr increase with fractionation, but sample 4 is odd.

Nb distribution is governed by the distribution of pyrochlore which, being an early phase, can produce local cumulates and hence the Nb-MgO diagram shows scatter (Fig. 5.18).

All these rocks were subjected, with a variable degree, to a late mineralization and dolomitization. However, Group IV was strongly affected, this is reflected in the crystallization of dolomite e.g. in MKY4 (see Plate 5.2 c,d,e,f) and BY26D1 (Plate 5.3 c,d). Furthermore, the accumulation or clustering, of the dyke sample points, towards the Mg apex in the triangular plot (Fig. 5.8), and the scatter of sample points in the other geochemical variation diagrams of the Group IV, is possibly attributed to this extensive late mineralization and dolomitization, to which Group IV have been subjected.

### 5.7 Conclusion

Of the many sheet-like carbonatite bodies which occur in the granitoid gneiss, mainly those which occur as dykes cutting the gneiss at Um Sallamiah and which are either apatite-bearing or RE-mineral-bearing are identified as carbonatites. Although some of the other sheets have the appearance of dykes, neither their mineralogy nor their geochemistry (groups I and II) reveal any characters which support an interpretation that they may be carbonatites, and they are considered to be sheets of slightly mineralized sedimentary marbles enveloped by the granitoid gneisses.

The apatite-bearing and RE-mineral-bearing carbonatites, have distinctive trace element patterns, giving rise to the group III and group IV carbonatite rocks described earlier in this chapter. Within groups III and IV, patterns of fractionation are identified (Fig. 5.8). The group III carbonatites follow a fractionation pattern of increasing Mg, Sr and REE (Fig. 5.11 and Fig. 5.12), in common with other carbonatites of the world (Wooley and Kempe, 1989; Le Bas, 1989). The group IV carbonatites follow an unusual pattern of decreasing REE and Ba on Mg increases, (Fig. 5.13 and Fig. 5.16) and is accounted for

by the primary crystallization in the carbonatite magma of monazite, barite and ? bastnaesite.

The geochemical plots indicate no simple chemical relation between the group III and group IV carbonatites, but since both occur at the same locality at apparently the same period, it is considered that the two groups must be related. The simplest relation is that both are derived at slightly different times from a carbonatite magma chamber undergoing fractionation.

Whether, there is any genetic relationship between these carbonatite dykes, and the mafic-ultramafic suites at Mukeras, Yemen (to the west of the Lowder-Mudiah area), is not known so far, since geographically they far away from each other, no direct field contact relationships, and no age dates available for both to be correlated age wise.

However, it should be indicated that the author is proposing, based on comparison with localities having similar characteristics in the Afro-Arabian Shield, for the A-type Lowder-Mudiah granitoids, Mudiah bimodal metavolcanics and the bimodal Mukeras dyke swarms, an extensional tectonic regime. Whether, the carbonatites can be fit within this proposed tectonic scenario is debatable and cannot be established, at present, with the lack of direct field contact relationships and age dates.

## CHAPTER 6

### DISCUSSION AND CONCLUSIONS

#### 6.1 Chapters 1 - 4

The Lowder-Mudiah area is made up predominantly of crystalline basement rocks, unconformably overlain by a cover of Jurassic limestone and Quaternary basalt. The Precambrian rocks can be divided into three main belts separated by two northeast-striking ductile shear (thrust) zones. The central belt is highly metamorphosed and composed of grey and pink granitic gneisses, including lenses of sheared quartz-biotite gneiss and amphibolite. These gneissose rocks are intruded by grey and pink pegmatitic granites. Migmatites occur locally and carbonatite dykes intrude the grey granitic gneiss. The eastern belt comprises northeast-trending metavolcanics with subordinate marbles and sulphide-bearing veins; these rocks were metamorphosed under low-grade greenschist facies conditions, and deformed in open antiforms and synforms. The third belt occupies the western part of the area (Mukeras Escarpment), essentially composed of intrusive batholiths of medium-grained granite ( $740 \pm 22$  Ma) in the northeast and of quartzdiorite, diorite and gabbro in the southwest. These rocks are traversed by two bimodal dyke swarms: a major early swarm trends NE-SW ( $709 \pm 21$  Ma) and a minor late ( $587 \pm 18$  Ma) one E-W to NW-SE. The earlier swarm (NE-SW) is generally parallel to that of the major transcurrent faults in the area.

Multiple deformation produced three deformation episodes, each with its own distinctive style and orientation. Northeast-trending recumbent isoclinal folds were followed by open folds with vertical axial planes, and by northwest-trending crossfolds and kink bands. Thrust-lineation relationships suggest that there was an early phase of thrusting which produced down-dip lineations, and that these thrust surfaces were later reactivated to become transcurrent ductile shear zones which gave rise to the present predominant shallow-plunging lineations. Most kinematic evidence indicates that the transcurrent shear zones have a dextral sense of movement. Block faulting, along reactivated Precambrian thrust planes, is expressed in the uplift of the Mukeras Escarpment, and the

down-faulted Jurassic limestone.

Lithologies of the Lowder-Mudiah area are generally similar to those in the southern Saudi Arabian Shield (Greenwood, et al., 1980; Roobol et al., 1983; Stoeser et al., 1983; Jackson et al., 1984; Jackson, 1986) and in the Northeastern Desert of Egypt (Stern et al., 1988; Stern and Gottfried, 1986; Stern and Hedge, 1985). They are also comparable with those of northern Somalia, which is regarded as part of the Mozambique belt of eastern Africa (Warden and Daniel, 1984, Warden and Horkel, 1984). Warden and Horkel (1984) suggested that the north-eastern branch of the Mozambique belt extends into southern Arabia and constitutes a distinct geotectonic entity, characterized by a predominantly ensialic structure and lengthy polycyclic evolution. Hawkins et al. (1981) stated that a small segment of the Pan-African Shield in the southeastern part of Arabia at Dhofar is composed of quartz-feldspathic gneisses, granites, pegmatites, and aplites, and suggested that a basic dyke swarm underlies the Mirbat plain. Gass et al. (1990) also showed that there are late Precambrian (604 - 490 Ma) dyke swarms in northeast and southeast Oman (near Mirbat).

The granitoids of the Lowder-Mudiah area are peraluminous, high silica, "A-type" granites that formed from LILE- and LREE-enriched crustal melts; such granites would be expected in an extensional tectonic regime. These granitoids are similar to the younger (686 - 517 Ma) A-type granitoid assemblage (Fig. 3.1) of the Central Hijaz, Saudi Arabia (Jackson et al. 1984).

The bimodal Mudiah metavolcanics were formed from LILE- and LREE-enriched source(s), and exhibit Andean-type convergent margin characteristics. However, a large degree of compositional overlap may be expected between magmas in rapidly distending rifts, and Andean-type convergent margins (Stern et al. 1988).

The early NE-SW dyke swarm ( $709 \pm 21$  Ma -K/Ar,  $694.1 \pm 23.1$  Ma -<sup>39</sup>Ar/<sup>40</sup>Ar) of the Mukeras Escarpment indicates NW-SE directed crustal extension accompanied by widespread intrusion of bimodal igneous magmas which were derived from LILE- and LREE-enriched source(s), and which exhibit Andean-type convergent margin characteristics.

The mafic Mukeras dykes comprise two groups reflecting different sources or different

amounts of partial melts; they might represent hypabyssal conduits for the surficial eruption of the mafic component of the bimodal Mudiah metavolcanics. Basaltic melts were predictably generated by melting in the upper mantle, the basaltic-andesite melts being produced either by a lower-degree of melting of a hydrous upper mantle, or of eclogite. In contrast, the felsic dykes probably represent the feeders of the felsic component of the bimodal Mudiah metavolcanics, and they might be related to the "A-type" granitoids of Lowder-Mudiah.

The felsic Mudiah metavolcanics and the felsic Mukeras dykes are chemically similar to the "A-type" granites of the Central Hijaz of the Arabian Shield, which were explained by a fusion - refusion model by Jackson et al. (1984), to the felsic dykes in the Northeastern Desert of Egypt (Stern et al. 1988), and to the crustal-melt monzogranites in the Karakoram of N. Pakistan (Crawford 1988; Crawford and Windley, 1990).

Petrochemical data combined with geological evidence lead to the following conclusions. The accretion of arc systems in the late Precambrian forming the Afro-Arabian Shield resulted in a thickening of the (juvenile) crust, which led to deep crustal melting (anatexis), which was probably triggered by mantle disturbance and upper mantle upwelling, diapirism and adiabatic decompression, that led to/or was caused by updoming, stretching, crustal thinning (extensional regime), and the injection of mantle-derived basaltic magma, that gave rise to the basaltic (mafic) Mudiah metavolcanics and the basaltic (mafic) Mukeras dyke swarms. In contrast, crustal melts gave rise to the felsic Mudiah metavolcanics, the Lowder-Mudiah "A-type" granitoids, and the felsic Mukeras dyke swarm.

The Mukeras dyke swarms (709 - 587 Ma), the Mudiah metavolcanics, the bimodal dyke swarms of the Northeastern Desert of Egypt (592 - 580 Ma) (Stern and Gottfried 1986; Stern et al. 1988; Stern and Hedge 1985) and the "sequence" A volcanics of the Central Arabian Shield are very comparable in chemistry and type (see Table 3.5; Figs. 3.3, 3.4, 3.5). They are all late Proterozoic bimodal basaltic-andesite to rhyolite suites that are LILE- and LREE-enriched and have marked Nb troughs, and thus they all probably contain an inherited subduction zone signature. Their felsic component is also comparable to the Lowder-Mudiah granitoids (Figs. 3.2, 3.4) and they both represent

melts that developed from a remelted accreted arc in an extensional tectonic regime. Moreover, these rocks are similar to the bimodal "sequence" A (700 - 570 Ma) volcanics of the Central Arabian Shield (Roobol et al. 1983), which were considered by Agar (1986) to have extruded in pull-apart grabens of the Najed strike-slip orogen.

The host rocks ( $740 \pm 22$  Ma -K/Ar) of the Mukeras dyke swarms range in composition from granite, quartzdiorite, diorite to gabbro. They collectively have a calc-alkaline subduction zone signature, and were probably emplaced in the roots of contemporary island arcs, similar to the old granodiorite association (720 Ma) of the Central Hijaz of Saudi Arabia (see Fig. 3.7), which is calc-alkaline ranging in composition from gabbro through monzogranite (Jackson et al. 1984), and therefore they possibly formed along path A in the Lowder-Mudiah magmatic evolution (see Fig. 6.1). However, the only granitic sample available is similar to the Lowder-Mudiah granitoids and the monzogranite (Fig. 3.7a) of the younger (A-type granitoids) of the Central Hijaz (Jackson et al., 1984), leading to the possibility that the host rocks of the dykes were post-tectonic and formed along path B rather than A in the proposed Lowder-Mudiah magmatic evolution (see Fig. 6.1). This model, which is based on petrochemistry and age relationships, suggests that there are two possible paths along which the magmatic history of the Lowder-Mudiah area evolved:

Path A. The calc-alkaline granite-diorite-gabbro suite (host rocks of the Mukeras dyke swarms) formed as a result of subduction. This was followed by accretion, crustal thickening, mantle diapirism, crustal melting, extension, intrusion of the Lowder-Mudiah A-type granitoids, injection of the bimodal Mukeras dyke swarms and extrusion of the bimodal Mudiah metavolcanics.

Path B. Some granites in the host rock suite are peraluminous and contain normative corundum. This raises the possibility that there is a second environment in which the granitic host rocks evolved. These are post-collisional crustal melts triggered and contaminated by intrusion of LILE-enriched mantle melts, rather than by subduction-related magmatism (see Fig 6.1).

The late generation ( $587 \pm 18$  Ma) of Mukeras dykes are comparable in age to the alkali basalts of the Saudi Arabian Shield (see Table 3.6) and they also trend NW-SE in the

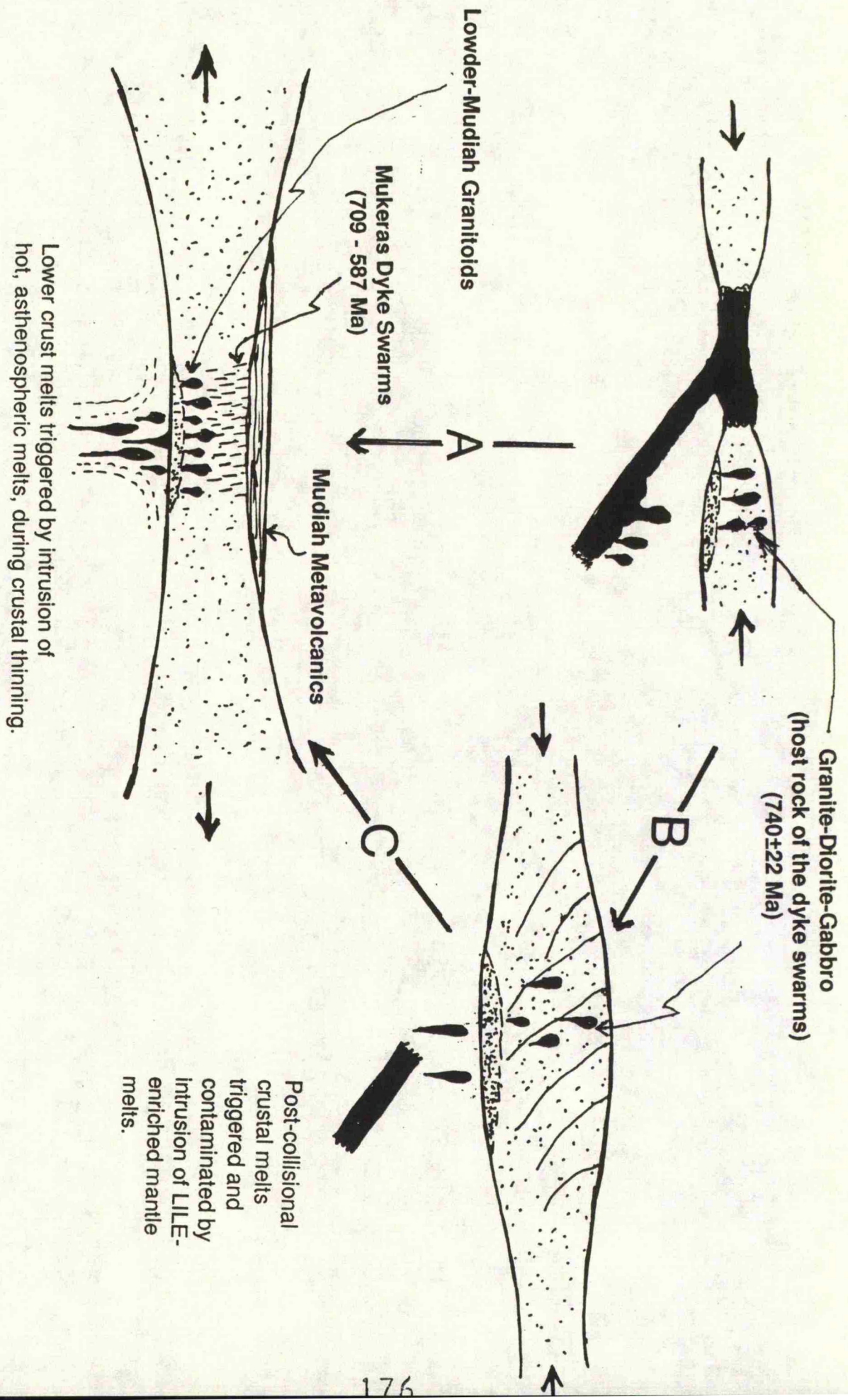


Fig. 6.1 Sketch illustrating possible paths for the magmatic evolution of the Lower-Mudiah granitoids, Mudiah metavolcanics, Mukeras dyke swarms and their host rocks.

same direction as the Najid Fault System and its pull-apart basins (Delfor, 1979; Agar, 1986).

The relationships between the mafic Mudiah metavolcanics and the mafic Mukeras dyke swarms on the one hand, and the Lowder-Mudiah granitoids, the felsic Mudiah metavolcanics and the Mukeras felsic dyke swarms on the other, are all based on their mutual spatial relations and their geochemical characteristics. More precise relationships require age determinations of the granitoids and metavolcanics.

The proposed mechanisms and relationships between the Lowder-Mudiah granitoids, Mudiah metavolcanics and the Mukeras dyke swarms should be considered as preliminary, due to the lack of isotopic constraints. This study is a first attempt to explore in modern detail the geology of South Yemen. It attempts to establish a possible mechanism(s) and evolutionary tectonic model especially by comparison with well-analysed comparable rocks in the Arabian and Afro-Arabian Shields. Further detailed study is recommended especially isotopic analysis in order to determine, confirm, develop, or reject the mechanism(s) and the evolutionary model proposed here.

## 6.2 Chapter 5

Field relations indicate that all the carbonatitic dykes are parallel and look alike, apart from their colour. Petrographically and mineralogically the presence of apatite, monazite and pyrochlore, in group III and IV indicate that these are typical carbonatites. This is supported by spiderdiagram patterns, in addition to possible fractional crystallization trends and paths. Therefore, field relations, petrography, mineralogy, and chemical evidence, suggest to the author that groups III and IV are definitely carbonatites. As to groups I and II, neither their mineralogy, nor their geochemistry support an interpretation that they may be carbonatites; they are considered as sedimentary marbles enveloped by the granitoid gneisses.

Whether there is any genetic relationship between these carbonatite dykes, and the mafic-ultramafic suites at Mukeras, Yemen (to the west of the Lowder-Mudiah area), is not known because geographically they are far away from each other, and there are no age dates to enable correlation.

However, based on comparison with similar rocks in the Afro-Arabian Shield, the author

---

proposes that the A-type Lowder-Mudiah granitoids, Mudiah bimodal metavolcanics and bimodal Mukeras dyke swarms, were formed in extensional tectonic regimes. Whether the carbonatites were related to this extensional regime is not known.

This study is the first attempt to understand the geology of southern Yemen in a plate tectonic framework.

References

---

**REFERENCES**

---

## REFERENCES

- Abouov, A.K. Lysitsin, E.S. Potroukhin, I.I. Lychkovsky, B.P. and Abdulaziz, I.S., 1981. Report on the results of prospecting and estimation within the Lowder field of carbonatites for 1977-1981. Unpublished technical report. Board of Petroleum and Minerals. Dept. of Geol. & Miner. Exploration, Aden.
- Agar, R.A., 1986. The Bani Ghay Group: sedimentation and volcanism in pull-apart grabens of the Najd Strike-slip orogen, Saudi Arabian Shield. *Precambrian Res.*, 31: 259-274.
- Al-Derweesh, K.A.S., 1988. Geology of Batais Al-Husn area, (Upper Abyan Delta), Abyan Governorate, People's Democratic Republic of Yemen. Unpublished M.Sc. Thesis, Kuwait University.
- Almond, D.C. 1984. "The Concepts of Pan-African Episode" and "Mozambique Belt" in Relation to the Geology of East and North-East Africa. *Bull. Fac. Earth Sci. King Abdulaziz Univ.*, 6: 71-87.
- Almond, D.C., Ahmed, R. and Dawoud, A.S. 1984a. Tectonic, metamorphic and magmatic styles in the Northern Red Sea Hills of Sudan. *Bull. Fac. Earth Sci. King Abdulaziz Univ.*, 6: 449-458.
- Almond, D.C., Curtiss, P.A.S., McCormac, M. O'Halloran, D.A. and Vail, J.R. 1984b. Migrating younger granite ring-complexes in the Bayunda Desert, Northern Sudan. *Bull. Fac. Earth Sci. King Abdulaziz Univ.*, 6: 271-176.
- Al-Shanti, A.M., 1979. The aims, objectives and scope of IGCP project no. 164 'Pan-African crustal evolution in the Arabian-Nubian Shield'. - Newsletter 'Pan-African crustal evolution in the Arabian-Nubian Shield'. 2: 9-13.
- Al-Shanti, A.M.S. and Mitchell, A.H.G. 1976. Late Precambrian subduction and collision in the AlAmar-Idsas region, Arabian Shield, Kingdom of Saudi Arabia. *Tectonophysics* 30: pp.T41-T47.
- Andersen, T. 1989. Carbonatite-related contact metasomatism in the Fen-Complex, Norway: effects and petrogenetic implications. *Mineralogical Magazine*, 53: 395-414.

## References

- Anderson, J.L. and Cullers, R.L. 1978. Geochemistry and evolution of the Wolf River batholith, a late Precambrian Rapikivi massif in north Wisconsin, U.S.A. *Precambrian Res.*, 7: 2825-324.
- Apted, M.J. 1981. Rare earth element systematics of hydrous liquids from partial melting of basaltic eclogite: a re-evaluation. *Earth Planet. Sci. Lett.* 52:172-182.
- Ba-bttat, M.A., 1978. The Geology of Wadi Al-Maragh area, Saudi Arabia. Unpubl. High Diploma Thesis, Fac. Earth Sci., K.A.U., Jeddah.
- Ba-bttat, M.A., 1981. Geology and Mineralization of the Jabal Samran and Jabal Abu-Mushut area. Unpubl. M.Sc. Thesis. K.A.U. Fac. Earth Sci., Jeddah.
- Ba-bttat, M.A. and Hussein, A.A., 1984. Geology and mineralization of the Jabal Samran Jabal Abu-Mushut area. *Bull. Fac. Earth Sci., K.A.U.* 6: 571- 578.
- Ba-bttat, M.A., 1985. The Geology of Wadi Al-Maragh area, Saudi Arabia. *Proceedings of the Second Jordanian Geological Conference.* Amman, Jordan. pp. 428-456.
- Ba-bttat, M.A., Windley, B.F., Mishwat, A.T., Almond, D.C., 1987. Geology of Lowder-Mudiah Area, Abyan Governorate, People's Democratic Republic of Yemen. *Proceedings of GEOSOM 87. Conference on the geology of Somalia and the surrounding regions.* Special issue *Journal of African Earth Sciences* (in press).
- Ba-bttat, M.A., Windley, B.F., Mishwat, A.T., Almond, D.C. 1989. Sutures, Dyke swarms and Carbonatites in People's Democratic Republic of Yemen. *Proceedings of the first Saudi Symposium on Earth Sciences.* Jeddah (in press).
- Bakor, A.R., Gass, I.G. and Neary, C.R. 1976. Jabal El-Wask: an Eocambrian back-arc ophiolite in NW Saudi Arabia. *Earth Planet. Sci. Lett.* 30:1-9.
- Barberi, F., Santacroce, R. und Varet J., 1982. Chemical aspects of rift magmatism. In: Palmason, G. (ed.). *Continental and Oceanic Rifts. Geodynamics Series 8*, Am. Geophys. Union. Washington, D.C., pp.223-258.
- Barker, F. 1979. Trondhjemite; definition, environment and hypothesis of origin. In: Barker, F. (ed.) *Trondhjemites, dacites and related rocks.* Elsevier, pp1-12.
- Barnes, J.W. 1988. *Ores and Minerals: Introducing Economic Geology.* Open University Educ. Enterp. Ltd. Milton Keynes. pp. 17-20.
- Basta, E.Z., Kotb, H. and Awadallah, M.F. 1980. Petrochemical and geochemical

### References

- characteristics of the Dokhan Formation at the type locality, Jabal Dokhan, Eastern Desert, Egypt. In: Al-Shanti, A.M.S. (ed). Evolution and Mineralization of the Arabian-Nubian Shield. I.A.G. Bull. 3: 122-140.
- Berger, A.R. 1982. The importance of small-scale mining: A general review. In: J.M. Neilson (Editor). Strategies for small-scale mining and mineral industries. AGiD Report No. 8, pp. 1-2.
- Berhe, S.M., 1988. The geologic and tectonic evolution of the Pan-African/Mozambique belt in east Africa. Unpubl. Ph.D. Thesis, The Open University, U.K.
- Berhe, S.M. 1990. Ophiolites in northeast and east Africa: Implications for Proterozoic crustal growth. Journal Geol. Soc. Lond., 147: 41-57.
- Berhe, S.M. and Rothery, D.A., 1986. Interactive Processing of Satellite Images for structural and lithological mapping in northeast Africa. Geological Magazine. 123: 393-403.
- Beydoun, Z.R. 1964 The Stratigraphy and Structure of the Eastern Aden Protectorate. Overseas Geology and Mineral Resources Bull., Supp. Ser.5. 107p.
- Beydoun, Z.R. 1966. Geology of the Arabian Peninsula. Eastern Aden Protectorate and Part of Dhufar. United States Geological Survey, Professional Paper. 560-H, 49p.
- Beydoun, Z.R. 1970. Southern Arabia and Northern Somalia: Comparative geology. Phil. Trans. Royal Soc. London. A267: 267-292.
- Black, R., 1966. Sur l'existence d'une orogeni ripheenne en Afrique de l'Ouest. C.R., Ac.Sc., 262, Ser. D, pp. 1-46-1049.
- Blumenthal, J.I.C.S. 1978. Geologicka expedicev LDR Jemen (The first Czechoslovakian geologic expedition to Southern Yemen): Geol. Pruzkum, Ostrava, Sb. GPO, No.
- Brown, G.C. 1979. Calc-alkaline Magma Genesis: The Pan-African Contribution to Crustal Growth? In: Al-Shanti, A.M.S. Evolution and Mineralization of the Arabian-Nubian Shield. Pergamon Press. Oxford. 1: 19-29.
- Brown, G.C. 1980. Calc-alkaline magma genesis: the Pan-African contribution to crustal growth ? Inst. Applied Geol. King Abdulaziz University, Jeddah, Bull. 4: 19-29.
- Brown, C.G. 1982. Calc-alkaline intrusive rocks: their diversity, evolution and relation to volcanic arcs. In: Thorpe R.S. (Editor) Andesites: John Wiley and Sons pp437-461.

## References

---

- Brown, G.C. and Hennessy, J. 1978. The initiation and thermal diversity of granite magmatism. *Phil. Trans. R. Soc. London, Ser. A.* 288: 631-643.
- Brown, G.F. 1972. Tectonic map of the Arabian Peninsula. Map AP-2, Dir. Gen. Min. Res., Kingdom of Saudi Arabia.
- Burke, K. and Sengor, C. 1986. Tectonic escape in the evolution of the continental crust. In: Barazangi, M. and Brown, L. (eds). *Reflection Seismology: The Continental Crust. Geodynamics Series 14.* Am. Geophys. Union. Washington, DC, pp41-53.
- Cahen, L. and N.J. Snelling, 1966. *The geochronology of Equatorial Africa.* North-Holland, Amsterdam, 195 pp.
- Calvez, J.-Y. , Alsac, C., Delfour, J., Kemp, J. and Pellaton, C. 1983. Geological evolution of western, central and eastern parts of the northern Precambrian Shield, Kingdom of Saudi Arabia. Saudi Arabian Deputy Ministry for Mineral Resources Open-File Report BRGM-OF-03-17.
- Calvez, J.Y., Pellaton, C., Alsac, C., and Tegye, M. 1982. Geochronology and geochemistry of plutonic rocks in the Umm Lajj and Jabal al Buwanah areas. Saudi Arabian Deputy Ministry for Mineral Resources Open-File Report BRGM-OF-02-36.
- Camp, V.E. 1984. Island arcs and their role in the evolution of the Western Arabian Shield. *Geol. Soc. of America Bull.* 95: 913-921.
- Chappel, B.W. and Stephens, W.E. 1988. Origin of infra- crustal.(I-type) granite magmas. In: *The Origin of Granites.* Transactions of the Royal Society of Edinburgh: Earth Sciences, 79: 71-86.
- Chappell, B.W. and White, A.J.R., 1974. Two contrasting Granite Types. *Pacific geology,* 8: 173-174.
- Church, W.R. 1988. Ophiolites, sutures and micro-plates of the Arabian-Nubian Shield: A Critical Comment. In: El-Gaby, S. and Greiling, R.O. (Editors) *The Pan-African Belt of Northeast Africa and Adjacent Areas; Tectonic Evolution and Economic Aspects of A late proterozoic Orogen.* Fried Vieweg Sohn Verlagsgesellschaft mbH, Braunschweig, Germany. pp.289-316.
- Clark, M.D. 1981. Geologic map of the Al Hamra' quadrangle, sheet 23C: Saudi Arabian Deputy Ministry for Mineral Resources Geoscience Map series, GM-49A (1:250,000).

## References

---

- Clemens, J.D. and Vielzeuf, D. 1987. Constrains on melting and magma production in the crust. *Earth Planet. Sci. Lett.* 86: 287-306.
- Clemens, J.D. and Wall, V.J. 1981. Origin and crystallisation of some peraluminous (S-type) granitic magmas. *Can. Mineral.* 19: 111-131.
- Clifford, T.N. 1967. The Damaran episode in the Upper Proterozoic-Lower Palaeozoic structural history of southern Africa. - *Geol.Soc. Amer., Spec. Paper* 92.
- Clifford, T.N., 1970. The structural framework of Africa. In: T.N. Clifford and I.G. Gass (eds.) *African magmatism and tectonics*. Oliver and Boyd, Edinburgh, 1-19.
- Collins, W.J., Beams, S.D., White, A.J.R. and Chappell, B.W. 1982. Nature and origin of A-type granites with particular reference to southeastern Australia. *Contrib. Mineral. Petrol.* 81: 189-200.
- Cox, K.G. 1980. A model for flood Basalt vulcanism. *Journal. Petrol.* 21: 629-650.
- Cox, K.G., Bell, J.D. and Pankhurst, R.J. 1979. *The Interpretation of Igneous rocks*. Allen and Unwin. London. pp. 12-41.
- Cox, K.G., Gass, I.G. and Mallick, D.I.J., 1977. The Western Part of the Shugra Volcanic Field, South Yemen. *Lithos.* 10: 185-191.
- Craig, J.R. and Vaughan, D.J. 1981. *Ore microscopy and Ore Petrography*. John Wiley and Sons. New York. 406 p.
- Crawford, M.B., 1988. Leucogranite of the NW Himalaya: Mantle-Crust interaction beneath the Karakoram and the magmatic evolution of collisional belts. Unpublished. Ph.D. Thesis, Leicester University, U.K.
- Crawford, M.B. and Windley, B.F. 1990. Leucogranites of the Himalaya/Karakoram: Implications for magmatic evolution within collisional belts and the study of collision related leucogranite petrogenesis. *Journal of Volcanology and Geothermal Research.* 44: 1-19.
- Darbyshire, D.P.F., Jackson, N.J., Ramsay, C.R. and Roobol, M.J. 1983. Rb-Sr isotope study of latest Proterozoic volcano-sedimentary belts in the Central Arabian shield. *J. Geol. Soc. London*, 140: 203-213.
- Deer, W.A., Howie, R.A. and Zussman, J. 1965. *Rock-Forming Minerals*. Longman, U.K. 528 p.

### References

---

- Delfour, J. 1979. Upper Proterozoic volcanic activity in the northern Arabian shield. Kingdom of Saudi Arabia. Bull. Inst. Applied Geol. (Jeddah), 3(2): 59-75.
- De Paolo, D.J. and Johnson R.W. 1979. Magma genesis in the New Britain island-arc: constraints from Nd and Sr isotopes and trace-element patterns. Contrib. Mineral. Petrol. 70: 367-379.
- Dixon, T.N., 1981. Gabal Dahanib, Egypt: A Late Precambrian layered sill of komatiitic composition. - Contrib. Mineral. Petrol. 76: 42-52.
- Dobrenky, A.E., Aruthunyan, G.S., Bolkovoy, B.I., Agaronyan, L.V. and Pogosyan, G.A., 1977. Geological Report on Results of Search and estimation at Mukeyras Deposit. Soviet Team, Board of Petroleum and Minerals, Dept. of Geology and Mineral Exploration, People's Democratic Republic of Yemn, Aden.
- Dostal, J. Caby, R. and Dupency, C. 1979. Metamorphosed alkaline intrusions and dyke complexes within the Pan-African belt of western Hoggar (Algeria): geology and geochemistry. Precambrian Res., 10: 1-2.
- Du Bray, E.A. 1983. Petrology of muscovite-bearing granitoids in the eastern and southeastern Arabian Shield. Deputy Ministry for Mineral resources, Open-file Report, USGS-OF-03-10, 36p.
- Du Bray, E.A. 1986a. Specialized granitoids in the southeastern Arabian Shield - case history of a regional assessment. J. Afr. Earth Sci. 4: 169-176.
- Du Bray, E.A. 1986b. Jabal Silsilah tin prospect, Najd region, Kingdom of Saudi Arabia. J. Afr. Earth Sci. 4: 237-247.
- Drysdall, A.R., Jackson, N.J., Ramsay, C.R., Douch, C.J. and Hackett, D. 1984. Rare element mineralization related to Precambrian alkali granites in the Arabian Shield. Econ. Geol. 79: 1366-1377.
- Duyverman, H.J., Harris, N.B.W., Hawkesworth, C.J. 1982. Crustal accretion in the Pan African: Nd and Sr isotope evidence from the Arabian Shield: Earth Planet Sci. Lett. 59: 315-326.
- El-Gaby, S., El-Nady, O.M. and Khudeir, A.A. 1984. Tectonic evolution of the basement complex in the CED of Egypt. Geol. Rdsch., 73: 1019-1036.
- El-Gaby, S. and Greiling, R.O. 1988. Introduction. In: El-Gaby, S. and Greiling, R.O.

## References

---

- (Editors) The Pan-African Belt of Northeast Africa and Adjacent Areas; Tectonic Evolution and Economic Aspects of a Late Proterozoic Orogen. Fried Vieweg Sohn Verlagsgesellschaft mbH, Braunschweig. Germany. pp.1-3.
- El-Gaby, S., List, F.K. and Tehrani Resa, 1988. Geology, Evolution and Metallogenesis of the Pan-African Belt in Egypt. In: El-Gaby, S. and Greiling, R.O. (Editors) The Pan-African Belt of Northeast Africa and Adjacent Areas; Tectonic Evolution and Economic Aspects of a Late Proterozoic Orogen. Fried Vieweg Sohn Verlagsgesellschaft mbH, Braunschweig. Germany. pp.15-68.
- El-Ramly, M.F. 1988. Preface In: El-Gaby, S. and Greiling, R.O. (Editors) The Pan-African Belt of Northeast Africa and Adjacent Areas; Tectonic Evolution and Economic Aspects of a Late Proterozoic Orogen. Fried Vieweg Sohn Verlagsgesellschaft mbH, Braunschweig. Germany. pp. 1-3.
- Embleton, J.C.B., Hughes, D.J., Klemenic, P.M., Poole, S. and Vail, J.R. 1983. A new approach to the Stratigraphy and Tectonic Evolution of the Red Sea Hills, Sudan. Bull. Fac. Earth Sci. King Abdulaziz Univ., 6:101-112.
- Engel, A.E.J., Dixon, T.H. and Stern, R.J. 1980. Late Precambrian evolution of Afro-Arabian Crust from ocean arc to craton. Geol. Soc. of America Bull. 91: 699-706.
- England, P.C. and Thompson, A. 1986. Some thermal and tectonic models for crustal melting in continental collision zones, in: Collision Tectonics, M.P. Coward and A.C. Ries, (eds.) Geol. Soc. Spec. Publ. 19: 83-94.
- Evans, A.M. 1987. An Introduction to Ore Geology. Black-Well Scientific Publication, Oxford. pp. 214-279.
- Evans, B.W. and Leake, B.E. 1960. The Composition and Origin of the Striped Amphibolites of Connemara, Ireland. Journal of Petrology. 1: 337-363.
- Eyal, Y. and Eyal, M. 1987. Mafic Dyke Swarms in the Arabian-Nubian Shield. Isr. J. Earth Sci. 36: 195-211.
- Fleck, R.J., Greenwood, W.R., Hadley, G.G., Anderson, R.E. and Schmidt, D.L. 1978. Age and evolution of the southern part of the Arabian Shield (Abstract). Precambrian Res. 6: A21-2.
- Fleck, R.J., Greenwood, W.R., Hadley, D.G. Anderson, R.E. and Schmidt, D.L. 1980.

## References

---

- Rubidium-strontium geochronology and the plate-tectonic evolution of the southern part of the Arabian Shield. USGS Prof. Paper 1131, 38p.
- Fleck, R.J. and Hadley, D.G. 1982. Ages and strontium initial ratios of plutonic rocks in a transect of the Arabian Shield. Saudi Arabian Deputy Ministry for Mineral Resources Open-File Report USGS-OF-03-38.
- Fleuty, M.J. 1964. The description of folds. In: Proceedings of the Geologists Association. 75: 461-492.
- Furnes, H., Shimron, A.E. and Roberts D. 1985. Geochemistry of Pan-African volcanic arc sequences in southeastern Sinai Peninsula and plate tectonic implications. Precambrian Res. 29: 359-382.
- Gardner, J.N., Goff, F., Garcia, S. and Hagan, R.C. 1986. Stratigraphic relations and lithologic variations in the Jemez Volcanic Field, New Mexico. J. Geophys. Res. 91: 1763-1778.
- Garson, M.S. and Shaiaby, I.M. 1976. Precambrian-Lower Paleozoic plate tectonics and metallogenesis in the Red Sea region. Geol. Ass. Canada Sp. Pap. 14. pp. 573-596.
- Gass, I.G. 1977. The evolution of the Pan-African crystalline basement in NE Africa and Arabia. J. Geol. Soc. London. 134: 129-138.
- Gass, I.G. 1981. Pan-African (Upper Proterozoic) plate tectonics of the Arabian-Nubian Shield. In: Kroner, A. (ed.) Precambrian Plate Tectonics. Elsevier, Amsterdam, pp387-405.
- Gass, I.G., Mallick, D.I.J. and Cox, K.G. 1965. Royal Society volcanological expedition to the South Arabian Federation and the Red Sea. Nature. 205: 952-955.
- Gass, I.G., Ries, A.C., Shackleton, R.M. and Smewing J.D. 1990. Tectonics, geochronology and geochemistry of the Precambrian rocks of Oman. In: Robertson, A.H.F., Searle, M.P., Ries A.C. (eds). The Geology and Tectonics of the Oman Region. Geol. Soc. Spec. Publ. 49: 585-599.
- Gellatly, D.C. 1962. A preliminary note on the Darkainie alkaline complex, Borama District, Somali Republic: Univ. of Leeds Res. Inst. African Geo., 6th Ann. Rept., 1960-1961. pp. 22-23.
- Gellatly, D.C. 1963a. The Geology of the Darkainie Nepheline Syenite Complex, Borama

## References

---

- District, Somali Republic: PhD. thesis. Univ. of Leeds, England.
- Gellatly, D.C. 1963b. Carbonatites of the Darkainle alkaline complex, Somali Republic: Univ. of Leeds Res. Inst. African Geol., 7th Ann. Rept. 1961-1962. pp.15-16.
- Gellatly, D.C. 1964. Nepheline and feldspar orientations in nepheline syenites from Darkainle, Somali Republic: *Am. Jour. Sci.* 262: 635-642.
- Geukens, F. 1966. Geology of the Arabian Peninsula, Yemen. United States Geological Survey, Professional Paper. 560-B: pp. 6-8.
- Gill, J. 1981. *Orogenic Andesites and Plate Tectonics*. Springer-Verlag, New York, 390p.
- Gittins, J. 1966. Carbonatite in Somalia Republic. In: Tuttle, O.F. and Gittins (Eds.) *Carbonatites*. John Wiley & Sons Ltd., New York. pp.461-462.
- Govindarajou, K. 1989. Compilation of working values and sample descriptions of 272 Geostandards. *Geostandards Newsletter*, 18: 1-113.
- Greenberg, J.K., 1981. Characteristics and origin of Egyptian younger granites: summary. *Geol. Soc. Am. Bull.* 1(92): 224-232.
- Greenwood, J.E.G.W. 1961. The Inda Ad Series of the former Somali land Protectorate: London, *Overseas Geology and Mineral Resources Bulletin*, 8: 288-296.
- Greenwood, J.E.G.W. and Bleackley, 1967. *Geology of the Arabian Peninsula. Aden Protectorate*. USGS Professional Paper. 560-C, Washington, U.S.A. 96 p.
- Greenwood, W.R., Anderson, R.E., Fleck, R.J. and Roberts, R.J. 1980. Precambrian Geologic History and Plate Tectonic Evolution of the Arabian Shield. *Bulletin*. 24. D.G.M.R., Jeddah, Saudi Arabia.
- Greenwood, W.R., Hadley, D.G., Anderson, R.W. Fleck, R.J. and Schmidt, 1976. Late Proterozoic cratonization in south-western Saudi Arabia. *R. Soc. Phil. Trans. Ser. A*, 280: 517-527.
- Greiling, R.O., Kroner, A., El-Ramly, M.F. and Rashwan, A.A. 1988. Structural Relationship between the Southern and Central parts of the Eastern Desert of Egypt: Details of Fold and Thrust Belt. In: El-Gaby, S. and Greiling, R.O. (Editors) *The Pan-African Belt of Northeast Africa and Adjacent Areas; Tectonic Evolution and Economic Aspects of a Late Proterozoic Orogen*. Fried Vieweg Sohn Verlagsgesellschaft mbH, Braunschweig. Germany. pp. 120-145.

---

#### References

---

- Grolier, M.J. and Overstreet, W.C. 1978. Geologic Map of the Yemen Arab Republic (Sana'). Miscellaneous Investigations Series, Map I-1143-B. United States Geological Survey.
- Harris, N.B.W., and Marriner, G.F. 1980. Geochemistry and petrogenesis of peralkaline granite complex from the Midian Mountains, Saudi Arabia. *Lithos* 13: 325-337.
- Harris, N.B.W., Marzouki, F.M.H. and Ali, S. 1986a. The Jabel Sayid complex, Arabian Shield: geochemical constraints on the origin of peralkaline and related granites. *J. geol. Soc. Lond.* 143: 287-295.
- Harris, N.B.W., Pearce, J.A. and Tindle, A.G. 1986b. Geochemical characteristics of collision-zone magmatism. In: M.P. Coward and A.C. Ries. *Collision Tectonics*. *Geol. Soc. Special Publ.* 19: 67-81.
- Hawkesworth, C.J., Mantovani, M.S.M., Taylor, P.N. and Palacz, Z. 1986. Evidence from the Paranaa of South Brazil for a continental contribution to DUPAL basalts, *Nature* 322: 356-359.
- Hawkins, T.R.W., Hindle, D. and Strugnell, R. 1981. Outlines of the stratigraphy and structural framework of south Dhofar (Sultanate of Oman), *Geologie en Mijnbouw*. 60: 247-256.
- Heinrich, E.W.M. 1966. *The Geology of Carbonatites*. Rand McNally Co. Chicago. pp.465-466.
- Henney, P.J., Evans, J.A., Holden, K.P., and Rock, N.M.S. 1989. Granite-lamprophyre associations in the Scottish Caledonides: trace element and isotopic evidence for mantle involvement in Caledonian granite genesis. *Terra abstracts* 1: 285-286.
- Hepworth, J.V., 1979. Does the Mozambique belt continue into Saudi Arabia ? *Inst. Appl. Geol. Jeddah, Bull.* 3, vol. 1, pp. 39-51.
- Hergt, J.M., Chappel, B.W., McCulloch, M.T., McDogall, I and Chivas, A.R. 1989. Geochemical and Isotopic Constraints on the Origin of the Jurassic Dolorites of Tasmania. *Jour. Petrol.* 30: 841 - 883.
- Hildreth, W. 1981. Gradients in Silicic Magma Chambers: Implications for Lithospheric Magmatism. *Journal of Geophysical Research.* 86 (B11):10153-10192.
- Hirdes, W. and Brinkmann, K. 1985. The Kabus and Balula serpentinite and Metagabro

## References

- Complexes - A Dismembered Proterozoic Ophiolite in the Northeastern Ndsba Mountains, Sudan. *Geol. Jb.* B58: 3-43.
- Hogarth, D.D. 1989. Pyrochlore, apatite and amphibole: distinctive minerals in carbonatite. In: Keith Bell (Ed.), *Carbonatites: genesis and evolution*. Unwin Hyman Ltd. London, pp. 105-148.
- Holmes, A., 1951. A sequence of Precambrian orogenic belts in South and Central Africa. 18th Int. Geol. Congr. London, 14: 254-269.
- Huppert, H.E. and Sparks, R.S.J. 1988. The generation of granitic magmas by intrusion of basalt into continental crust. *J. Petrol.* pp.599-624.
- Hussein, I.M., Kroner, A. and Durr, S.T. 1984. Wadi Onib: A dismembered Pan-African Ophiolite in the Red Sea Hills of Sudan. *Bull. Fac. Earth Sci. King Abdulaziz Univ.*, pp.319-327.
- Irvine, T.N. and Baragar, W.R.A., 1971. A guide to the chemical classification of the common volcanic rocks. *Canadian Journal of Earth Sciences*, 8: 523-548.
- Jackson, N.J., 1986. Petrogenesis and evolution of Arabian felsic plutonic rocks. *Journal of African Earth Sciences*. 4: 47-59.
- Jackson, N.J., Walsh, J.N. and Pegram, E. 1984. Geology, geochemistry and petrogenesis of Late Precambrian granitoids in the Central Hijaz Region of the Arabian Shield. *Contr. Miner. Petrol.* 87: 205-219.
- Kay, R.W. and Gast, P.W. 1973. The rare earth content and origin of alkali-rich basalts. *J. Geol.* 81: 653-682.
- Kazmin, V., Schiferaw A. and Balcha, T. 1978. The Ethiopian basement: Stratigraphy and possible manner of evolution. *Geol. Rdsch.*, 67: 531-546.
- Kazmin, V., M. Teferra, S.M. Behre and Chowaka, S. 1979. Precambrian structure of Western Ethiopia. *Annals. Geol. Surv. Egypt.* 9: 1-8.
- Kennedy, W.Q. 1964. The structural differentiation of Africa in the Pan-African tectonic episode. *Ann. Rept. Res. Inst. African Geol. Univ. Leeds*, 8: 48-49.
- Kopecny, V., 1981. Petrology of crystalline complex in Yaffa country, P.D.R. Yemen. Olomouc, Palacky Univ., *Prirodoved. fAk., Sb., Geogr., Geol.*, Vol.62, No.18, pp. 107-134.

## References

- Kroner, A., 1979. Pan-African plate tectonics and its repercussions on the crust of northeast Africa. *Geologisches Rundschau*. 68: 565-583.
- Kroner, A. 1984. Late Precambrian plate tectonics and orogeny: a need to redefine the term 'Pan-African'. In: J. Klerks and J. Michsot (eds), *African Geology*, Musee r. Afr. Centr., Tervurend, pp23-28.
- Kroner, A., Greiling, R., Reischmann, T., Hussein, I.M., Stern, R.J., Durr, S. Kruger, J. and Zimmer M. 1987. Pan-African crustal evolution in the Nubian segment of northeast Africa. *Am. Geophys. Union, Geodynamics Series*, 17.
- Kroner, A., Reischman, T., Wust, H.J. and Rashwan, A.A. 1988. Is there any Pre Pan-African (>950 Ma) Basement in the Eastern Desert of Egypt? In: El-Gaby, S. and Greiling, R.O. (Editors) *The Pan-African Belt of Northeast Africa and Adjacent Areas; Tectonic Evolution and Economic Aspects of A late proterozoic Orogen*. Fried Vieweg Sohn Verlagsgesellschaft mbH, Braunschweig. Germany. pp. 95-119.
- Kroner, A., Rooboi, M.J., Ramsay, C.R. and Jackson, N.J. 1979. Pan African ages of some gneissic rocks in the Saudi Arabian Shield. *J. Geol. Soc. London*. 136: 455-461.
- Kroner, A., Stern, R.J., Dawoud, A.A., Compston, W. and Reischmann, T. 1987. The Pan-African continental margin in NE Africa: Evidence from a geochronological study of granulites in Sabaloka, Sudan. *Earth Planet. Sci. Lett.*
- Leat, P.T., Thompson, R.N. Morrison, M.A., Trayhorn, S.C. and Hendry, G.L. 1987. Geodynamic significance of post-Variscan intrusive and extrusive potassic magmatism, in SW England, *Trans. R. Soc. Edinburgh Earth Sci.* 77: 349-360.
- Le Bas, M.J. 1989. Diversification of carbonatite. In: Keith Bell (Editor) *Carbonatites: genesis and evolution*. Unwin Hayman Ltd. London, pp. 428-447.
- Le Bas, M.J. Le Maitre, R.W. Streckeisen, A. and Zanettin, B., 1986. A chemical classification of volcanic rocks based on the total alkali-silica Diagram. *Journal of Petrol.* 27: 745-750.
- Le Maitre, R.W. 1989. *A Classification of Igneous Rocks and Glossary of Terms*. Blackwell Scientific Publ. Oxford. 193 p.
- Lewis, F.M., Pierce, J.C., Potter, G.M. and Bhappu, R.B. 1983. Technology and economics of small mines: Mining. In: M. Woakes and J.S. Carman (Editors). *AGiD*

## References

---

- guide to mineral resources development. AGiD Report Series: No.10: pp. 267-282.
- Lightfoot, P. and Hawkesworth, C. 1988. Origin of Deccan Trap Lavas: evidence from combined trace element and Sr-, Nd- and Pb-isotope studies. *Earth Planet. Sci. Lett.* 91: 89-104.
- Loiselie, M.C., Wones, D.R., 1979. Characteristics of anorogenic granites: *Geol. Soc. Am. AGM (1979). Abstr with Progr:* 539.
- Mantovani, M.S.M., Marques, L.S., De Sousa, M.A., Civetta, L., Ataila, L. and Innocenti, F. 1985. Trace element and Strontium Isotope Constraints on the origin and Evolution of Parana Continental Flood Basalts of Santa Catarina State (South Brazil). *Journal Petrol.* 26: 187-209.
- Marsh, N.G., Saunders, A.D., Tarney, J. and Dick, H.J.B. 1980. Geochemistry of basalts from the Shikoku and Daito basins, Deep sea Drilling Project Leg 58. In: Klein et al (Editors), *Init. Report, Washington, 58:* pp. 805-842.
- Marsh, N.G., Tarney, J. and Hendry, G.L. 1983. Trace elements geochemistry of basalt from Hole 50B, Panama Basin, D.S.D.P. Leg 69 and 70. In: Can, J., et al (Editors). *Init. Report of the D.S.D.P. Washington, 69:* 747-763.
- McWilliams, M.O. 1981. Palaeomagnetism and Precambrian tectonic evolution of Gondwana. In: A. Kroner (ed.), *Precambrian plate tectonics*, Elsevier, Amsterdam, pp. 649-687.
- Mian, I., 1987. The Mineralogy and Geochemistry of the Carbonatites, Syenites and Fenites of Northwest Frontier Province, Pakistan. Unpublished Ph.D. Thesis. University of Leicester, U.K.
- Mian, I. and Le Bas, M.J., 1986. Sodic amphiboles in fenites from the Loe Shilman Carbonatite Complex, NW Pakistan. *Mineralogical Magazine*, 50: 187-197.
- Miyashiro, A. 1973. *Metamorphism and Metamorphic Belts*. George Allen and Unwin Ltd. London. pp. 273-309.
- Miyashiro, A. 1978. Nature of alkalic volcanic rock series. *Contrib. Mineral. Petrol.* 66: 91-104.
- Miyashiro, A., Aki, K. and Sengor, A.M.C. 1979. *Orogeny*. John Wiley and Sons, Chichester. pp. 213-233.

## References

---

- Moller, P., Morteau and Schley, F. 1980. Discussion of REE distribution patterns of carbonatites and alkalic rocks. *Lithos*, 13: 171-179.
- Molnar, P. 1984. Structure and tectonics of the Himalaya: constraints and implications from geophysical data. *Ann. Rev. Earth Planet. Sci.* 12: 489-518.
- Molnar, P. and Tapponier, P. 1975. Cenozoic tectonics of Asia: effects of a continental collision. *Science* 189. pp. 419-26.
- Mysen, B.O. and Boettcher, A.L. 1975. Melting of a hydrous mantle: II. Geochemistry of crystals and liquids formed by anatexis of mantle peridotite at high pressures and high temperatures as a function of controlled activities of water, hydrogen, and carbon dioxide. *J. Petrol.* 16: 549-593.
- Neary, C., Gass, I.G. and Cavanagh, B.J. 1976. Granitic association of northeastern Sudan. *Geol. Soc. Amer. Bull.* 87: 1501-1512.
- Norry, M.J. and Fitton, J.G., 1983. Compositional differences between oceanic and continental basic lavas and their significance. In: C.J. Hawkesworth and M.J. Norry (Editors). *Continental Basalts and Mantle Xenoliths*. Shiva Pub.
- Nurmi, P.A., and Haapala, I. 1986. The Proterozoic granitoids of Finland: granite types, metallogeny, and relation to crustal evolution. *Bull. Geol. Soc. Finland*, 58: 203-233.
- Pearce, J.A. 1983. Role of the sub-continental lithosphere in magma genesis at active continental margins. In: C.J. Hawkesworth and M.J. Norry (Editors). *Continental Basalts and Mantle Xenoliths*. Shiva Pub. Ltd. pp 230-249.
- Pearce, J.A., Harris and Tindle, A. 1984. Trace element discrimination diagrams for the tectonic interpretation of granite rocks. *Journal of Petrology*, 25: 956-983.
- Pearce J. and Norry, M.J. 1979. Petrogenetic Implications of Ti, Zr, Y and Nb Variation in volcanic rocks. *Contrib. Mineral. Petrol.* 69: 33-47.
- Pellaton, C. 1979. Geologic map of the Yanbu al Bahr quadrangle, sheet 24C. Saudi Arabian Deputy Ministry for Mineral Resources. Geoscience Map Series GM-48A (1:250,000).
- Pellaton, C. 1981. Geologic map of the Al Madinah quadrangle, sheet 24D. Saudi Arabian Deputy Ministry for Mineral Resources. Geoscience Map Series, GM-52A (1:250,000).

## References

---

- Pitcher, W.S. 1979. Comments on the geological environment of granites. In: Atherton, M.P. and Tarney, J. Origin of Granite Batholiths, Geochemical evidence. Shiva Pub. pp. 1-8.
- Pohl, W. 1988. Precambrian Metallogeny of NE-Africa. In: El-Gaby, S. and Greiling, R.O. (Editors) The Pan-African Belt of Northeast Africa and Adjacent Areas: Tectonic Evolution and Economic Aspects of a Late Proterozoic Orogen. Fried Vieweg Sohn Verlagsgesellschaft mbH, Braunschweig, Germany. pp.318-314.
- Radin, A.A.M., Fyfe, W.S. and Kerrich, R. 1981. Origin of Peralkaline Granites of Saudi Arabia. *Contrib. Mineral. Petrol.* 78: 358-366.
- Ramdohr, P. 1980. *The Ore Minerals and their Intergrowths*. Pergamon Press, Oxford, 2nd ed., Vol. 1,2.
- Ramsay, C.R., Drydali, A.R. and Clark, M.A. 1986a. Felsic plutonic rocks of the Midyan region, Kingdom of Saudi Arabia - I. Distribution, classification and resource potential. *J. Afr. Earth Sci.* 4: 63-77.
- Ramsay, C.R., Stoesser, D.B. and Drysdall, A.R. 1986b. Guidelines to classification and nomenclature of Arabian felsic plutonic rocks. *J. Afr. Earth Sci.* 4: 13-20.
- Ressetar, R. and Monrad, J.R. 1983. Chemical composition and tectonic setting of the Dokhan Volcanic formation, eastern desert, Egypt. *J. Afr. Earth Sci.* 1: 103-112.
- Rock, N.M.S., and Hunter, R.H. 1987. Late Caledonian dyke-swarms of northern Britain: spatial and temporal intimacy between lamprophyric and granitic magmatism around the Ross of Mull pluton, Inner Hebrides. *Geologische Rundschau*, 76: 805-826.
- Rooboi, M.J., Ramsay, C.R., Jackson, N.J. and Darbyshire, D.P.F. 1983. Late Proterozoic lavas of the Central Arabian Shield - evolution of an ancient volcanic arc system. *J. Geol. Soc. London* 140: 185-202.
- Rutter, M.J. and Wyllie, P.J. 1988. Melting of vapour-absent tonalite at 10kbar to simulate dehydration-melting in the deep crust, *Nature* 331: 159-160.
- Ryerson, F.J. and Hess, P.C. 1978. Implications of liquid-liquid distribution coefficient to mineral-liquid partitioning. *Geochim. Cosmochim. Acta.* 42: 921-932.
- Saeedan, A. 1984. *Geology and Mineralization of Am Saiui Mukeras*. Unpublished Ph.D. Thesis (in Russian) from a Russian University. Directorate of Geology and Mineral

## References

---

- Exploration, Ministry of Oil and Minerals. Aden.
- Saunders, A.D., Tarney, J., Marsh, N.G. and Wood, D.A. 1980. Ophiolites as ocean crust or marginal basin crust: A geochemical approach. In: A. Panayiotou (Editor), *Ophiolites Proc. Int. Ophiolite Symp. Cyprus*, pp. 193-204.
- Schandeimeier, H., Darbyshire, D.P.F., Harms, U. and Richter, A. 1988. The East Saharan Craton: Evidence for Pre Pan-African Crust in NE Africa West of the Nile. In: El-Gaby, S. and Greiling, R.O. (Editors) *The Pan-African Belt of Northeast Africa and Adjacent Areas; Tectonic Evolution and Economic Aspects of A late proterozoic Orogen*. Fried Vieweg Sohn Verlagsgesellschaft mbH, Braunschweig. Germany. pp. 69-74.
- Self, S., Goff, F., Gardner, J.N. Wright, J.V., and Kite, W.M. 1986. Explosive rhyolitic volcanism in the Jemez Mountains: Vent locations, caldera development and relation to regional structure. *J. Geophys. Res.* 91: 1779-1798.
- Serencsits, C.M., Faul, H., Foland, K.A., El Ramley, M.F. and Hussein, A.A. 1979. Alkaline ring complexes in Egypt: their ages and relationships to tectonic development of the Red Sea. *Annals of the Geological Survey of Egypt*. 9: 102-116.
- Shackleton, R.M. 1979. Precambrian tectonics of NE Africa. *Institute of Applied Geology (Jeddah-Saudi Arabia), Bulletin*, 3: 1-6.
- Shackleton, R.M. 1986. Precambrian collision tectonics in Africa. In: MP. Coward and A.C. Ries (Editors), *Collision Tectonics*. *Geol. Soc. Lond. Spec. Publ.*, 19: 329-349.
- Shackleton, R.M. 1988. Contrastive Structural Relationships of Proterozoic Ophiolites in Northeast and Eastern Africa. In: El-Gaby, S. and Greiling, R.O. (Editors) *The Pan-African Belt of Northeast Africa and Adjacent Areas; Tectonic Evolution and Economic Aspects of A late proterozoic Orogen*. Fried Vieweg Sohn Verlagsgesellschaft mbH, Braunschweig. Germany. pp.181-193.
- Shackleton, R.M., Ries, A.C., Graham, R.H. and Fitches, W.R. 1980. Late Precambrian ophiolitic melange in the eastern Desert of Egypt. *Nature* 285, pp. 472-474.
- Shearman, D. 1988. Sulphure and Pb/Zn Sulphide deposition, during carbonate diagenesis, in the presence of hydrocarbons, bacteria and gypsum/anhydrite. Unpublished lecture notes. Kuwait University.

#### References

---

- Shimron, A.E. 1984. Evolution of the Kid Group, Southeast Sinai Peninsula: Thrusts, melanges, and implications for accretionary tectonics during the late Proterozoic of the Arabian-Nubian Shield. *Geology* 12: 242-247.
- Simpson, C. and Schmid, S.M. 1983. An evaluation of criteria to deduce the sense of movement in sheared rocks. *Geol. Soc. of America Bull.* 94: 1281 - 1288.
- Stacey, J.S. and Hedge, C.E. 1984. Geochronologic and isotopic evidence for early Proterozoic crust in the eastern Arabian Shield. *Geology*. 12: 310-313.
- Stacey, J.S., Stoesser, D.B., Greenwood, W.R. and Fischer, L.B. 1984. U-Pb Zircon geochronology and geological evolution of the Halaban-Ai Amar region of the Eastern Arabian Shield, Kingdom of Saudi Arabia. *Journal Geol. Soc., London*, 141: 1043-1055.
- Stern, R.S. 1979. Late Precambrian Crustal Environments as Reconstructed from Relict Igneous Minerals, Central Eastern Desert of Egypt. *Annals of the Geological Survey of Egypt*. IX: pp.9-31.
- Stern, R.J. 1981. Petrogenesis and Tectonic Setting of Late Precambrian Ensimatic Volcanic Rocks, Central Eastern Desert of Egypt. *Precambrian Research*. 16: 195-230.
- Stern, R.J. 1985. The Najd fault system of Saudi Arabia and Egypt: a late Precambrian rift-related transform system? *Tectonics* 4: 497-511.
- Stern, R.J. and Gottfried, D. 1986. Petrogenesis of a late Precambrian (575-600 Ma) bimodal suite in northeast Africa. *Contrib. Mineral. Petrol.* 92: 492-501.
- Stern, R.J., Gottfried, D. and Hedge, C.E. 1984. Late Precambrian rifting and crustal evolution in the Northeastern Desert of Egypt. *Geology*. 12: 168-172.
- Stern, R.J. and Hedge, C.E. 1985. Geochronologic and isotopic constraints on Late Precambrian Crustal Evolution in the Eastern Desert of Egypt. *American Journal of Science*. 285: 97-127.
- Stern, R.J., Sellers, G. and Gottfried, D. 1988. Bimodal Dike Swarms in the Northeastern Desert of Egypt: Significance for the origin of Late Precambrian "A-Type" Granites in Northern Afro-Arabia. In: El-Gaby, S. and Greiling, R.O. (Editors) *The Pan-African Belt of Northeast Africa and Adjacent Areas: Tectonic Evolution and Economic Aspects of*

## References

---

- a Late Proterozoic Orogen. Friedr Vieweg Sohn Verlagsgesellschaft, mbH, Braunschweig. Germany. pp. 147-179.
- Stoeser, D.B. 1986. Distribution and tectonic setting of plutonic rocks of the Arabian Shield. *Journal of African Earth Sciences*, 4: 21-46.
- Stoeser, D.B. and Camp, V.E. 1985. Pan-African microplate accretion of the Arabian Shield. *Geol. Soc. of America, Bulletin*, 96: pp. 817-826.
- Stoeser, D.B., Fleck, R.J., and Stacey, J.S. 1983. Geochronology and origin of an early tonalite gneiss of the Wadi Traib Batholith and the formation of syntectonic gneiss complexes in the Southeastern Arabian Shield, Kingdom of Saudi Arabia. *Bull. Fac. Earth Sci., K.A.U.*, 6: 351-364.
- Stoeser, D.B. and Stacey, J.S. 1988. Evolution, U-Pb Geochronology and Isotope Geology of the Pan-African Nabitah Orogenic Belt of the Saudi Arabian Shield. In: El-Gaby, S. and Greiling, R.O. (Editors) *The Pan-African Belt of Northeast Africa and Adjacent Areas; Tectonic Evolution and Economic Aspects of a Late Proterozoic Orogen*. Fried Vieweg Sohn Verlagsgesellschaft mbH, Braunschweig. Germany. pp.227-288.
- Streckheisen, A. 1976. To each plutonic rock its proper name. *Earth sci. Reviews*. 12: 1-33.
- Streckheisen, A. and Le Maitre, R.W. 1979. A chemical approximation to the modal QAPF classification of Igneous rocks. *Neues Jahr. Min. Abh.* 136: 169-206.
- Stuckless, J.S., Hedge, C.E., Wenner, D.B. and Nkomo, I.T. 1984. Isotopic studies of postorogenic granites from the northeastern Arabian Shield, Kingdom of Saudi Arabia, Saudi Arabian Deputy Ministry for Mineral Resources Open-File Report USGS-OF-04-42.
- Stuckless, J.S., Van Trump, G., Jr. Christiansen, E.G., Bush, C.A., Bunker, C.M. and Bartell, A.J. 1983. Preliminary assessment of the geochemistry and mineral favourability of the postorogenic granites of the southeastern Arabian Shield, Kingdom of Saudi Arabia. Saudi Arabian Deputy Ministry for Mineral Resources Open-File Report USGS-OF-03-64.
- Sun, S.S. and McDonough, W.F. 1989. Chemical and isotopic systematics of Oceanic

## References

---

- basalts: implications for mantle composition and processes. In: Saunders, A.D. and Norry, M.J. (Editors) *Magmatism in the Ocean basins*. Geol. Soc. Special Publication. 42: 313-345.
- Sylvester, A.G. 1988. Strike-slip faults. *Geol. Soc. of America Bulletin*, 100: 1666-1703.
- Tait, R.E. and Harley, S.L. 1988. Local processes involved in the generation of migmatites within mafic granulites. In: *Origin of Granites*. Trans. Royal Soc. of Edinburgh: Earth Sciences. 79: 209-222.
- Tapponnier, P. and Molnar, P. 1976. Slip-line field theory and large scale continental tectonics. *Nature* 264: 319-324.
- Tapponnier, P., Peltzer, G., Le Dain, A.Y and Armijo, R. 1982. Propagating extrusion tectonics in Asia: new insights from simple experiments with plasticine. *Geology*, 10: 611-616.
- Tarney, J. and Saunders, A.D. 1979. Trace element constraints on the origin of Cordilleran batholiths. In: M.P. Atherton, and J. Tarney, (Editors) *Origin of Granite Batholiths*. Shiva. Pub., pp. 90-105.
- Tarney, J., Saunders, A.D., Weaver, S.D., Donnellan, N.C.B. and G.L. Hendry, 1979. Minor-element geochemistry of basalts from Leg 49, North Atlantic Ocean. In: Luyendyk, B.P., Cann, J. (Editors) *Init. Reports DSDP 49*: 657-691.
- Tarney, J. and Weaver, B.L., 1987. Geochemistry and petrogenesis of early Proterozoic dyke swarms; In: H.C. Halls and W.F. Fahrig (Editors). *Mafic Dyke Swarms*, Geological Association of Canada Special Paper. 34: 81-94.
- Taylor, S.R. and McLennan, S.M. 1981. The composition and evolution of the continental crust: rare earth element evidence from sedimentary rocks. *Phil. Trans. Royal Soc. London*. A301: p. 381.
- Taylor, S.R. and McLennan, S.M. 1985. *The continental crust: its composition and evolution*. Blackwell Scientific Pub., Oxford, 312 p.
- Thompson, R.N.; Morrison, M.A., Dickin, A.P. and Hendry, G.L. 1983. Continental Flood Basalts.... Arachnids Rule OK? In: C.J. Hawkesworth and M.J. Norry (Editors). *Continental Basalts and Mantle Xenoliths*. Shiva Pub., England. pp. 158-185.
- Thompson, R.N.; Morrison, M.A.; Hendry, G.L. and Parry, S.J. 1984. An assessment of
-

## References

---

- the relative roles of crust and mantle in magma genesis: an element-approach. *Phil. Trans. Royal Soc. Lond.*, A310: 549 - 590.
- Uytenbogaardt, W. Burke, E.A.J., 1971. *Tables for Microscopic Identification of Ore Minerals*. Elsevier, Amsterdam. 2nd revised ed. 430 p.
- Vail, J.R. 1983. Pan-African crustal accretion in northeast Africa. *J. African Earth Sci.*, 1, 285-294.
- Vail, J.R. 1984. Distribution and tectonic setting of post-kinematic Igneous Complexes in the Red Sea Hills of Sudan and the Arabian Nubian Shield. *Bull. Fac. Earth. Sci., K.A.U.* 6: 259-269.
- Vail, J.R. 1988. Tectonics and Evolution of the Proterozoic Basement of Northeastern Africa. In: El-Gaby, S. and Greiling, R.O. (Editors) *The Pan-African Belt of Northeast Africa and Adjacent Areas; Tectonic Evolution and Economic Aspects of A late Proterozoic Orogen*. Fried Vieweg Sohn Verlagsgesellschaft mbH, Braunschweig, Germany. pp.194-226.
- Vielzeuf, D. and Holloway, J.R. 1988. Experimental determinations of the fluid-absent melting relations in the pelitic system. Consequences for crustal differentiation. *Contrib. Mineral. Petrol.* 98: 257-276.
- Voegeli, D.A., 1985. The origin of composite dike rocks from the northeastern desert and Sinai, Egypt. MS thesis, U. Texas at Dallas, 165p.
- Walsh, J.N., Buchley, F. and Barker, J. 1981. The simultaneous determination of R.E.E.'s in rocks using the Inductively Coupled Plasma Spectrometer. *Chem. Geol.* 33: 141-153.
- Warden, A.J. and Daniels, J.L. 1984. Evolution of the Precambrian of Northern Somalia. *Bull. Fac. Earth Sci. King Abdul Aziz Univ.* 6: 145-164.
- Warden, a.J. and Horkel, A.D. 1984. The Geological Evolution of the NE-Branch of the Mozambique Belt (Kenya, Somalia, Ethiopia). *Mitt. Osterr. Geol. Ges.*, Vol. 78.
- Watson, E.B. 1976. Two-liquid partition coefficients: experimental data and geochemical implications. *Contrib. Mineral. Petrol* 56: 119-134.
- Weaver, B.L. and Tarney, J. 1981. The Scourie Dyke Suite: Petrogenesis and geochemical nature of the Proterozoic sub-continental mantle". *Contrib. Mineral.*

## References

---

- Petrol. 78: 175-188.
- Weaver, B.L. and Tarney, J. 1983. Chemistry of the Sub-Continental Mantle: Inferences from Archean and Proterozoic Dykes and Continental Flood Basalt, In: C.J. Hawkesworth and M.J. Norry (Editors). Continental Basalts and Mantle Xenoliths. Shiva Publishing Ltd. pp. 209-229.
- Weaver, B.L., Wood, D.A., Tarney, J. and Joron, J.L. 1987. Geochemistry of ocean island basalts from the South Atlantic: Ascension, Bouvet, St. Helena, Gough and Tristan da Cunha. In: J.G. Fitton and B.G.J. Upton. Alkaline Igneous Rocks. Geol. Soc. London. Spec. Publ. 30: 253-267.
- White, A.J.R. and Chappell, B.W. 1977 Ultrametamorphism and granitoid gneiss. Tectonophysics 43: 7-22.
- White, A.J.R. and Chappell, B.W. 1988. Some supracrustal (S-type) granites of the Lachlan Fold Belt. Transactions of the Royal Society of Edinburgh: Earth Sciences, 79: 169-181.
- Wickham, S.M. 1987. The segregation and emplacement of granitic magmas. J. Geol. Soc. London 144: 281-297.
- Wilson, M. 1989. Igneous Petrogenesis: A global tectonic approach. Unwin Hyman Ltd. London, 466 p.
- Windley, B.F. 1977. The Evolving continents. John Wiley & Sons, London, 399 p.
- Windley, B.F. 1981. Precambrian rocks in the light of the plate tectonic concept. In: Kroner, A (Editor) Precambrian Plate Tectonics. Elsevier Scientific Pub. pp. 1-20.
- Windley, B.F. 1983. A tectonic review of the Proterozoic. Geol. Soc. of America. Memoir 161: pp. 1-10.
- Windley, B.F. and Tarney, J. 1986. The structural evolution of the lower crust of orogenic belts, present and past. In: Dawson, J.B., Carswel, D.A, Hall, J and Wedepohl, K.H. (Editors). The Nature of the Lower Continental Crust, Geol. Soc. Lond. Spec. Publ. 24: 221- 230.
- Woolley, A.R. 1982. A discussion of carbonatite evolution and nomenclature and the generation of Sodic and Potassic fenites. Mineralogical Magazine, 46: 13-17.
- Woolley, A.R. 1989a. The Spacial and Temporal Distribution of Carbonatites, in: Bell, K.

#### References

---

- (Ed.) Carbonatites: genesis and evolution. Unwin Hyman Ltd., London, pp.15-37.
- Woolley, A.R. and Kempe, D.R.C. 1989b. Carbonatites: nomenclature, average chemical compositions and element distribution. In: Keith Bell (Editor), Carbonatites: genesis and evolution. Unwin Hyman Ltd. London, pp. 1-14.

## **APPENDICES**

---

A2

---

Table (A2.1 Appendix) Statistical Measurement of Dykes

Traverse	No. of dykes	Thickness in meters
A	1	5.10
	2	3.60
	3	8.00
	4	8.80
	5	19.80
	6	23.70
	7	1.70
	8	30.80
	9	6.50
	10	1.30
	11	1.00
	12	0.90
	13	4.50
	14	20.00
B	15	4.50
	16	14.30
	17	12.30
	18	8.60
	19	9.80
	20	2.00
	21	21.00
C	22	20.20
	23	8.00
	24	0.80
	25	9.80
	26	7.70
	27	5.50
	28	14.80
	29	5.20
	30	22.10
Total		302.30

Average thickness of dykes  $302.30/30 = 10.076666 = 10$  ms.  
Those tape measurements of dykes were carried at  
Wadi Taran (Lowder) along the three traverses A, B and C.  
When related to the length of the host rock section, the  
following results were obtained:

Traverse A loct.122:

Total thickness = 159.6 m

Dyke thickness = 117.7 m

% of dykes to the country rocks =  $117.7/159.6 \times 100$   
= 73.74686  
= 74.00 %

Traverse B loct.123:

Total thickness = 123.0 m

Dyke thickness = 72.5 m

% of dykes to the country rocks =  $72.5/123.0 \times 100$   
= 58.94308  
= 59.00 %

Traverses A+B:

T.T. =  $159.6+123.0 = 282.6$  m

D.T. =  $117.7+72.5 = 190.2$  m

% of dykes to C. rocks =  $190.2/282.6 \times 100$   
= 67.3036  
= 67.00 %

Traverse C loct.124:

T.T. = 124.00

D.T. = 94.10

% of dykes to C. rocks =  $94.10/124.00 \times 100$   
= 75.88709  
= 76.00 %

Average of % of dykes to country rocks =  $74+59+76/3=76\%$

Table (A2.2 Appendix) Classes and frequency of dykes

Class	Frequency	Fr. %
0-5	9	30
5-10	11	36.6
10-15	3	10
15-20	2	6.66
20-25	4	13.3
25-30	0	0
30-35	1	3.33
Total	30	100

Table A2.3 Appendix: K-Ar analytical data

SAMPLE	No.	Type	%K	Ar No.	Vol. Ar <sup>40</sup> RAD. cc STP/g x 10 <sup>-5</sup>	% Ar <sup>40</sup> RAD.	Age m.y.
Biotite	BY109	Granite host rock	7.29	4625	25.894	99.3	740 ± 22
Hornblende	BY104	Alkali granite	0.829	4626	3.4816	95.8	847 ± 26
Hornblende	BY116	NE-SW dyke	0.806	4627	2.7228	94.2	709 ± 2
Hornblende	BY119	E-W dyke	0.200	4628	0.5399	86.6	587 ± 1

Table A2.4 Appendix: K/Ar analysis for hornblende concentrate of alkali granite (Sample BY104)

BY 104 Hnb., run 1001, weight = 0.06649 gms. J value = 0.003900 +/- 1.0%

Temp	39K (	37Ca Vol. *10 <sup>-9</sup>	38Cl cc	Ca/K	*40/39K	%Atm 40	Age	Err
710	1.266	2.094	0.088	3.291	170.382	17.4	919.22	2.56
845	9.129	8.862	0.321	1.932	152.546	2.1	842.21	1.29
910	1.385	1.720	0.041	2.472	148.203	4.0	822.95	1.41
970	1.825	2.311	0.055	2.519	149.782	3.3	829.97	1.24
1060	1.442	3.567	0.050	4.921	147.503	6.7	819.82	1.42
1120	0.265	0.838	0.009	6.285	137.736	11.4	775.66	3.12
1285	0.025	0.114	0.001	9.004	109.907	80.8	643.56	200.75
1385	0.011	0.029	0.001	5.176	62.393	91.4	392.92	512.42

Integrated values, analytic & J errors (2 sigma)

Age (My) 841.70 1.37 13.52

\*40/39K 152.432 0.20 %

Wt %K = 0.844 , \*40 = 351.90 x 10<sup>-7</sup> cc/gm

BY116 Hnb., run 1082, weight =0.05777 gms. J value =0.006860 +/- 2.0 %  
 Atmos 40/36 =298.0 +/- 0.2 Sensitivity =1.850 \*10-7cc/volt.

Temp	39K	37Ca	38Cl	Ca/K	*40/39K	%Atm	Age	Err	%39
C	{	Vol. *10-9	cc	}		40	{	Ma	}
675	1.841	1.545	0.030	1.670	67.862	24.8	689.56	5.32	10.6
740	1.871	1.745	0.026	1.856	71.515	12.7	720.15	5.39	10.8
795	1.419	1.940	0.022	2.722	70.317	7.5	710.18	5.18	8.2
850	2.485	12.746	0.066	10.206	71.411	7.1	719.29	4.10	14.3
890	2.736	23.388	0.093	17.008	70.504	4.6	711.73	4.20	15.8
950	3.995	30.786	0.156	15.337	65.384	4.6	668.52	3.41	23.0
1030	1.621	15.116	0.067	18.555	62.180	8.4	640.93	4.47	9.3
1200	1.286	22.518	0.052	34.845	70.379	8.2	710.69	7.65	7.4
1345	0.096	1.365	0.002	28.379	55.930	46.0	585.87	61.80	0.6

Integrated values, analytic & J errors(2 sigma)

Age (Ma) 694.11 1.95 23.13  
 \*40/39K 68.401 0.34 %

Wt %K = 0.624, \*40 = 205.42 x 10-7 cc/gm

Table A2.5 Appendix: Analytical data for hornblende concentrates of NE-SW (old) dyke (sample BY116).

BY 119 Hnb., run 1083, weight = 0.05431 gms. J value = 0.006860 +/- 2.0 %  
 Atmos 40/36 = 298.0 +/- 0.2 Sensitivity = 1.850 \*10-7cc/volt.

Temp C	{ 39K Vol. *10-9 cc }	37Ca *10-9 cc	38Cl cc	Ca/K	*40/39K	%atm 40	{ Age Ma }	Err }	%39
700	0.614	2.254	0.010	7.312	48.489	60.0	518.06	24.55	12.1
750	0.417	0.998	0.001	4.762	57.051	27.1	595.87	12.46	8.2
800	0.202	0.794	0.003	7.839	52.677	25.7	556.54	18.57	4.0
865	0.461	6.703	0.011	28.939	54.080	16.7	569.25	15.48	9.1
920	1.262	35.585	0.062	56.118	58.939	11.7	612.59	6.37	24.8
960	0.657	17.425	0.035	52.779	59.547	14.1	617.94	8.21	12.9
1120	0.811	24.409	0.039	59.885	59.122	22.2	614.20	6.56	16.0
1340	0.659	17.564	0.034	53.041	51.204	23.6	543.10	13.21	13.0

Integrated values, analytic & J errors(2 sigma)

Age (Ma) 585.95 4.56 20.52  
 \*40/39K 55.938 0.91 %

Wt %K = 0.195, \*40 = 52.34 x 10-7 cc/gm

Fig. A2.6 Appendix: Analytical data for hornblende concentrates of E-W (Young) dyke (sample BY119).

Table A2.7 Sample Grid Reference, initiated for Lowder-Mudiah area, according to the standard British System. Relevent grid line numbers are marked on all the maps.

Sample No.	Rock Type	Grid Reference	Remarks
BY30C	Granite	710 134	Sc, Ch alteration
BY16N	Granite	428 153	Sc alteration
BY18A	Granite	605 130	
BY36C	Granite	612 139	
BY9A	Granite	805 125	
BY18C	Granite	605 130	
BY19A	Granite	45 14	
BY18B	Granite	605 130	
BY74	Granite	6000 1295	
BY91	Granite	1800 1635	Sc alteration
BY93	Granite	250 162	
BY106	Granite	6300 1284	
BY14A	Granite	750 119	
BY36D	Granite	612 139	Pegmatitic & Sc, Ch
BY37B	Granite	705 129	Pegmatitic
BY24E	Granite	4880 1435	Sc alteration
BY94	Granite	490 118	
BY104	Alkali Granite	370 119	Ch alteration
BY15E	Granitic Gneiss	6400 1282	Ch, Sc alteration
BY30A	Granitic Gneiss	7050 1335	
BY26N	Granitic Gneiss	482 1462	
BY21	Granitic Gneiss	5550 1385	Sc alteration
BY30B&D	Granitic Gneiss	7000 1348	Sc alteration
BY36B	Granitic Gneiss	612 139	
BY92	Granitic Gneiss	230 164	
BY16G	Granitic Gneiss	4250 1505	
BY26F	Granitic Gneiss	4820 1462	
BY24A	Amphibolite	4880 1442	Scp alteration
BY42F	Amphibolite	4450 1495	Scp alteration
BY16K1	Amphibolite	438 150	Scp alteration
BY16K2	Amphibolite	438 150	Scp alteration
BY2A	Meta-Rhyolite	7550 1407	Ch alteration
BY2B	Meta-Rhyolite	7550 1407	Ch alteration
BY3	Meta-Rhyolite	74 14	Porphyritic
BY7B	Meta-Rhyolite	8550 1275	Porphyritic
BY2C	Meta-Basalt	7550 1407	
BY2G	Meta-Basalt	7550 1407	Ep alteration
BY40B	Meta-Rhyolite	61 15	
BY85	Meta-Rhyolite	7520 1412	
BY86	Meta-Rhyolite	715 143	
BY87	Meta-Basalt	749 141	
BY70	Meta-Rhyolite	8480 1275	Porphyritic

BY8B1	Meta-Rhyolite	885 127	Porphyritic, & Gossan
BY34D1	Basaltic dyke	235 128	Early (NE-SW)
BY61	Basaltic dyke	229 127	Early (NE-SW)
BY62	Andesitic dyke	2210 1281	Early (NE-SW)
BY65	Basaltic dyke	235 129	Early (NE-SW)
BY66	Basaltic dyke	2400 1292	Early (NE-SW)
BY95	Basaltic dyke	202 126	Early (NE-SW)
BY97	Andesitic dyke	210 127	Early (NE-SW)
BY100	Basaltic dyke	2490 1299	Early (NE-SW)
BY101	Basaltic dyke	2200 1279	Early (NE-SW)
BY110	Basaltic dyke	Between	} Refer to Fig. 2.7
BY112	Basaltic dyke	170 132	
BY114	Basaltic dyke	and	
BY116	Basaltic-andesite dyke	200 135	
BY64	Rhyolitic dyke	2300 1285	Porphyritic
BY99	Rhyolitic dyke	250 130	Early (NE-SW)
BY102	Rhyolitic dyke	2190 1275	Early (NE-SW)
BY118	Rhyolitic dyke	170 132 & 200 135	Refer to Fig. 2.7
BY103	Rhyolitic dyke	2180 1272	Late (E-W)
BY119	Rhyolitic dyke	170 132 & 200 135	Late (E-W) Refer to Fig.2.7
BY96	Basaltic dyke	2100 1265	Late (E-W)
BY105	basaltic dyke	380 118	Late (E-W)
BY111	Gabbro	Between	} Refer to Fig. 2.7
BY113	Diorite	170 132	
BY115	Qz-Diorite	and	
BY117	Qz-Diorite	200 135	
BY63	Granite	2250 1282	
BY98	Rhyolitic dyke	2500 1305	Late (E-W)
BY35A1	Limestone	345 163	
BY35A2	Limestone	345 163	
BY35A4	Limestone	345 163	
BY1	Marble	760 141	
BY6	Marble	8100 1452	
BY26A	Carbonatite	4820 1462	
BY26C	Carbonatite	4820 1462	
BY26D1	Carbonatite	4820 1462	
BY26D2	Carbonatite	4820 1462	
BY25B	? Carbonatite	4800 1452	?=mineralized marble
BY25C	Carbonatite	4800 1452	
BY25D	Carbonatite	4800 1452	
BY25E	Carbonatite	4800 1452	
BY25A	Carbonatite	4800 1452	
BY26E	Carbonatite	4820 1462	

BY11	Carbonatite	485 146	
BY16J1	? Carbonatite	4200 1528	
BY16J2	? Carbonatite	4200 1528	
BY42D1	Carbonatite	47 15	
BY42D4	? Carbonatite	47 15	
BY42G1	? Carbonatite	4920 1507	
BY44	? Carbonatite	155 159	} From one dyke
BY45	? Carbonatite	155 159	
BY46	? Carbonatite	155 159	
BY47A	Carbonatite	1580 1592	
BY48	? Carbonatite	1550 1583	
BY49	? Carbonatite	1600 1585	
MKY4	Carbonatite	4820 1455	
MKY6	Carbonatite	4800 1448	
BY89A	Carbonatite	4820 1455	} From one dyke
BY89D	Carbonatite	4820 1455	
BY89E	Carbonatite	4820 1455	
BY90A	Carbonatite	4920 1455	} From one dyke
BY90B	Carbonatite	4920 1455	
BY90C	Carbonatite	4920 1455	
BY32	Meta-basalt	7490 1415	
BY32A - N	Meta-rhyolite	740 141	
BY32O	Meta-rhyolite	725 140	
BY30P	Qz-vein	7200 1395	
BY52	Meta-basalt	7520 1408	
BY85	Meta-rhyolite	7520 1412	
BY86A - B	Meta-rhyolite	715 143	
BY87	Meta-basalt	749 141	
BY88	Meta-rhyolite	7350 1405	
BY42A	Granitic Gneiss	5650 1535	
BY42B - C	Granitic Gneiss	5300 1503	
BY42G	Carbonatite	4920 1507	
BY42D	Carbonatite	47 15	
BY42E	Granitic Gneiss	47 15	
BY42F	Amphibolite	4450 1495	
BY68	Granitic Gneiss	535 152	
BY39	Granitic Gneiss	5220 1455	
BY56A	Granitic Gneiss	5050 1452	
BY56B	Granitic Gneiss	4880 1445	
BY17A - N	Qz-biot-hornb Gneiss	4970 1445	
BY84A - B	Qz-biot-hornb Gneiss	4950 1442	
BY24A,B,C,D,F	Amphibolite	4880 1442	
BY24E	Granite	4880 1435	
BY90	Carbonatite	4920 1453	
BY89	Carbonatite	4820 1455	

BY25A - E	Carbonatite	4800 1452	
BY26A - E,G,H,K,L	Carbonatite	4820 1462	
BY26I	Amphibolite	4820 1462	
BY26F,J,M,N	Granitic Gneiss	4820 1462	
BY57A	Granitic Gneiss	405 151	
BY57B,C,D	Granitic Gneiss	4350 1498	
BY16A - I	Granitic Gneiss	4250 1505	
By16J,M	Carbonatite	4200 1528	
BY16K	Amphibolite	438 150	
BY16N	Granite	428 153	
BY35A	Jurassic Limestone	345 163	
BY35B	Jurassic Limestone	348 162	
BY35C	Jurassic Limestone	3470 1625	
BY92	Granitic Gneiss	230 164	
BY93	Granite	250 162	
BY91	Granite	1800 1635	
BY29	Granitic Gneiss	202 162	
BY28	Granitic Gneiss	135 152	
BY60	Qz-biot Gneiss	1750 1458	
BY27	Qz-biot Gneiss	175 145	
BY67A	Garnet-qz-bio Schist	178 143	
BY67B	Garnet-qz-biot Schist	1800 1435	
BY82	Garnet-qz-biot Schist	51 11	
BY77	Granite	480 119	
BY78	Amphibolite	520 116	
BY14B	Granitic Gneiss	805 118	
BY14C	Granitic Gneiss	820 119	
BY58A - I	Rhyolitic dyke	2310 1275	
BY59	Rhyolitic dyke	2300 1272	
BY33	Granite	4050 1299	
BY31	Granitic Gneiss	3200 1335	
BY69A,B	Qz-biot-horn Gneiss	4600 1235	
BY75	Granitic Gneiss.	4550 1255	
BY80A - D	Granite	4950 1260	
BY19B - D	Granitic Gneiss	47 14	
BY71	Granite	5150 1283	
BY72	Granite	5300 1265	
BY73	Granite	5350 1255	
BY81	Granite	5450 1245	
BY83A - D	Granitic Gneiss	595 130	
BY79A	Granitic Gneiss	6500 1245	
BY79B	Granite	6450 1236	
BY76	Granitic Gneiss	6850 1284	
BY37A	Granitic Gneiss	7050 1282	
BY54	Granitic Gneiss	6900 1252	

BY15D	Granitic Gneiss	6950 1250	
BY51	Granitic Gneiss	75 13	
BY38	Granitic Gneiss	7580 1295	
BY20	Basalt	758 127	
BY15A - C	Granitic Gneiss	7580 1215	
BY13	Granitic Gneiss	8100 1237	
BY50A - D	Granitic Gneiss	8150 1242	
BY10	Granitic Gneiss	8220 1245	
BY36A,B	Granitic Gneiss	612 139	
BY36C,D	Granite	612 139	
BY36E	Qz-biot-hornb Gneiss	612 139	
BY55	Granitic Gneiss	6350 1398	
BY41	Granitic Gneiss	6850 1399	
BY41A - F	Granitic Gneiss	670 142	
BY40A - B	Granitic Gneiss	61 15	
BY17O - X	Meta-rhyolite	6400 1512	
BY23A	Meta-rhyolite	7750 1365	
BY23B	Meta-rhyolite	7900 1345	
BY23C	Meta-rhyolite	8000 1335	
BY22	Basalt	8300 1335	
BY1	Marble	760 141	
BY2D - F	Basaltic-andesite	7550 1407	
BY2A,B	Meta-rhyolite	7550 1407	
BY2C,G	Meta-basalt	7550 1407	
BY3	Meta-rhyolite	74 14	
BY4	Basalt	780 142	
BY5	Meta-rhyolite	8050 1448	
BY6	Marble	8100 1452	
BY53	Meta-basalt	825 145	
BY43A	Meta-rhyolite	750 144	
BY43B	Meta-basalt	7900 1462	
BY43C	Meta-rhyolite	8000 1477	

Table A2.8 Locality Grid Reference, initiated for the Lowder-Mudiah area, according to the standard British System. The relevent grid line numbers are marked on all the maps.

Locality	Grid Reference
Lowder town	35 13
Mudiah town	77 122
Mukeras Escarpment	20 125
Thereh	17 134
W. Taran	24 129
W. Mekhbezeh	38 12
Um Sallamiah	50 146
Al-Arakbi	42 15
Durib	19 158
Al-Gashaber	70 127
Um Ain	41 146
Al-Majil	19 144
Zarah	33 133
J. Yusuf	41 13
J. Khuruf	45 14
Al-batan	66 146
Al-Guriah	75 137
J. Al-Mugut	70 134
Um Madarah	78 132
Al-Waznah	81 129
Uramah	85 125
W. Maran	79 116
W. Kabran	66 12
J. Khamaah	595 123
W. Barrani	52 124
Al-Hafah	52 129
Um Najdah	46 127
Um Shaah	44 122
J. Um Hamra	49 119
Um Jarubah	485 115
Asswedah	605 131
Um Glaitah	97 126
Um Goaz	86 13
Wadi Azzan	5 13
Um Humayshah	4 167

**A3**

---

### A3 SAMPLE PREPARATION

#### 1) Rock Crushing

The first step in this process is to make sure the crushing room and all equipment is thoroughly cleaned.

Start by removing any weathered crust on the rock sample by using either the hand splitter or the hydraulic splitter. Both splitters are located in the Bulk Store. The unweathered remainder can then be split up into cubic lumps of 2-3cm. At least 1000 times the grain size is a general guide to the amount that is required for representative samples.

This "cubed" material can then be placed in the flypress pan and reduced to a gravel with a grain size no greater than 2-3mm. Try to confine crushing to the hardened steel disc in the centre of the flypressing pan. A fraction of this material may then be put in the grinding mill to be used. There are several types of grinding mill to choose from, each with its own advantages and disadvantages. On the choice of tema, consultation with NGM is advisable. However, for most general geochemical work the Agate tema is used as this does not produce any appreciable contamination, except for SiO<sub>2</sub> and perhaps a little Pb. For other purposes eg Pb isotope work, one of the other grinding mills may have to be used.

Not less than 50cc of sample should be used in the tema, and a plastic beaker marked with the minimum, optimum and maximum volumes for the grinding mills is available. The material should be spread evenly between the barrel, ring and block. Any loose material on top of the barrel, ring and block should be brushed down as failure to do so may result in damage to the lid. The seal should be properly fitted or loss of sample during grinding will occur. Place the lid on the mill and check the "O" ring seal is fitted correctly.

The grinding mill is then clamped securely into its correct motor drive unit and switched on. The length of time necessary for this grinding depends on the type of rock and the grinding mill being used, but the powder should not feel gritty when the process is finished.

Empty the powder onto a clean sheet of computer paper and then tip onto a plastic bag. A 1-2 cm cut off paintbrush is useful for cleaning out the powder. The coarse crush should also be retained in a larger plastic bag. All the equipment used, especially the tema and flypress should be cleaned thoroughly between each sample and after use, to avoid contamination, using dampened tissue and then dried with dry tissue. Stubborn material, eg clays from altered basalts can be removed with some silver sand for 4-5 minutes - there is usually a sack of this in the crushing room.

If you have not used the crushing room before ask for a

demonstration first from either Nick Marsh, Rob Kelly or Adelaide Holmes. If you consistently damage the facilities or endanger other workers through abusing the equipment you will be banned from using it (regardless of the consequences to any research you may wish to do !!) and charged for any repairs and/or replacements that are necessary.

#### GRINDING MILLS AVAILABLE

Grinding mills cost approx. £1700 - most of your grant if you break one!

Podmore Agate

For general geochemical use

(silver case)

XRF Trace and Major elements

(low speed motor unit)

REE separations for ICP work

Nd isotope work and most Rb and Sr

O and C isotope work on carbonates (where CO<sub>2</sub> is released by H<sub>3</sub>PO<sub>4</sub>)

Crushing time  
8-15 mins

Contamination - Si, O plus possibly very minor Pb (suspected but unproven)

Si:- High levels in most geological material, so negligible effect unless dealing with hard, SiO<sub>2</sub> poor (<5% ) material

O:- Most rock forming minerals can be assumed to consist of an oxygen lattice, so there is a negligible effect except for some oxygen isotope work, the only instance when oxygen itself is actually analysed.

DO NOT USE FOR:-

O isotope work on silicates

Pb isotope work (?)

Phosphate rocks

Sulphides and other ore minerals

Heavily mineralised samples

Tema Agate  
 (green case)  
 (low speed  
 motor unit)  
 Crushing time  
 8-15 mins

Can be used for sulphides, ore minerals, phosphate rocks, and anything else which may contaminate the grinding mill. This is an older mill which has already suffered from serious abuse and has had to be pensioned off from routine work. It will give slightly more contamination of SiO<sub>2</sub> etc than the Podmore barrel due to the damaged annulus.

Podmore WC  
 (tungsten carbide)  
 (high speed  
 motor unit)  
 Crushing time  
 1-2 minutes total  
 in 20 second  
 runs with 40  
 second breaks  
 between runs  
 to allow  
 heat to  
 dissipate

For:-(1) Pb, O, S isotope work  
 on silicates  
 :-(2) marginally preferred for  
 Rb & Sr isotope work  
 :-(3) samples with higher than  
 trace amounts of very hard  
 minerals eg perovskite, sphene,  
 diamond and some garnets

Contamination:-  
 W, C, Co, Ta, Nb, HREE?  
 DO NOT USE FOR:-  
 Nd isotope work  
 W, C, Co, Ta, or Nb  
 Probably best to avoid if  
 high accuracy REE determinations  
 are required  
 For organic carbon analyses or  
 C isotopes

Also available are Cr steel and Ni steel grinding mills. Their use, in general, is not advised unless Fe, Cr, V, Ni, Mn and C contamination is acceptable. These mills are all used with the high speed motor unit.

## 2) Powder Pellets

Having obtained a rock powder the next process for XRF analysis is making a pressed powder pellet. The equipment used for this process is in the XRF lab.

Weigh approx. 15g of powder into a small beaker, add to this enough Mowiol 88 solution (this is a solution of polyvinyl alcohol in a 1:5 mix of methanol and distilled deionised H<sub>2</sub>O) to bind the powder together in small lumps, but not so much that the powder looks wet when thoroughly mixed. The amount required depends on the rock type and the abundance of clay minerals, but usually varies from about 15-20 drops. This mixture is then placed in the die, the surface smoothed, and then the top of the die and the plunger are then replaced. The complete die is then placed in the hydraulic press, the valve closed and pumped up to 15 tons on the red scale. The valve should then be opened slightly so that the pressure falls gently to avoid breaking the pellet. When no longer under pressure the die is removed, inverted and replaced on the ram with the aluminium ring in place of the bottom section, and pumped up until the pellet is above the barrel section of the die. The pellet is given a Leicester number which is written in the pellet log book. The pellet is placed on the rack to dry. All the equipment must be thoroughly cleaned between samples, and after use, with damp tissue and then thoroughly dried with dry tissue, to avoid contamination.

When the pellet is dry ie the next day the Leicester pellet number should be written in the side, and it should be placed in a polythene bag giving the sample number, the Leicester pellet number and the name of the person submitting this for analysis. Suites of samples should be put in a cardboard pellet box. There are two sizes depending on the number of samples. The smaller size takes approx. 20-25 and the larger 45-50 samples. Try and ensure that the pellets are put in numerical pellet number order. Put your name and the lowest and highest pellet number on the lid and one end of the box and place it on the racks. Then fill out a card for the XRF booking rack - one card per analysis program per 50 pellets.

### 3) Fusion Beads

Fusion beads are the best way of determining major element concentrations in rocks by XRF. All the equipment for their preparation is located in the Pure Geochemistry Lab.

For this stage of the sample preparation about 4 to 5 grams of the sample powder are put into a 10 ml glass vial. N.B. The vials should be labelled using a felt tip marker pen with your initials and some unambiguous sample name or number e.g. their Leicester pellet number. This rock powder is then dried overnight in a drying oven at 110°C to remove surface water. These powders are then stored in a dessicator. Plastic snap tops should be put on the vials once they have cooled to room temperature to avoid sample loss through spillage and cross contamination.

The next step is to determine the weight loss on ignition. This is generally performed in Pd/Au or Pt crucibles. The weight of the crucible (W1) and the weights of the crucible plus sample before (W2) and after ignition (W3) are recorded in order to determine the weight loss. The ignitions are normally performed in the larger of the two muffle furnaces at 950°C for 1 to 1.5 hours. After ignition the samples are allowed to cool down to room temperature in a dessicator before reweighing. After reweighing the ignited powders can then be transferred to clean 10 ml glass vials with plastic snap tops for storage in a dessicator prior to preparing fusion beads. N.B. Remember to label these vials as described above.

The percentage weight loss (LOI) can then be determined from the following simple formula :-

$$\text{LOI} = 100 * (\text{W2} - \text{W3}) / (\text{W2} - \text{W1})$$

For some rocks e.g. magnesian carbonatites a higher temperature (ca. 1000°C - 1100°C) and a longer time may be required to remove all the CO<sub>2</sub> or other volatiles present. For other rocks, notably peralkaline basalts and their more evolved brethren, a lower temperature must be used to avoid fusing the rock sample, temperatures of around 700°C to 750°C and ignition times of 3 to 4 hours are often required although in extreme cases temperatures as low as 500°C are needed. The details given here for carbonatites and alkaline igneous rocks are only guidelines; experience has shown that each suite of these rock types have to be experimented with to find viable conditions for complete ignition and sample oxidation. Another problem to be aware of with carbonate rich samples is that the partial pressure of CO<sub>2</sub> in the furnace can rise sufficiently high to effectively buffer further breakdown of carbonates. To prevent this it is worth opening the furnace door for two to three minutes every 20 minutes or so and restricting the number of carbonate rich samples in the furnace to a maximum of six samples at any one time. Great care must always be taken with the ultra-alkaline rocks to avoid alkali

loss (particularly Na) during any high temperature sample preparation techniques; in some cases alkali loss may be unavoidable with these rock types and alternative analytical strategies will have to be developed to deal with them.

Before making fusion beads it is advisable to dry the flux, a eutectic mixture of lithium metaborate and lithium tetraborate (Johnson - Mathey Spectroflux JM100B or Englehard XRF Fusion Flux(Standard Grade)), overnight at 500°C to remove any absorbed water or other volatiles taken up from the atmosphere. The dried flux should always be stored in a dessicator and it is advisable to only work with it for two days before redrying as it will absorb water and possibly CO<sub>2</sub> from the air during weighing out.

On starting to make a batch of fusion beads and initially on each day a flux weight loss determination should be made. Approximately 2 - 4 grams of previously dried flux is accurately weighed into a Pt/5% Au crucible and placed in one of the vertical tube furnaces for 15 minutes. It is then taken out and stood on a piece of furnace brick in a dessicator and allowed to cool to room temperature (this takes approximately 25-30 minutes). When cooled the crucible and flux are reweighed and the weight loss determined. The normal range of weight losses is 0.1-0.3 weight percent.

Then a sample may be prepared as follows. 5g plus the previously determined weight loss of dried flux is accurately weighed into a Pt/Au crucible. Then 1g of the ignited sample is weighed on top of the flux. These are then thoroughly mixed together. Then the crucible and its contents is placed in the vertical tube furnace. For carbonatites read the saga in the next section. N.B. The flux used for the weight loss determination can be used for the first sample to avoid wastage!

At various times during the fusion process the liquid must be agitated in order to remove particles of powder stuck to the crucible sides and to remove bubbles from the liquid. This may be done by a rolling or swirling motion of the crucible held in the Pt tipped tongs. To facilitate good mixing the crucible can be kept warm by swirling over the meker burner on the window bench. While the rock is fusing it is a good idea to put two holders onto the die hotplate to bring them up to the same temperature as the dies.

When the liquid is satisfactorily homogenised and there are no particles left on the side or base of the crucible, the fusion must be brought to 1250 C in the furnace. When it reaches this temperature, the crucible is removed from the furnace using the Pt tipped tongs, held back to front for ease of pouring. The contents are poured onto the die and stamped into a disc, aiming to pour the liquid in the middle of the die. The resulting disc is left for a few seconds in the press and then the bottom die can be removed with the bead and inverted over a holder. The complete holder is put on another hotplate at 300 C to allow the glass beads to anneal for at least 3 hours. It is a good policy to put a sticky label on the top of the holder to identify the rock sample. The remnants of the fusion adhering to the crucible must then be carefully removed from the crucible; it is worth keeping this with the bead in case the bead breaks as there should then be sufficient to recast the bead which saves having to weigh out the flux and sample again. To clean the crucible completely it should be simmered in a weak nitric acid solution for about 20 minutes. After 3 hours the beads in the holder may be taken off the hotplate and put to cool. When cool an adhesive label with the sample number must be

stuck to the back face of the bead and the bead can then be stored in a resealable polythene bag.

Table A3.1: Accepted values for international and internal standards

	BOB-1*	MRG-1	NIM-G	BEN	TYG*	GH	UB-69*	BR	GA
Nb	4.7	20	53	100	12.6	85	2.5	98	12
Zr	100	108	300	265	198	150	62	250	150
Y	26	14	143	30	46	75	21	30	21
Sr	190	266	10	1370	65	10	266	1320	310
Rb	6	8.5	320	47	67	390	81	47	175
Th	1.4	0.9	51	11	16.8	87	7	11	17
Ga	16	17	27	17	15	23	16	19	16
Zn	63	191	50	120	70	85	180	160	80
Ni	115	193	8	267	4	3	18	260	7
Cr	304	430	12	360	8	6	25	380	12
V	234	526	2	235	15	5	198	235	38
Ba	44	61	120	1025	416	20	950	1050	840
La	5.6	9.8	109	82	31	25	13	82	40
Ce	14.7	26	195	152	65	60	26	151	76
Nd	10.9	19.2	72	70	28	29	14	65	27

\* denotes an internal standard adopted by Leicester

This appendix contains tables showing the accepted values for elemental abundances in international standards (from Govindaraja, 1989), internal standards used at Leicester, and values obtained for both by XRF.

All trace element abundances are given in ppm.

The XRF results quoted in Table A3.2 are taken from four rhodium tube runs (RHT) and four tungsten tube runs (WT) taken at random from runs where the Lowder-Mudiah, Yemen, samples were included.

Table A3.2: Comparison of XRF results for international and internal standards

Accepted values for standards BOB-1 etc given in Table A3.1.  
 RHT denotes rhodium tube, WT denotes tungsten tube on XRF spectrometer.  
 The number following RHT/WT indicates the Leicester XRF run number

	BOB-1				Average	St. Dev.
	RHT380	RHT383	RHT410	RHT384		
Nb	4.9	4.7	5.1	5.4	5.03	0.30
Zr	104	104.1	101.2	102.7	103.00	1.36
Y	27.3	27.4	27	26.6	27.08	0.36
Sr	192.1	192.2	196.1	191.7	193.03	2.06
Rb	6.1	7.8	7	8.4	7.33	1.00
Th	0.6	0.7	2.9	1	1.30	1.08
Ga	12.9	17.4	16.9	17.4	16.15	2.18
Zn	67.8	64.6	65.8	64	65.55	1.68
Ni	106.8	108.2	105	104.6	106.15	1.67
	WT307	WT306	WT285	WT315		
Cr	270.1	273.6	303.7	280.7	282.03	15.11
V	218.8	224.8	232.7	217.5	223.45	6.94
Ba	39.6	36.8	37.2	37.6	37.80	1.24
La	3.8	6.4	6.9	5.8	5.73	1.36
Ce	14.1	14.6	12.7	14.5	13.98	0.88
Nd	11.4	12	9.1	11.6	11.03	1.31

	MRG-1				Average	St. Dev.
	RHT380	RHT383	RHT410	RHT384		
Nb	20.2	19.8	19.8	20.3	20.03	0.26
Zr	108.6	107.5	109.8	107.8	108.43	1.03
Y	14	14.6	13.5	14.1	14.05	0.45
Sr	273.2	276	277.4	271.8	274.60	2.56
Rb	12.5	5.9	8	7.4	8.45	2.84
Th	2.3	0	0	1.6	0.98	1.16
Ga	21.2	21.8	22.8	22.2	22.00	0.67
Zn	229	221.6	229.3	227.9	226.95	3.62
Ni	201.1	199.2	200.3	204.3	201.23	2.19
	WT307	WT306	WT285	WT315		
Cr	519.4	453	413.7	489.4	468.88	45.72
V	556.6	514.3	502.7	538.1	527.93	24.14
Ba	53.7	52.7	57.8	57.5	55.43	2.60
La	7.6	7.1	7.9	9	7.90	0.80
Ce	20.8	29.8	27.7	27.6	26.48	3.92
Nd	16.2	18.5	20.5	17.7	18.23	1.79

	NIM-G				Average	St. Dev.
	RHT380	RHT383	RHT410	RHT384		
Nb	55.8	56.3	56	55.3	55.85	0.42
Zr	303.3	303	297.1	302.8	301.55	2.97
Y	148.7	140.8	142.1	143.3	143.73	3.47
Sr	11.9	11.6	12.3	11	11.70	0.55
Rb	317.8	320.1	330	321.3	322.30	5.33
Th	51.7	50.7	53.6	49.5	51.38	1.73
Ga	29	29.5	29.1	30.4	29.50	0.64
Zn	51	52.5	52.2	50.7	51.60	0.88
Ni	6.9	6	5.7	5.8	6.10	0.55
	WT307	WT306	WT285	WT315		
Cr	14.8	17.4	14.7	18.9	16.45	2.06
V	1.2	0	0	0.6	0.45	0.57
Ba	116.9	112.8	115.8	117.5	115.75	2.09
La	105	102.8	101.7	104.6	103.53	1.55
Ce	201.7	197.4	204.2	198.3	200.40	3.14
Nd	75.7	74.3	76.5	75.4	75.48	0.91

Table A3.2: Comparison of XRF results for international and internal standards

RHT denotes rhodium tube, WT denotes tungsten tube on XRF spectrometer.  
The number following RHT/WT indicates the Leicester XRF run number

BEN					Average	St. Dev.
	RHT380	RHT383	RHT410	RHT384		
Nb	108.1	110.9	106.5	107.4	108.23	1.90
Zr	265.8	270.4	267.3	265.8	267.33	2.17
Y	30.8	29.7	30.9	29.8	30.30	0.64
Sr	1401.8	1397.5	1396.5	1388	1395.95	5.78
Rb	50.8	50.9	51.6	48.2	50.38	1.49
Th	12.8	12	11.4	12.7	12.23	0.66
Ga	19.7	18.6	20.3	20.6	19.80	0.88
Zn	142.1	142.3	123.1	141.7	137.30	9.47
Ni	285.1	285.6	278.5	285.4	283.65	3.44
WT307 WT306 WT285 WT315						
Cr	369	364.5	384.1	377.3	373.73	8.71
V	262	266.1	246.4	251.7	256.55	9.08
Ba	1096.4	1063.1	1098.5	1100.1	1089.53	17.68
La	81.1	81	80.7	80.5	80.83	0.28
Ce	154.6	155	153.9	151.6	153.78	1.52
Nd	67.9	69.1	65.6	70	68.15	1.91
TYG					Average	St. Dev.
	RHT380	RHT383	RHT410	RHT384		
Nb	12.7	12.3	13.1	12.5	12.65	0.34
Zr	215.5	216.3	212.1	219.6	215.88	3.08
Y	46.7	46.6	48.6	47.7	47.40	0.94
Sr	65.3	66.2	64.9	66.8	65.80	0.86
Rb	68.6	67.2	69.1	68.8	68.43	0.84
Th	17.1	18.7	15.7	17.4	17.23	1.23
Ga	15.2	15.3	14.8	16.8	15.53	0.88
Zn	77.7	83.5	73.4	77.1	77.93	4.17
Ni	3	3.5	3.1	3.4	3.25	0.24
WT307 WT306 WT285 WT315						
Cr	0.9	2.6	1.6	2.3	1.85	0.76
V	14.3	15.8	14.1	13.8	14.50	0.89
Ba	406.4	401	412.9	413.4	408.43	5.89
La	33.2	33.9	31.4	32.6	32.78	1.06
Ce	67.7	66.7	68.7	67.7	67.70	0.82
Nd	30.3	30.6	31.1	31.4	30.85	0.49
GH					Average	St. Dev.
	RHT380	RHT383	RHT410	RHT384		
Nb	89.3	90.1	88.3	89.8	89.38	0.79
Zr	154.6	152.5	150.8	155.7	153.40	2.18
Y	86.4	84.4	86.4	87.2	86.10	1.19
Sr	9.4	9.8	10.7	10	9.98	0.54
Rb	387.4	383.9	396.8	385.4	388.38	5.80
Th	71.4	76.5	70.2	71.3	72.35	2.82
Ga	24.6	23.2	23	24.1	23.73	0.75
Zn	59.8	62.6	74.2	62.5	64.78	6.42
Ni	9	9.9	8.1	10.8	9.45	1.16
WT307 WT306 WT285 WT315						
Cr	9.2	9.1	8.2	8.5	8.75	0.48
V	2.4	1.1	0	0.8	1.08	1.00
Ba	22.9	24	23.2	25.4	23.88	1.12
La	22.4	22.2	18.1	21.4	21.03	2.00
Ce	51.7	51.7	48.5	51.2	50.78	1.53
Nd	27	27.2	25.8	27	26.75	0.64

Table A3.2: Comparison of XRF results for international and internal standards

RHT denotes rhodium tube, WT denotes tungsten tube on XRF spectrometer.  
The number following RHT/WT indicates the Leicester XRF run number

UB-69					Average	St. Dev.
	RHT380	RHT383	RHT410	RHT384		
Nb	1.5	3.6	2.5	2.6	2.55	0.86
Zr	58.4	60.8	59.2	58.8	59.30	1.05
Y	21.9	22.1	21.6	21.2	21.70	0.39
Sr	271.2	269.8	273	268.9	270.73	1.79
Rb	80.7	79.8	83.8	82.4	81.68	1.78
Th	6.7	8.4	9.9	8.8	8.45	1.33
Ca	18.4	18.5	16.1	19.5	18.13	1.44
Zn	182.3	198.3	175.3	182.4	184.58	9.73
Ni	13.1	10	8.7	10.1	10.48	1.86
WT307 WT306 WT285 WT315						
Cr	11.7	14	21.2	17.2	16.03	4.12
V	186.8	190.9	196.3	190.4	191.10	3.92
Ba	943.4	933	973.7	955.2	951.33	17.46
La	16.9	16.3	17.2	14.5	16.23	1.21
Ce	28	28.3	21.3	29.7	26.83	3.76
Nd	14.3	14.6	13.2	14.4	14.13	0.63

BR				Average	St. Dev.	
	RHT380	RHT383	RHT410	RHT384		
Nb	106.7	104.7	105.9	107.8	106.28	1.31
Zr	267.5	263.8	268.4	266.1	266.45	2.00
Y	29.9	31.4	28.5	28.9	29.68	1.29
Sr	1372.2	1370.2	1371.2	1389.4	1375.75	9.14
Rb	50.7	47.3	49.1	54	50.28	2.85
Th	7.4	10.7	9.8	11.4	9.83	1.74
Ca	20.9	20.4	19	22	20.58	1.24
Zn	166.3	172	162.7	167	167.00	3.83
Ni	282.4	284.1	279.1	287	283.15	3.30
WT307 WT306 WT285 WT315						
Cr	362.2	359	377.2	364.4	365.70	7.98
V	266.9	257	254.6	251.1	257.40	6.78
Ba	1171.7	1142.2	1193.5	1174.1	1170.38	21.17
La	81.6	80.1	83.4	81.8	81.73	1.35
Ce	153.2	154.1	144.9	153.4	151.40	4.35
Nd	66.5	67.4	66.9	68.1	67.23	0.69

GA				Average	St. Dev.	
	RHT380	RHT383	RHT410	RHT384		
Nb	12.9	11.3	12.2	12.5	12.23	0.68
Zr	139.6	135.9	135.5	139	137.50	2.10
Y	24.3	23.7	23.7	23.4	23.78	0.38
Sr	296.3	295.1	295.6	295	295.50	0.59
Rb	168.8	169.4	176.9	171.1	171.55	3.70
Th	15.5	13.8	16.6	17.9	15.95	1.74
Ca	17.3	16.5	16	18.6	17.10	1.13
Zn	73.8	71.2	71.7	71.9	72.15	1.14
Ni	6.2	5	4.3	4	4.88	0.98
WT307 WT306 WT285 WT315						
Cr	23.4	25.3	26.6	25.3	25.15	1.32
V	39	41	38.5	38.3	39.20	1.24
Ba	839.7	836.2	857.6	851.8	846.33	10.06
La	33.4	34.6	29.3	33.2	32.63	2.30
Ce	59.7	61.1	61.3	60.3	60.60	0.74
Nd	23.6	24	23.9	23.5	23.75	0.24

Table A3.3 Reference data for Central Hijaz granitoid rock associations (After, Jackson et al., 1984).

Average chemical data for central Hijaz granitoid rock associations

	Younger assemblage						Older assemblage			
	Alkali granite association		Alkali-feldspar granite association		Monzogranite association		Trondhjemite association		Granodiorite association	
	$\bar{x}$ (n=14)	(s)	$\bar{x}$ (n=29)	(s)	$\bar{x}$ (n=17)	(s)	$\bar{x}$ (n=7)	(s)	$\bar{x}$ (n=11)	(s)
SiO <sub>2</sub>	74.04%	0.64	75.31%	1.32	72.64%	1.28	71.72%	3.53	68.03%	1.17
Al <sub>2</sub> O <sub>3</sub>	11.40	0.47	13.04	1.66	14.14	0.39	15.27	1.10	15.36	0.46
Fe <sub>2</sub> O <sub>3</sub>	3.48	0.66	1.15	0.53	1.44	0.44	1.50	0.84	1.69	0.73
FeO	0.50	0.14	0.45	0.21	0.79	0.34	0.83	0.31	1.75	0.66
MgO	0.02	0.04	0.08	0.09	0.45	0.15	0.50	0.33	1.19	0.36
CaO	0.43	0.11	0.63	0.28	1.63	0.36	2.57	0.97	2.96	0.67
Na <sub>2</sub> O	4.11	0.52	4.13	0.39	3.99	0.37	5.19	0.90	4.26	0.45
K <sub>2</sub> O	4.54	0.24	4.49	0.44	3.90	0.60	1.49	0.50	3.07	0.54
TiO <sub>2</sub>	0.28	0.03	0.15	0.06	0.34	0.10	0.34	0.21	0.62	0.20
P <sub>2</sub> O <sub>5</sub>	0.05	0.18	0.04	0.02	0.96	0.03	0.08	0.05	0.16	0.04
MnO	0.10	0.03	0.05	0.02	0.05	0.01	0.05	0.02	0.08	0.23
LOI	0.61	0.31	0.50	0.36	0.53	0.33	0.74		0.67	
Total	99.56		100.09		100.00		100.30		100.00	
Ba	237 ppm	207	253 ppm	182	648 ppm	188	389 ppm	87	609 ppm	255
Be	4	2	2	3	1	1	<1	-	<1	-
Ce	168	69	71	48	50	11	23	4	48	16
Co	4	0.30	5	1	6	3	9	2	13	3
Cu	10	2	7	3	10	6	9	5	14	4
F	627	316	834	661	673	237	363	74	682	289
La	71	40	36	25	28	6	13	3	24	8
Li	22	9	26	22	30	13	11	7	21	11
Nb	63	32	37	22	24	16	11	1	24	11
Rb	111	18	146	59	114	20	28	6	95	14
Sc	3	0.70	4	1	5	1	5	1	9	4
Sn	17	6	18	14	7	3	-	-	-	-
Sr	24	15	65	70	239	93	378	72	308	127
Ta	2	3	0	0	14	20	-	-	-	-
Th	14	4	22	7	10	3	-	-	-	-
U	4	1.4	5.8	2.3	2.2	0.3	-	-	-	-
V	9	3	8	4	21	7	14	10	47	19
Y	80	41	39	22	24	13	11	3	27	13
Zn	148	51	80	126	8	8	35	12	59	20
Zr	823	326	231	178	190	62	105	93	250	84
Fe <sub>2</sub> O <sub>3</sub> /FeO	7		2.56		1.82		1.81		0.97	
K <sub>2</sub> O/Na <sub>2</sub> O	1.10		1.09		0.98		0.29		0.72	
K/Rb	322		242		272		419		255	
Th/U	3.50		3.80		4.60		-		-	

$\bar{x}$  = mean; n = number of samples; s = standard deviation (n = 1)

Table A3.4 a - d Reference data for Central Hijaz Arabian Shield volcanics (After, Roobol et al., 1983).

TABLE A. Averaged compositions of lavas from the Bidah, Shayban, Aqiq and Ishmas suites (including some data from Jackaman 1972)

Rock type	Bidah suite				Shayban suite				Aqiq suite		Ishmas suite		
	B	BA	A	R	B	BA	A	R	B	R	A	D	R
	3	4	2	1	1	2	1	3	4	4	2	1	2
Pheno-crysts	No data	40% sauss fsp; aug.; pseud.	40% seric Ksp; qtz.	10% turbid fsp.	One aphyric; other 15% seric plag; aug.	25% sauss plag; pseud.	5% Ksp; An <sub>13</sub> ; ±qtz.	5% cpx; sauss ±albite pseud.	0-30% seric fsp; pseud.	<5% seric plag.	One aphyric; the other 30% pseud.	<10% seric plag; ox.	<10% qtz; seric fsp.
SiO <sub>2</sub>	49.49	53.23 <sup>1</sup>	58.6	72.7	51.82	53.97	62.26	72.07	50.97	74.83	57.86	63.10	78.50
TiO <sub>2</sub>	0.70	1.43(3)	0.5	0.2	1.19	0.72	0.43	0.41	1.29	0.34	0.36	0.92	0.18
Al <sub>2</sub> O <sub>3</sub>	13.54	16.10	14.6	13.7	17.61	15.07	14.83	13.64	14.55	12.45	10.11	15.26	10.38
Fe <sub>2</sub> O <sub>3</sub>	3.40(2)	4.74(1)	10.0*	3.1*	6.06	4.27	2.73	1.68	10.76*	2.49*	8.70*	8.10*	2.24*
F <sub>2</sub> O	6.83(2)	5.63(1)	n.d.	n.d.	4.83	5.72	3.61	3.39	n.d.	n.d.	n.d.	n.d.	n.d.
MnO	0.20	0.19(3)	0.2	0.1	0.14	0.19	0.08	0.06	0.19	0.03	0.15	0.11	0.03
MgO	10.36	5.41	4.6	0.5	6.39	7.16	4.92	2.06	8.33	0.56	10.20	1.73	0.61
CaO	12.26	10.00	9.6	3.6	9.02	7.59	4.56	0.44	9.90	2.28	10.63	3.21	2.90
Na <sub>2</sub> O	1.26	1.80(3)	1.5	6.0	2.55	5.00	5.68	6.04	2.53	6.26	1.36	3.72	3.17
K <sub>2</sub> O	0.84	0.35	0.6	0.0	0.24	0.24	0.75	0.08	0.93	0.67	0.61	3.44	1.98
P <sub>2</sub> O <sub>5</sub>	0.20	0.13(3)	0.1	0.1	0.14	0.14	0.14	0.12	0.32	0.09	0.05	0.41	0.06
Total	99.08	99.01	100.3	100.0	99.99	100.03	99.99	99.99	99.77	100.00	100.03	100.00	100.05
Vols	3.22	4.90	n.d.	n.d.	5.22	5.97	2.91	3.23	n.d.	n.d.	n.d.	n.d.	n.d.
Rb	11(1)	5(2)	12	<5	<5	5	5	<5	20	8	<5	54	22
Sr	279(1)	343(2)	330	168	405	256	112	48	396	118	125	256	68
Zr	54(1)	65(2)	67	50	115	82	90	105	149	284	23	181	135
Y	14(1)	14(2)	17	16	20	18	14	28	30	71	9	39	62
Nb	<10(1)	<10(2)	<10	<10	<10	<10	<10	<10	<10	20	<10	<10	<10

N is the number of analyses averaged. Rock type is defined by SiO<sub>2</sub> contents thus: B = basaltic andesite (52-56%); BA = basaltic andesite (56-63%); A = dacite (63-69%); D = dacite (63-69%); R = rhyolitic (>69%). Phenocrysts: fsp = feldspar; qtz = quartz; plag = plagioclase; Ksp = potassium feldspar; aug = augite; cpx = clinopyroxene; opx = orthopyroxene; ol = olivine; pseud = mafic pseudomorphs; hbl = hornblende; ox = oxide; musc = muscovite; sauss = saussuritized; seric = sericitized. Vols: corrected loss on ignition. Bracketed numbers are numbers of analyses averaged where <N. \*Total Fe as Fe<sub>2</sub>O<sub>3</sub>. n.d. = not determined.

TABLE A. Averaged compositions of lavas from the Balas and Idsas suites

Rock type	Balas suite (units 1 & 2)				Balas suite (unit 3)			Balas suite (unit 6)			Idsas suite			
	B	BA	A	R	B	BA	A	A	D	R	B	BA	A	D
	5	1	1	1	1	6	1	1	4	4	1	2	3	1
Pheno-crysts	Mostly aphyric; one with 30% plag & aug	15% sauss plag; pseud.	20% sauss plag; pseud.	20% sani; dine; plag An <sub>13</sub>	5% aug	10-40% sauss plag; aug; opx pseud.	40% sauss plag; pseud.	40% cpx; sauss ±albite pseud.	1-20% Ksp; sauss ±pseud.	5% Ksp; albite ±ox.	30% sauss plag; ox.	30-40% sauss plag; seric fsp; ±cpx.	5-30% sauss plag.	5% plag; An <sub>13-22</sub> hbl.
SiO <sub>2</sub>	48.19	55.89	58.05	72.15	50.91	54.87	57.06	56.89	67.02	74.86	51.93	54.29	57.77	66.64
TiO <sub>2</sub>	2.08	1.55	0.81	0.43	1.15	1.06	0.93	0.94	0.88	0.49	0.89	1.16	1.04	0.54
Al <sub>2</sub> O <sub>3</sub>	14.81	18.60	15.33	14.81	17.07	16.97	18.57	14.46	14.37	12.55	15.49	15.38	14.68	16.65
Fe <sub>2</sub> O <sub>3</sub>	5.23	4.18	3.95	0.82	3.79	2.91	5.20	3.24	1.48	1.24	12.24*	10.83*	10.11*	3.95*
FeO	7.50	3.04	4.34	1.31	6.91	6.09	3.03	5.50	4.51	1.63	n.d.	n.d.	n.d.	n.d.
MnO	0.20	0.10	0.16	0.02	0.20	0.16	0.16	0.16	0.07	0.03	0.19	0.17	0.14	0.04
MgO	9.02	5.25	5.82	0.54	7.64	6.16	3.63	8.79	3.13	1.22	6.06*	5.50	4.70	1.56
CaO	8.39	4.63	6.20	1.89	9.05	7.70	6.02	7.03	2.58	1.50	9.54	7.07	7.35	4.99
Na <sub>2</sub> O	2.89	3.95	3.83	6.90	2.43	2.95	3.70	2.77	5.48	6.22	2.70	2.97	2.93	4.72
K <sub>2</sub> O	1.16	2.30	1.20	1.03	0.63	0.93	1.43	0.11	0.10	0.12	0.73	2.30	0.92	0.73
P <sub>2</sub> O <sub>5</sub>	0.53	0.52	0.31	0.09	0.23	0.21	0.27	0.11	0.32	0.15	0.22	0.35	0.35	0.18
Total	100.00	100.01	100.00	99.99	100.01	100.01	100.00	100.00	99.94	100.01	99.99	100.02	99.99	100.00
Vols	4.66	3.17	2.68	2.26	3.29	3.12	3.57	3.85	2.57	1.44	n.d.	n.d.	n.d.	n.d.
Rb	12	41	19	13	7	12	24	<5	<5	<5	18	30	13	12
Sr	264	447	452	140	220	336	427	198	218	132	394	343	309	733
Zr	175	294	191	357	136	170	177	84	153	111	102	142	140	199
Y	40	34	27	53	29	27	25	16	30	22	18	25	30	7
Nb	<10	15	<10	12	<10	11	16	16	<10	<10	<10	<10	<10	<10

TABLE c. Averaged compositions of lavas from the Fatimah and Arfan suites

Rock type	Fatimah suite					Arfan suite				
	B	BA	A	D	R	B	BA	A	D	R
N	4	5	1	1	2	3	3	1	1	4
Pheno-crysts	5-30% sauss plag; cpx; ox; pseuds.	5-30% sauss plag; ±ox; ±pseuds.	Aphyric	<10% sauss fsp; ox; pseuds.	<10% sauss plag An <sub>36</sub> ; ±pseuds.	0-15% seric plag; ol pseuds.	0-50% seric plag; ol pseuds.	20% plag An <sub>82</sub> ; pseuds; ox.	Aphyric	0-20% ox; ±plag; ±Ksp; ±pseuds.
SiO <sub>2</sub>	49.68	54.34	56.00	69.00	69.78	51.37	52.70	58.24	65.78	73.14
TiO <sub>2</sub>	1.65	1.39	1.49	0.53	0.65	1.60	1.41	1.31	0.42	0.15
Al <sub>2</sub> O <sub>3</sub>	13.09	14.57	13.95	15.62	14.88	16.79	17.70	15.67	16.93	14.14
Fe <sub>2</sub> O <sub>3</sub>	13.55*	11.38*	11.40*	4.12*	4.12*	6.40	6.21	3.47	2.14	1.29
FeO	n.d.	n.d.	n.d.	n.d.	n.d.	4.12	3.23	3.90	2.65	0.62
MnO	0.19	0.16	0.15	0.06	0.06	0.15	0.15	0.11	0.19	0.05
MgO	9.72	6.62	5.67	0.77	0.85	5.34	5.04	4.95	1.01	0.29
CaO	8.45	6.00	6.83	2.27	1.55	8.85	7.92	7.71	3.62	1.29
Na <sub>2</sub> O	3.05	3.81	2.82	5.91	5.61	3.34	3.69	2.59	5.22	5.91
K <sub>2</sub> O	0.31	1.33	1.25	1.54	2.31	1.70	1.59	1.67	1.73	3.04
P <sub>2</sub> O <sub>5</sub>	0.34	0.37	0.42	0.19	0.21	0.35	0.35	0.38	0.30	0.09
Total	100.03	99.97	99.98	100.01	100.02	100.01	99.99	100.00	99.99	100.01
Vols	n.d.	n.d.	n.d.	n.d.	n.d.	2.55	2.41	1.96	1.68	0.37
Rb	8	25	20	30	33	44	38	41	50	70
Sr	334	340	307	107	107	623	659	583	569	274
Zr	152	190	211	188	177	157	173	211	370	146
Y	36	39	48	40	40	29	28	28	32	17
Nb	<10	<10	<10	<10	<10	8	7	8	8	7

Explanation as in Table a.

TABLE d. Averaged compositions of lavas from the Jujuju, Jahhad and Hummah suites

Rock	Jujuju suite					Jahhad suite					Hummah suite		
	B	BA	A	D	R	B	BA	A	RD	R	BA	A	D
N	1	2	3	3	1	2	2	2	1	4	7	4	2
Pheno-crysts	20% plag An <sub>70</sub> ; pseuds.	5-30% plag An <sub>70</sub> ; ±ox.	0-5% plag An <sub>63</sub> ; ±ox.	10-20% plag; ox; ±pseuds.	2% musc.	20-30% aug; ±ol; pseuds.	0-10% plag; ±ol; pseuds; ±ox.	0-5% ±aug; ±sauss; plag.	5% qtz; Ksp.	0-20% Ksp; ±plag; An <sub>10</sub> .	0-15% seric plag; ±aug; ±ox.	1-10% seric plag; ±aug; ±ox.	10-20% seric plag; ox.
SiO <sub>2</sub>	51.31	53.52	61.87	67.94	72.11	49.51	53.84	58.57	69.29	77.15	54.25	56.70	64.65
TiO <sub>2</sub>	1.28	1.69	1.75	0.74	0.19	1.48	1.70	1.03	0.66	0.16	1.26	1.22	1.04
Al <sub>2</sub> O <sub>3</sub>	16.84	17.19	15.81	15.76	15.68	17.33	16.45	16.29	14.08	11.44	17.79	17.13	15.92
Fe <sub>2</sub> O <sub>3</sub>	5.50	5.60	4.05	4.02	2.29	5.70	5.59	4.23	1.48	2.36	4.84(4)	5.99(2)	5.73
FeO	3.52	3.62	3.13	0.21	0.00	4.89	4.93	4.11	3.79	0.67	3.99(4)	2.40(2)	0.00
MnO	0.14	0.12	0.09	0.08	0.09	0.17	0.16	0.13	0.14	0.06	0.13	0.13	0.08
MgO	7.27	4.47	1.97	0.51	0.24	7.36	4.13	3.47	1.23	0.02	3.70	3.11	1.07
CaO	10.09	8.92	3.80	2.55	2.76	9.92	8.11	6.83	4.73	0.60	7.44	6.52	2.62
Na <sub>2</sub> O	3.36	2.84	4.83	5.36	4.33	2.84	2.95	3.80	2.90	3.57	3.97	4.28	5.54
K <sub>2</sub> O	0.46	1.64	2.14	2.54	2.24	0.61	1.77	1.41	1.57	3.95	1.76	1.59	2.98
P <sub>2</sub> O <sub>5</sub>	0.22	0.41	0.57	0.29	0.08	0.22	0.38	0.15	0.12	0.05	0.36	0.42	0.40
Total	99.99	100.02	100.01	100.00	100.01	100.03	100.01	100.02	99.99	100.03	99.49	99.49	100.03
Vols	1.26	1.88	1.60	1.08	0.60	3.22	2.42	2.52	0.86	0.49	4.92	4.18	1.82
Rb	10	35	56	51	56	19	50	29	42	118	36	31	62
Sr	604	574	370	367	602	314	335	325	132	48	705	498	486
Zr	126	213	327	297	203	127	223	178	185	873	149	158	234
Y	n.d.	35	38	40	25	33	51	35	50	158	25	27	31
Nb	4	6	10	12	6	5	7	5	7	23	9	10	9

Explanation as in Table a. RD = rhyodacite.

Table A3.5 a - b Reference data for the bimodal dyke swarms of the Northeastern Desert of Egypt (After, Stern et al., 1988).

Major and Trace Element Data, Mafic Dikes

	195A	195B	195D	195E	195H	196A	196B	198C	199	201A	204B	204G	204H	204J	204M	195D
SiO <sub>2</sub>	63.67	54.31	61.12	52.79	58.20	62.92	59.46	51.92	50.53	61.95	55.74	58.56	59.37	49.05	65.90	56.23
TiO <sub>2</sub>	1.14	1.54	1.26	1.54	1.50	1.51	1.11	2.03	2.01	1.40	1.71	1.09	1.31	2.40	1.05	1.28
Al <sub>2</sub> O <sub>3</sub>	15.52	14.80	15.12	13.84	15.99	15.21	16.32	15.86	15.12	15.03	16.06	16.21	16.51	15.90	15.63	17.90
Fe <sub>2</sub> O <sub>3</sub> <sup>†</sup>	6.54	10.92	7.22	9.83	8.61	7.24	8.01	11.92	12.44	8.21	9.33	7.85	7.70	13.13	5.17	8.53
MgO	2.15	6.94	3.65	8.90	3.57	1.99	3.81	5.47	6.81	1.64	4.31	3.89	2.96	5.36	2.67	3.28
MnO	0.14	0.16	0.10	0.15	0.16	0.11	0.11	0.16	0.22	0.12	0.10	0.12	0.10	0.21	0.07	0.10
CaO	3.42	7.32	5.28	7.50	5.21	3.57	5.04	8.10	8.75	4.01	5.93	6.38	5.00	9.75	3.98	6.53
Na <sub>2</sub> O	3.96	2.69	3.29	3.16	3.86	4.49	3.64	3.34	2.65	4.06	4.30	3.68	4.55	2.89	3.20	4.04
K <sub>2</sub> O	3.11	0.97	2.59	1.77	2.47	2.54	2.24	0.76	1.15	3.14	2.06	1.95	2.16	0.87	2.05	1.79
P <sub>2</sub> O <sub>5</sub>	0.35	0.35	0.37	0.52	0.43	0.42	0.26	0.44	0.32	0.44	0.46	0.27	0.34	0.44	0.28	0.32
Total	100.00	100.00	100.00	100.00	100.00	100.00	100.00	100.00	100.00	100.00	100.00	100.00	100.00	100.00	100.00	100.00
L.O.I.	1.30	2.45	6.02	4.31	1.72	1.99	2.39	3.02	1.25	2.03	3.75	2.89	2.46	5.02	1.60	1.21
Trace Elements (ppm)																
Cr	<20	286	131	556	48	<20	115	98	157	<20	123	109	<20	23	93	<20
Ni	< 5	143	46	176	33	6	43	33	82	< 5	55	41	11	67	37	13
Cu	9	31	20	46	9	18	26	20	99	8	30	23	22	31	14	4
Zn	103	112	106	94	105	106	103	118	133	111	117	106	105	112	110	71
Rb	65 <sup>†</sup>	23 <sup>†</sup>	61 <sup>†</sup>	27 <sup>†</sup>	83 <sup>†</sup>	44	49	14 <sup>†</sup>	30	89	65	62	59	18 <sup>†</sup>	59	67
Sr	489 <sup>†</sup>	552 <sup>†</sup>	632 <sup>†</sup>	626 <sup>†</sup>	573 <sup>†</sup>	473	629	717 <sup>†</sup>	539	488	953	569	705	614 <sup>†</sup>	1164	1036
Y	34	26	22	26	28	35	27	30	27	38	18	23	20	28	12	21
Zr	300	291	231	265	279	351	236	273	205	413	235	208	255	257	250	235
Nb	10	11	<10	11	11	13	<10	11	12	21	<10	<10	<10	13	<10	<10
Ba	687	759	1130	649	755	742	505	369	294	697	1048	435	526	288	690	474
Element Ratios																
Fe <sub>2</sub> O <sub>3</sub> /MgO	3.0	1.6	2.0	1.1	2.4	3.6	2.1	2.2	1.8	5.0	2.2	2.0	2.6	2.5	1.9	2.6
K <sub>2</sub> O/Na <sub>2</sub> O	0.79	0.36	0.79	0.56	0.64	0.57	0.62	0.23	0.43	0.77	0.48	0.53	0.47	0.30	0.64	0.44
K/Rb	397	350	352	544	246	479	379	441	318	293	263	261	304	401	288	222
K/Ba	38	11	19	23	27	28	37	17	32	37	16	37	29	25	25	31
Rb/Sr	0.13	0.04	0.10	0.04	0.14	0.09	0.03	0.02	0.06	0.18	0.07	0.11	0.08	0.03	0.05	0.06

Fe<sub>2</sub>O<sub>3</sub><sup>†</sup> = total iron as Fe<sub>2</sub>O<sub>3</sub>  
L.O.I. = % wt. loss on ignition  
† = analysis by isotope dilution

Major and Trace Element Data, Felsic Dikes

	195F	195I	196C	196E	198B	200C	200F	201C	201D	202G	202J	202B	203E	203F	204D	204E	204F	204I	204L
SiO <sub>2</sub>	71.00	74.89	77.51	77.30	77.41	77.42	77.80	75.81	72.45	69.94	72.63	76.91	78.35	70.14	73.96	77.80	77.33	76.58	71.28
TiO <sub>2</sub>	0.53	0.17	0.12	0.14	0.13	0.18	0.08	0.15	0.41	0.64	0.55	0.13	0.09	0.49	0.31	0.11	0.12	0.23	0.51
Al <sub>2</sub> O <sub>3</sub>	14.61	14.14	12.25	12.84	12.82	12.45	12.55	12.47	13.75	14.13	14.03	11.99	11.68	14.19	13.85	11.99	12.6	12.48	14.71
Fe <sub>2</sub> O <sub>3</sub> <sup>†</sup>	2.08	0.95	1.02	0.46	0.40	0.73	0.86	1.75	2.48	1.26	2.21	1.40	0.93	2.85	1.83	0.91	0.88	1.01	1.91
MgO	0.45	0.14	0.10	0.08	0.06	0.08	0.01	0.07	0.66	1.02	0.38	0.08	0.01	0.36	0.56	0.09	0.06	0.08	0.38
MnO	0.09	0.04	0.02	0.02	0.02	<0.01	0.01	0.03	0.04	0.06	0.09	0.03	0.03	0.03	0.03	0.02	0.03	0.01	0.11
CaO	1.20	0.67	0.38	0.72	0.55	0.46	0.63	0.79	2.03	2.22	1.30	0.40	0.48	1.27	1.15	0.49	0.50	1.27	0.94
Na <sub>2</sub> O	5.85	4.90	3.90	3.87	3.98	3.96	4.83	4.30	4.10	4.63	4.97	4.08	3.89	4.40	3.63	3.83	3.88	3.13	5.59
K <sub>2</sub> O	4.12	4.01	4.60	4.49	4.60	4.64	3.16	4.53	3.94	3.92	3.70	4.88	4.46	5.88	4.57	4.71	4.54	5.12	3.77
P <sub>2</sub> O <sub>5</sub>	0.07	0.09	0.09	0.08	0.03	0.08	0.07	0.10	0.14	0.18	0.14	0.10	0.09	0.14	0.11	0.05	0.04	0.09	0.10
Total	100.00	100.00	100.00	100.00	100.00	100.00	100.00	100.00	100.00	100.00	100.00	100.00	100.00	100.00	100.00	100.00	100.00	100.00	100.00
L.O.I.	0.59	0.48	0.61	0.46	0.45	0.77	0.59	0.73	0.79	1.17	0.74	0.69	0.57	0.72	1.81	0.90	0.72	1.82	0.51
Type**	H	H	H	H	H	H	H	H	H	H	A	H	H	H	P	H	H	H	H
Trace Elements (ppm)																			
Cr	<20	<20	<20	<20	<20	<20	<20	<20	<20	<20	<20	<20	<20	<20	<20	<20	<20	<20	<20
Ni	< 5	< 5	5	8	< 5	12	< 5	< 5	7	13	9	7	7	< 5	8	< 5	13	< 5	6
Cu	7	< 2	9	14	3	15	26	6	4	15	14	11	10	< 2	< 10	< 2	17	2	9
Zn	56	48	65	60	43	60	83	95	73	85	101	118	94	88	64	44	77	42	99
Rb	55 <sup>†</sup>	90 <sup>†</sup>	223 <sup>†</sup>	99	82.8 <sup>†</sup>	211	125 <sup>†</sup>	194	150	110	80	167	330	124	206	256	212 <sup>†</sup>	219	77
Sr	183 <sup>†</sup>	70.3 <sup>†</sup>	37.6 <sup>†</sup>	120	92.5 <sup>†</sup>	43	122 <sup>†</sup>	53	295	394	458	20	5	89	118	55	22 <sup>†</sup>	70	228
Y	39	25	68	11	13	26	118	58	28	25	38	45	103	48	34	74	76	46	44
Zr	413	221	241	104	109	191	252	310	277	389	428	379	237	783	238	248	242	202	459
Nb	16	15	57	11	12	39	98	33	15	10	16	23	87	24	21	60	62	36	17
Ba	1076	849	63	743	851	50	443	710	809	1268	66	18	481	572	56	45	116	973	
Element Ratios																			
Fe <sub>2</sub> O <sub>3</sub> /MgO	4.6	6.8	10.2	5.8	6.7	9.1	86	25	3.8	3.2	5.8	17.5	9	7.9	3.3	10.1	14.7	12.6	5.0
K <sub>2</sub> O/Na <sub>2</sub> O	0.70	0.82	1.18	1.16	1.16	1.17	0.65	1.05	0.96	1.35	0.74	1.20	1.15	1.34	1.26	1.23	1.17	1.64	0.67
K/Rb	622	340	171	376	461	183	210	194	218	296	384	243	97	394	184	153	177	194	406
K/Ba	32	39	606	50	45	770	610	85	46	40	24	614	2060	101	66	698	837	366	32
Rb/Sr	0.30	1.39	5.9	0.83	0.90	4.9	1.0	3.7	0.51	0.28	0.17	8.4	76	1.4	1.7	4.7	9.6	3.1	0.34

Fe<sub>2</sub>O<sub>3</sub><sup>†</sup> = total iron as Fe<sub>2</sub>O<sub>3</sub>  
L.O.I. = % wt. loss on ignition  
Type\*\*: A = Peralkaline, H = Metaluminous, P = Peraluminous  
(Notes: Peraluminous/Metaluminous cutoff at molar Al<sub>2</sub>O<sub>3</sub>/Na<sub>2</sub>O+CaO+K<sub>2</sub>O = 1.05 (Stuckless et al., 1986))

Table A3.6 Reference data for the bimodal dyke swarms of the Northeastern Desert of Egypt (After, Stern et al., 1988), plotted for comparison with Mudiah metavolcanics and Mukeras dyke swarms of the Lowder-Mudiah area Yemen.

	Rare Earth Element Data (ppm)									
	-----Mafic Dikes-----					-----Felsic Dikes-----				
	195B	199	204J	204M	205D	195F	195I	203E	204E	
La	21.9	16.3	21.5	20.6	21.4	41.3	35.1	23.5	24.6	
Ce	51.4	41.0	54.3	47.3	49.3	95.5	71.3	66.5	105.8	
Nd	29.3	25.4	32.3	24.6	26.3	48.2	26.8	34.0	35.5	
Sm	6.30	5.86	7.23	4.76	5.22	9.55	4.48	10.6	9.50	
Eu	1.81	1.90	2.15	1.40	1.64	2.35	0.74	0.04	0.11	
Gd	6.35	5.76	6.72	3.96	4.52	9.00	3.73	12.1	8.78	
Dy	4.54	4.75	5.31	2.59	3.52	6.50	3.37	13.6	9.04	
Er	2.43	2.29	2.51	1.12	1.79	3.56	1.50	8.12	5.24	
Yb	2.06	1.91	1.97	0.79	1.51	2.81	1.40	7.70	4.73	
<hr/>										
(La/Yb) <sub>n</sub>	7.1	5.7	7.2	17.5	9.4	9.7	16.7	1.9	3.5	
Ce/Ce <sup>*</sup> <sub>n</sub>	0.99	1.01	1.04	1.00	0.99	1.01	0.96	1.18	1.78	
Eu/Eu <sup>*</sup>	0.85	0.99	0.93	0.97	0.99	0.77	0.51	0.01	0.04	
(Yb/Er) <sub>n</sub>	0.85	0.85	0.81	0.72	0.86	0.81	0.97	1.02	0.92	

Ratios with subscript "n" refer to chondrite-normalized abundances.

Ratios with asterisk refer to ratios of observed to expected concentrations.

**A5**

---

A5.1  
Detailed Petrographic Description of Representative  
Carbonatite rock samples:

MKY6 (Um Sallamiah)

Hand specimen Description

The rock is yellowish brown, medium- to coarse-grained phaneritic, with lenticular bands of coarse-grained, white crystalline calcite, and opaque mineral magnetite. This rock reacts vigorously with HCl.

Thin-Section Description

The rock is medium to coarse grained, phaneritic altered, and foliated and lineated, as expressed by the mica and apatite. It is composed of:

Carbonate mineral about 70%, early generation (dusty-looking with indefinite boundaries) in the groundmass (Dolomite ?) and a later generation, crystalline colourless and with definite boundaries.

Apatite, about 10%, 0.5-1.5 mm in size, elongated, subrounded, sometimes in hexagonal prisms. The apatite prisms show flow orientation, have typical stubby morphology of carbonatitic apatites, and they are full of fluid inclusions.

Amphibole about 10%, altered and with broken crystal (deformed). Phlogopite about 5%, subhedral golden yellow, bent flakes, with wavy extinction. Opaque iron oxides, magnetite about 1%, with six sided cross-sections.

The texture in this rock indicate that it is wholly primary in its mineral assemblage, but bent flakes of phlogopite and the broken crystals of amphibole indicate deformation.

#### Ore microscopy

Ore microscopic study reveals that the opaque minerals are magnetite slightly martitized, sulphides [(euhedral cubs of pyrite, pyrrhotite (altered to goethite)] and goethite mantled with magnetite (Ramdohr, 1980; Utengbogaardt and Burke, 1971).

#### MKY 4 (Um Sallamiah)

#### Hand Specimen Description

This rock is phaneritic, medium- to coarse-grained, pinkish in colour, with patches of barite, in addition to carbonates, mica and opaque iron oxide (magnetite-rich), large crystals of elongated, reddish-brown amphibole. The rock has high specific gravity and react vigorously with HCl. It is weakly foliated.

#### Thin-Section Description

This rock is coarse-grained, phaneritic, inequigranular, very weakly foliated and composed of:-

Carbonate I (dolomite) is coarse-grained. This is replaced by carbonate II (calcite) along fracture lines in a preferred direction, it is coarse grained, mosaic-textured. A third generation of carbonate (calcite) forms small veins. Barite is pinkish, pleochroic and shows perthite-like intergrowth textures with the 1st generation of carbonates (dolomite and/or calcite). The amphibole is pale-green to brownish (honey) and shows rim replacement by calcite. Other constituents are honey coloured monazite, golden yellow phlogopite, apatite, and magnetite.

BY11 (Um Sallamiah)

#### Hand Specimen Description

Deep pink in colour, phaneritic and coarse-grained, inequigranular, composed of carbonates, patches of pink barite, mica, amphiboles and opaque iron oxides.

#### Thin-Section Description

This rock is coarse- and medium-grained, phaneritic, inequigranular, composed of dusty carbonate dolomite and clean calcite. Barite is pink in colour, showing perthite-like intergrowth texture with the dolomite and/or calcite.

Amphibole, apatite, phlogopite, in addition to opaque iron oxides, are also present.

## A5.2

### Sample preparation

Analysed samples were first broken into small cubes (approx. 2.5 centimeters across) using a hydraulic jaw splitter, and any weathered crust was discarded. Enough rock to represent over 1000 times the average grain size by volume (about 1 kg for a medium-coarse grained granite) was then further crushed in a fly press to produce a coarse gravel with a grain size of less than 3mm. About 100g of this crush was then ground to a fine powder in an agate Tema mill. All the apparatus was cleaned thoroughly between samples to avoid contamination. Samples which were too small to give a representative amount of crushed material or which were heavily weathered were not used.

### X-ray Fluorescence (XRF) analysis

Samples were analysed on the Philips PW 1400 automatic X-ray spectrometer with a 72-position sample changer at Leicester University. Fusion beads were prepared from a pre-ignited sample of powder mixed in the proportions one part to five parts (0.9 g/4.5 g) with dried lithium metaborate/lithium tetraborate flux in a Pt/5% Au crucible. Each batch of flux was dried and a proportion fused to determine its weight loss on fusion so that this could be allowed for. Ignition of samples was

carried out in a furnace for 1.5 hours at 900<sup>0</sup>C and weight loss on ignition (LOI) is included in the major element listings and recalculated totals. Fusion was carried out at 1200<sup>0</sup>C in a vertical tube furnace for about 20 minutes before the liquid was caste into a 46mm glass disc which was allowed to anneal at 250<sup>0</sup>C for several hours. Powder pellets were made by mixing 15g of rock powder with around 20 drops of a 7% aqueous solution of polyvinyl alcohol ('Moviol') and then pressing the mixture into 46 mm diameter pellets under 15 tons of pressure using a steel dye and hydraulic ram.

A rhodium anode X-ray tube was used with fusion beads for analysing the following major element:

SiO <sub>2</sub>	TiO <sub>2</sub>	Al <sub>2</sub> O <sub>3</sub>	Fe <sub>2</sub> O <sub>3</sub>	MnO	MgO
CaO	Na <sub>2</sub> O	K <sub>2</sub> O	P <sub>2</sub> O <sub>5</sub>		

Two programs were run on the rhodium (Rh) anode tube and one on a tungsten (W) anode tube in order to analyse powder pellets for the following trace elements:

Rh Traces: Nb Zr Y Sr Rb Th Ga Zn Ni

Rh Ores: Zr Sr Zn Mo W Pb Cu

W Traces: TiO<sub>2</sub> V cr Ba La Ce Nd

The Zr, Sr, and Zn analyses from the Rh Traces program were used as these are more accurate due to higher

count times. The Mo and W analyses are not listed as they were usually zero or very small for all samples. The Rh Ores program was not run for all samples. A special program on the rhodium tube was used to measure U for selected samples and this also measured Rb, Th and Pb values which were comparable with those values used from the main programs. Details of the Rh anode excitation technique are given by Marsh et al (1980) and of the W anode excitation technique by Tarney et al. (1979). Quality control was maintained on trace element programs by running one international standard for every five samples.

### REE analysis

Rare-earth elements for carbonatite samples were measured using an inductively coupled plasma (ICP) source spectrometer. Sample preparation involved the standard HF - HClO<sub>4</sub> attack followed by dissolution in HCl (Walsh et al, 1981) as outlined below:

0.5 g of ignited powder is accurately weighed into a PTFE beaker and dampened with a few drops of distilled and deionised water (ddH<sub>2</sub>O). 15 ml of HF and 4 ml of HClO<sub>4</sub> are added and the mixture is then evaporated to incipient dryness at 180<sup>0</sup>C on a hot plate. A further 4 ml of HClO<sub>4</sub> is added and the mixture again taken down to incipient dryness. By this stage any undissolved material may be apparent and, if this is the case, the process from the addition of the first batch of acid is repeated. The final residue is redissolved in 20 ml of warmed 25% HCl, transferred to a 100 ml pyrex beaker, rinsing out with ddH<sub>2</sub>O and finally made up to 50 ml with ddH<sub>2</sub>O.

Chromatographic glass columns with an internal diameter of 20 mm were used for the REE separation. They were filled with Dowex AG 50W-XB(H), 200-400 mesh resin to a settled height of approx. 12cm in a distilled water medium. 250 ml of ddh<sub>2</sub>O is initially run through the columns followed by a 250 ml 4N HCl wash and a 250 ml 1N HCl wash. The sample solution is now added followed by

450 ml of 1.7N HCl. The REE's and Y are diluted with 600 ml of 4N HCl and the solution is evaporated to dryness, being transferred to a 50 ml pyrex beaker when only a small amount remains. At this stage 2 ml of concentrated nitric acid is also added. When the samples come to be run the nitrate residue is redissolved in 10% HCl for injection into the ICP.

Two controls were run to try to highlight any errors:

- a) Each batch of six samples included one blank, whereby the above method is followed exactly except that no sample is added. At least one blank was run through each column and all yielded negligible results when run through the ICP. This indicates that there is minimal contamination during the preparation process.
- b) Each batch of six samples contained one international standard.

Table A5.1: Results obtained for standard BOB-1 by ICP, and recommended values

A. BOB-1 (number after forward slash indicates batch number during REE preparation for ICP)

	/1	/2	/3	/4	/5	/6	Av.	Rec
La	5.20	5.03	5.09	5.62	5.44	4.99	5.23	4.72
Ce	14.60	14.62	13.94	15.14	14.68	14.06	14.51	13.76
Nd	11.24	11.21	11.12	11.69	10.66	11.13	11.18	10.70
Sm	3.58	3.77	3.68	3.75	4.10	3.78	3.78	3.32
Eu	1.35	1.34	1.37	1.42	1.33	1.35	1.36	1.25
Gd	4.71	4.88	4.7	4.99	5.07	4.75	4.85	4.16
Dy	5.08	5.07	5.02	5.27	5.20	4.88	5.09	0.00
Er	2.88	2.34	3.01	3.13	2.41	2.85	2.77	0.00
Yb	2.78	2.72	2.79	2.93	2.60	2.62	2.74	2.63
Lu	0.41	0.42	0.41	0.44	0.38	0.40	0.41	0.44

Rec = recommended values (A. Saunders, pers. comm.)

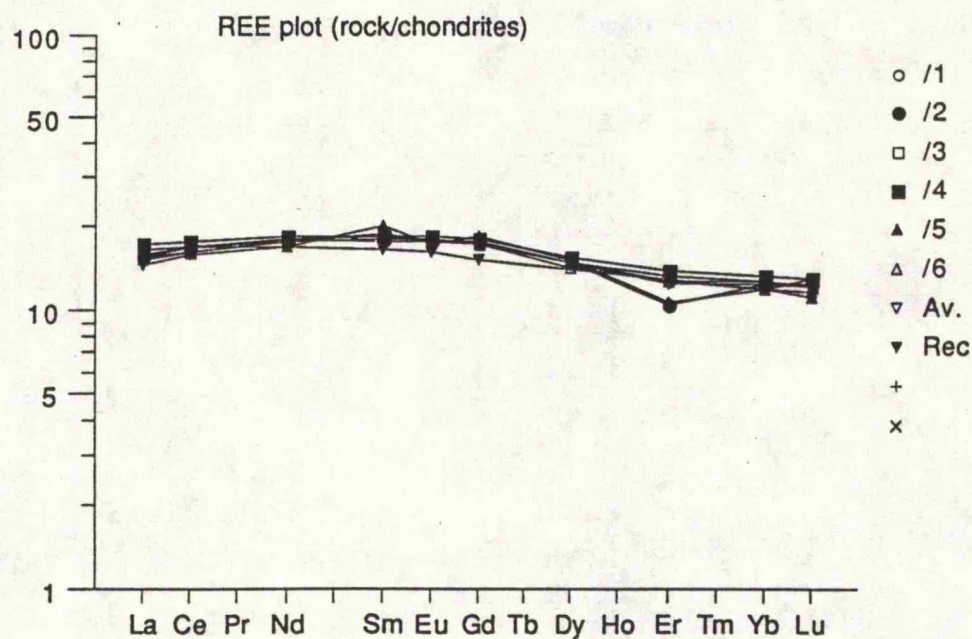


Fig. A5.1 REE plot of BOB-1 analysis, including an average of 6 ICP batches and recommended values (Saunders, pers. comm.).

REE plot (rock/chondrites)

---

Primitive mantle (ppm)

Na	2500
K	180
Ti	960
Rb	0.55
Sr	17.8
Y	3.4
Zr	8.3
Nb	0.56
Ba	5.1
La	0.551
Ce	1.436
Nd	1.067
Hf	0.27
Ta	0.04
Pb	0.120
Th	0.064
U	0.018
P O	0.024

---

Table A5.2 Appendix: Normalising values for primitive mantle (Taylor and McLennan, 1985).

**MAHFOOD ALI OBAID BA-BTTAT, PH.D. THESIS**

**GEOLOGY, PETROCHEMISTRY AND TECTONICS OF THE LOWDER-MUDIAH,  
ABYAN PROVINCE, YEMEN REPUBLIC**

**Enclosure contains:**

Fig. 2.1 Geological map of the Lowder-Mudiah area, Yemen Republic.

Fig. 2.2 Locality map and Geographical names of the Lowder-Mudiah area, Yemen Republic.

Fig. 2.3 Sample Location map of the Lowder-Mudiah area, Yemen Republic.

Fig. 2.5 Patterns of Late Precambrian dykes in the southeastern part of Mukeras Escarpment

Fig. 2.6 Distribution of the host rocks of the dykes shown in Fig. 2.5.

Fig. 4.1 Structural map of the Lowder-Mudiah area, Yemen Republic.